OCT 31 1966

IA - 1082

MASTER

RELEASED FOR ANNOUNCEMENT
IN NUCLEAR SCIENCE ABSTRACTS

RESEARCH LABORATORIES ANNUAL REPORT

for the period
January - December 1965

Israel Atomic Energy Commission

DISCLAIMER

This report was prepared as an account of work sponsored by an agency of the United States Government. Neither the United States Government nor any agency Thereof, nor any of their employees, makes any warranty, express or implied, or assumes any legal liability or responsibility for the accuracy, completeness, or usefulness of any information, apparatus, product, or process disclosed, or represents that its use would not infringe privately owned rights. Reference herein to any specific commercial product, process, or service by trade name, trademark, manufacturer, or otherwise does not necessarily constitute or imply its endorsement, recommendation, or favoring by the United States Government or any agency thereof. The views and opinions of authors expressed herein do not necessarily state or reflect those of the United States Government or any agency thereof.

DISCLAIMER

Portions of this document may be illegible in electronic image products. Images are produced from the best available original document.

AVAILABILITY

Israel Atomic Energy Commission reports and bibliographies may be obtained on application to:

TECHNICAL INFORMATION DEPARTMENT
ISRAEL ATOMIC ENERGY COMMISSION
SOREQ RESEARCH ESTABLISHMENT
YAVNE, ISRAEL

IA-1082

RESEARCH LABORATORIES ANNUAL REPORT

for the period

January-December 1965

RELEASED FOR ANNOUNCEMENT

IN NUCLEAR SCIENCE ABSTRACTS

Israel Atomic Energy Commission

Soreq Nuclear Research Center

CONTENTS

	Page
IRR-1 OPERATION	1
RADIOISOTOPE PRODUCTION	21
RADIOISOTOPE TRAINING CENTER	25
PHYSICS	
1. Elementary Particle Physics	27
2. Reactor Physics	32
3. Nuclear Physics	43
4. Solid State Physics	58
5. Plasma Physics	73
MATHEMATICS	75
CHEMISTRY	
1. Inorganic Chemistry	77
2. Radiation Chemistry	109
3. Nuclear Chemistry	159
4. Biochemistry	177
5. Analytical Laboratories	
A. Analytical Chemistry	180
B. Spectroscopy	189
C. Activation Analysis	196
BIOLOGY AND MEDICINE	203
NUCLEAR SAFETY	217
HEALTH PHYSICS	235
APPLICATIONS	255
A. Industrial Applications	256
B. Irradiation of Agricultural Products	270
INSTRUMENTATION	289
ELECTRONICS	295
PHYSICS TECHNOLOGY	310
MECHANICAL ENGINEERING	311
NUCLEAR EDUCATION	319
CONTRACTS	320
DOCUMENTATION	321
IA-reports	323
Published Papers	331
Papers Presented at Conferences	335
AUTHOR INDEX	339
SUBJECT INDEX	343

INTRODUCTION

This report sums up the progress made in the research and service programs of the Soreq Nuclear Research Center during 1965. In contrast to our previous reports, which covered six-month periods, the present report reviews the work of the whole year. Some of the results have been published during the year in the form of Israel AEC IA-reports (75), papers in scientific journals (44) and papers presented at conferences (30) . These publications are listed on p.323. Abstracts of some of them appear in the appropriate sections.

The main research topics are outlined below, as well as some other facets of our work.

Research

In Elementary Particle Physics progress was made in the application of higher symmetry groups to elementary particle reactions. Methods were developed for theoretical calculations on the basis of which the production of higher spin particle resonances were successfully predicted.

In the field of Reactor Physics, a complete group-diffusion theory was developed for the calculation of fast reactors. Other fast reactor investigations include the derivation of a simple analytical solution to the slowing-down equation, calculation of the sodium void and Doppler effects for different core sizes and types of fuel, the effect of the cross section increments used on the calculated Doppler effect, and Monte Carlo calculations of the heterogeneity of fast reactor cores and the interaction between the resonances of the fertile and fissile isotopes.

In Nuclear Physics, experimental work on neutrons emitted during triple fission of Cf^{252} has been completed and the results are being evaluated. In addition, progress has been made in the research on α-particle associated triple fission in U^{235}. In this connection several technical problems were overcome and data collection is continuing. Several Mössbauer

effect experiments were carried out, including studies with magnetic substances, ferroelectrics and iodine compounds. Further results have been obtained in the study of resonant scattering using capture gamma rays.

The Solid State Physics department has set up a nuclear magnetic resonance laboratory, and the NMR technique was used to study some transition metal hydrides. In other areas, several studies were carried out on the subject of crystal lattice dynamics, particularly with regard to vibronic states and the Jahn-Teller effect. Work on a theoretical model for the motion of krypton in a clathrate has been completed. Quantum mechanical calculations of spectra were made for various cases, including the infra-red spectra of small ionic crystals and intensity calculations of absorption bands in tetrahedral symmetry. Further infrared studies of the ferroelectric phase transition in ammonium dihydrophosphate gave support to the model suggested previously concerning the proton potential well. A model for the structure of water was suggested on the basis of quasielastic neutron scattering. Paramagnetic resonance studies include the spectrum of Co^{1+} in single crystals of CaO and radiation damage in simple oxides. The investigation of the properties of semi-conducting diamonds was continued.

In the field of Inorganic and Physical Chemistry, research on several topics was concluded and the results summed up. These topics include the interaction between lanthanide and nitrate ions in solution, molten salt studies of lanthanide ions, and the reactions between alcohols and phosphorus pentoxide. Further studies were carried out on electrolyte solution theory, solvent extraction of Am and Ga, and various investigations connected with molten salts - particularly extraction of Zn halides, electrodeposition of Ta, cation exchange, and the water content of molten salts. Methods were investigated for the preparation of several compounds - for example PrO_2, PrF_4, $AsOF_3$ and O^{18}-labelled H_2O_2. The properties of three molecules, viz. H_2O_2, NH_3 and $CH_2 = CH_2$, were computed with the aid of computer codes written for this purpose.

In Radiation Chemistry, considerable progress was made in the understanding of the mechanism of reaction of hydrated electrons with organic and inorganic compounds, and additional information was gained on the behavior of the intermediates formed in these reactions e.g. CO_2^-, $BrO_3^=$ and Zn^+. Kinetic data obtained for the reactions of hydrated electrons, H atoms and OH radicals with organic compounds, provided an understanding of the mechanisms of the reactions studied, as well as a basis for the quantitative prediction of the radiolytic degradation of most organic compounds when in aqueous solution. The investigation of the primary steps in the radiolysis of water by measuring H/D isotope effects, revealed new information which may lead to a revision of the existing theory concerning the radiolytic decomposition of water.

The Nuclear Chemisty department has made further progress in the study of high energy chemical reactions. The high energy particles used in the experimental work were fission recoils, but preparations are being made to use accelerated ionic beams in the future. A theoretical study of the mechanism of high energy chemical reactions has been initiated, the first step being concerned with the scattering and slowing-down of energetic atoms in a gaseous medium. Rapid radiochemical separation of short-lived fission products, cross section measurements and nuclear structure studies by high resolution gamma ray spectroscopy and fast neutron spectroscopy, were carried out. These investigations are part of a more general program of using an electromagnetic isotope separator on line with a fission source at the reactor, expected to go into operation in 1967.

Industrial Applications

Continued efforts, started during 1964, have resulted in the recognition by the National Council for Research and Development, of the national scope of the program for the application of large radiation sources in agriculture and industry. Special committees have been set up by the Council to guide the programs and approve the necessary budgets, supplied by the Council, the Ministry of Agriculture, the AEC and other organizations.

Agricultural products already approved for study include citrus, potatoes, onions, avocadoes, bananas, strawberries and peppers. A study of the control of the Mediterranean Fruit Fly by irradiation, and sterilization of hospital supplies, have also been approved. A contract was obtained to study sand movement on the sea bottom near shores and harbour facilities. To promote commercial developments of the new technology, the ISORAD company was set up.

Nuclear Desalination

During 1965 a joint U.S.A.- Israel Board, appointed by the heads of the two governments, carried out a feasibility study on the erection of a dual-purpose nuclear plant for the production of 200 Mwe electricity and the desalination of 120 million cubic meters per year of sea water. The study was conducted by Kaiser Engineers (with Catalytic Construction Company as sub-contractor). The Israel Atomic Energy Commission participated in several aspects of the study: a) supply of the data required; b) the active participation of the Technical Director of the Soreq Research Reactor in the study team; c) analysis and criticism of the interim reports presented by the study team, made by an engineering group specially appointed for this purpose; d) determination of the nuclear safety requirements of the project, taking into account the particular conditions in Israel; e) participation of an Israel AEC representative on the Israel Board of Directors of the project. Upon receipt of the results of the feasibility study and its publication at the end of 1965, the Israel Board of Directors of the project began preparing the final report to be presented to the Prime Minister.

Some of the research carried out during the year was performed under contracts awarded by various bodies. The contracts are listed on p. 320. In accordance with our policy, considerable effort was also put into the promotion of nuclear education. The activities in this direction are described on p.319.

Sh. Yiftah

Shimon Yiftah
Scientific Director

I R R-1 R E A C T O R

Operation

During the period covered by this report the maximum power output of the reactor was 2500 kW. Normal operation was at 2000 kW, scheduled in 1, 2 or 3 shifts depending on the demand.

Details of the reactor operation are given in Table 1. The nomimal cumulative output during this period is plotted in Fig. 1.

TABLE 1

Operation of the reactor

1.1.1965 - 31.12.1965

	Hours	Per Cent
On-load operation	2600	29.6
Critical experiments and load changes	78	0.9
Reactor experiments for training	90	1.0
Not available due to faults	164	1.8
Planned maintenance	90	1.0
Planned non-operation, mainly non-shift operation (including visits, holidays, weekends, etc.)	5738	65.7
Total hours per year	8760	100.0

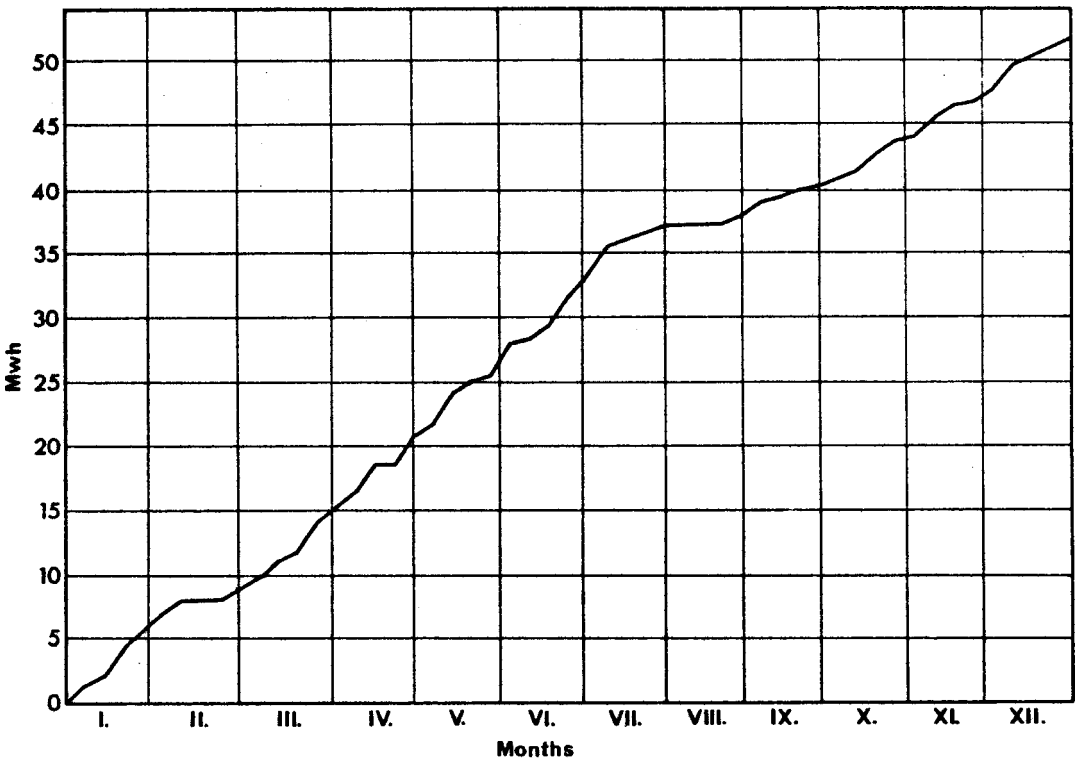

Fig. 1

Nominal cumulative output during 1965

Utilization

The utilization of the reactor falls into three categories:

a) Beam tube and thermal column experiments

b) Gamma irradiation

c) Radioisotope production.

a) The following experiments are in progress or in the running-in stage in the beam tubes and thermal column:

Beam Tube No.1 - Capture gamma ray spectroscopy

- Nuclear resonance fluorescence using an in-pile gas loop

- Mössbauer experiments using capture gamma rays

Beam Tube No.2 - Cold neutron time-of-flight for solid state studies

Beam Tube No.3 - Neutron diffractometer experiments

Beam Tube No.4 - Fast shuttle rabbit for nuclear spectroscopy

Beam Tube No.6 - Gas loop for nuclear chemistry studies

Thermal Column - Nuclear fission studies

- Study of (n,α) reactions

- Resonance fluorescence using capture gamma rays

- Exponential experiments

These experiments are conducted by the Nuclear Physics, Solid State Physics and Nuclear Chemistry departments, and more details are given in the appropriate sections of this report.

b) In the gamma cell, irradiation experiments are carried out by the Industrial Applications Group, using the 30,000 curies Co^{60} source which is installed in the reactor pool.

c) Details of radioisotope production are given in the next section.

Table 2 shows the utilization of the reactor by the various departments.

TABLE 2

Number of irradiations ordered by different users

1.1.1965 - 31.12.1965

Department	In-core irradiation	Pneumatic tube irradiation
Health Physics	-	32
Industrial Applications Group	3	305
Inorganic Chemistry	-	25
Nuclear Chemistry	485	2750
Nuclear Physics	279	101
Radiation Research	80	2
Radioisotope Training Centre	-	8
Reactor	27	21
Solid State Physics	8	-
Technion	1	25

Neutron Activities in the Reactor Coolant Water: A. Notea* and S. A. Scott**

Neutrons which are detected in reactor coolant water originate from two main sources: 1) delayed neutron precursors, such as 4.14 sec N^{17} produced from $O^{17,18}$ by fast neutrons, and fission product delayed neutron emitters, 2) the (gamma,n) reaction on deuterium with gammas of energies exceeding 2.22 MeV. The expected sources of high energy gammas are 2.25 sec C^{15}, Bremsstrahlung and gammas from fission products and N^{17}, and the most important source - 7.10 sec N^{16}. The following experiment was conducted to determine the contribution of the various sources to the total neutron activity.

The neutron activity of the coolant was measured with a BF_3 counter attached to the water pipe at a point which the water passes approximately 5 seconds after leaving the core (Fig. 2). The output of the counter was

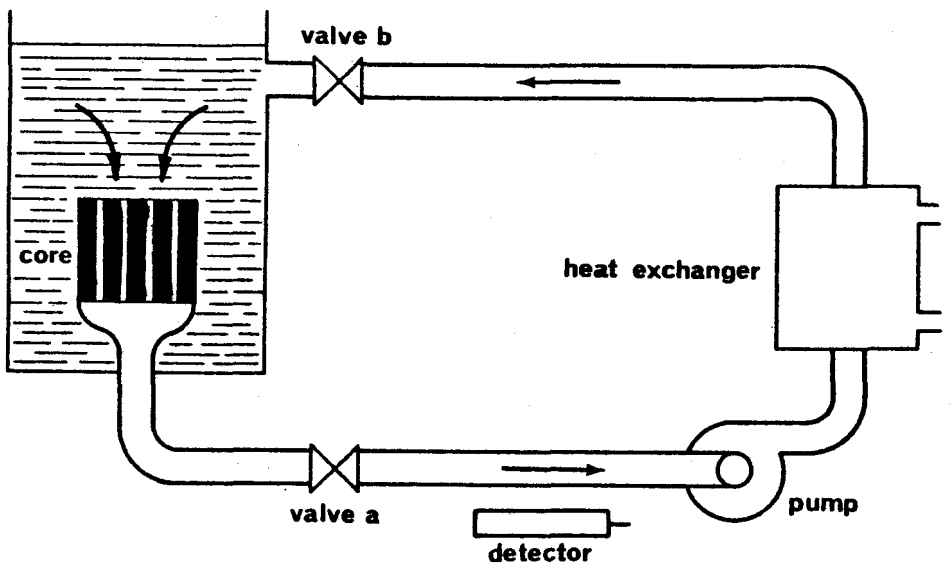

Fig. 2

The IRR-1 coolant water flow system

---

* Soreq Nuclear Chemistry Dept.

** Technion - Israel Institute of Technology, Haifa

fed to a multiscaler with suitable discrimination against gammas. To measure the composite decay curve the multiscaler was started, the coolant pump switched off, and valves A and B closed. Due to the automatic safety system, this operation "scrams" the reactor. The decay curves were analysed using a computer. From a typical run it was found that the main source of neutrons is N^{17}, which accounts for 98% of the total activity. Less than 1% of the total is due to N^{16}, about 1% is from the second fission delayed neutron group (22.7 sec) and 0.03% is from the first fission group (55.7 sec).

Since the N^{17} activity is the dominant one in the coolant during the first 20 seconds after leaving the core, it can be used for monitoring the reactor power (see p.9,12). The neutron count rate 40 seconds after exit is due primarily to the fission products and thus can be used to monitor the fission product level in the water to detect a possible failure of a fuel rod.

The N^{16} Activity in the Reactor Coolant Water[1]: S. A. Scott* and A. Notea**

The primary coolant loop of water cooled reactors must be heavily shielded due to the presence of N^{16} during reactor operation. This isotope decays to O^{16} with the subsequent emission of 7.12 and 6.13 MeV gamma rays. The half-life of this activity has been variously reported[1-3] as 7.35, 7.31 and 7.14 sec.

A series of measurements was carried out on the gamma radiation emitted from the IRR-1 primary coolant loop. A 9.2 cm ϕ x 9.2 cm NaI(Tl) detector was used in conjunction with standard pulse analysis techniques.

* Technion - Israel Institute of Technology, Haifa
** Soreq Nuclear Chemistry Dept.

The pulse height spectrum showed, in addition to the N^{16} photo- and escape-peaks, a contribution from Na^{24}. The counting rate above a 4.5 MeV discrimination level was not linearly dependent on the reactor power level, an effect attributed to pulse pile-up.

The decay of the high energy gamma radiation was measured by simultaneously switching off the primary circuit pump and shutting off the inlet and outlet coolant valves (see Fig.2 , previous item). The reactor power level, coolant flow rate, detector position and counting period were selected so as to reduce to a minimum such effects as dead time losses, pulse pile-up distortions and interfering contaminant activities. The decay curve was fitted to an exponential series by the general least squares method. The N^{16} half-life was found to be 7.10 ± 0.03 sec.

References:

1. SCOTT, S. A. and NOTEA, A., Nuclear Physics, 1966 (in press)
2. ELLIOT, J. O. and YOUNG, F. C., Nucl. Sci. and Eng., 5, 55 (1959)
3. MALMSKOG, S. and KONIJN, J., Nucl. Phys., 38, 196 (1962)
4. BIENLEIN, J. K. and KALSCH, E., Nucl. Phys., 50, 202 (1964)

Measurement of the Reactor Coolant Flow Rate : S. A. Scott*, A. Notea**

Accurate determination of the thermal power level of a research reactor is usually limited by the error involved in the measurement of the primary coolant flow rate. Mechanical or hydraulic gauges are generally employed, calibrated where possible by volume-time measurements in a hold-up tank of known geometry.

Two new techniques have been investigated for measuring coolant flow rate. Both involve detection of induced activity in the primary coolant loop - the high energy gamma radiation from 7.1 sec N^{16} in the one method, and the delayed neutrons emitted by 4.1 sec N^{17} in the other.

---

* Technion - Israel Institute of Technology, Haifa
** Soreq Nuclear Chemistry Dept.

The first method involves measurement of the drop in coolant activity along the primary loop, as a function of distance from the core, with the reactor operating at constant power and flow rate. Due to the instability of both reactor and detector, the measurements at the different points must be carried out simultaneously with separate detectors. The counting rate R_i for the i^{th} detector at a distance X_i from the reactor grid plate is given by

$$R_i = k[1 - \exp(-\frac{\lambda X_o}{v_o})] \exp(-\frac{\lambda X_i}{v})$$

where v_o and v are the coolant velocities in the core and primary loop respectively, X_o is the effective length of the core, λ the induced activity decay constant and k a constant involving geometrical and calibration factors. Any pair of detectors can be used to determine the coolant velocity, since

$$v = \frac{\lambda(X_j - X_i)}{\ln(\frac{R_i}{R_j})}$$

which involves only λ and the relative detector distances. Unfortunately, the use of N^{16} gamma radiation is restricted by the opposing demands of high energy gamma detection (large NaI(Tl) crystals) and pile-up rejection (low counting rate). This problem does not arise if the N^{17} neutron activity is measured, but there are other complications in that the (γ,n) and fission product neutron contributions necessitate the definition and measurement of an effective decay constant instead of λ.

The second method avoids all the above problems. Three detectors are used, one in the reactor reflector and the other two at positions along the primary coolant loop. Each detector is connected to a multichannel analyser operated as a multiscaler at 0.1 sec per channel. With the reactor operating at a suitable power level and flow rate, all the multiscalers are started simultaneously and, after a short delay, the

reactor is scrammed. A typical set of curves is shown in Fig. 3 .

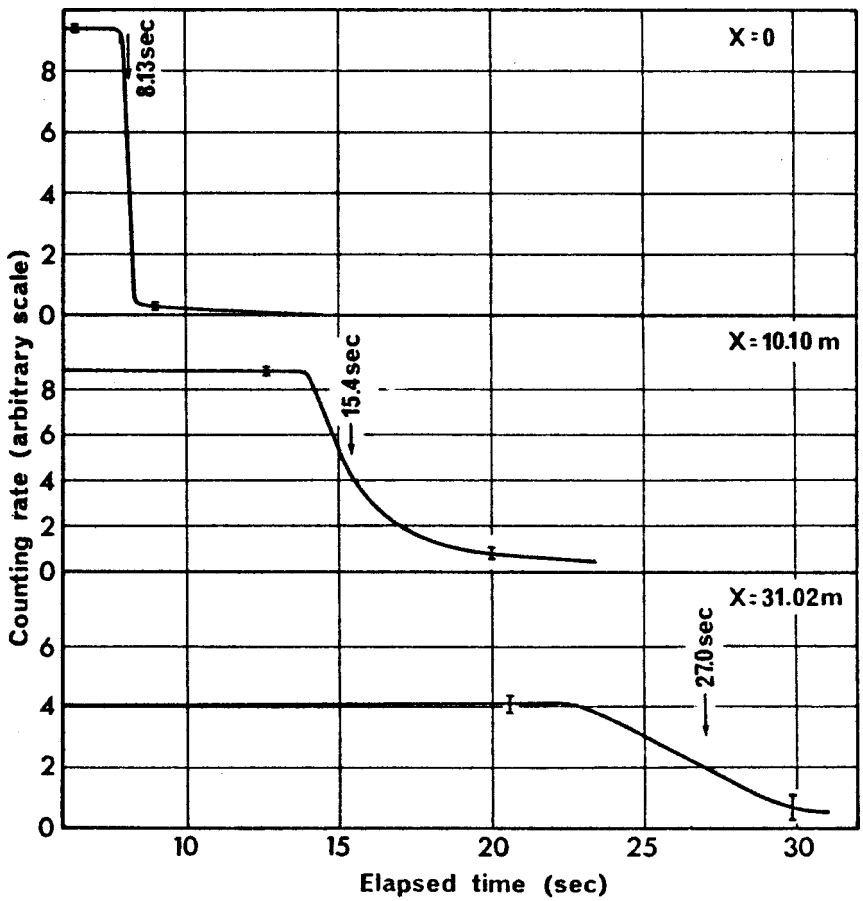

Fig. 3

Measurement of reactor coolant flow rate by three detectors following reactor scram. Flow rate = 330 m^3/h. X = distance from reactor grid plate

Both coolant velocity v and "the effective core length X_o" (different from the X_o on p. 7) are obtained directly from time and distance measurements. Flow rate results accurate to about 1% were obtained for both N^{16} and N^{17} measurements, and improved collimation would probably increase this accuracy considerably.

Comparison between Local and Integral Reactor Power Measurements : A. Notea, A. P. Hoffmann, S. A. Scott*

Direct power measurements in swimming pool reactors are possible only above about 1 MW. Even at power levels of several megawatts the coolant temperature rise through the core is only a few degrees, and thermocouple readings together with coolant flow rate measurements give relatively inaccurate values of the reactor power. The determination of reactor power levels less than about 1 MW requires the use of a more sensitive system, calibrated against temperature measurements at high power.

There are two types of secondary power monitoring systems. The first, or "local" type, involves the measurement of the thermal neutron density at some point in or near the core, usually with a compensated ionization chamber or fission chamber. In order that there be a linear relationship between thermal power and local thermal neutron density, the thermal neutron flux profile at the time of the calibration must remain undisturbed throughout subsequent power measurements. This situation is never realised in practice since the relative thermal neutron density at the detector is dependent on the control rod configuration, fuel burn-up, fission product poisoning, etc.

In the second, "integral" type of monitoring system the induced coolant activity is measured. This method assumes a linear relationship between the thermal power and the average fast neutron flux, and consequently should be less sensitive to changes in the flux profile. In the present work the delayed neutron activity due to the 4.1 sec N^{17} was determined.

The IRR-1 swimming pool reactor was equipped with two "local-type" monitors (a compensated ionization chamber and a fission chamber, located on opposite sides of the core), and two "integral-type" monitors (to measure coolant temperature rise and coolant delayed neutron activity).

---

* Technion - Israel Institute of Technology, Haifa

The nominal operating power, as given by the compensated ionization chamber (CIC), was maintained at 2 MW for a series of control rod configurations. The results are shown in Table 3 . It is apparent that the two integral measurements show excellent mutual agreement, while the local measurements differ by up to 30% both among themselves and relative to the integral results.

TABLE 3

Comparative local and integral power measurements

Control rods inserted					Local measurements		Integral measurements	
1	2	3	4	5	Ionization chamber	Fission chamber	Coolant temperature	N^{17} monitor
x	x	x	x	x	100 ± 1	100.0 ± 0.2	100 ± 2	100.0 ± 0.2
		x		x	100	70.7	82	84.3
		x			100	80.6	74	78.7
	x				100	108.8	82	88.8
			x		100	97.7	88	89.2
	x		x		100	115.1	96	97.9

Xenon build-up, occurring preferentially in high flux regions, will perturb the thermal flux spatial distribution while having a much reduced effect on the fast flux. Figure 4 shows typical results obtained when the reactor is operated continuously at 2 MW CIC nominal power level. The thermal power drop of over 25% is monitored relatively accurately by the integral detector.

It has been shown[1] that the N^{17} monitor is linear in response down to at least 10 W (see next item). Its insensitivity to local flux changes makes it a convenient and accurate method of measuring the thermal power level.

The above work was carried out in cooperation with the Nuclear Chemistry Department.

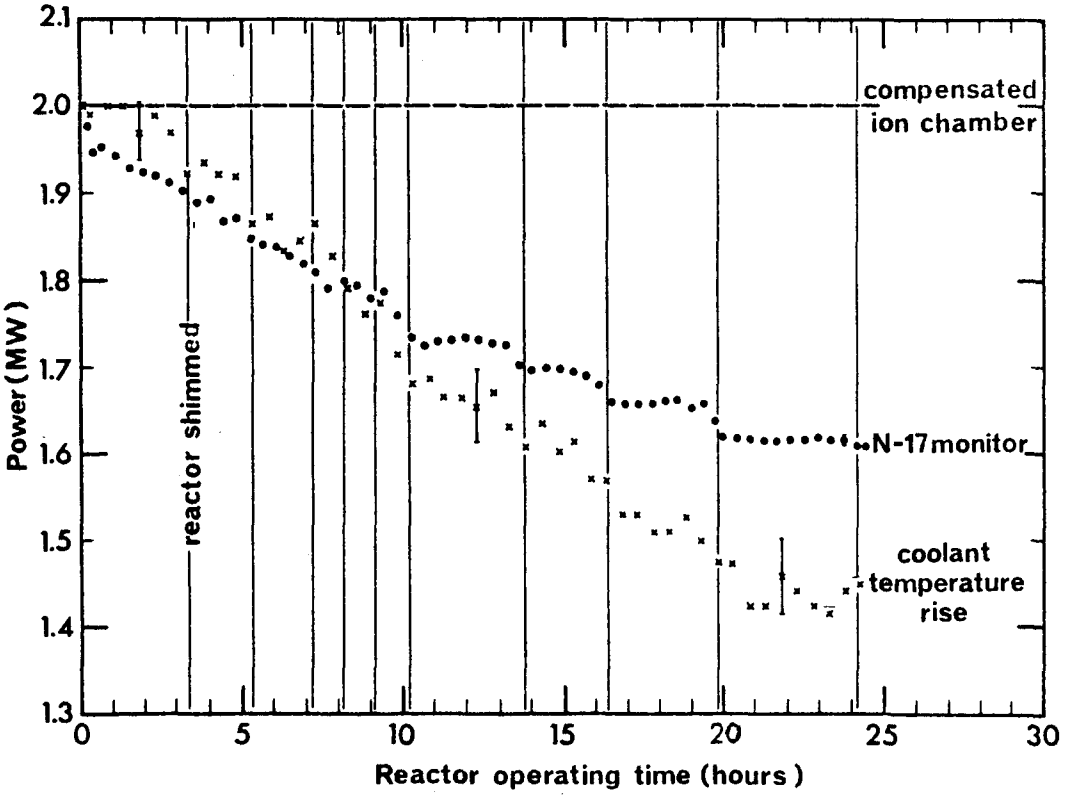

Fig. 4

Reactor output as measured by local and integral monitors

Reference :

1. SCOTT, S.A. and NOTEA, A., Trans. Am. Nucl. Soc., 8, 70 (1965)

Monitoring Reactor Power by N^{17} Neutron Decay[1]: S.A. Scott* and A. Notea**

A primary coolant loop neutron monitoring system for measuring reactor power (see p. 4,9) was constructed and tested at the IRR-1 swimming pool reactor. A high efficiency BF_3 counter was attached to the coolant pipe between the reactor pool outlet and the primary circuit pump. Pulse height discrimination was used and the detection system was shown to be completely insensitive to gamma rays over the entire power range. The compensated ionization chamber of the reactor was calibrated in terms of the power level by measurements of the coolant flow rate and temperature rise. The counting rate of the coolant loop monitor was then recorded as a function of the reactor power level over the range 10 W to 2.5 MW. The relationship is linear over the entire range, as seen from Fig. 5 .

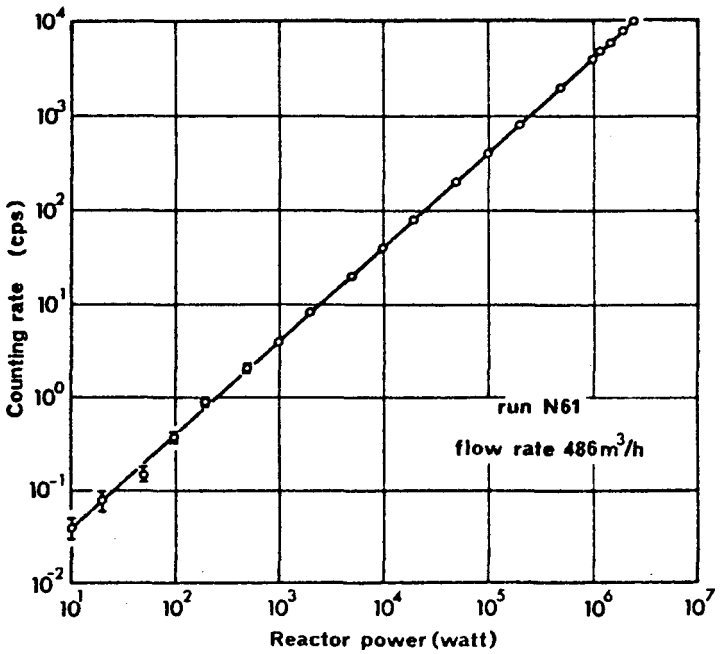

Fig.5

Measurement of the linearity of the coolant loop system

Reference:

1. SCOTT, S. A. and NOTEA, A., Am. Nuc. Soc. Trans. 8, 1, 70 (1965)

* Technion - Israel Institute of Technology, Haifa
** Soreq Nuclear Chemistry Dept.

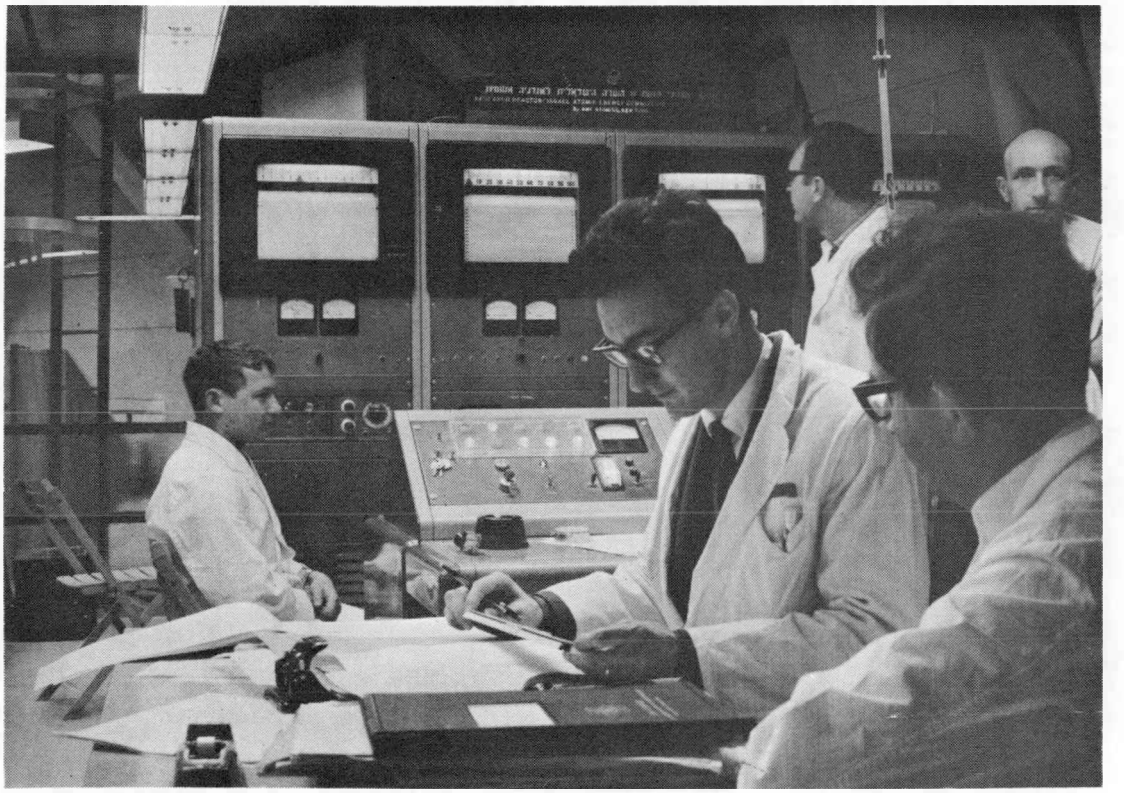

Reactor control room

Proposed Automatic Control of the Reactor Power by Monitoring Delayed Neutrons from N^{17} : A. P. Hoffmann and D. Segal

In the original design of the IRR-1 reactor, automatic control is accomplished through the output of a compensated ionization chamber placed near the reactor core. This output is very sensitive to the thermal neutron flux distribution, which is subject to large variations during one- and two-shift reactor operation, due to the nuclear poisons present in the reactor.

We propose to use a reactor power monitor based on the N^{17} delayed neutrons in the coolant water (see previous item) for the automatic control of the reactor power. This system would be added to the existing control equipment, as shown in the following figure. Experiments are being planned to check the system.

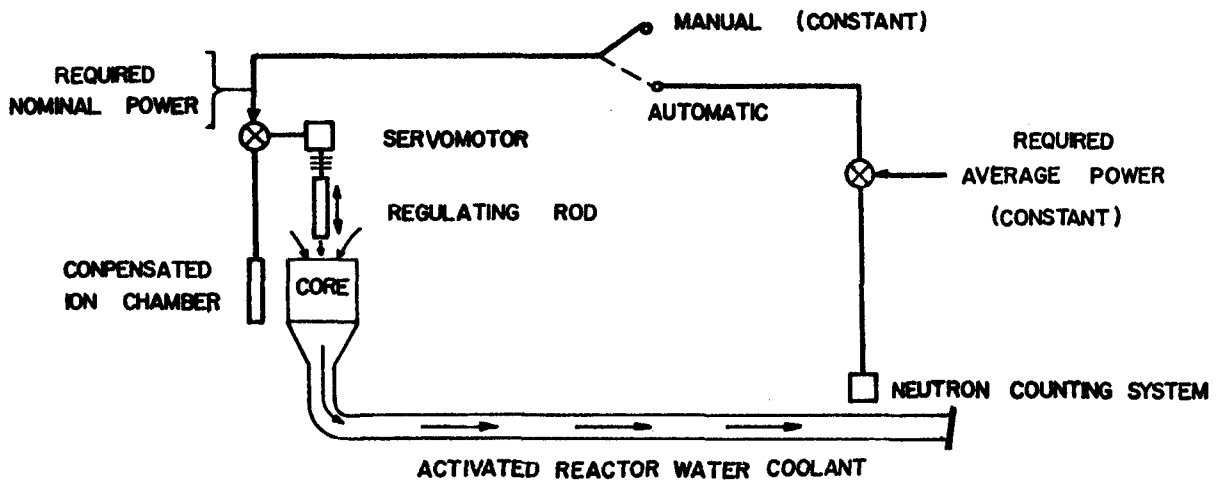

Fig. 6

Proposed automatic reactor power control system

Non-Destructive Experimental Evaluation of the Burn-up in an MTR Type Fuel Element : A. P. Hoffmann

A rather simple non-destructive experimental method has been proposed to determine the burn-up of an MTR type fuel element in our reactor.

The reactor is fueled by highly enriched U^{235} fuel elements arranged in a rectangular grid array so as to give a small core. In such a small core of parallelipipedal shape the neutron flux is greatly affected by any local or distributed perturbation like nuclear poisons, beam tube experiments, and in-core irradiations for radioisotope production. Thus the calculation of the burn-up rate in every fuel element is very inaccurate, besides being tedious.

The proposed method uses a reference cold critical core (Fig. 7)

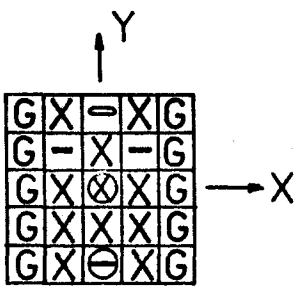

Fig. 7

Reference cold critical core for burn-up measurements

- ⊠ new fuel element
- ⊗ replace irradiated fuel element
- ⊟ safety rod (always 100% out) + control fuel element
- ⊖ regulating rod + control fuel element
- ⊖ control rod + control fuel element
- G graphite reflector element

in which one new cold fuel element is replaced by an irradiated fuel element and the excess reactivity difference between the two is determined experimentally. This reactivity difference is converted to burn-up value by considering the changes in the four-factor formula.

The reference core configuration gives, with our standard fuel elements, a slight excess reactivity just enough to check the burn-up of irradiated standard fuel elements burned to (30-35%).

There are several advantages to this configuration:

- it is symmetrical with respect to the y axis
- the replace position is surrounded only by fuel elements (safety rods always 100% out)
- the excess reactivity difference is achieved by one single control rod
- the replace position has the highest weighted factor
- it has a rectangular cross section and can be quite easily interpreted.

A more detailed report will be published.

Determination of the Gamma Flux in a Nuclear Reactor by the $N_2^{1414} - N_2^{1515}$ Isotopic Exchange Reaction[1]

M. Anbar* and P. Perlstein*

In a previous study[2] it was shown that the radiolytically induced isotope exchange $N_2^{1515} + N_2^{1414} \rightarrow 2\ N_2^{1415}$ proceeds linearly with dose with a G-value of $G_{exch} = 9.5 \pm 0.25$. The same value was obtained with both X- and gamma-rays, and no deviations from linearity were observed up to a total dose of 1.25×10^8 rad. As this system does not undergo any chemical change on irradiation and its behavior is predictable up to complete isotopic equilibrium, it was suggested that it be applied as a gas dosimeter for high radiation doses.

The high dose rates as well as the mixed radiation prevailing in nuclear reactors make it hard to find a satisfactory dosimetric

* Radiation Research Dept.

system. In the present work the $N_2^{1515} - N_2^{1414}$ system was successfully used to determine high level gamma radiation doses in the IRR-1 research reactor.

Irradiation vessels were evacuated to 10^{-5} mm Hg and then filled with different mixtures of N_2^{14} and N_2^{15}, using a Toepler pump under a pressure of 200 mm Hg as measured with a mercury manometer. A special cold-trap held in a dry-ice + acetone bath ($-78^{\circ}C$) was attached to the filling manifold to remove mercury vapor originating from the Toepler pump and the manometer.

After irradiation the vessels were allowed to "cool" for a minimum of 24 hours (Si^{31} has a half-life $t_{\frac{1}{2}} = 2.6$ h) and the gas was then analyzed with a CEC 21-401 analytical mass spectrometer. The masses 28 (N_2^{1414}), 29 (N_2^{1415}) and 30 (N_2^{1515}) were measured. The masses 32 (O_2) and 40(Ar) were also measured to check for possible air contamination. The ratio R of scrambled N_2^{1415} to total N_2 was calculated, taking into account the initial amount of "scrambled" nitrogen N_2^{1415} which was 0.4 - 6.8%, depending on the enrichment of the nitrogen-15 used.

The results obtained at different mole ratios of N_2^{15} and N_2^{14} and with different irradiation times ranging from 10 to 50 minutes are presented in Table 4 .

The gamma flux of the IRR-1 reactor was determined some time ago at low power output using the Fricke dosimeter, and again recently using the N_2O dosimeter. Both determinations were of low accuracy, the average value being 1.05 ± 0.2 Mrad/min at 1.6 MW. Although this value can hardly serve as a quantitative check on the $N_2^{1515} - N_2^{1414}$ dosimeter, it indicates that the G value used, which was determined at much lower dose rates, is applicable to the dose rates measured in the present study.

The linearity of the dosimeter response with dose in the region of equimolecular composition of N_2^{15} and N_2^{14} , which is the most sensitive region for mass spectrometric measurements, makes this system a suitable

TABLE 4

The nitrogen exchange reaction as a dosimeter in pile irradiation

Reactor power level (MW)	Mole fraction N_2^{1515}/N_2^{1414}	Time of irrad. (min.)	$R_o \times 10^3$	$R_t \times 10^3$	Total dose (Mrad)	Dose rate Mrad/min
1.6	1/2.5	30	16.80	20.92	41.5	1.38
1.6	1/2.5	40	16.80	22.13	49.8	1.24
1.6	1/2.5	50	16.80	23.50	62.6	1.25
						Ave. 1.29 ± 0.08
1.6	1/1.15	10	42.54	44.17	10.8	1.08
1.6	1/1.15	20	42.54	45.50	19.7	0.99
1.6	1/1.15	30	42.54	47.29	31.5	1.05
1.6	1/1.15	20	42.54	45.48	19.2	0.96
1.6	1/1.15	30	42.54	47.07	29.8	0.99
1.6	1/1.13	20	48.66	51.91	21.3	1.07
1.6	1/1.13	40	48.66	55.15	42.4	1.06
1.6	1/1.13	50	48.66	56.79	53.0	1.06
1.6	1/0.35	20	31.06	33.22	18.3	0.92
1.6	1/0.35	30	31.06	34.95	33.0	1.10
1.6	1/0.35	50	31.06	36.99	50.2	1.00
1.6	1/0.13	40	73.44	75.99	38.1	0.95
						Ave. 1.20 ± 0.05
2.0	1/0.8	15	4.27	6.60	17.4	1.16
2.0	1/0.8	30	4.27	9.04	37.0	1.23
						Ave. 1.20 ± 0.05

dosimeter for reactor radiation. Although the maximum dose in our experiments was only 5×10^7 rad, the behavior of the system remains predictable up to much higher doses.

In the measurement of gamma fluxes of high intensity, the precision-limiting factor becomes the measurement of the time of irradiation. High sensitivity of the dosimeter is thus not essential, it being

more important to have a linear and reproducible response at high doses. The $N_2^{1515} - N_2^{1414}$ isotope exchange dosimeter fulfills these requirements.

References:

1. ANBAR, M. and PERLSTEIN, P., Israel AEC Report, IA-1048 (1965)

2. ANBAR, M. and PERLSTEIN, P., J. Phys. Chem., 68, 1234 (1964)

Reactor Water Analysis[1] : Y. Prulov*, M. Stiller*, Y. Feige*

A detailed report[1] on the reactor water analyses performed was prepared. The report includes results already summarized[2,3] as well as quantitative gamma spectrometry results obtained during 1965.

The radioactive isotopes and their concentrations usually found in the pool water were: Na^{24} - about 1 μc/l; Cu^{64} and Np^{239} - about 10^{-1} to 10^{-2} μc/l; Mn^{56}, Cd^{115} and W^{187} - about 10^{-3} μc/l; and I^{131}, I^{133}, I^{134}, I^{135}, Br^{82}, Sr^{91}, Sr^{92} in smaller concentrations (10^{-4} μc/l or less).

In the regeneration eluates of the "hot" ion exchanger unit the concentrations per liter of eluate usually found were 1 to 5 x 10^{-1} μc/l for I^{131}, Ag^{110m}, Ce^{141} and Ce^{144}, Mn^{54}, Zn^{65}, and Ba^{140} - La^{140}; 10^{-1} to 10^{-2} μc/l for Sb^{124}, Np^{239}, Zr^{95}, Co^{60}, Sr^{90} and Cs^{137}; and lower concentrations (below 10^{-2} μc/l) for Hf^{181}, Ta^{182}, Cd^{115}, Se^{75}, Sp^{113}, Fe^{59}, Co^{58} and Cs^{134}.

Based on the average concentration of Cs^{137} usually found in the eluate, and taking into account the operating conditions of the reactor, the weight of U^{235} which generates the fission products in the above mentioned concentrations was calculated. Assuming that this U^{235} comes from the external contamination of the fuel elements, then for a loading of 27 fuel elements (having a total surface of 47 m^2) an external U^{235} contamination of 1.7 x 10^{-2} μg/cm^2 was derived. Thus it seems that the only source

* Health Physics Dept.

of fission products found in our coolant system is indeed the external uranium contamination of the fuel elements, since similar values of external contamination (1.2×10^{-2} $\mu g/cm^2$) were found for a similar type of reactor by Moeller[4] and are within the range of the supplier specifications.

References:

1. PRULOV, Y., STILLER, M. and FEIGE, Y., Israel AEC Report, IA-1077 (1966)
2. KRIEGER, H. L., PRULOV, Y., STILLER, M. and FEIGE, Y., Israel AEC Semi-Annual Report, July-Dec. 1963, IA-900, p.9
3. PRULOV, Y., STILLER, M. and FEIGE, Y., Israel AEC Report, IA-1021 July-Dec. 1964, p.2
4. MOELLER, D. W., ORNL 2311, (1957)

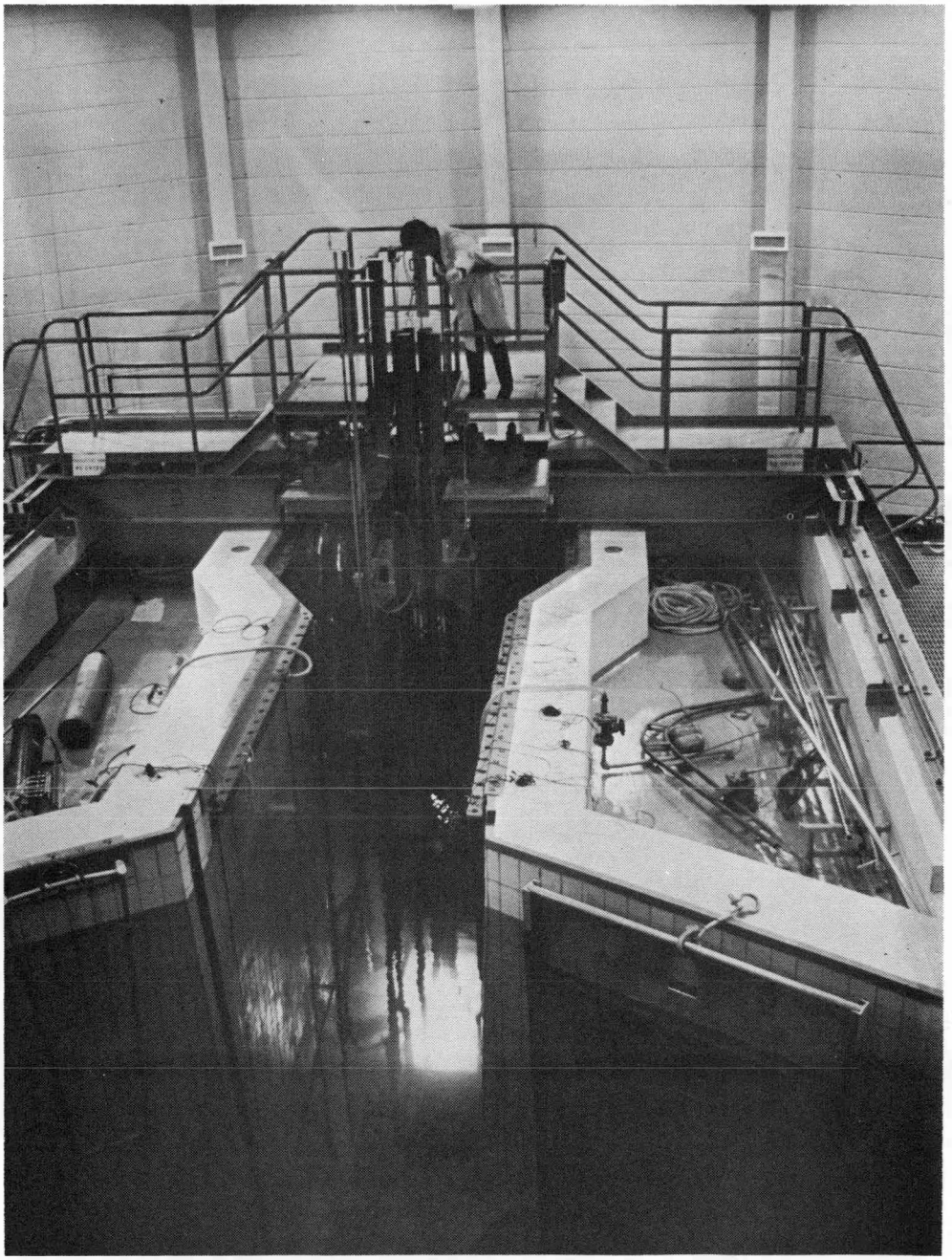

The IRR-1 swimming pool reactor showing the Cerenkov effect in the core

RADIOISOTOPE PRODUCTION

The isotopes delivered during 1965 are listed in Table 5, p.23. New products include high specific activity Cu^{64} and carrier-free K^{43}.

Progress has been made toward the production of beta and gamma standard calibration sources for energy calibration and as quantitative standards. It is hoped that these will soon be available for purchase from the Isotope Production Unit.

Production of Tc^{99m} : M. Boazi and E. Yellin

Carrier-free Tc^{99m} in the form of pertechnetate is used in medicine for diagnostic and therapeutic purposes. Its favourable characteristics are a 6-hour half-life, the clean 140 keV gamma ray and the absence of primary particle radiation. At the request of many physicians, this compound is now being prepared routinely.

Tc^{99m} is obtained from its longer-lived parent, Mo^{99} ($T_{\frac{1}{2}}$ = 66 h), which in turn can be obtained either by fission[1] or by neutron activation of Mo^{98} [2]. The molybdate is adsorbed on alumina, from which the daughter is eluted with dilute acid. Further purification and neutralization are accomplished by passing the solution through a cation exchange column.

The activity of the Tc^{99m} solution is calibrated in comparison with a Co^{57} standard, which has a gamma ray of 0.122 MeV with approximately the same abundance as the 0.140 MeV gamma belonging to Tc^{99m}.

References:

1. HARPER, P.V., LATHROP, K.A., JIMINEZ, F., FINK, R. and GOTTSCHALK, A., Radiology, 85, 101 (1965)
2. MURANO, R. and NELP, W.B., J. Nucl. Medicine, 6, 610 (1965)

Preparation of Neohydrin-Hg^{197} : M. Boazi

The synthesis of Hg^{197}-labelled neohydrin for the scanning of brain and kidney tumours has already been described(1).

In the production of Hg^{197} the major contaminant is 47 d Hg^{203} which is produced through the reaction Hg^{202} $(n,\gamma)Hg^{203}$. The optimum conditions for obtaining a high yield of Hg^{197}, with a relatively low concentration of Hg^{203}, are short irradiation at high neutron flux. The product should be used as soon as possible after irradiation. The concentration of Hg^{203} is determined by measuring its 0.279 MeV gamma peak using a 3" x 3" NaI scintillation detector.

The activity of the Hg^{197} is calibrated by scintillation counting of its 0.077 MeV gamma peak using Am^{241} as a standard, or by 4π gamma counting.

Reference:

1. BOAZI, M., Israel AEC Semi-Annual Report, July-Dec. 1964, IA-1021, p.7

Carrier-Free S^{35}: H. L. Finston* and M. Boazi

The preparation of carrier-free S^{35} by irradiation of organo-sulphur compounds has been investigated. The compounds were irradiated in a neutron flux of 2.5 x 10^{13} n/cm^2.sec, dissolved in a suitable solvent and extracted with water. The compounds irradiated were CS_2, $S-[(CH_2)_4-CO_2H]_2$,

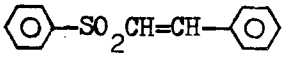

and

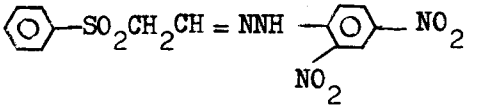

No appreciable S^{35} activity was detected in the aqueous or organic solutions.

---

* Israel AEC Fellow. Permanent address: N.Y. City University, Brooklyn College, N.Y.

Production of Colloidal Au^{198}: M. Boazi and T. Sonnino

The laboratory scale procedure described previously[1] for the production of colloidal Au^{198} for medical purposes has been adapted for full scale production.

Metallic gold is dissolved in aqua regia, the excess acid evaporated, and the resulting crystals dissolved in water. This solution is made alkaline and added slowly with stirring to a warm aqueous solution of gelatin containing traces of a "germ" solution of colloidal gold. Finally the solution is refluxed for three hours and sterilized at 121°C.

The problem of gelation, which may arise during the addition of the $HAuCl_4$ solution to the gelatin, preventing uniform particle formation, is overcome in the above procedure by the prolonged refluxing which dissolves the gel.

The product obtained meets the medical requirements regarding ionic content and particle size:

1. The maximum permissible ionic concentration is 5%, since ionic gold enters the bloodstream giving a high background which masks any concentration of the colloidal gold in specific organs. In our product the refluxing and sterilization stages reduce the ionic content to less than 3%, as checked by paper chromatography.

2. The optimum particle size for maximum concentration in the organs is 200-400 Å. Smaller particles are absorbed in the bloodstream. The particle size is controlled by the relative amounts of "germ" and $HAuCl_4$ used in the reaction. The size is checked with an electron microscope.

Reference:

1. EDGÜER, E. and ABRASHKIN, S., Israel AEC Jan-June 1964, IA-984 p. 11

TABLE 5

Production of radioisotopes - 1965

ISOTOPE	NO. OF ORDERS	ACTIVITY (mCi)	VALUE (IL)	CUSTOMER *														TYPE OF PROCUDTION **				
				BH	BIU	HH	HMS	HTA	HU	NH	RH	SNRC	T	TH	VI	WI	OTHERS	CI	SI	S	SR	P
ANTIMONY-124	2	0.02	158														2			2		
ARGON-41	9	15	232												9			9				
ARSENIC-76	1	0.01	39														1			1		
BISMUTH-210m	1	0.01	39														1			1		
BROMINE-82	7	22	248	4								1				2				7		
CERIUM-141	1	0.5	61																			
CERIUM-143	33	9.75	2014						33									33				
CERIUM-134m	1	1	61						1									1				
CHLORINE-38	3	6	219											3						3		
CHROMIUM-51	3	1445	510									1				1	1			3		
COBALT-60	12	163.23	1805		1				1			3			4		3			1	4	7
COPPER-64	1	0.003	39														1			1		
DYSPROSIUM-159	1	0.05	43									1						1				
EUROPIUM-152m	2	1	82									1					1	1		1		
GADOLINIUM-159	10	217	979						10									10				
GALLIUM-72	9	0.225	537									9						1	8			
GOLD-198	41	3632.7	2294.40	7				3	3	4	3	11		10				1	3	7	3	27
GOLD-199	2	0.015	122													2		2				
HAFNIUM-181	2	2	82						2									2				
HOLMIUM-166	1	0.010	39														1			1		
IRIDIUM-192	1	2.7	65	1															1			
IRON-59	4	2.042	328										1				3	1		3		
LANTHANUM-140	18	390	1186						15			3						15	1	2		
MERCURY-197	2	17	136											2								2
MERCURY-203	3	12.212	311											2			1			1		2
NICKEL-63	1	-	250													1					1	
OSMIUM-193	33	70	2444						32								1	32		1		
PHOSPHORUS-32	2	0.03	136		2																	2
POTASSIUM-42	30	37.83	2073	16					6							7	1			30		
POTASSIUM-43	2	0.05	210													2						2
PRASEODYMIUM-142	1	0.003	39														1			1		
RHENIUM-186	7	29	476									7								7		
RUBIDIUM-86	3	0.645	146												2		1			3		
RUTHENIUM-103	1	0.01	68														1			1		
SAMARIUM-183	1	1	61						1									1				
SCANDIUM-46	1	0.01	39														1			1		
SILVER-110m	2	0.01	122									2						2				
SODIUM-24	31	146.7	1774	19			4					1		6			1			31		
SULPHUR-35	5	357	1197	2								3							1			5
TANTALUM-182	1	4	68	1																		
TELLURIUM-131m	2	6	136						2									2				
TERBIUM-161	11	36.27	2220						10								1	10		1		
THULLIUM-170	3	2.68	172									2					1	1		2		
TUNGSTEN-187	1	0.01	43										1					1				
YTRIUM-90	23	499.5	1456	16		6						1						22		1		
ZINC-65	2	0.02	216									1					1			2		
ZIRCONIUM-97	1	0.003	39														1			1		
CUSTOM IRRADIATIONS	5		1003									3	2					5				
TOTALS	339	7130.238	26017.40	66	3	6	4	3	116	4	3	50	4	23	15	15	27	153	14	117	8	47

* BH = Beilinson Hospital, Petah Tikva.
BIU = Bar Ilan University, Ramat Gan.
HH = Hadassah Medical Org., Jerusalem.
HMS = Hadassah Medical School, Jerusalem.
HTA = Municipal Hospital "Hadassah", Tel Aviv.
HU = Hebrew University, Jerusalem.
NH = Negev Central Hospital, Beersheba.
RH = Rambam Hospital, Haifa.
SNRC = Soreq Nuclear Research Center, Yavne.
T = Technion, Haifa.
TH = Tel Hashomer Hospital, Tel Hashomer.
VI = Vulcani Inst. for Agricultural Research, Rehovot.
WI = Weizman Institute, Rehovot.

** CI = Custom irradiation (customer provides target)
SI = Service irradiation (center provides target)
S = Solution
SR = Source
P = Specially processed

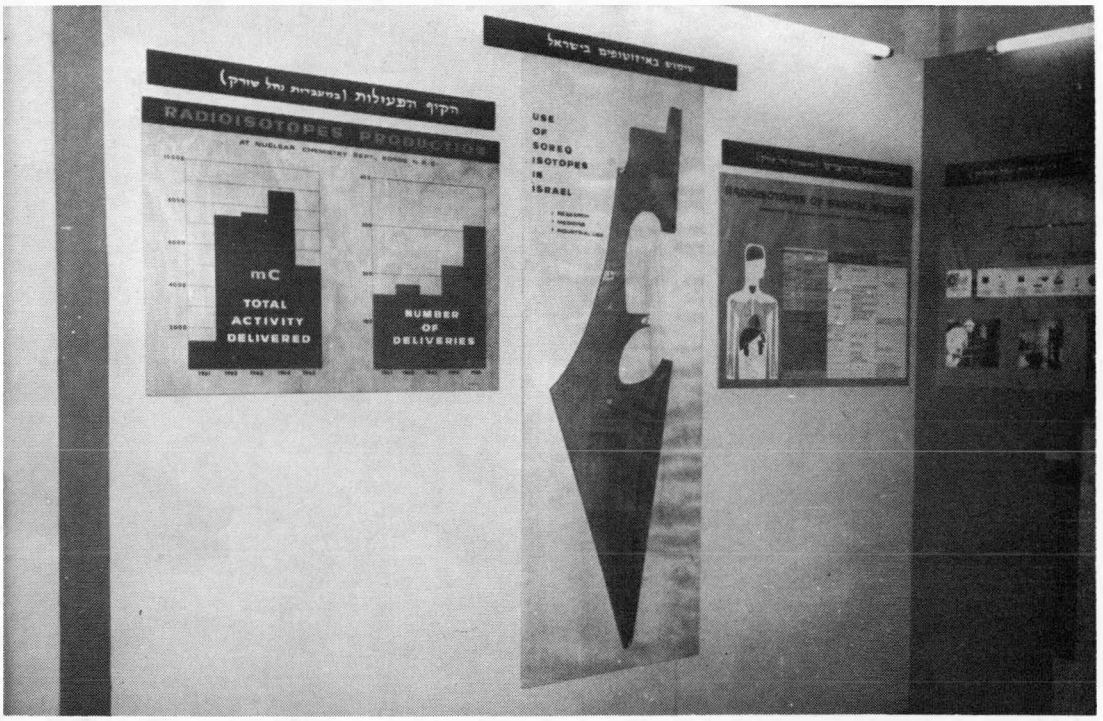

Radioisotope Production - Exhibit at the Second National Conference on Nuclear Medicine, Tel-Aviv, December 1965

RADIOISOTOPE TRAINING CENTER

Director: C. Braudo
Chemistry: B. Carmon
Nuclear Instrumentation: M. Kanter

Courses

During the year 1965 the following courses were held:

Course	Duration	No. of Participants
Laboratory Technicians	31.1.65 - 17.2.65	40
Physicians	21.3.65 - 29.3.65	23
Biologists and Agriculturists	16.5.65 - 17.6.65	11
Laboratory Technicians (University of Tel Aviv - High Grade Technicians School)	18.7.65 - 29.7.65	13

Lecture Demonstrations

Fortnightly lecture demonstrations for high school physics pupils were continued.

Research

Reports on the research undertaken by the Center appear in the appropriate sections. In connection with the salinity of Lake Kineret, experiments were performed on the tracing of the water flow from submerged radioactive springs (p.267). Other topics being studied are reverse transpiration in plants (p.218) and the catalytic effect of chloride on the thermal decomposition of perchlorates (p. 96).

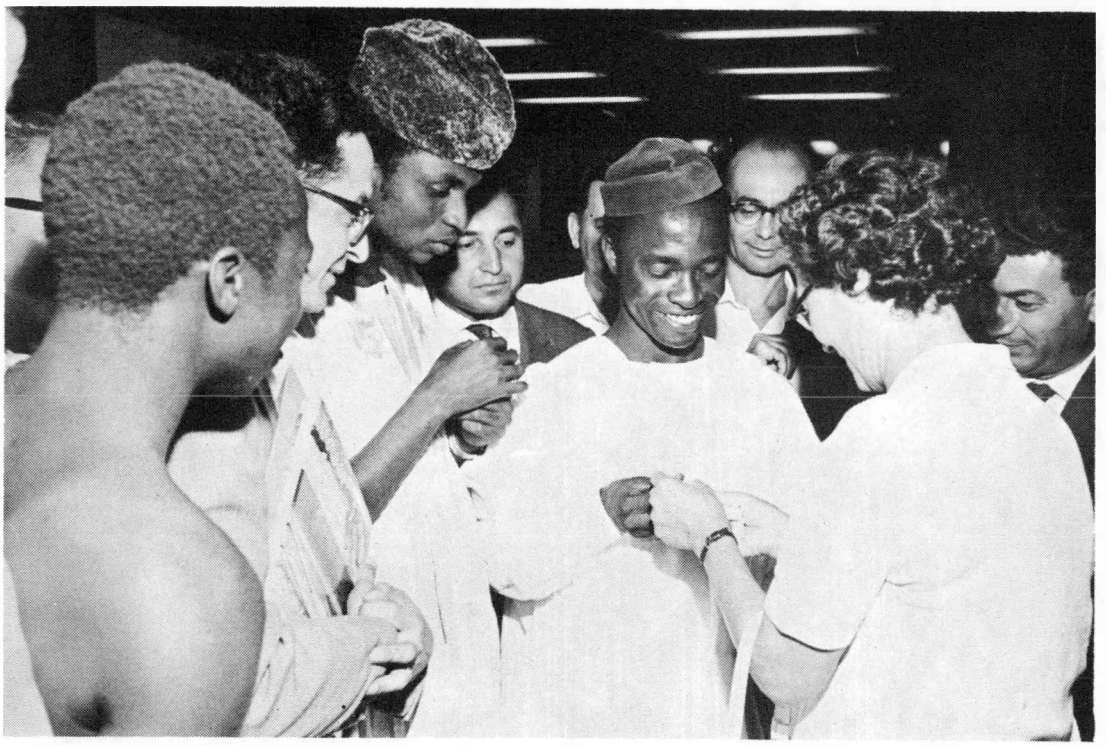

A friendly atmosphere reigns at the Radioisotope Training Center's International Course

PHYSICS

1. ELEMENTARY PARTICLE THEORY

Explicit Wave Functions for any Spin[1]: Y. Frishman* and E. Gotsman

A general method is given for calculating the exact form of the helicity amplitudes of a wave-function for any spin. Explicit expressions of the wave-functions for spin J = 1, 3/2, 2 and 5/2 are listed. Examples of helicity amplitudes for the production of $J = 3/2^+$ and $J = 5/2^+$ isobars in proton-proton scattering are computed.

Reference:

1. FRISHAMN, Y. and GOTSMAN, E., Phys. Rev. 140, B1151 (1965), and Israel AEC Report, IA-1040 (1965)

A Bootstrap Calculation for the Mass of the Intermediate Vector Boson[1]: E. Gotsman and D. Horn**

Assuming that the weak interactions are mediated by a neutral intermediate vector boson, W_o, a bootstrap type calculation is carried out to determine the mass of the particle (in the neutrino anti-neutrino channel). The requirement of self-consistency between input and output parameters leads to the result that the mass of the W_o is approximately one thousand times the proton mass.

Reference:

1. GOSTMAN, E. and HORN, D., Phys. Rev. Letters, 15, 714 (1965)

---

* Weizmann Institute of Science, Rehovoth
** Physics Department, Tel Aviv University

Tests of Relativistic SU(6) in Proton - Antiproton Annihilation : H. Harari and H. J. Lipkin*

The proton - antiproton annihilation at rest into two mesons is proposed as a critical test of the various relativistic generalisations of the SU(6) theory. It is shown that every relativistic extension of SU(6) in which mesons with finite momenta are still in the 35-dimensional representation of SU(6) leads to a ratio of 16 between the production rates of charged and neutral K mesons. This ratio is clearly in contradiction with experimental data, and symmetry breaking effects must be introduced in order to reconcile the theoretical predictions with experimental results.

Reference:
1. HARARI, H. and LIPKIN, H. J., Phys. Letters, 15, 286 (1965)

Γ_o Selection Rules in SU(12) Proton - Antiproton Annihilation : H. Harari H. J. Lipkin* and S. Meshkov**

The operators $\Gamma_{op'}$, $\Gamma_{on'}$, $\Gamma_{o\lambda'}$, are defined by the operation of the Dirac matrix γ_o on the SU(3) triplet of Dirac quarkspinors p', n', and λ' respectively. It is shown that these operators represent quantities conserved in SU(12), forbidding various processes. In particular, particles at rest are eigenstates of these operators. The annihilation,at rest,of the pp system into some multimeson final states is forbidden. The process $\bar{p}+p \rightarrow K^o + \bar{K}^o + \pi^+ + \pi^-$ is forbidden,while the processes :

---

* Weizmann Institute of Science, Rehovoth
** National Bureau of Standards, Washington, D.C.

$$\bar{p}+p \rightarrow K^{+} + K^{-} + \pi^{+} + \pi^{-}$$

$$\bar{p}+p \rightarrow K^{o} + K^{-} + \pi^{+} + \pi^{o}$$

$$\bar{p}+p \rightarrow \bar{K}^{o} + K^{-} + \pi^{-} + \pi^{o}$$

are allowed, at rest. At finite energies the cross sections of processes which are forbidden at rest are reduced by factors of v/c. At low velocities this may be detected experimentally.

Reference:

1. HARARI, H., LIPKIN, H. J. and MESHKOV, S., Phys. Rev. Letters, 14, 845 (1965)

Meson and Baryon Masses in SU(6) Symmetry[1]: H. Harari and H. J. Lipkin*

The question of deriving mass formulae for the baryon and meson supermultiplets in the SU(6) symmetry model is studied. It is shown that the experimental values of meson and baryon masses are in disagreement with the assumption that the mass splittings in both SU(6) supermultiplets are given by the expectation values of the operators having the same definite transformation properties under SU(6). It is further argued that simple tadpole-type symmetry breaking mechanisms tend to give a definite linear combination of SU(3) singlet and octet terms of the mass operator, which transforms like the 405 representation of SU(6). Hence such theories are not capable of explaining the mass spectrum of the low-lying mesons and baryons.

Reference:

1. HARARI, H. and LIPKIN, H. J., Phys. Rev. Letters, 14, 570 (1965)

* Weizmann Institute of Science, Rehovoth

Electromagnetic Interactions and the Subgroups of SU(6)[1,2]: H. Harari

Various sets of relations concerning the electromagnetic properties of the constituents of the SU(6) supermultiplets were recently derived by various authors. A systematic study of these relations is presented, using subgroups of SU(6) which are generalizations of the U-spin subgroup of SU(3). It is shown that two different assumptions on the transformation properties of the electromagnetic contributions to the particle masses are not in contradiction with present data.

References:

1. HARARI, H., Phys. Rev., 139, B1323 (1965)
2. HARARI, H., Israel AEC Report IA-1023 (1965)

Intrinsic Spin and U(12) Theory[1] : H. Harari

A complete classification of all the possible spin states of a system of any number of quarks and anti-quarks within the framework of U(12) is presented. A one-to-one correspondence is shown to exist between all finite irreducible representations of U(12) and the pair of numbers (N, J) where N is the total number of basic spinors in a system with a given total spin J. A set of Sp(4) selection rules which are valid in any U(12) invariant theory is derived.

Reference:

1. HARARI, H., Phys. Rev. Letters, 14, 1100 (1965)

Experimental Tests of Broken U(12) and Approximate U(6) × U(6)[1]:
H. Harari and H. J. Lipkin*

It is shown that predictions based on certain subgroups of U(12) remain valid both in broken U(12) (to all orders in kinetons and simple derivative coupling) and in the Dashen Gell-Mann non-chiral U(6) × U(6)

---

* Weizmann Institute of Science, Rehovoth

approximate symmetry. Examples are also given of new predictions which follow from the W-spin collinear subgroup.

Reference:

1. HARARI, H. and LIPKIN, H. J., Phys. Rev. (in press)

Algebraic Aspects of Regge Recurrences[1]: E. Gotsman and Y. Ne'eman*

The algebraic structure of Regge recurrences is examined and its relation to symmetry schemes underlying various models is established. The relationships between Spectrum Generating Algebras (S.G.A.) and the Regge non-compact sub-algebras are discussed for the Coulomb potential, the three-dimensional oscillator, the signature which appears in exchange potentials, as well as for the U(6,6) symmetry of hadron physics.

Reference:

1. GOTSMAN, E. and NE'EMAN, Y., Math. Phys. (in press)

Three-Particle Final States and Unitary Symmetry[1]: I.M. Bar-Nir* and H.Harari

A large number of new predictions of SU(3) are derived for processes with three outgoing particles. All the reactions treated involve scattering of charged particles on protons, with no more than one neutral particle in the final state. They can all be measured by the present experimental techniques. A detailed comparison between the available data and the predictions is presented. In a few cases, disagreement is found, but when we allow symmetry breaking contributions within the matrix elements which describe the processes the data are always consistent with the predictions. The general problem of comparing the predictions of a broken symmetry with scattering data is discussed and various possibilities for performing such comparisons are suggested.

Reference:

1. BAR-NIR, I. M. and HARARI, H., Phys. Rev. (in press)

---

* Physics Department, Tel Aviv University

2. REACTOR PHYSICS

One-Dimensional Multigroup Perturbation Codes : M. Lemanska and S. Yiftah

The PERTR[1,2] code was adapted to solve the material replacement problem for ZPR-III assemblies and for the fast, small, critical assemblies Jezebel, Godiva and Topsy. The results obtained for the central and non-central reactivity contributions of various samples were compared with the experimental values. In addition, the reactivity coefficients were computed and the results compared with the experimental data [3,4] and with the values computed by other investigators[5,6]. The dependence of the computed results on the interval division in the perturbing sample and on the change of the fluxes resulting from the presence of the sample were considered.

A comparison was made between the perturbation method and the direct method for treating the central reactivity contribution problem.

The PERDIF[1] code was adapted to compute the Doppler effect for large fast breeder power reactors. The results were compared with those given by the diffusion code.

References:

1. LEMANSKA, M., and YIFTAH, S., Israel AEC Semi-Annual Report Jan.-June 1964, IA-984, p. 34.
2. LEMANSKA, M. and YIFTAH, S., Israel AEC Semi-Annual Report July-Dec., IA-1021, p. 17.
3. LANG, J.K., LOEVENSTEIN, W.B., BRANYAN, L.E., BRUNSON, G.S., KIVU, F.S., OKRANT, D., RICE, R.E. and THALGOTT, F.W., Fast Neutron Power Reactor Studies with ZPR-III A/CONF.15/8/598, July 1958.
4. ENGLE, L.B., HANSEN, G.E. and PAXTON, H.C., Nucl. Sci. and Eng. 8, 543 (1960).
5. HANSEN, G.E. and MAIER, Cl., Nucl. Sci. and Eng. 8, 532 (1960).
6. DAVEY, W.G., A Comparison of Experimental and Calculated Prompt Neutron Lifetimes and Central Reactivity Coefficients in ZPR-III Assemblies and their Relationship to other Reactor Parameters. ANL-6682, June 1963.

Fundamentals of Fast Reactor Calculations : M. Segev and S. Yiftah

A complete group-diffusion theory was developed for the calculation of fast reactors. The main features are set out below.

a) The P_1 approximation for the Boltzman equation is formally, and without any physical assumptions, reduced to group equations and group cross sections.

b) The exact meaning of flux separation (into energy and spatial parts) for reactor calculations is elucidated.

c) It is shown that all (not only the transport) effective group-diffusion cross sections are higher (typically by 3-5%) than the corresponding effective group-physical ones.

d) Approximate formulae are derived for the intergroup transfer parameters in elastic scattering. These are simple to apply and for $A \geqslant 10$ yield values which are within 1% of the exact ones.

e) A theorem is proved which shows "Placek oscillations" in the collision density for elastic slowing-down in any moderator (excluding H) with any absorption and scattering laws.

f) The asymptotic slowing-down equation is expanded in "slowing-down" moments. This expansion describes various problems such as anisotropy of scattering and scattering in mixtures.

g) Simple analytical forms are derived for the solution of the slowing-down equation for typical homogeneous fast reactor mixtures. These solutions take into account the complicated nature of slowing-down such as the narrow and dense resonances of heavy elements; the resonances of structural elements and the mixtures of several elements.

h) The above analytical formulae for the flux were compared with a numerical solution of the slowing-down equation coded for the Philco-2000. The comparisons show a very good agreements between the results. A full report is being written.

Collision Density for Typical Fast Reactor Conditions : M. Segev and S. Yiftah

A search for analytical solutions of the slowing-down equation under fast reactor conditions was motivated by the following considerations.

a) In calculating effective cross sections, a constant collision density is assumed. Disregarding absorption this assumption is valid for heavy isotope resonances which are mostly narrow resonances (N.R.). The flux decay towards lower energies, caused by absorption, is to a certain extent taken into account by averaging the effective cross sections over some gross behaviour of the flux between the group limits. However such a fixed behaviour cannot account for changes in the rate of decay due to changes in the relative amount of absorbers.

b) Neither narrow resonance (N.R.) nor wide resonance (W.R.) techniques apply to resonances of the lighter elements such as Fe, Na, O, C. The Elmoe Code finds the flux in such cases by iterations, through hundreds of groups. It is an involved technique since any change in the relative amount of the light elements calls for a recalculation of the flux and hence of the "coarse" (i.e. usual) group cross sections. Also the lack of an explicit relation between the amount of light elements and the flux is a disadvantage.

c) An analytical knowledge of the collision density in a fast reactor will enable one to calculate group cross sections for wider, and hence less, groups than usual, thus reducing the time for a criticality computation. This is particularly important for two-dimensional calculations.

A later report will describe in detail the steps leading to an approximate and simple analytical solution of the slowing-down equation under fast reactor conditions. This solution depends explicitly on the relative amounts of each isotope in the mixture, on the isotope masses and on the energy-dependent cross sections. It does not depend on anything else; in particular, no iterations are involved. It thus describes in an analytic way the flux decay caused by absorption and the flux depressions under light-element resonances.

It is found that, in the energy range of fast reactors and for typical mixtures, the collision density under a scattering resonance of a heavy isotope is quite constant. Under a symmetrical resonance of a light or structural element it is depressed in an asymmetrical way. Such asymmetries were found and estimated in an iterative way by Goldstein[1] for intermediate resonances (I.R.).

For the sake of comparison and checking, a numerical solution to the slowing-down equation was coded for the Philco-2000 and run for several typical mixtures. The analytic solution was found to give a good estimate of the flux and a very good estimate of effective cross sections.

Reference:

1. GOLDSTEIN, R., Nucl. Sci. and Eng. 19, 359 (1964)

Sodium Void and Doppler Effects in Large Fast Power Reactors[1]: S. Yiftah, L. Gitter and Y. Ilamed

Calculations were made in order to study the sodium void and Doppler effects in a series of fast reactors which differ in core volume, isotopic content (type) of Pu fuel, and chemical composition of fuel (metal, oxide, carbide). The sodium void and Doppler effects were obtained from criticality factors computed for 486 spherical systems. Details of the computations and results are given in ref.1. Since the calculations were undertaken in connection with parametric studies, the computational results were analysed to find analytical expressions useful for these studies. The following conclusions were drawn.

For a given reactor the sodium void effect at normal temperature, as a function of sodium leakage, is described to a good approximation by a parabola with negative curvature. Three criticality factor calculations are enough to obtain the parameters of the parabola.

For a particular composition and type of fuel, the parameters of the parabola are functions of the core volume. Using the parameters obtained, the sodium void effect for any volume can be calculated by interpolation.

The sodium void effect for any initial sodium content can be calculated as a simple difference, if the sodium void effect vs. leakage is known for one initial sodium content. For any given leakage the effect is more negative for lower initial sodium content.

The concept of "stationary volume" can be defined as the volume for which any change in sodium density (leakage or addition of sodium) will have a negative effect on the reactivity of the reactor. The stationary volume for any initial sodium content can be read directly from the graph of X_m (the leakage for which the sodium void effect is maximal) vs. volume, as obtained for one initial sodium content. Stationary volumes increase with decrease of initial sodium content.

For any given assembly at any temperature the sodium void effect becomes more positive as the volume increases. The stationary volume is the maximal volume for which the sodium void effect is non-positive at any leakage at normal temperature. For any leakage the negative Doppler effect increases with volume. For a given volume the Doppler effect does not change much with sodium leakage.

With respect to composition of fuel it appears that the oxide fuels have the most negative sodium void effect and consequently the largest stationary volumes. For large volumes with a given sodium content the Doppler effect is also most negative for oxide assemblies.

With respect to fuel type, the presence of greater amounts of the higher isotopes causes a more negative sodium void effect and thus the corresponding stationary volume is larger. The presence of higher isotopes also causes a more negative Doppler effect for any particular sodium content.

Thus oxide assemblies allow for the largest reactors with combined non-positive reactivity effects, and the change in the isotopic composition of the fuel occurring during operation will not affect this safety characteristic of the reactor unfavourably.

Reference:

1. YIFTAH, S., GITTER, L. and ILAMED, Y., Israel AEC Report, IA-1057, (1965)

Effect of Changes in Cross Section Increments on the Total Doppler Effect in Fast Reactors : S. Yiftah, L. Gitter and Y. Ilamed

We recently calculated the Doppler effect in large fast reactors[1]. The cross section increments which enter into these calculations are affected by many complex factors, and it is possible that some of these may have been inadequately taken into account.

In order to obtain a better understanding of the dependence of the change in criticality factor, $\Delta c/c$, on the increments of the cross sections, $\Delta\sigma$, criticality changes were computed for a number of systems, with several different reasonable sets of $\Delta\sigma$ for each system. The various sets of $\Delta\sigma$ were computed by Dr. G. Shaviv by simplified Doppler calculations, taking into account effects that had previously been neglected. Computations were also carried out for increments equal to half the given increments $\Delta\sigma$; in addition the Doppler effect for each energy group ("local" effects) were calculated.

The following conclusions seem to be warranted from inspection of the computed reactivities and flux integrals of the systems:

(i) In general, in the range of variation of $\Delta\sigma$ considered, i.e. for "small" $\Delta\sigma$ $(\Delta\sigma \ll \sigma)$, the Doppler coefficient is additive in $\Delta\sigma$:

$$\frac{\Delta c}{c}\left(\Delta_1\sigma_f+\Delta_2\sigma_f,\ \Delta_1\sigma_a+\Delta_2\sigma_a\right) = \frac{\Delta c}{c}\left(\Delta_1\sigma_f,\ \Delta_1\sigma_a\right) + \frac{\Delta c}{c}\left(\Delta_2\sigma_f,\ \Delta_2\sigma_a\right)$$

For increasing $\Delta\sigma$ the Doppler coefficient becomes subadditive:

$$\frac{\Delta c}{c}(\Delta_1\sigma_f+\Delta_2\sigma_f,\ \Delta_1\sigma_a+\Delta_2\sigma_a) < \frac{\Delta c}{c}(\Delta_1\sigma_f,\ \Delta_1\sigma_a) + \frac{\Delta c}{c}(\Delta_2\sigma_f,\ \Delta_2\sigma_a)$$

(ii) The contribution to the Doppler effect from neutrons of the lowest energy groups is small in metal assemblies, and high in carbide and oxide assemblies, the contribution being higher in oxide than in carbide assemblies. This is apparently due to the difference in the flux distribution. In metal assemblies there is a relatively small flux in the lowest energy group where the increase in cross section is relatively high, while in carbide and oxide systems there is a marked shift toward lower energies.

(iii) The contribution to the Doppler effect from the lowest energy group decreases with the sodium leakage. This again seems to be due to the shift of the spectrum of the flux towards higher energies with the leakage of sodium.

A detailed report with tables of the computed results is in preparation.

References:

1. YIFTAH, S., GITTER, L. and ILAMED, Y., Israel AEC Report IA-1057 (1965)

Results of Doppler Coefficient Calculations for Fast Reactors and Comparison of Different Methods*(1) : Part I by R. Froelich** and K. Ott **, Part II by G. Shaviv and S. Yiftah

Doppler coefficients of dilute fast reactors were calculated by the successive k method and by perturbation theory. The results obtained by the two methods were compared and discussed in detail over the temperature range

---

* This work was supported in part by the Kernforschungszentrum Karlsruhe - Euratom Association on Fast Reactors

** Kernforschungszentrum Karlsruhe

of interest. The Doppler coefficient during excursions was treated by taking into account the space distribution of the additional energy release and the dynamic spectra for reasonable asymptotic periods.

Reference:

1. FROELICH, R., OTT, K., SHAVIV, G. and YIFTAH, S., Paper Presented at International Conference on Safety, Fuels and Core Design in Large Fast Power Reactors, Argonne, October 11-13, 1965

Effect of Pu Isotopic Composition on the Doppler Coefficient in Fast Reactors : G. Shaviv and S. Yiftah

The effect of the plutonium isotopic composition on the Doppler coefficient was examined in fast reactors having different chemical compositions of the fuel and different core volumes. It was found that for a given core volume and chemical composition the absolute value of the Doppler coefficient increases with increase in the amount of high plutonium isotopes (Pu^{240}, Pu^{241} and Pu^{242}).

Monte Carlo Investigation of the Heterogeneity of Fast Reactor Cores : G. Shaviv and S. Yiftah

In a reactor the effective cross section for a reaction over a given energy group is usually defined as that value which when multiplied by the group flux gives the reaction rate in the group under consideration. Thus for the energy group between E_g and E_{g+1}

$$\tilde{\mu}_x = \frac{\int_{E_g}^{E_{g+1}} \phi \mu_x dE}{\int_{E_g}^{E_{g+1}} \phi dE} \qquad (1)$$

Eq. (1) can be written in the form

$$\tilde{\mu}_x = \frac{\int_{E_g}^{E_{g+1}} \frac{F\mu_x}{\mu_t}\, dE}{\int_{E_g}^{E_{g+1}} \frac{F}{\mu_t}\, dE} \qquad (2)$$

Using eq. (2) effective cross sections were calculated by means of a Monte Carlo code adapted from the NYU program which calculates resonance capture in thermal reactors[1]. This method is based on the fact that the collisions recorded in a Monte Carlo history in an element R of phase space (volume, energy, direction) give an estimate of the collision density integrated over R. Consequently, appropriate summations of (μ_x / μ_t) and $(1/\mu_t)$ at these collisions provide estimates of the reaction rates and the integrated flux over R, which are the terms required to evaluate equation (2).

The Monte Carlo results for a typical fast reactor lattice confirm the fact that core heterogeneity has only a slight influence on the effective group cross sections in fast reactors. In the calculations a number of effects which are normally ignored in analytical studies of this problem were included. The statistical inaccuracies inherent in the Monte Carlo method are small enough not to invalidate the general conclusions reached.

Reference:

1. RICHTMYER, R. D., VAN-NORTON, R. and WOLFE, A., The Monte Carlo Calculation of Resonance Capture in Reactor Lattices, Proc. 2nd UN Conf. Geneva 16, 180 (1958)

Monte Carlo Investigation of the Interaction between the Resonances of Fertile and Fissile Isotopes in Fast Reactor Cores : G. Shaviv and S. Yiftah

The problem of the interaction between the resonances of the fertile and fissile isotopes in fast reactor cores and its influence on the effective and group effective cross sections has been treated analytically by various

authors[1,2]. In all analytic methods the simplifying assumption is made that the total collision density is constant. This assumption is generally a good approximation for a single resonance which is narrow compared with the energy degradation occurring in the collisions of a neutron with the atoms of the medium. However fluctuations in the total collision density may arise due to interaction between resonance sequences belonging to different isotopes. The aim of this work was to see whether these fluctuations have any effect on the interaction between the resonances of the fertile and fissile isotopes in fast reactors.

The effective cross sections were calculated by the Monte Carlo method, in which it is not necessary to assume that the total collision density is constant over the resonance. Table 6 summarizes the results obtained for the effective cross section of Pu at two energies and two temperatures. It can be seen that the effect of the resonances of U^{238} on those of Pu^{239} is to reduce the effective absorption and fission cross sections by a few per cent. The results are in good general agreement with those obtained by Codd and Collins[1] who used different conditions and energies. This shows that the assumption of constant collision density is adequate for the situation discussed here.

TABLE 6

Effect of the interaction between the U^{238} and Pu^{239} resonances on the effective cross section of Pu^{239}

E (keV)	T (°K)	Effective cross section for fission (Fermi)		Effective cross section for absorption (Fermi)	
		without U^{238} resonances	with U^{238} resonances	without U^{238} resonances	with U^{238} resonances
4-5	300	2.179±0.0034	2.043±0.0029	1.216±0.0017	1.167±0.0015
	1500	2.241±0.0028	2.087±0.0031	1.247±0.0014	1.197±0.0015
9-10	300	2.291±0.0034	2.036±0.0037	0.7792±0.0017	0.7658±0.0016
	1500	2.327±0.0030	2.054±0.0032	0.7868±0.0015	0.7711±0.0016

The large errors inherent in the Monte Carlo method prevent any definite conclusions with regard to the temperature variation of the effect studied. An investigation of the temperature effect must await the compilation of a Monte Carlo code aimed specifically at the study of temperature variations.

References:

1. CODD, J. and COLLINS, P.J., Some Calculations Concerning the Influence of Resonance Overlapping on the Doppler Effect in a Dilute Fast Reactor, Proc. of the Conf. on Breeding, Economics and Safety in Large Fast Power Reactors, Oct. 7-10, 1963, ANL-6792.

2. HWANG, R.N., An Improved Method of Doppler Effect Calculation for Fissile Materials in the Intermediate Energy Region, ibid.

3. NUCLEAR PHYSICS

During the past year three new experiments have been installed in Beam Tube 1 of the IRR-1 reactor. Two of them - capture gamma ray spectroscopy, and Mössbauer studies with capture gamma rays - use the newly completed external neutron beam (see p. 312). The third experiment utilises a radioactive gas loop, the gas being irradiated at the core face, for fluorescence gamma scattering experiments. Mössbauer studies during the year have been centered on the use of I^{129} to investigate the structure of molecular crystals, and on the study of phase transitions in ferro-electric materials. The Mössbauer source, 70 min Te^{129}, is prepared in the reactor. The range of the low temperature Mössbauer experiments has recently been extended by acquiring a Cryo-Tip open cycle Joule-Thompson cryostat, using commercial hydrogen.

Resonant Scattering: G. Ben-David, B. Arad, Y. Schlesinger

(I) Resonant Scattering from Highly Excited Nuclear Levels

The fifty resonance levels so far discovered were re-examined, and the effective cross sections evaluated more precisely, making use of improved stability of the electronic equipment, and more accurate methods of calculation. The results have been submitted for publication[1]. It may be possible to achieve a large increase in the number of measurable resonances by increasing the flux of gammas and using detectors of higher resolution. A brief summary of the results was presented at the Antwerp conference on nuclear structure[2].

(II) Measurement of the 7.64 MeV Level in Tl by Self-Absorption Technique

The strong resonance observed for the 7.64 MeV level in Tl permitted measurement of the level width using the self-absorption method. For a target thickness of 3.81 g/cm^2, and resonant and non-resonant absorber thicknesses of 14.85 g/cm^2 each, the self-absorption coefficient was re-measured and a value of 0.17 $\pm$ 0.2 obtained. Making use of the known temperature dependence of the resonance, and the measured effective cross section, the level width was estimated assuming the Doppler approximation for the cross section. A value of $\Gamma/\alpha g \cong 0.6$ eV was obtained, where α is the natural abundance of the resonant isotope and g the ratio of the spins of the excited and ground states. Accurate computation of the cross section requires the use of a computer programme, which has just been completed (see next paragraph).

(III) Evaluation of the Doppler Integral $\psi(x,t)$ using Computer Methods

Accurate analysis and interpretation of experimental resonant scattering data requires calculation of the Doppler integral in a very broad region of the parameters (x,t). The existing compilation of this function[3] does not cover the whole region required. In addition, the Doppler and Lorentzian approximations used in the calculations can cause large errors if not applied strictly in the appropriate regions of x and t. It was found possible to calculate the integral using a particularly simple numerical procedure, to an accuracy as high as 1 in 10^8, which is far better than the accuracy of any previous compilation in the required range of parameters. The sub-routine PSI (x,t) is now being used for general analysis of the experimental data, and will be described in an IA-report. In Table 7 the values obtained for the ψ-function are compared with those given in the published tabulations.

TABLE 7

Comparison of values of the ψ-function from different tabulations

β	Ref.	X				
		0.0	0.1	1.0	10.0	100.0
10^{-3}	C	1.000000	.990099	.500000	.009901	.000010
	D	.9999987	.99009853	.50000012	.009900990	.000009999
1.0	A	.75783054	.75510317	.5401622	.01004972	
	B	.75957	.75684	.54082	.010049	
	C	.757872	.755143	.540145	.010050	.000100
	D	.75787296	.75514314	.54014446	.01004971	.00010000499
10^{2}	A	.017527		.017525	.017354	.006524
	C	.017526	.017526	.017525	.017354	.006535
	D	.0175263108	.01752629	.0175245	.0173548	.00653508
10^{4}	D	.00017722551	.0001772255	.0001772255	.00017722533	.00017720779

A - Rose, Miranker, Leak, Rosenthal and Henriekson. WAPD.SR.506 Vol. I and II (1954).

B - Seth and Tabony. TID.21304 (1964).

C - Dandeu, Gautier, Guillerniu, Olivie and Roche. CEA.R2824 (1965).

D - Present work.

(IV) Coincidence Measurement of the 7.53 MeV Level in Tellurium

The complex scattered spectrum found in the scattering of Ni capture gamma rays from a Te scatterer has been examined by a coincidence technique, in an attempt to identify the inelastic scattering components. Both a two-dimensional pulse height analyser and a one-dimensional multichannel analyser gated by the sum-coincidence pulse were used. The preliminary results are in agreement with the assumption that inelastic scattering gives rise to the 6.7 MeV and 5.8 MeV components. A further

study of this resonance, using lithium drifted germanium detectors, will be performed to establish finally the inelastic energy levels and isotopes responsible for the resonance.

References:

1. BEN-DAVID, G., ARAD, B., BALDERMAN, J. and SCHLESINGER, Y., Israel AEC Report IA-1050 (1965) and Phys. Review, April 1966, (in press).
2. BEN-DAVID, G., ARAD, B., BALDERMAN, J. and SCHLESINGER, Y., Intern. Conf. on the Study of Nuclear Structure with Neutrons, Antwerp, Belgium, July 1965.
3. DANDEU, Y., OLIVIE, G. and ROCHE, F., Table de L'integrale $\psi(\beta,x)$, Rapport No. 43 bis, Section Aut. de Calcul Electr.

Measurement of the Mean Life of the First and Second Excited States in Na^{23}:

R. Moreh and J. Balderman

An experimental set-up is now ready for the measurement of the lifetime of the first (0.44 MeV) and second (2.07 MeV) excited states of Na^{23}, using the resonance fluorescence technique. The levels of Na^{23} are populated by Ne^{23}, which is obtained from the $Ne^{22}(n,\gamma)$ reaction by irradiating spectroscopically pure neon in the IRR-1 reactor.

The thermal neutron flux around the activation chamber is $\sim 10^{13} n/cm^2 sec$. To obtain an equilibrium Ne^{23} source, the gas is circulated through a loop by means of an ordinary rotary pump, the oil contamination being removed using a liquid air trap containing glass wool. The cylindrical copper source container (diameter 40 mm, length 60 mm, wall thickness 1.5 mm) is placed inside a large perspex chamber surrounded by a shielding installation to reduce the high background of γ-rays. The sodium scatterer was prepared by melting the metal under paraffin oil, then cooling it and pressing the solid sodium into the appropriate shape under oil and covering it with 0.3 mm PVC foil.

The positions of several energy levels in O^{18} and O^{19} were established, and the angular distribution of proton groups leading to several levels in O^{17}, O^{18} and O^{19} were measured.

The experimental results were analysed using the Bulter-Born theory and an estimate was obtained of the amplitudes of the simple shell model configuration and deformed states in several levels of O^{18}. The results compare fairly well with recent theoretical estimates by Federman and Talmi[5].

(III) Gamma Transitions in O^{18} *

The levels at 5.25 and 5.37 MeV in O^{18} have been investigated using the $O^{17}(d,p\gamma)O^{18}$ reaction. The 5.25 MeV level was found to decay 41 ± 6% to the 1.98 MeV level and 59 ± 6% to the ground state. The 5.37 MeV level was found to decay 89 ± 3% to the 1.98 MeV level and 11 ± 3% to the 3.92 MeV level, with an upper limit of 3% and 2% to the 3.55 MeV and ground state respectively. The results are in agreement with the assignment of 2^+ to the 5.25 MeV level and 3^+ to the 5.37 MeV level.

References:

1. MOREH, R., Nucl. Phys. 70, 293 (1965).
2. MOREH, R. and DANIELS, T., Nucl. Phys., 74, 403 (1965).
3. JAFFE, A.A., et. al , Proc. Phys. Soc. 76, 914 (1960)
4. MIDDLETON, R. and PULLEN, D.J., Nucl. Phys. 51, 50 (1964)
5. FEDERMAN, P. and TALMI, I., Phys. Letters 15, 165 (1965)

Mössbauer Studies of Various Ferrite Structures: T. Rothem and D. Kedem

A Mössbauer spectrometer of good resolution and linearity has been built. Its saw-tooth drive is provided by the Intertechnique 400 channel analyser.

The resolution is 0.2 mm/sec, as measured with a thin absorber of natural Fe.

---

* The experimental work was carried out at the University of Manchester.

The comparison scatterer was made by filling a ring-shaped aluminium container with the appropriate weight of MgO, matched for both Compton scattering and pair production to give the same effect as the sodium scatterer.

Energy Levels of Oxygen Isotopes: R. Moreh

(I) Study of the (t,p) Reaction on O^{16}, O^{17} and O^{18} using 5.55 MeV Tritons*[1,2]

The (t,p) reaction on O^{16}, O^{17} and O^{18} was studied at a triton bombarding energy of 5.55 MeV. Special attention was given to the reaction $O^{17}(t,p)O^{19}$. The position of several energy levels in O^{19} was established. Good agreement was obtained in some cases between the measured proton angular distributions and the predictions of the plane wave double stripping theory. In other cases the contribution of other reaction modes seems to be appreciable.

The spin and parity of the ground and 3.153 MeV levels in O^{19} obtained by the $O^{17}(t,p)$ reaction were determined unambiguously to be $5/2^+$, arising from the $d^3_{5/2}$ and $d_{5/2}s^2_{1/2}$ configurations respectively. The 0.093 and 2.775 MeV levels were identified with the $3/2^+$ and $9/2^+$ levels respectively of the $d^3_{5/2}$ configuration.

The results for the $O^{16}(t,p)O^{18}$ reaction agreed with those of Jaffe et al.[3]., who used tritons of 5.50 MeV. In the $O^{18}(t,p)O^{20}$ reaction the spin and parity assignments for the ground and first three excited levels of O^{20} were in essential agreement with those of Middleton et al.[4] who used tritons of 10 MeV.

(II) The Level Structure of O^{18} and O^{19} by Stripping Reactions*

The (d,p) reactions on O^{16}, O^{17} and O^{18} were investigated at a deuteron energy of 5.56 MeV, with a view to studying the O^{18} energy levels.

The Q values of the ground state transitions in the reactions $O^{17}(d,p)O^{18}$ and $O^{18}(d,p)O^{19}$ were determined to be 5.820 ± 0.010 and 1.734 ± 0.010 MeV respectively.

---

* The experimental work was carried out at the University of Manchester.

Mössbauer Effect in Molecular Iodine Crystals[1] : M. Pasternak, A. Simopoulos*, Y. Hazony

The Mössbauer effect of the 27.7 keV transition in I^{129} has been studied in molecular iodine crystals. From the quadrupole splitting of the transitions (see Fig.8) the ratio $Q_{26.8}/Q_{gnd}$, the quadrupole coupling $e^2q\,Q_{gnd}$, and the isomer shift were determined. The sign of the quadrupole coupling shows that the sign of the iodine field gradient is positive. From the isomer shift of I_2 and from those of alkali iodides, a linear dependence of the isomer shift on the number of p-holes was derived. The intensities of the peaks give a strong indication of an angular dependence of the recoilless fraction $f(\theta)$. The θ_D of the I_2 crystal, as well as that of the KI crystal, was derived from the temperature dependence of the recoilless fraction.

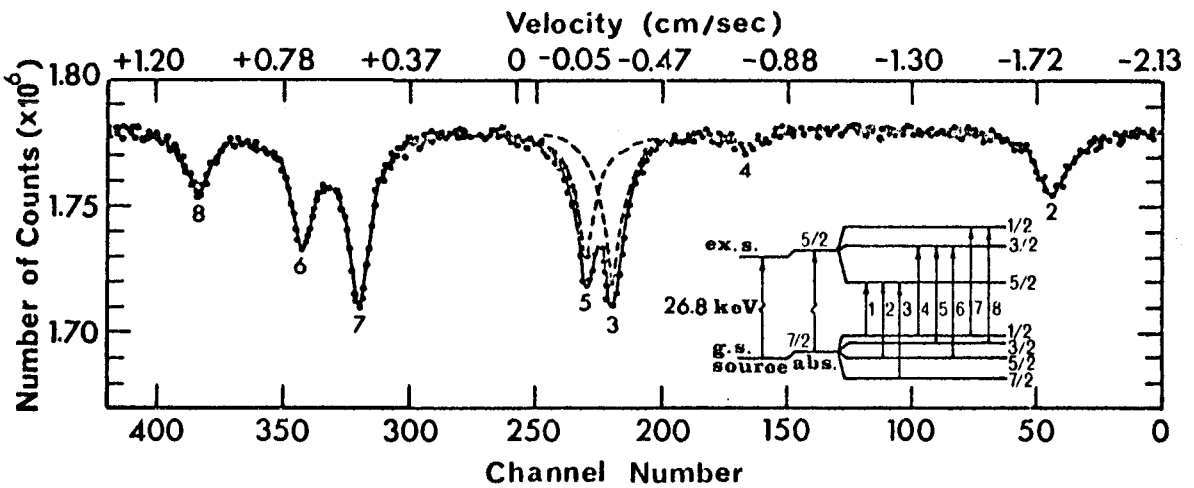

Fig. 8

Quadrupole splitting of I_2 (molecular iodine crystal), measured with a Zn^{66}-Te^{129} source. Both source and absorber were at liquid nitrogen temperature

Reference :

1. PASTERNAK, M., SIMOPOULOS, A., HAZONY, Y., Phys. Rev., 140 6A 1892, (1965)

* IAEA fellow, on leave from the Nuclear Research Center "Democritos", Athens, Greece

Measurements have been performed on ferrite absorbers of $ZnFe_2O_4$, $CuFe_2O_4$ and $CdFe_2O_4$. The results indicate that the internal magnetic field of a Fe nucleus varies according to the site at which it is located in the ferrite crystal lattice. Zinc ferrite, for instance, which is a normal spinel where Fe atoms are all situated in octahedral sites, gave no magnetic splitting either at room temperature or at liquid nitrogen temperature. It did show, however, a significant quadrupole splitting (0.32 mm/sec).

Measurements are in progress to determine the behaviour of these compounds at lower temperatures.

Absolute Recoilless Fraction of ZnTe: S. Bukshpan and M. Pasternak

The absolute recoilless fraction, f, of ZnTe was measured at 104°K using a cubic absorber - CuI^{129}. The experiment was performed by measuring the Mössbauer efficiency at increasing absorber thicknesses, in order to find the "saturation" absorption depth.

The absorption depth $\epsilon(0)$ is related to f_s according to the following formula[1]

$$\epsilon(0) = f_s \left(1 - \exp\left(-\frac{T_a}{2}\right) \cdot J\left(i\,\frac{T_a}{2}\right)\right)$$

where $T_a = f_a n_a t_a \sigma_o$. Due to the behaviour of the Bessel function $J(i\,\frac{T_a}{2})$, $\epsilon(0)$ was saturated at $\sim f_s \times 0.85$. The following values were obtained:

$$f\ (ZnTe) = 0.21 \pm 0.01$$

$$f\ (CuI) = 0.10 \pm 0.01$$

By plotting the absorber line width as a function of the absorber thickness, the half-life of the 27.7 keV level was derived. It was found to be $T_{\frac{1}{2}} = 15$ nsec, which is shorter by 10% compared with the data obtained by the conventional electronic technique[2].

References:

1. MARGULIES, S. and EHRMAN, J.R., Nuclear Instr. 12, 131 (1961).

2. DEWAARD, H., private communication

Mössbauer Effect in I_2Cl_6 : M. Pasternak

The I_2Cl_6 molecule has a planar structure. The field gradient acting on the iodine nucleus is produced by the p electron lone pairs directed perpendicular to the I-Cl bond.

An I_2Cl_6 absorber was prepared by direct combination of chlorine and I_2^{129} at -75°C. The quadrupole coupling at 90°K was determined from the positions of the quadrupole lines. It was found to be e q Q = + 2144 Mc/sec, which agrees to within 1% with the data obtained by the N.Q.R. technique. The plus sign indicates that the field gradient is produced by the lone electron pairs. The isomer shift related to the ZnTe source was found to be ± 0.35 cm/sec, indicating that the I-Cl bonds are chiefly produced by p electrons. The quadrupole peak intensities give no indication of anisotropy in the recoilless fraction.

Mössbauer Effect in Ferroelectric Compounds of Iodine : S. Bukshpan

A study has been initiated of the Mössbauer effect in ferroelectric iodine compounds, specifically NH_4I, $(NH_4)H_3IO_6$, $Ag_2H_3IO_6$ and BiSI. Preliminary measurements made with NH_4I show a very low effect near the temperature of phase transition. Attempts will be made to get a higher effect by using a source with higher efficiency, for instance, a solid solution of V and 5% Te. Experiments to prepare such a source are in progress. Of the other compounds, BiSI has been prepared by a chemical process. It has a low transition temperature (- 160°C) and can be used with the standard ZnTe source.

Mössbauer Effect of Co^{57} Impurities Diffused in LiOH Crystals: A. Simopoulos*

The excitation of approximately localized modes in light crystals doped with heavy impurities has been theoretically predicted and experimentally observed by the infrared technique(1). On the basis of theoretical calculations(2) for the use of the Mössbauer technique to study these modes, we have started a project in this direction. Experiments with the conventional Mössbauer technique (zero phonon transitions) are being conducted using LiOH crystals as a host matrix and Co^{57} as impurity.

Results with single crystals show anisotropy of the binding of the impurity atoms in accordance with the anisotropy of the crystal. The overall spectrum suggests the existence of two impurity sites in the crystal, one corresponding to an Fe^{3+} ion (the decay product of Co^{57}) and the other probably to an Fe^{+} ion. Work is in progress to relate the atomic motion of the host atoms to that of the impurity and to establish, with more confidence, the existence of the Fe^{+} site. The temperature dependence of the recoil-free fraction will give information about the existence of approximately localized modes.

Three other related projects are in the planning stage :

a) Further experiments with $Mg(OH)_2$ and $Ca(OH)_2$ as host matrices.

b) Study of vanadium hydrides doped with Co^{57}. These hydrides have been studied by neutron inelastic scattering and the results show new low-frequency modes not present in the spectrum of the vanadium metal. Such modes could also be detected by the Mössbauer technique.

c) Study of KI crystals doped with LiI. Electrocalorimetric measurements(3) have shown tunneling modes of the Li impurity inside the crystal. These modes amount to $1^{\circ}K$. Such a mode could be detected easily with a "one-phonon transition" experiment by using the Mössbauer technique.

References:

1. SIEVERS, A.J., Phys. Rev., Letters 13, 310 (1964)
2. BROUT, R. and VISSCHER, W.M., Phys. Rev. Letters 9, 54 (1962)
3. LOMBARDO, G. and POHL, R.O., Phys. Rev. Letters 15, 291 (1965)

* IAEA fellow, on leave from the Nuclear Research Center "Democritos", Athens, Greece

of nucleons in the smaller sphere, A, and the ratio between the heavy and light spheres, α, which gives the degree of asymmetry. Mathematical saddle points were calculated in the two dimensional space of A and d for various values of α. The energies of these points are plotted as a function of α in Fig. 9. The curves go through a minimum for α different from 1, indicating that the nuclear shape at the saddle point is asymmetric.

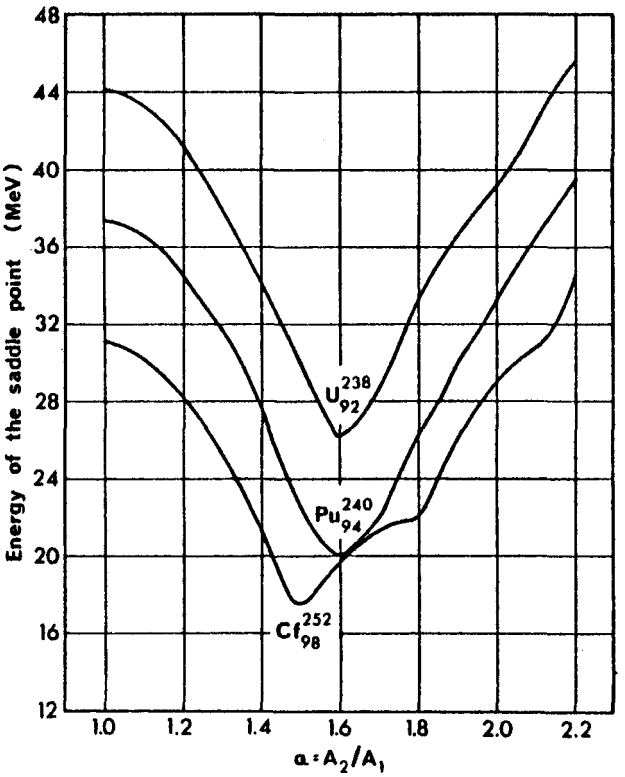

Fig. 9
Energy of saddle point as a function of the ratio α between the heavy and light spheres

Reference:
1. SWIATECKI, W., Proc. of the Second International Conference on Nuclidic Masses (1965) p.58, IAEA Vienna.

Alpha Particle Associated Fission in U^{235} : Y. Gozez, G. Ben-David, R. Moreh and A. Katase *

The preliminary experimental results, obtained with the apparatus described previously[1], showed excessive pile-up due to the high gamma fluxes present in the reactor thermal column. This was sufficient to distort

* Permanent address : Kyashu University, Japan.

Mean Square Displacement of Iodine in ICN: M. Pasternak and T. Sonnino

The ICN crystal is an interesting compound for measuring the atomic mean square displacement $\langle x^2 \rangle$. The crystal consists of covalently bonded ICN, forming linear chains bound by weak Van der Waals forces[1]. The aim of the present experiment is to measure $\langle x^2 \rangle$ by depositing oriented crystals and measuring the absolute Mössbauer fraction f ($\theta = 90^\circ$).

Assuming $\langle r^2 \rangle = \langle x^2 \rangle_\perp \cos^2\theta + \langle x^2 \rangle_\parallel \sin^2\theta$, we have derived, using a computer, the relation between $\langle x^2 \rangle_\perp - \langle x^2 \rangle_\parallel$ and the ratio $\frac{R\ (\Delta m = 0)}{R\ (\Delta m = 1)}$, where R ($\Delta$m) is the normalized quadrupole intensity for $\Delta m = 0$ and $\Delta m = \pm 1$ transitions. The values of f ($\theta = 90^\circ$) and f for randomly oriented crystals will be measured, and from these and the R (Δm) ratios (Goldanskii effect[2]) the anisotropy of the recoilless fraction will be derived.

References:

1. WYCKOFF, R.W.G., Crystal Structures, Vol 1 Interscience, N.Y. 1948
2. GOLDANSKII, V.I., MAKAROV, E.F. and KHRAPOV, V.V., J. Exper. and Theor. Phys. 17, 508 (1963).

Saddle Point Calculations for Fission, Taking into Account Shell Effects: E. Nardi, E. Cheifetz*, Y. Boneh*

Saddle point calculations which take into account shell effects have been carried out for fission in heavy nuclei. The nuclear shape at and around the saddle is described by two spherical clusters connected by a cylindrical neck. Shell effects are introduced by attributing to each spherical cluster the shell correction term for an equivalent nucleus, taken from the liquid drop mass formula of Swiatecki[1]. The parameters describing the problem are the distance between the centers of the spheres, d, the number

* Weizmann Institute of Science, Rehovot.

the alpha spectrum considerably. The electronic set-up has now been modified by using biassed amplifiers to cut out the low energy pulses. Improvements in the three-dimensional analyser have been effected, and data collection is continuing.

Reference:

1. GOZEZ, Y., BEN-DAVID, G., and MOREH, R., Israel AEC Semi-Annual Report July-Dec. 1964, IA-1021, p.25.

Neutron Emission in Triple Fission: E. Nardi and Z. Fraenkel*

Measurements are being continued in the experiment to determine the number of prompt neutrons emitted in the ternary fission of Cf^{252}. The pulse height data are recorded on an N.D.A. 4-dimensional analyser. Preliminary values of the total number of ternary fission neutrons have been obtained. A Monte-Carlo calculation was performed to compute the efficiency of the plastic scintillator and the time distribution for neutrons of different energies and incident angles. Specifically, a calculation was made for the geometry of the experiment (25 cm source-to-crystal distance). The results indicate the crystal to be relatively insensitive to differences in neutron energies.

Reference:

1. NARDI, E. and FRAENKEL, Z., Israel AEC Semi-Annual Report, July-Dec. 1964, IA-1021, p.27.

Evaporation Calculations: L. Meilen and Z. Fraenkel*

A computer programme for computing the evaporation of particles from a nucleus on the basis of the compound nucleus and statistical models has been improved and completed.

---

* Weizmann Institute of Science, Rehovot

The programme can be used for two different types of processes:

a) Evaporation from nuclei bombarded with particles of medium energy (<50 MeV)

b) Evaporation from excited nuclei after a prompt cascade.

The programme can compute the competition between fission and neutron emission in heavy elements, and the evaporation of neutrons from the fission fragments.

The output table gives the spectrum of the residual nuclei and the spectra of the emitted particles.

Resonance Fluorescence of γ-Rays Using Gaseous and Liquid Sources : T. Rothem and B. Locker *

An experimental arrangement has been completed for the study of resonance fluorescence of γ-rays using gaseous and liquid sources. The resonant nuclei are embedded in ferrites. Sources include Co^{60} in the form of $CoCl_2$ and Mn^{56} in the form of $MnCl_2$. Resonance scattering measurements in $NiO.Fe_2O_3$ and $CoO.Fe_2O_3$ have been started.

Decay Schemes of Sn^{121m} and Te^{121m} : B. Locker* and Y. Hazony

Coincidence measurements have been performed for a) the ~ 400 keV β-rays of a Sn^{121m} source and the low energy gamma spectrum; b) the 1.1 MeV gamma rays of Te^{121m} and the low energy gamma spectrum. Both measurements showed a gamma transition of ~ 9 keV. This transition is in cascade with a ~28 keV gamma transition to the ground state of Sb^{121}. The results have been prepared for publication.

The various methods used for the preparation and purification of the Sn^{121m} source will be published as an IA report(IA-1081) .

---

* Bar-Ilan University

Study of (n,α) Reactions using Thermal Neutrons: G. Hazan, R. Moreh, A. Katase* and G. Gozez.

Experiments have been continued on the (n,α) reaction induced by thermal neutrons in medium weight nuclei[1]. A small reaction chamber was used, with 10 cm thick lead shielding walls to reduce background due to gamma rays. The whole arrangement, including preamplifier, was inserted into the thermal column by means of a special loading device. Modifications were introduced in the electronic circuit to reduce the effect of gamma pile-up which limited the sensitivity of the experiment for low cross section reactions. After fast differentiations, a biassed amplifier is used to cut off the low energy signals, the stretched output being fed to a P.H.A. The apparatus can now be used to measure (n,α) cross sections as low as a few tens of μ-barns.

A preliminary 30 hour run with Mo^{95} has not shown any significant peak near the energy of the expected Q value for the ground state transition. This experiment is continuing. Further studies are planned for Xe, Hg, and Sm.

Reference

1. CHEIFETZ, E., GILAT, J., YAVIN, A.I., ASHERI, D., COHEN, S.G. and OPATOWSKY, A., Phys. Letters 1, 289 (1962).

* Permanent address : Kyashu University, Japan.

4. SOLID STATE PHYSICS

During the past year an NMR Laboratory has been set up. It is equipped with a 15" electromagnet capable of producing a field of 23,000 gauss in a 2" air gap. A pulsed nuclear resonance spectrometer operating between 2 and 30 Mc has been built. The RF pulse output power is 5 kW over most of the range. This spectrometer is suitable for experiments in solids. Various other instruments for the NMR experiments in solids have also been built.

Nuclear Magnetic Resonance Study of Hydrogen Alloying in the Early Transition Metals (Group V B) [1] : D. Zamir

The Knight shifts and spin lattice relaxation times of vanadium and niobium in the VH_x and NbH_x systems respectively have been measured. From the observed temperature dependence of the relaxation time the contribution of the conduction electrons to the nuclear relaxation was found. A comparison of the Knight shifts and relaxation times of V and Nb in the hydrides with those for the corresponding alloys, VCr_x and $NbMo_x$, shows a great similarity between the two types of systems. Some of the implications of this similarity have been examined. Using a Korringa-type relation for Nb in the NbH_x system, the type of conduction electrons giving rise to the Knight shift and relaxation rate was investigated.

Reference:

1. ZAMIR, D., Phys. Rev. 140, A 271 (1965)

Infrared Spectra of Small Ionic Crystals*: R. Englman and R. Ruppin

The long wavelength part of the dispersion curves for a thin disc-shaped rocksalt type crystal is calculated by means of an approximate model,

* This research was sponsored by the Air Force Materials Laboratory, Research and Technology Division, AFSC, through the European Office of Aerospace Research, United States Air Force, Contract AF 61 (052) - 753.

which employs cyclic boundary conditions. It is found that for wavelengths of the same order as, or smaller than, the thickness of the crystal, significant shifts in the frequencies of the optical branches occur.

Absorption frequencies and oscillator strengths are calculated as a function of the thickness of the specimen and of the angle of incidence of the infrared radiation. It is found that, in addition to the usual transverse optical frequency, the crystal absorbs at other frequencies which are either less than the transverse optical frequencies, or between the transverse and the longitudinal frequencies or greater than the longitudinal frequencies.

Recently we have developed an approach which can be applied to finite solids of very general shapes in order to obtain those vibrational modes and frequencies which are affected by the presence of the boundary.

The Operator for Spin-Forbidden Transitions* : R. Englman

With the Dirac equation as a basis we have shown that the matrix element of the dipole moment, taken between four-component spinors, gives the fundamental transition amplitude for spin-forbidden transitions. It was found that very frequently it is sufficient to take the same matrix element, but only between the large components, those which are the solutions of the Pauli-Hamiltonian. Finally, it was shown that because it excludes hole-excitations, the Pauli-Hamiltonian cannot possibly give a rigorous expression for the transition matrix.

* This research was sponsored by the Air Force Cambridge Research Laboratories through the European Office of Aerospace Research, United States Air Force, Contract AF 61 (052) - 806.

Studies in the Vibronic Theory of Ferroelectrics* : R. Englman and C. Yatom

It was shown in ref. 1 that the vibronic theory of ferroelectricity reduces to a simple solvable form (the Wigner-Jaynes formulation) in the mean interaction approximation. We have now derived the parameters appearing in the Devonshire phenomenological expression for the free energy. The parameters depend on the temperature explicitly and are functions of several constants of the microscopic theory.

The results of Bell and Rupprecht[2] for the dielectric constant $\epsilon = \epsilon_L + C(T - T_o)^{-1}$ in five perovskites show that ϵ_L is an order of magnitude smaller than C/T_o. We investigated the consequences for ϵ_L of an electronic band scheme rather than a degenerate level scheme, and found that ϵ_L may be affected considerably provided that the Fermi-level is near to the crossing point of the energy bands or to the point (in k space) of closest approach of these bands. For the calculations to be significant for a real crystal, the distance between the Fermi-level and the crossing point or the point of closest approach must be of the order of the transition temperature.

References:

1. ENGLMAN, R., Israel AEC Report IA-994 (Chapter 4)
2. RUPPRECHT, G. and BELL, R. D., Rev. 135, A748 (1964)

* This research was sponsored by the Air Force Materials Laboratory, Research and Technology Division, AFSC, through the European Office of Aerospace Research, United States Air Force, Contract AF 61 (052)-753.

Covalency Effects in Trigonal Distortion* : R. Englman

The strength of the axial field, as derived from the splittings of the optical bands of paramagnetic metal ions in crystals of trigonal symmetry, fluctuates greatly from band to band. We have made a qualitative analysis of the effect on the assumption that, in addition to the (mostly) positive trigonal field splitting parameter acting on the metal ions, there is also a larger and negative trigonal field splitting parameter acting on the molecular orbitals formed from the ligand orbitals. Covalency mixing results in an effective splitting parameter that differs for each configuration (in the t^3 and e^2 subshell). Of equivalent configurations, the one possessing greater interelectronic interaction energy is likely to have smaller convalency coupling and consequently a more positive trigonal field splitting parameter.

It appears that covalency may result in the stabilization of the Jahn-Teller instability or even in a distortion in the opposite sense to that which obtains in the absence of covalency.

The Jahn-Teller Effect for Threefold Degeneracies : M. Caner and R. Englman

We have treated the case of a triply degenerate electronic state interacting with a set of triply degenerate vibrational modes.

The vibronic states (being sums of products of electronic states with vibrational states) have been classified according to the irreducible representations of the group (O or T_d) of the Hamiltonian. The eigenvalues, eigenvectors and certain transition probabilities have been computed.

* This research was sponsored by the Air Force Cambridge Research Laboratories through the European Office of Aerospace Research, United States Air Force, Contract AF 61 (052) - 806.

Intensity Calculations for Absorption Bands in Tetrahedral Symmetry : Z. Yager

A general method has been developed for calculating the intensities of $d^n \rightarrow d^n$ transitions for paramagnetic ions in tetrahedral symmetries. Electric dipole transitions of this type would be forbidden in a crystal with inversion symmetry. In tetrahedral symmetry two mechanisms may be responsible for the transition: a) the odd static electric field, b) the odd vibrational motion of the neighbours. Either of these mechanisms causes an inmixture of charge transfer states in the even-parity metal states.

With this physical background we have classified both the electronic states and the vibrational motion by means of group theory, thereby also reducing the number of overlap integrals entering the transition probabilities. These overlap integrals are calculated for Slater-type wave functions of the metal and the ligand. They, as well as other related quantities, have been tabulated. Numerical calculations have been made for Ni^{2+} in ZnO.

Calculation of Jacobi Polynomials and Angular Momentum Transformation Matrix Elements[1] : M. Gazith

Angular momentum transformation matrix elements were calculated directly from Jacobi polynomials by using an appropriate form of the explicit expression for these polynomials. The use of this form of the

---

This research was sponsored by the Air Force Cambridge Research Laboratories through the European Office of Aerospace Research, United States Air Force, Contract AF61(052) - 806

Jacobi polynomials obviates the need for lengthy calculations by recurrence formulae. Matrix elements for $j = 3$ and 5 were calculated and tabulated. The results obtained were used for numerical calculations by Z. Yager (see previous item).

Reference :

1. GAZITH, M., Israel AEC Report IA-1067 (1966)

A Theoretical Model for the Motion of Krypton in a Clathrate[1] : B. Barnett and Y. Hazony

A theoretical model of the potential inside a hydroquinone clathrate is suggested on the basis of data obtained from Mössbauer effect experiments and specific heat measurements. The experimental evidence suggests that the guest particle lies in a narrower potential well at low temperatures than at high ones. The three dimensional interpretation of the model has been given as well as thermodynamic considerations regarding the relationship between the experimental specific heats and the theoretical C_V. A comparison between the experimental and theoretical specific heats is made for the hydroquinone-krypton clathrates.

Reference :

1. BARNETT, B. and HAZONY, Y., J. Chem. Phys. 43,3462 (1965) and Israel AEC Report IA-1019 (1965)

$NH_4H_2PO_4$ Phase Transition Studies by Infrared Absorption: I. Pelah, E. Wiener (Avnear) and S. Levin

The phase transition of antiferroelectric $NH_4H_2PO_4$ (ADP) was studied by measuring the infrared absorption spectrum in the wavelength region 250 cm^{-1}

to 4000 cm^{-1}. The changes in the spectrum which occurred on crossing the antiferroelectric Curie temperature (148°K), were compared with those found earlier[1] for the ferroelectric transition point (123°K) of KDP (KH_2PO_4). Above their Curie temperature the spectra of ADP and KDP are very similar, except of course for the addition of the NH_4 characteristic lines in the case of ADP. Below the phase transition the spectra differ considerably: the PO_4 lines are split in a different manner, especially the broad peak at 250cm^{-1} to 450 cm^{-1} which is split into 6 lines in ADP instead of 4 as in KDP. Changes are also in the NH_4^+ lines on cooling below the Curie temperature. The positions of the hydrogens in the short O-H..O bonds are not known as yet[2] for the low temperature ADP phase. It is most important for an understanding of the antiferroelectric phenomena that these positions should be established. Taking into account the static and dynamic crystal effects on the symmetry, our results indicate[4] that below the Curie temperatures the symmetry of the PO_4 group is C_1 in $NH_4H_2PO_4$ and C_2 in KH_2PO_4.

This may support Nagamiya's[3] theory on the different arrangement of the hydrogens in the PO_4 tetrahedra. Similar results were found when comparing the spectra of KH_2AsO_4 and $NH_4H_2AsO_4$ above and below their Curie temperatures. The effect of phase transition on the infrared spectra of the deuterated compounds of $NH_4H_2PO_4$ were studied for different percentages of deuteration in order to determine the role played by the hydrogens and to aid in the assignment of the infrared lines.

The results support our previous idea[1] that in the upper phase there is a low frequency hydrogen mode which changes drastically on phase transition. This mode is explained as resulting from a splitting of the ground level of the proton in a slightly asymmetric double minimum potential well, where tunneling of the proton takes place.

References:

1. IMRY, Y., PELAH, I. and WEINER, E., J. Chem. Phys. 43, 2332 (1965)
2. TENZER, L., FRAZER, B.C. and PEPINSKY,R., Acta Cryst. 11, 505 (1958)
KEELING, R.O. and PEPINSKY, R., Z. Kristallogr. 106, 236 (1955)

3. NAGAMIYA, T., Prog. Theor. Phys. 7, 275 (1954)

4. WIENER (Avnear), E., PELAH, I. and IMRY, Y., ADP Phase Transition Studied by Infrared Absorption , 8th European Congress on Molecular Spectroscopy. Copenhagen, Denmark, August 14-20, 1965.

A New Interpretation of the Quasielastic Scattering of Slow Neutrons in Water[1]: I. Pelah and Y. Imry

A refinement was made in our previous simple model[2] for liquid water which depicted it as a "gas" of aggregates of a few hundred molecules each. In the limit where the aggregates do not interact, the model gave the same neutron scattering as from a "gas" of molecular weight about 300 times that of H_2O. The "Doppler shift" in scattering from this "gas" gives the right order of magnitude for the quasielastic broadening and its dependence upon momentum transfer[2].

In the present work the interactions between the aggregates are taken into account. The system is described as a "quasisolid" composed of the aggregates as units, with a characteristic temperature which is presumably low (because of the large aggregates). Neutron scattering from this system for small energy transfers will be the sum of many phonon contributions. Machine calculations of the differential cross section for scattering of slow neutrons from this model were made using Sjölander's[3] phonon expansion and assuming a simple frequency distribution for the "phonons". It was found that for high values of the Debye Waller exponent, 2W, the cross section tends to the gas approximation. For $2W \cong 3$, which is obtained for $\theta \approx 3^{\circ}K$, the scattering cross section consists of a series of peaks whose total envelope is given by the gas approximation. This is found to agree with the experimental results of Bajoric et al[4] and to give qualitatively the right temperature behaviour - contrary to former diffusion models. The physical implications of the model are discussed.

References:

1. PELAH, I. and IMRY,Y.,Israel AEC Report IA-875 (1963)
2. PELAH, I. and IMRY, Y., Phys. Letters, to be published.
3. SJÖLANDER, A., Arkiv för Fysik, 14,315 (1958)
4. BAJORIC, A., GOLYKOV, E.B., ZHUKOVSKAYA, I., SHAPIRO, F.L., SHKATULA, A. and JANIK, E.A., Proc. of the Symposium on Inelastic Scattering of Neutrons in Solids and Liquids, Vienna (1962) pp.363.

Paramagnetic Resonance Spectrum of Co^{1+} in Single Crystals of Calcium Oxide[1]:

W. Low* and J.T. Suss

The investigation of the paramagnetic resonance spectrum of Co^{1+} in CaO was completed. Co^{1+} was obtained by gamma irradiation of crystals containing Co^{2+}. The resonance results are:

$A = (31.6 \pm 0.3) \times 10^{-4}$ cm^{-1} ; $g = 2.2743 \pm 0.0008$ at 20°K and

$g = 2.2756 \pm 0.0008$ at 12°K.

A comparison was made of the internal magnetic field due to effective core polarization for Co^{1+} in MgO, Co^{1+} in CaO and Ni^{2+} in MgO. The core polarization for similar ions was found to be nearly independent of the crystal host.

Reference:

1. LOW, W. and SUSS, J.T., Phys. Rev. Letters, 15, 519 (1965) and Israel AEC Report IA-1056.

E.S.R. Studies of Radiation Effects in Simple Oxides[1]: W. Low* and J.T. Suss

Gamma irradiation of single crystals of MgO, CaO and SrO, causes a number of effects which can be measured by means of electron spin resonance.

---

* The Hebrew University, Jerusalem.

In addition to valence changes of iron group impurities in MgO[2] and CaO[3],[4],[5] we have also observed H_1 centers (holes trapped near a positive ion vacancy) in CaO and SrO. These centers are not stable at room temperature. They have axial symmetry, with $g_{\|} = 2.0020$, $g_{\perp} = 2.0717$ in CaO, and $g_{\|} = 1.9999$, $g_{\perp} = 2.0757$ in SrO . Similar hole centers in MgO[6] were stable at room temperature.

A number of additional centers have been found in crystals of CaO and SrO. One of the most interesting is a center found at 20°K which can be expressed by means of a spin Hamiltonian :

$$\mathcal{H} = g_{\|}\,\beta H_z \cdot S_z + g_{\perp}\,\beta(H_x S_x + H_y S_y) + A S_z I_z + B S_y I_y + D\left[S_z^2 - \frac{1}{3}S(S+1)\right]$$

with $g_{\|} = 2.0010$, $g_{\perp} = 2.1232$, $A = 1.9 \times 10^{-4}$ cm^{-1} , $B = 3.6 \times 10^{-4}$ cm^{-1}, $D \sim 0.5 \times 10^{-4}$ cm^{-1} . This center is partially stable at 77°K and could arise from a hole trapped near a Na impurity.

References:

1. LOW, W. and SUSS, J.T., Proc. of the Intern. Conference on Electron Diffraction and the Nature of Defects in Crystals, Melbourne, Australia, 16-21 August, 1965.
2. ORTON, J.W., AUZINS, P., GRIFFITHS, J.H.E. and WERTZ, J.H., Proc. Phys. Soc., 78, 554 (1961)
3. LOW, W. and SUSS, J.T., Bull. Am. Phys. Soc. 9, 36 (1964)
4. LOW, W. and SUSS, J.T., Phys. Letters, 7, 310 (1965).
5. LOW, W. and SUSS, J.T., Phys. Rev. Letters, 15, 519 (1965) and Israel AEC Report IA-1056.
6. WERTZ, J.E., AUZINS, P., GRIFFITHS, J.H.E. and ORTON, J.W., Disc. Faraday Soc., 28, 136 (1959).

Electroluminescence and Dark-Current in Semiconducting Diamonds[*]: A. Halperin[**], V. Bar and J. Levinson.

The electroluminescence and conductivity of some specimens of semiconducting diamonds (type IIb) were investigated.

* This research was supported in part by the Air Force Cambridge Research Laboratories under Contract AF61(052)-759 through the European Office of Aerospace Research, United States Air Force.

** Hebrew University, Jerusalem.

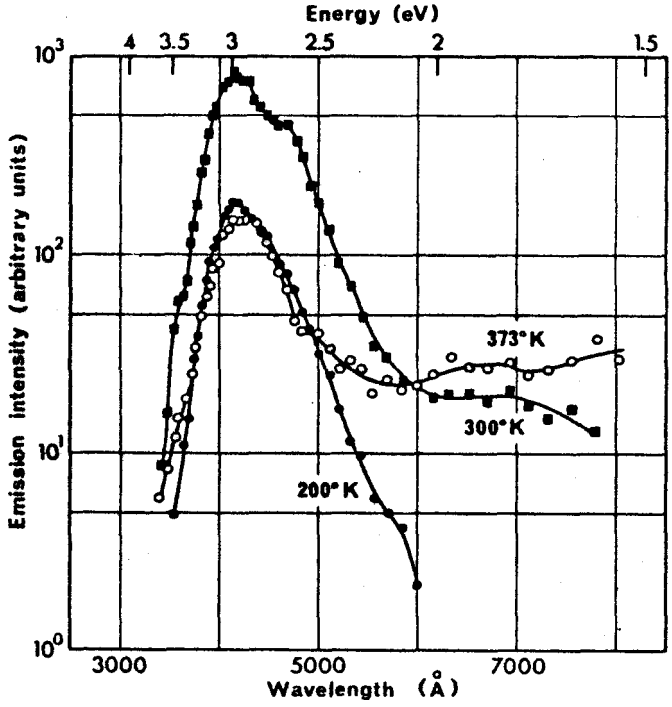

Fig. 10

Dependence of the electroluminescence emission spectrum on temperature, with 300 V applied across specimen C_5.

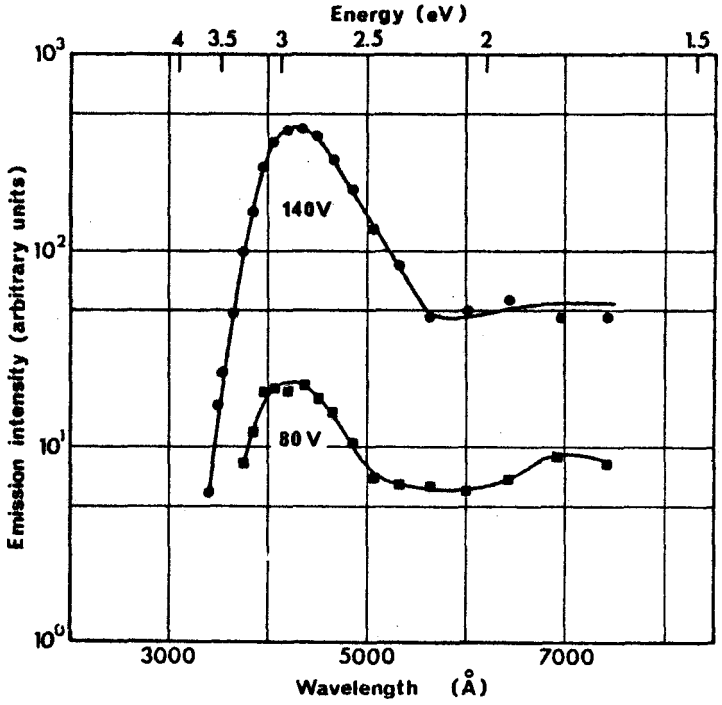

Fig. 11

Dependence of the electroluminescence emission spectrum on the applied voltage at room temperature in specimen C_2.

All the crystals showed p-type direction of rectification. The dependence of the current and the emitted light on the voltage and temperature was measured, as well as the spectrum of the emitted light. In most of the experiments short square voltage pulses were applied to the crystals. In some experiments, especially at low voltages and low temperatures, both DC and AC voltages were applied.

The electroluminescence was found to rise exponentially on warming the crystal, with an activation energy of 0.3 - 0.4 eV, which is close to the activation energy obtained from dark-current measurements[1].

The plot of log I against $\frac{1}{\sqrt{V}}$ (where I is the intensity of the emitted light and V the applied voltage) gives a constant slope up to about 100 volts across the crystals (about 300 volts per cm). At higher voltages the curve becomes steeper. It is interesting that electroluminescence has been observed with only 1.8 volts across the crystal, which is less than one third of the forbidden gap.

The emission spectrum consists of two broad bands, one in the blue-violet region[2] with a maximum around 4400 Å, and the other in the orange-red region (5500-8000 Å) with several maxima. Figure 10 shows the temperature dependence of the emission spectrum of one specimen (C_5 in our notation). When the temperature rises the ratio between the intensity of the blue band and that of the red band decreases. Figure 11 shows the dependence of the emission spectrum on the voltage for specimen C_2. The "red" band is more pronounced at low voltages.

References:

1. AUSTIN, I.G. and WOLFE, R., Proc. Phys. Soc., London B69, 329 (1961) ; also HALPERIN, A. and NAHUM, J., Phys. Chem. Solids, 18, 297 (1961).
2. WOLFE, R. and WOODS, J., Phys. Rev. 105, 921 (1957).

Thermoluminescence in Semiconducting Diamonds*: A. Halperin** and R. Chen

The thermoluminescence glow curves of semiconducting diamonds have been measured in earlier work(1). It was shown that after excitation with UV light (2250 Å) at liquid air temperature the glow obtained during the warm-up of the crystal consists of a weak peak below 150°K, a very strong composite peak near 250°K and weaker glow peaks at higher temperatures. The emission was found to be blue-green. The most efficient excitation wavelength was a sharply defined peak near 2250 Å .

In the present work the thermoluminescence was examined in greater detail, and the following new information obtained:

a) The blue glow peaks are accompanied by red peaks at about 175°K and 280°K.

b) The blue peaks could be excited not only by wavelengths near the absorption edge (2250 Å) but also by longer wavelengths up to about 4000 Å.

c) The excitation spectrum for the red peak (at 280°K) extended to wavelengths up to 6000 Å and more.

d) The dependence of the intensity of the main thermoluminescence peak on the total dose of the exciting light was also examined in detail. For excitation with light near the edge (2200 to about 2600 Å) the intensity of the 250°K peak was strictly proportional to the excitation dose. For excitation with wavelengths of 2700 to nearly 4000 Å the dependence was superlinear, being proportional to the second power of the dose at 3000 Å and to the third power at 3600 - 3700 Å. For wavelengths above 4000 Å only the red peak (at 280°K) could be excited, and its intensity was strictly proportional to the dose. Fig.12 shows some representative curves of the maximum intensity of the 250°K peak as a function of the dose for some

---

* This research was supported in part by the Air Force Cambridge Research Laboratories under Contract AF 61(052)-759, through the European Office of Aerospace Research, United States Air Force.

** The Hebrew University, Jerusalem.

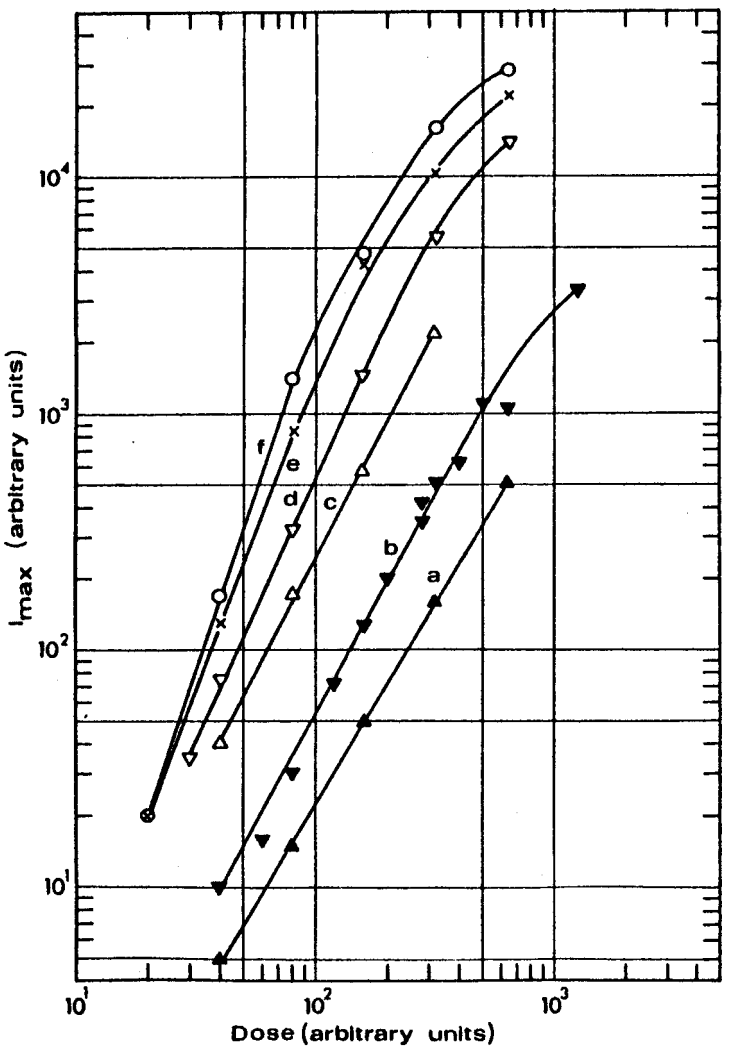

Fig. 12

Intensity of the main peak as a function of the irradiation dose Type IIb diamond (specimen C_3)

a) 2800 Å, initial slope (n) = 1.7
b) 3000 Å, n = 1.9
c) 3200 Å, n = 2.1
d) 3400 Å, n = 2.3
e) 3500 Å, n = 2.7
f) 3600 Å, n = 3.0

wavelengths of excitation. On the log-log scale used the slope gives the power of the dose to which the intensity is proportional (at low doses).

e) The blue peak at about 150°K was found to depend linearly on the dose at low doses and sublinearly at higher ones. At a certain dose the intensity of the peak reaches a maximum and when higher doses are used, the intensity of the peak drops. This seems to be the result of competition between excitation and bleaching effects. Bleaching effects are also observed when illuminating the crystal with visible or infrared light after excitation in UV.

Reference:

1. HALPERIN, A. and NAHUM, J., J. Phys. Chem. of Solids, 18, 297 (1961).

5. PLASMA PHYSICS

Radiation by Growing Plasma Oscillations : S. Cuperman

The electromagnetic radiation emitted from bounded plasmas by growing (in time) plasma oscillations was studied. Such growing oscillations occur when for some reason a plasma instability is set up. Specifically, the growing plasma oscillations arising from the nonconvective electrostatic instability in an infinitely long current carrying cylindrical plasma of finite radius were considered.

Using the linearized equations of motion, the fields and the dispersion relation corresponding to free boundaries were obtained. Under certain circumstances the solution of the dispersion equation leads to complex values for the frequency, the wave number being kept constant. The phase velocity of the propagating field is near the constant axial velocity of the electrons, thus being smaller than the velocity of light.

An approximation for the electromagnetic power density, valid for the case in which the rate of growth γ is much smaller than the real part of the frequency, was obtained and its asymptotic expression considered. The particular value of the e.m. power density for the stationary regime (i.e. vanishing rate of growth) was found. This quantity is vanishing if the phase velocity of the propagating fields is smaller than the velocity of light. However, with $\gamma \neq 0$, the electromagnetic power density builds up from zero to nonvanishing values.

Theory of the Buildup of a Beam-Generated Plasma: S. Cuperman

Recent experiments on beam - plasma interactions in which the plasma is produced by the interaction of a monoenergetic electron beam

with neutral hydrogen gas have shown an unusual behaviour of the degree of ionization of the neutral gas as a function of the neutral gas density. The electron density of the plasma initially increases as a linear function of the density of the neutral background gas; then an abrupt jump occurs, corresponding to a density rise of 300 - 400 %, or even much larger if a mirror magnetic confinement is present. Following this discontinuity, the plasma electron density again rises linearly with the neutral background. During the unusual rise, intense radiofrequency activity is observed. Moreover, the emerging electron beam spreads considerably and diffuses in the direction of lower energies. Under certain circumstances beam-electrons with energies several times larger than the initial one are observed.

An attempt is being made to derive the theory of this enhanced ionization by electron beam - plasma interaction. The theory involves the non-linear interaction between the strongly time dependent microscopic electric fields (which appear when a beam - plasma electrostatic instability is set up), and the beam particles and cold plasma particles.

Review of Experimental and Theoretical Studies on Plasma Formation by Laser Beams : J. Joskowicz*

Several experimental and theoretical studies have been carried out over the past three years on ionisation and gas breakdown phenomena associated with laser beams. Experiments proved to be perfectly concordant, but the theories were contradictory at first. However, a crystallisation seems to be on the way: gas-breakdown is essentially governed by inverse bremsstrahlung, whereas the first ionisations are due to multiphoton absorption. The present work summarizes the various theories on plasma formation by laser beams.

---

* On an Israel AEC Fellowship. Permanent address: Euratom-CEA, Fontenay-Aux-Roses, France.

M A T H E M A T I C S

On the Structure of T A - Algebras : Y. Ilamed

The idea of studying the structure of T A - algebras (Taussky A algebras) was suggested by Olga Taussky[1] who proposed studying the structure of an algebra whose composition law is given by the generalised Jordan product $MN + N^*M^*$, where M and N are complex n by n matrices and * denotes the complex conjugate and transpose operation.

Corresponding to an associative algebra A we define a T A algebra by the composition law ab

$$ab = \frac{1}{2}(a.b + b^*.a^*) \tag{1}$$

where a.b denotes multiplication in A and * denotes a one-to-one linear mapping of the algebra A onto itself such that

$$(a.b)^* = b^*.a^* \ , \ (a^*)^* = a \tag{2}$$

Denoting by [a,b] the commutator of a,b, namely [a,b] = ab - ba, and by (a,b,c) the associator of a,b,c, namely (a,b,c)= (ab)c - a(bc), the following identities are valid in T A - algebras

$$(ab)^* = b^*a^* \tag{3}$$

$$(ab)^* = ab \tag{4}$$

$$[a,b] = [b^*, a^*] \tag{5}$$

$$(a,b,c) + (c^*, b^*, a^*) = 0 \tag{6}$$

$$[ab,cd] = 0 \tag{7}$$

$$((ab)(ab), cd, ab) = 0 \tag{8}$$

$$(a,b,c) = (b,a,c^*) + (a^*, c,b) \tag{9}$$

$$(a,b^*,c) + (b,c^*,a) + (c,a^*,b) = 0 \tag{10}$$

$$(a,bc,d) + (d,bc,a) + (bc)[ad^*] = 0 \tag{11}$$

Reference:

1. TAUSSKY, O., Research Problem 17, Bull. Am. Math. Soc.,71, 711 (1965)

Hamilton-Cayley Theorem for Matrices with Non-Commutative Elements[1] :

Y. Ilamed

In this paper an example is given to show how the Hamilton-Cayley theorem for a matrix with non-commutative elements can be used to obtain identities in the enveloping algebra of a given Lie algebra.

Reference:

1. ILAMED, Y., Lectures in Theoretical Physics, Eds. W. E. Brittin and A. O. Barut, Vol. VIIA, p.295, Univ. of Colorado Press, 1965

Fourth Order Three Point Difference Scheme for Solving Linear Second Order Differential Equations : A. Gersten

The differential equation $y''(x) + A(x)y'(x) + B(x)y(x) = C(x)$ with its boundary conditions is approximated by finite differences with an accuracy of $O((\Delta x)^4)$. The formula connects entities for three values of the argument and can be applied in some cases of regular singularities.

CHEMISTRY

1. INORGANIC AND PHYSICAL CHEMISTRY

During the past year research on several of the topics studied in the department was concluded. Amongst these topics are: interaction between lanthanide and nitrate ions in solution, molten salt studies of lanthanide ions, reactions between alcohols and phosphorus pentoxide, and electroplating of tantalum from molten salts.

Interaction between Lanthanides and Nitrate Ions[1]: I. Abrahamer and Y. Marcus

The study of the interaction between lanthanide ions and nitrate ions has been concluded. The main results may be summed up as follows.

1) Lanthanide ions exist in two forms: a high-symmetry form,as for example in the fully hydrated and highly solvated ions, and a low symmetry form, as in the nitrate complexes.

2) From the linear variation of the molar absorption coefficient with nitrate concentration, it is apparent that no stable species are formed.

3) It seems that water is present in the inner coordination sphere of complexes with tributyl phosphate. The composition of the complex varies with water and nitrate ion concentration, and is not $M(NO_3)_3(TBP)_3$, as given in the literature.

4) A possible composition of the species existing in the triisooctylammonium nitrate is $M(NO_3)_3(TIOAN)_2$ (ref.2).

5) The affinity of lanthanide ions for various complexing and solvating agents decreases in the order: DMF $>>$ TBP $>$ NO_3^- $\approx$ H_2O $>$ EtOH $>$ dioxane.

6) The variation in the composition of the lanthanide complexes with increasing atomic number exhibits an odd-even effect which may be due to the alternating affinity of the lanthanide ion for ligands containing donor-oxygen.

References:

1. ABRAHAMER, I., ELIEZER, I. and MARCUS, Y., Israel AEC Semi-Annual Report, July-Dec. 1964, IA-1021, p.60

2. MARCUS, Y. and ABRAHAMER, I., J. Inorg. Nucl. Chem., 22, 141 (1961)

Ion-Solvent Interaction in Electrolytes: I. Abrahamer and J. Padova

It has been shown[1] that the partial molar volume of electrolytes, extrapolated to infinite dilution, can account for ion-solvent interactions, and that from these values the free energy of solvation can be calculated.

The densities of solutions of $(CH_3)_4NCl$, $(C_2H_5)_4NBr$ and $(C_3H_7)_4NBr$ in anhydrous methanol have been measured. The apparatus used was a bi-capillary pycnometer, which was calibrated with mercury and triple distilled water. Its accuracy was 5×10^{-5} $g.cm^{-3}$.

The apparent molar volumes at infinite dilution, ϕ_v^o, were found by extrapolating the apparent molar volume ϕ_v as a function of the square root of the concentration. The results are given in Table 8.

TABLE 8

Apparent molar volumes at infinite dilution

Salt	ϕ_v^o ml.mole^{-1}		S_v(methanol)
	methanol	water	
$(CH_3)_4NCl$	95.0 ± 0.1	107 [2]	10.80 ± 0.01
$(C_2H_5)_4NBr$	149.0 ± 0.1	175.3 [3]	7.73 ± 0.01
$(C_3H_7)_4NBr$	222.1 ± 0.1	240.8 [3]	6.06 ± 0.01

(S_v is the slope of the plot of ϕ_v vs. $C^{\frac{1}{2}}$)

The positive values of S_v indicate that the R_4N^+ ion may have a structure-forming effect, both in aqueous and in methanol solutions[4].

References:

1. PADOVA, J., J. Chem. Phys., 39, 1552 (1963); ibid.40, 691 (1964)
2. GILKINSON, W. R., STEWARD, L. J. L., J. Phys. Chem., 65, 1465 (1961)
3. WEN YANG WEN and SAITO, S., J. Phys. Chem., 68, 2639 (1964)
4. FRANKS, F. et al., XVI Meeting CITCE, Budapest (1965)

Electrolyte Solution Theory[1]: J. Padova

The thermodynamic treatment of a fluid in an electrostatic field has been applied to electrolytic solutions. It has been shown that for the ionic free energy of transfer, as well as for the primary medium effect and the solubility in mixed solvents, the so-called linear dependence on the

reciprocal of the dielectric constant is not to be expected on theoretical grounds, contrary to general belief. These thermodynamic quantities should be a linear function of the derivative of the differential dielectric constant.

On the basis of the theory it is possible to predict Harned's coefficient for mixtures of electrolytes by using the relation between dielectric constant and activity coefficient[2] to obtain the average field strength. The interaction between one ion and the average field of the other ion must be calculated to obtain the exact expression for $\log \gamma_{(o)B}$ and $\log \gamma_{B(o)}$[3]:

$$\log \gamma_{B(o)} = \log \gamma_{(o)B} - \alpha_B m.$$

A first approximation shows that cross terms drop out and it is possible to obtain a polynominal expansion of the form

$$\log \gamma_{(o)B} - \log \gamma_{B(o)} = A m + B m^2 + C m^3$$

where A, B, C are functions of the measured decrement in the dielectric constants.

It is hoped to simplify the above expression by assuming a specific model, the cell model, for a certain concentration of the main electrolyte.

References:

1. PADOVA, J., 16th Meeting of CITCE, Budapest, Sept. 1965, Abstract p.87.
2. PADOVA, J., Israel AEC Semi-Annual Report July-Dec. 1964, IA-1021 p.78; Israel J. Chem., 2 5a, 279 (1964).
3. ROBINSON, R.A. and SLOTY, R.M., Electrolyte solutions, 2nd Edition (1959) Butterworth London - p. 438.

Synergism in Solvent Extraction. Am(III) and Am(VI) in Nitric Acid :

M. Zangen

Synergistic extraction of Am(III) and Am(VI) from 0.05 M HNO_3 was studied, using a combination of a monoacidic phosphate or phosphonate ester (the chelating agent) with tributyl phosphate (the synergist) at varying

concentrations in carbon tetrachloride.

The results were found to agree with the extraction mechanisms derived previously[1,2]. The extracted species are a) $AmO_2X_3^-.AHXH^+$ (hexavalent) and b) $Am(HX_2)_3$ (trivalent), where HX represents the chelating agent 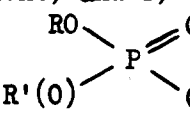 , dimerized as $(HX)_2$ in the organic phase, and A represents the synergist. The main species formed by interaction between A and HX is c) $A(HX)_2$ (III).

The following values were found for the equilibrium constants of the reactions leading to a), b) and c), respectively:

for HX = di(2-ethylhexyl) phosphoric acid: 1.3×10^6; 2×10^4; 15

for HX = n-octyl hydrogen phenylphosphonate: 2×10^7; 6×10^6; 90.

References:

1. ZANGEN, M., J. Inorg. Nucl. Chem., 25, 581 (1963).
2. ZANGEN, M., J. Inorg. Nucl. Chem., 25, 1051 (1963).

Extraction of Ga(III) from Bromide Solutions by Thenoyltrifluoroacetone and Tetraphenylarsonium Bromide in Chloroform: M. Zangen, E. Hecht and A.S. Kertes*.

The partition of Ga(III) between chloroform solutions of thenoyltrifluoroacetone (TTA) or tetraphenylarsonium bromide (TφAB) and aqueous bromide solutions of various acidities was investigated. The bromide concentrations ranged between 1 and 13 M. The complex extracted with TTA appears to be a mixed bromide-TTA complex. Increase in pH increases the distribution ratio in the case of TTA, but somewhat decreases it in the case of TφAB. Evidence was found of a synergistic effect between TTA and TφAB. The results are shown in Figs.13 and14.

* The Hebrew University, Jerusalem.

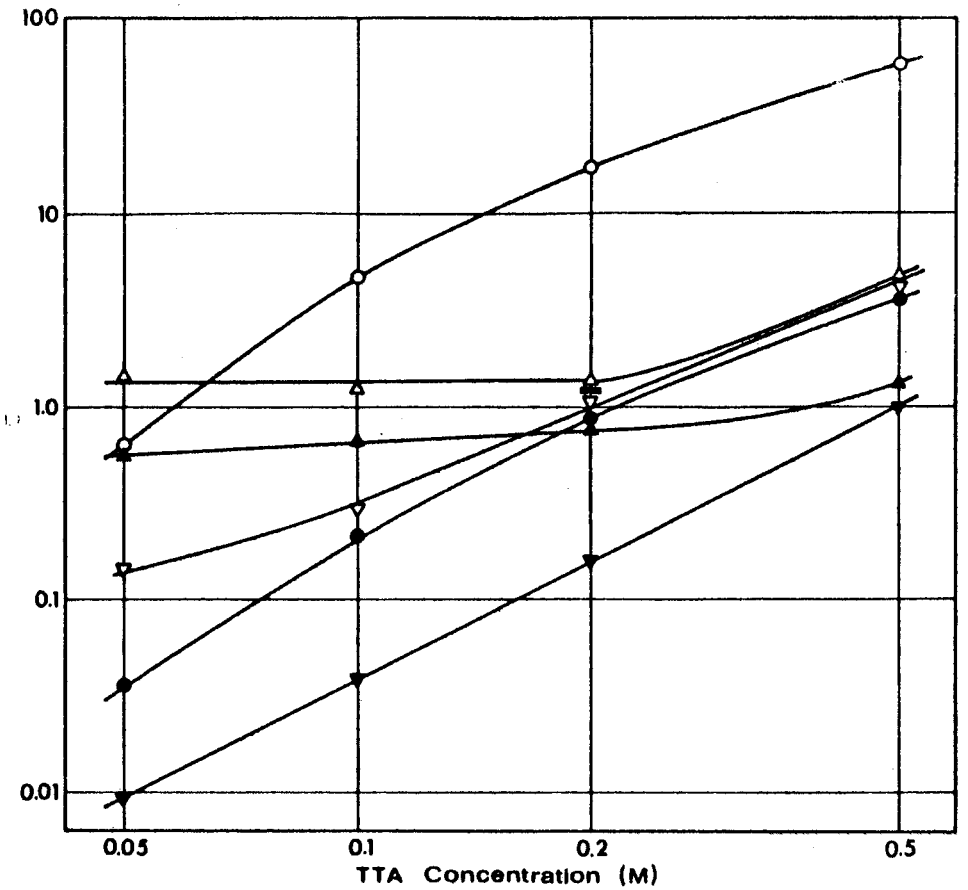

Fig. 13

Distribution ratio of Ga^{3+} between solutions of TTA in chloroform and aqueous LiBr, as a function of TTA concentration
full symbols: $[H^+]_{aq} = 10^{-2}$
empty symbols: $[H^+]_{aq} = 10^{-3}$

○ - 1 M $[Br^-]$
▽ - 3 M $[Br^-]$
△ - 13 M $[Br^-]$
▬ - 1 M $[Br^-]$ + 0.01 M TφAB

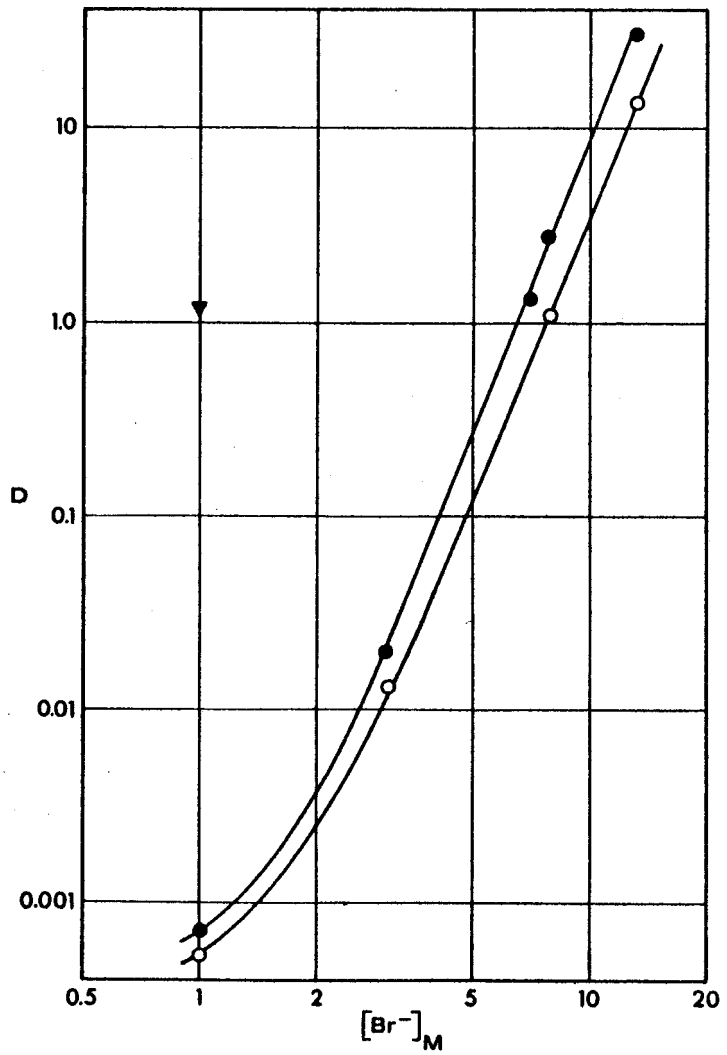

Fig. 14

Distribution ratio of Ga^{3+} between 0.01 M solutions of TφAB in chloroform and aqueous LiBr, as a function of bromide concentration

● $[H^+]_{aq} = 10^{-2}$
○ $[H^+]_{aq} = 10^{-3}$
▼ $[H^+]_{aq} = 10^{-2}$, plus 0.2 M TTA

Electrodeposition from Molten Salts: A. Aladjem and Y. Marcus

The study of the electrodeposition of tantalum from molten salts[1] has been completed. The media examined were molten nitrates, chlorides, thiocyanates and bromides. Thiocyanates were unstable and could not be used. Powdery deposits with a tantalum content of > 95% were obtained from mixed alkali-metal chlorides and nitrates containing Ta_2O_5 and potassium fluo-tantalate; this deposition was obtained at temperatures ~50°C above the m.p. of the mixture, with graphite anodes. Tantalum anodes could be used in chloride systems, but not in nitrate systems where they became coated with a non-conductive oxide film. The deposits were obtained over a wide range of current densities, in some cases from 0.1 to 10 amp/dm^2 . The current efficiency was low (< 50%) due to the codeposition of alkali metals, especially lithium. Compact deposits of tantalum-nickel alloys (with a tantalum content of up to nearly 20%) were obtained from the same media containing nickel chloride. In this case no codeposition of the alkali metal took place at low current density and the current efficiency was close to 100%. Of a large number of materials tested, impervious graphite was found to be the best structural material for vessels in contact with the molten salts.

From a theoretical analysis, as well as a literature survey, it was concluded that electrodeposition of tantalum from aqueous electrolytes cannot be achieved.

Experiments were also performed on the electrodeposition of tin from molten $SnCl_2$. Adherent deposits with a metallic lustre were obtained on copper, iron and brass, over the temperature range 280-400°C and cathodic current densities up to 10 amp/ dm^2 . The deposits on nickel and aluminium were non-adherent. The cathodic current efficiency was close to 100% and the "throwing power" was good. Insoluble graphite anodes or soluble tin anodes were used with equal success. The molten electrolyte was stable at the temperature used; graphite, ceramic and quartz crucibles were used as containers of the molten bath and were not attacked by it. The process is especially suitable for the plating of springs and other articles where hydrogen

embrittlement is a major problem.

Reference:

1. ALADJEM, A., Israel AEC Semi-Annual Report Jan.-June 1963, IA-900, p.129.

Cation Exchange in Molten Salts: M. Liquornik and Y. Marcus

The exchange reaction between NaZ^* and solutions of $CsNO_3$ or $Ca(NO_3)_2$ in molten $NaNO_3$ was studied. The same experimental methods as reported previously[1] were used, with slight variations. It was found necessary to analyze the zeolite as well as the melt after the exchange, especially in the cases where the concentration changes in the liquid phase were small or where changes in the occlusion were to be expected. For this purpose the melt was filtered through a porous plate, and the zeolite cooled and washed with water to remove the adhering melt. The results of the experiments are now being analysed.

The exchange isotherms of the system $KZ + KNO_3 + NaNO_3$ were measured at 350° and 450°. The results will be used to determine the heat of exchange of the system.

Attempts were made to use radioactive tracers to measure the diffusion coefficient of sodium and silver between their respective molten nitrates and zeolites. However it was found that the reaction was complete within one hour, and under the experimental conditions used no kinetic data could be obtained.

References:

1. LIQUORNIK, M. and MARCUS, Y., Israel AEC Semi-Annual Report, July-Dec.1964 IA-1021, p. 60.
2. MARCUS, Y. and ABRAHAMER, I., J. Inorg. Nucl. Chem., 22, 141 (1921).

Lanthanide Nitrates in Molten Alkali Nitrates: M. Peleg and J. Padova

The investigation of complex formation by neodymium nitrate in molten alkali nitrate has been completed. A potentiometric technique was

used, with the experimental set-up described previously[1]. A plot of the potential at the cell vs. the logarithm of the total Nd concentration is shown in Fig. 15 The break in the graph was confirmed to be about 0.6 molal (0.9 molar). The break indicates the occurrence of specific interactions at this concentration confirming the evidence from both density[2] and spectrophotometric[3] measurements. From the slope it would seem that the average charge of the species present in solution at concentrations above 0.9 m is one, pointing to a decrease in dissociation of $Nd(NO_3)_3$ as its concentration increases, with the possible existence of $Nd(NO_3)_2^+$. An attempt will be made to confirm this supposition polarographically.

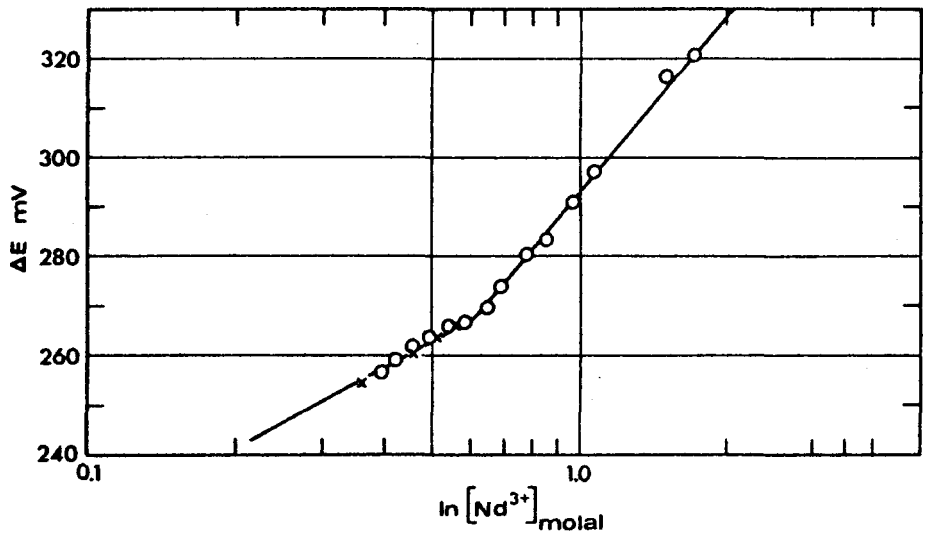

Fig. 15

ΔE as a function of $\ell n[Nd^{3+}]_{molal}$

T = 286.5° C

O - run 1

X - run 2

References:

1. PELEG, M. and PADOVA, J., Israel AEC Semi-Annual Report, July-Dec. 1964, IA-1021, p. 62.

2. PADOVA, J. and SORIANO, J., J. Chem. Eng. Data, 9, 510 (1964).

3. PADOVA, J. and SORIANO, J., unpublished data, and XIX Intern.Congr. Pure Appl. Chem., Paper B3-6, London 1963, Israel AEC Report,IA-1068.

Solubility of Water in Molten Salts: M. Peleg.

It is well established that certain molten salts dissolve large amounts of water and that the presence of the water affects the properties of the material concerned. This is of special importance in connection with the corrosive effects of the melt.

A limited number of solubility measurements have been carried out for the nitrates[1,2,3] and chlorides[4] of the alkali metals. All the results show that the solubility of the water is proportional to its vapour pressure above the melt. As a first stage in an investigation of the effect of water on the properties of molten salts it was decided to determine the solubility of water in various salts and to establish the state in which the water exists in the melt.

It has been noticed that if water is present in a melt, a polarographic wave is obtained at a certain voltage (depending on the reference electrode). As the water is removed, the "water" wave disappears[5,6,7]. This phenomenon was used in the present study. The experimental set-up is shown in Fig.16. Since a known pressure of water vapour was required over the sample, the polarographic cell was made vacuum tight. For high temperatures it is not convenient to use the normal dropping mercury electrode; thus a rotating platinum micro-electrode[8] was employed as the indicating electrode. The electrode was rotated at a constant speed of 200 r.p.m. The reference electrode was a platinum sheet of area 3 cm^2.

This satisfies the requirement of non-polarizability with respect to the indicating electrode. Heating was provided by means of a tube furnace which could be controlled to within $\pm$ 1°C. The required water vapour pressure was obtained by keeping a small amount of water at the appropriate temperature and checking the pressure with a mechanical pressure gauge.

The experimental technique was tested with a molten eutectic of $KNO_3/NaNO_3$ and was found to give results similar to those of other investigators.

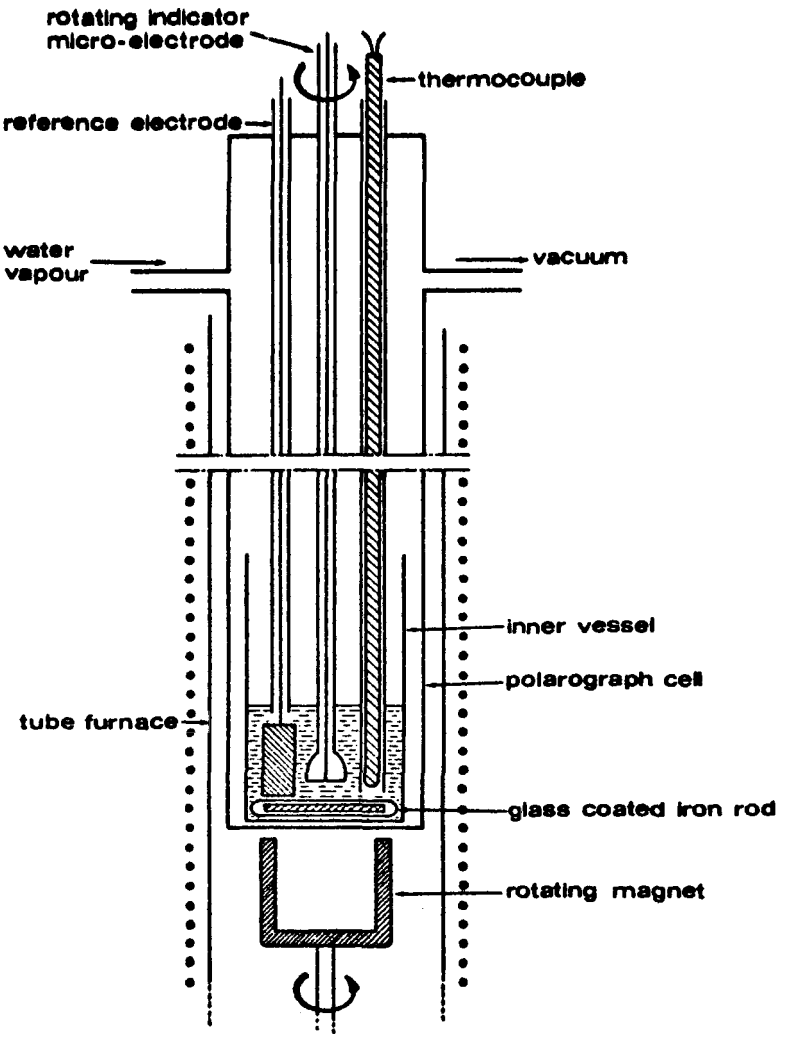

Fig.16

Experimental arrangement

The polarogram obtained is shown in Fig.17 . For cathodic polarization the residual current dropped to less than 1 μa after keeping the melt for 2 days under vacuum at 245°C. The persistence of the residual current seems to be due to traces of water still present. Similar results were found by Swofford[6]. Under the same drying treatment the anodic polarization showed a wave of about 5.0 μa and $E_{1/2}$ = - 0.103 volts. Addition of water vapour (17 to 40 mm Hg, the lower value being determined by the

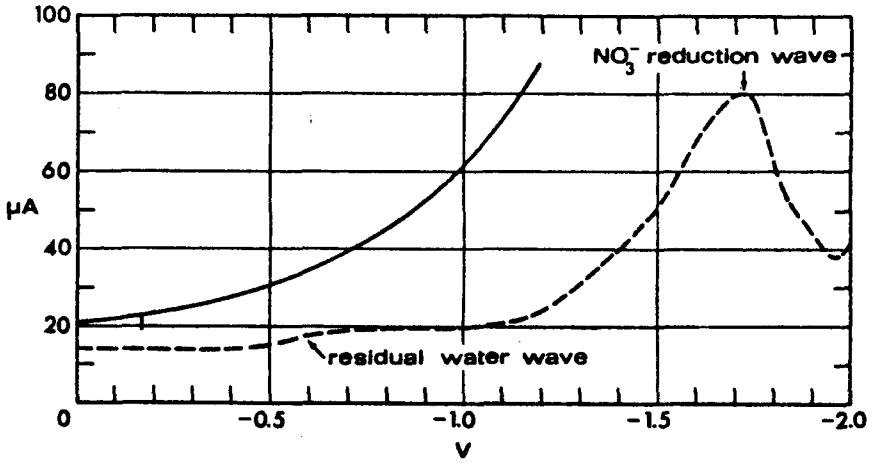

a

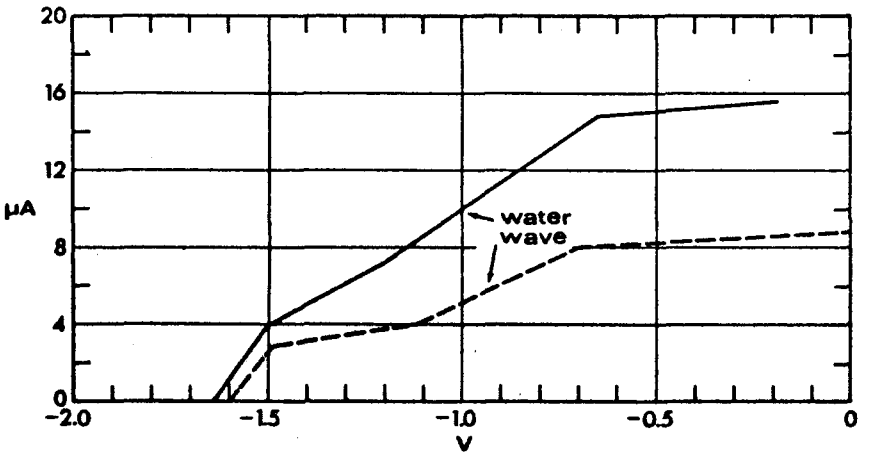

b

Fig.17

Polarograph of molten eutectic $NaNO_3/KNO_3$ (1:1). T = 245°C
a) cathodic polarization b) anodic polarization
— — — residual current ——— after addition of water vapour

limitations of the present experimental arrangement) gives an increase for both the cathodic and anodic waves. The cathodic wave proved difficult to interpret due to the proximity of the nitrate reduction wave, but a continuous increase in the height of the water wave with increasing water content was observed. The anodic wave for a pressure of 17 mm water showed a rapid increase to a limiting current of 8.5 μa, and virtually no further increase

as the pressure was increased to 40 mm. Thus it appears that the substance which causes the anodic wave reaches some saturation point. It was thought that perhaps O^{2-} ions were present as an impurity in the melt and reacted with the water to give OH^- ions[9]. However, addition of a small amount of sodium hydroxide did not produce any increase in the height of the anodic wave, but instead gave a wave in another position.

The next step in the investigation will be to attempt to identify the substance responsible for the anodic wave and also to find a method suitable for calibrating the water content of the melt to give absolute values of concentration.

References:

1. DUKE, F.R. and DOAN, A.S., Iowa State College, J. Sci., 32, 451 (1958).
2. BERTOZZI, G., Internal Report EURATOM, Ispra 827, June (1964).
3. FRAME, J.P., RHODES, E. and UBBELHODA, A.R., Trans. Far. Soc., 57, 1975 (1961).
4. BURKHARD, W.J. and CORBETT, J.D., J. Am. Chem. Soc., 79, 636 (1957).
5. LAITINEN, H.A., FERGUSON, W.S. and OSTERGOING, R.A., J. Electrochem. Soc., 104, 516 (1957).
6. SWOFFORD, H.S. and LAITINEN, H.A., J. Electrochem. Soc., 110, 814 (1963).
7. GECKLE, T.E., TID 21511 and N.S.A., 19, 17859 (1965).
8. AZIM, S. and RIDDIFORD, A.C., Anal. Chem., 34, 1023 (1962).
9. FRANCINE, M. and MARTINI, S., EUR 2496e.

Extraction of Zinc Halides from Molten Salts: M. Zangen

The distribution ratio D of $ZnCl_2$, $ZnBr_2$ and ZnI_2 between a eutectic mixture of molten $LiNO_3$ and KNO_3 (mole ratio K/Li = 1.33) and a eutectic mixture of polyphenyls[1] was determined radiometrically. The value of log D was found to decrease linearly with temperature in the range 150°-200°. The addition of potassium chloride or bromide to the nitrate melt caused a decrease in D. This can be explained by the formation of the inextractable anionic zinc halide complexes $ZnCl_3^-$, $ZnCl_4^=$ and $ZnBr_3^-$. The results are shown in Figs.18 and 19.

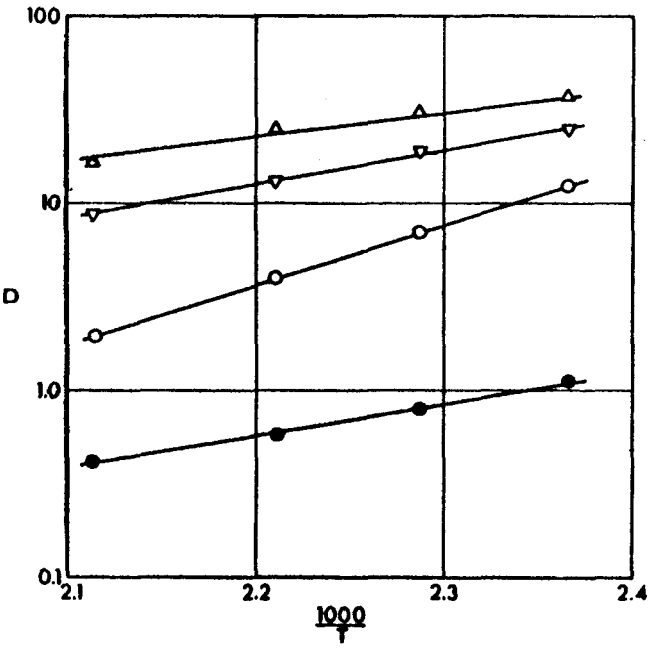

Fig.18

Distribution ratio of zinc halides between polyphenyl mixture and molten $LiNO_3$-KNO_3, as a function of temperature

△ - ZnI_2 ▽ - $ZnBr_2$ ○ - $ZnCl_2$ ● - $ZnCl_2$, with 0.3 molal KCl in the melt

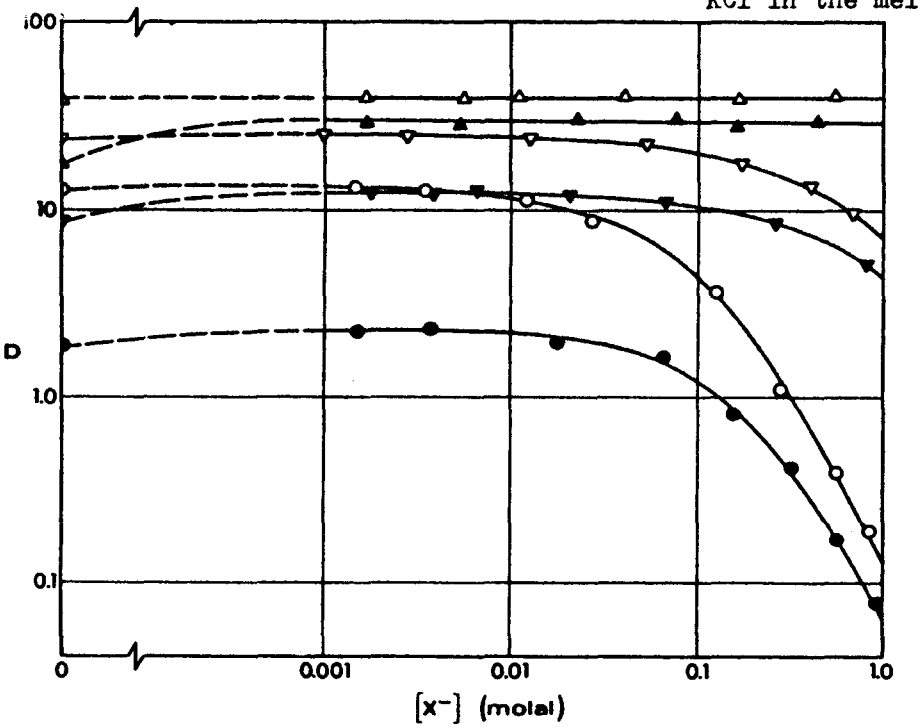

Fig. 19

Distribution ratio of zinc halides between polyphenyl mixture and molten $LiNO_3$-KNO_3, as a function of added potassium halide

○ - chloride ▽ - bromide △ - iodide

empty symbols - 150°; full symbols - 200°

Reference:

1. ZANGEN, M., MARCUS, Y., and FRIEDMAN, L. F., Israel J. Chem. 1, 312 (1963)

Phase Diagram of the System UCl_4-$PbCl_2$: R. Rafaeloff, J. L. Borowitz and A. Roy

The liquidus of the UCl_4-$PbCl_2$ system[1] has been completed and is shown in Fig.20 . It has been established that the system has only one eutectic, melting at 346°C and having a $UCl_4/PbCl_2$ ratio of 1:1. There is a single peritectic line at 387°C, on the $PbCl_2$-rich side of the diagram. The compound formed by the peritectic reaction seems to be very rich in $PbCl_2$, and will be further investigated by X-ray diffraction methods and differential thermal analysis. Mixtures around the presumed composition will be tested. Attempts will also be made to crystallize the compound and to analyse it chemically.

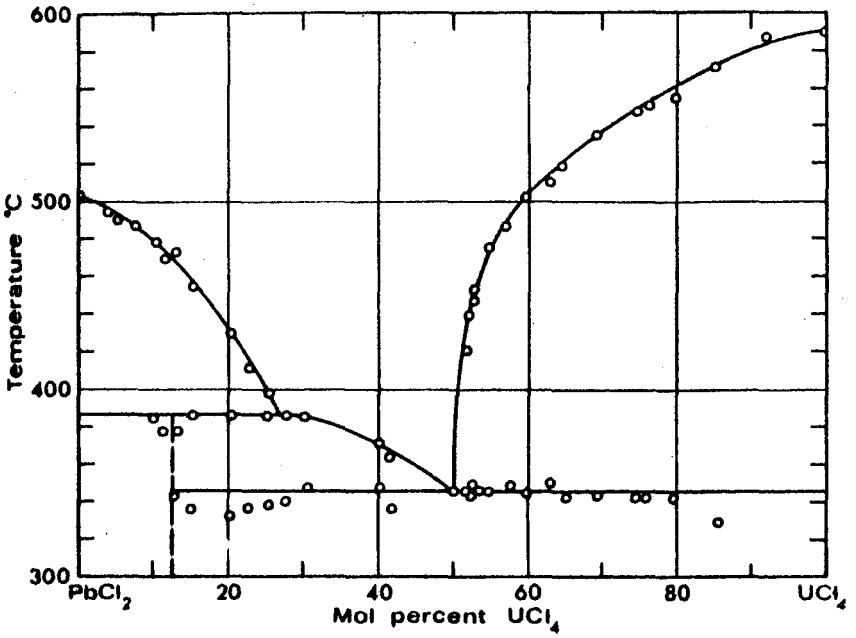

Fig. 20

Liquidus of the UCl_4-$PbCl_2$ system

From the phase diagram data, the thermodynamic ideality of the solutions and their regularity have been examined. A plot of $\ln N_A$ vs. $\frac{1}{T}$ (where N_A is the mole fraction of A, and T is the absolute temperature) is shown in Fig.21a for the $PbCl_2$-rich end of the liquidus line and in Fig. 21b for the UCl_4-rich end. The data fit the straight line for solutions between 100 and 88% $PbCl_2$ and between 100 and 70% UCl_4, indicating almost ideal behaviour of the solutions at these concentrations.

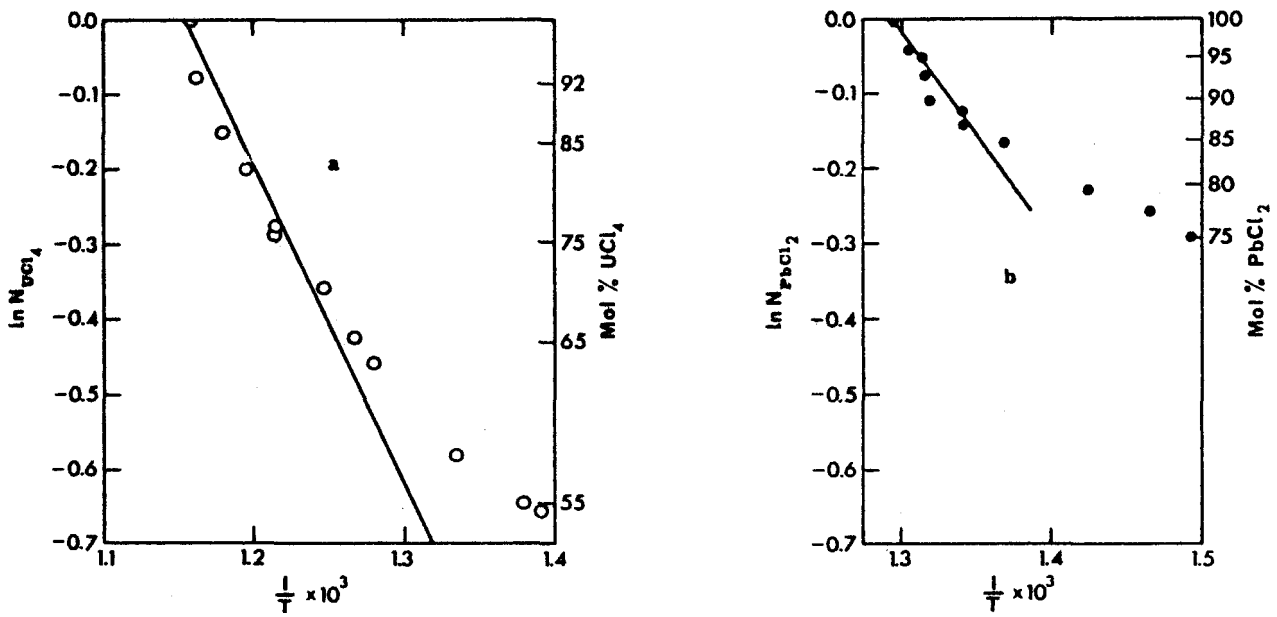

Fig. 21

Log of the mole fraction N_A as a function of the reciprocal of the absolute temperature T : a) for the $PbCl_2$-rich end of the liquidus line, b) for the UCl_4-rich end

Figure 22 shows the plots of the excess free energy of one component against the square of the mole fraction of the other component. The poor fit to straight lines indicates that the solutions are not regular, in the sense used by Hildebrand[2], beyond the ideal ranges of the diagram.

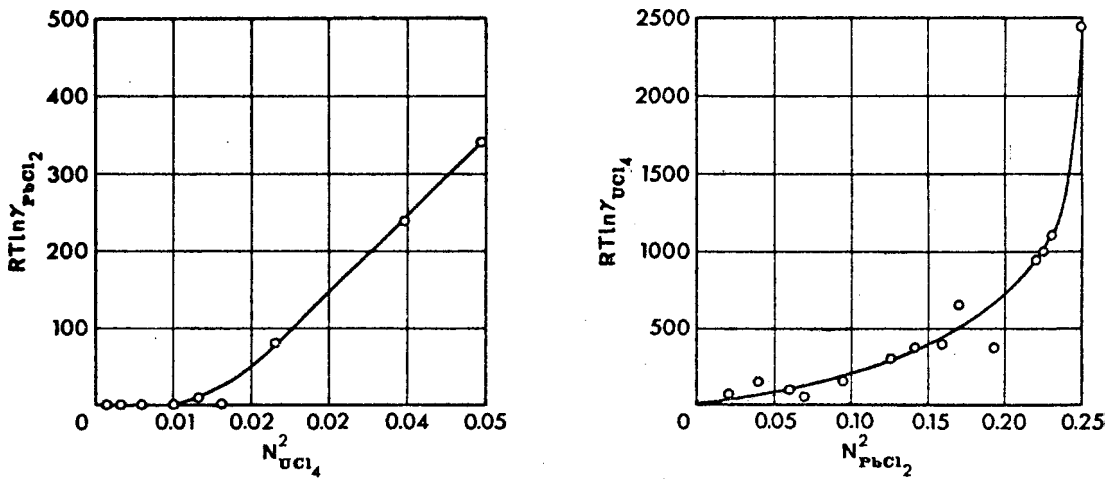

Fig.22

Excess free energy of one component as a function of the mole fraction of the other, for the UCL_4-$PbCl_2$ system

References:

1. BOROWITZ, J. L., RAFAELOFF, R. and ROY, A., Israel AEC Semi-Annual Report, July-Dec. 1964, IA-1021, p. 70

2. HILDEBRAND, J. H., J. Am. Chem. Soc., 51, 66 (1929)

Praseodymium Tetrafluoride: J. Soriano, M. Givon and J. Shamir*

The existence of PrF_4 has been a matter of controversy. Whereas Perros et al[1] stated that it should be thermodynamically stable, Cunningham et al[2] maintained that these calculations were based on erroneous data. All attempts to prepare the compound were unsuccessful (e.g. ref. 3).

---

* The Hebrew University, Jerusalem.

The only known fluorine compounds of Pr(IV) are complexes of the type Na_2PrF_6 which were prepared by Asprey and Keenan[4].

In our laboratory PrF_4 has been prepared by the following method. Na_2PrF_6 was transferred to a filter of porous P.T.F.E. in a vacuum system. Dry HF was distilled onto it, causing the complex to break up into its two components. The NaF dissolved in the HF and passed through the filter, while the PrF_4 remained behind. Analysis of the NaF showed it to be free of Pr. Analysis of the solid phase showed the presence of PrF_4, which decomposed into PrF_3 and HF when dissolved in the water. The yield was low, partly due to decomposition during the analysis since the very dry atmosphere required was not available.

References:

1. PERROS, T.P., MUNSON, T.R. and NAESER, C., J. Chem. Educ., 30, 402 (1953).
2. CUNNINGHAM, B.B., FEAY, P.C. and MOLLIER, M.A., J. Am. Chem. Soc., 76, 3361 (1954).
3. PERROS, T. and NAESER, C.R., J. Am Chem. Soc., 74, 1357 (1952).
4. ASPREY, L.B. and KEENAN, T.K., J. Inorg. Nucl. Chem., 16, 260 (1961).

Preparation of Praseodymium Dioxide: R. Rafaeloff.

A survey of the known methods of preparing tetravalent praseodymium compounds[1,2,3] indicated that the best starting material is PrO_2 [2]. Three techniques for preparing PrO_2 were tested:

a) refluxing Pr_6O_{11} in dilute acetic acid for a few hours;
b) oxidation of Pr_6O_{11} with oxygen at 350° and 50 atm for 100 hours;
c) oxidation of Pr_6O_{11} in $NaClO_3$ melt at about 300° for 8 hours.

In all three methods the product, a dark brown powder, was dried at 160°C for 24 hours. The purity of the prepared PrO_2 was tested by iodometric determination of the active oxygen, and by analysis for praseodymium

content by precipitation as oxalate. The oxalate was decomposed at 700°, and weighed as Pr_4O_7, or decomposed at 950° to Pr_6O_{11}. The praseodymium content of Pr_6O_{11} was determined by titration with EDTA. Both the first and third methods yield pure PrO_2, but the yield of the first method is low compared with the almost theoretical yield of the third. The PrO_2 obtained by oxidation under pressure according to the second method showed a lower content of active oxygen. The $NaClO_3$ melt method is thus recommended.

References:

1. PAJAKOFF, S.W., Nonatshefte fur Chemie, 74, 482 (1963).
2. SORIANO, J. and MARCUS, Y., Inorg. Chem., 3, 901 (1964).
3. PRANDTL, W. and HUTTNER, K., Z. anorg. allgem. Chem., 149, 235 (1925); PRANDTL, W. and RIEDER, G., Z. anorg. allgem. Chem., 233, 225 (1938).

Synthesis of Arsenic Oxyfluoride: J. Soriano and Y. Shamir*

Several methods have been tried for the synthesis of $AsOF_3$:

a) heating a mixture of As_2O_5 and AsF_5,

b) heating a mixture of As_2O_5 and CaF_2,

c) according to the series of reactions:

$$As_2O_3 + 3\ CaF_2 + 3\ H_2SO_4 \rightarrow 2\ AsF_3 + 3\ CaSO_4 + 3\ H_2O$$

$$2\ AsF_3 + 2\ Cl_2 \rightarrow 2\ AsCl_2F_3 \rightleftarrows [AsCl_4]^+\ [AsF_6]^-$$

$$[AsCl_4]^+\ [AsF_6]^- + 4\ N_2O_5 \rightarrow [As(ONO_2)_4]^+\ [AsF_6]^- + 4\ NO_2Cl$$

$$[As(ONO_2)_4]^+\ [AsF_6]^- \xrightarrow{400°C} 2\ AsOF_3 + 4\ NO_2 + O_2$$

In all three methods the yield were low (<10%). Chemical analysis, molecular weight determination and infra-red spectra showed that the product was not $AsOF_3$ as such, but possibly a polymer or an ionized species with composition $[AsO_2]^+\ [AsF_6]^-$.

The work is being continued in order to find better ways for synthesis, e.g. by oxidation of AsF_3 with ozone.

---

* The Hebrew University, Jerusalem.

Catalytic Effect of Chloride on the Thermal Decomposition of Perchlorates:
B. Carmon*, M. Steinberg**

It has been established by conventional methods that nitrogen-containing perchlorates oxidize Cr^{III} to Cr^{VI} in the presence of chloride[1]. No reaction occurs in the absence of chloride.

Experiments to investigate the role of the chloride were carried out using KCl labelled with Cl^{36}. The labelled KCl was mixed with NH_4ClO_4 at low pressure and heated to about 140°C. Preliminary results showed that the gaseous decomposition products contained about 1 to 5% of the Cl^{36} introduced. No radioactive gaseous products could be detected when KCl^{36} alone was heated. Similar experiments with $NOClO_4$ were less conclusive. The quantities used were between 0.3 and 0.5 millimoles of each of the reactants. The specific activity of KCl was about 1.5 μCi per gram.

Further experiments will be carried out with equimolar mixtures of KCl^{36} + NH_4ClO_4 and KCl^{36} + $KClO_4$ which will be decomposed at temperatures in the vicinity of 310, 370, 450 and above 520°C. The activity of the gaseous products will be compared with that of the residues. At a later stage decomposition will be carried out in presence of Cr_2O_3 and other oxides.

Reference:

1. STEINBERG, M., unpublished results.

Synthesis of O^{18}-Labelled Hydrogen Peroxide in H_2O^{16}: M. Anbar***, Z. Baruch*** and D. Meyerstein***

O^{18}-labelled hydrogen peroxide can be used to great advantage in the study of the mechanisms of auto-oxidative processes, the oxidation of water, and especially the reactions of hydrogen peroxide itself. In spite of this great potential demand no satisfactory method for preparing O^{18}-labelled H_2O_2 has been reported to date[1,2,3].

* Soreq Radioisotope Training Center
** Hebrew University, Jerusalem
*** Soreq Radiation Research Dept.

Many auto-oxidative processes produce hydroperoxides which yield H_2O_2 on hydrolysis. The problem was to prepare an O^{18}-labeled peroxide which could then be rapidly hydrolysed and the $H_2O_2^{18}$ removed as it is formed before it can be decomposed by any of the other products. The system chosen was the auto-oxidation of hydroxylamine in alkaline solution[4], in the presence of Ba^{++} ions which remove the peroxide in the form of sparingly soluble BaO_2. BaO_2 is then hydrolysed in acid solution and the H_2O_2 recovered by distillation under vacuum.

$Ba(ClO_4)_2$ was added to a solution of 0.2 M hydroxylamine sulphate, to give a 1 M solution of Ba^{+2} ions. The $BaSO_4$ was removed by centrifugation. 50 ml of the solution (0.2 M $NH_2OH.HClO_4$ + 1 M $BaClO_4$) was transferred into the reaction vessel, and 50 ml 2N NaOH added. The solution was then thoroughly degassed on a vacuum line (final concentration of $O_2 < 0.001$ mM). Approximately 250 ml O_2^{18} at 400 mm Hg was then added, and the solution stirred continuously for 18–24 hours with a magnetic stirrer. The overall pressure increases with time since, though the oxygen is absorbed, N_2 and N_2O are formed. BaO_2^{18} is precipitated. Over 90% of the oxygen was absorbed within 20 hours at room temperature. The BaO_2^{18} was separated by centrifugation and washed, after which it could be dried and stored. In order to recover $H_2O_2^{18}$, the BaO_2^{18} is dissolved in excess $HClO_4$ and then brought up to pH 4 with NaOH. The solution is distilled under vacuum, with a yield of 55 - 65%. Up to 0.2 M solutions of $H_2O_2^{18}$ were obtained by this procedure.

The overall yield based on the O_2^{18} used was 25 - 30%. The isotopic composition of the $H_2O_2^{18}$ produced, determined by the decomposition of H_2O_2 over Pt black, was the same as that of the oxygen used, within 1%. The yields were reproducible within ± 10% and the $H_2O_2^{18}$ obtained was free of impurities and could be stored for weeks in a polyethylene container without decomposition.

References:

1. ANBAR, M., GUTTMANN, S., and STEIN, G., J. Chem. Phys. 34, 703 (1961)

2. HALPERIN, P., and TAUBE, H., J. Am. Chem. Soc., 74, 380 (1952)

JARNAGIN, R. C. and WANG, J. H., J. Am. Chem. Soc. 80, 786 (1958)

VOLNOV, I. I., TSENTSIGER, A. B. and CHAMOVA, V. N., Izv. Akad. Nauk SSSR Otdel. Khim. Nauk, 1961, 531

3. ANBAR, M., J. Am. Chem. Soc. 83, 2031 (1961)

4. YAGIL, G. and ANBAR, M., J. Inorg. and Nucl. Chem. 26, 453 (1964)

On the Reaction of NO_2 with H_2O in the Presence of H_2O_2 : M. Anbar*, M. Faraggi* and D. Zehavi*

One of the problems raised during our study of the radiolytic behavior of nitric acid and nitrate ions was the possible reaction of nitrogen dioxide with hydrogen peroxide.

Nitrogen dioxide is known to react with water :

$$2\ NO_2 + H_2O \rightarrow NO_2^- + NO_3^- + 2\ H^+ \qquad (1)$$

Hydrogen peroxide would react with NO_2 according to:

$$2\ NO_2 + H_2O_2 \rightarrow 2\ NO_3^- + 2\ H^+ \qquad (2)$$

or

$$NO_2 + H_2O_2 \rightarrow O_2 + NO + H_2O \qquad (3)$$

In a system of NO_2, H_2O_2 and H_2O a decrease of the nitrite ion concentration compared with that in the absence of H_2O_2, or the appearance of O_2, would indicate a reaction between NO_2 and H_2O_2.

Two percent of nitrogen dioxide in argon were injected slowly (0.5 ml/min) into a stirred neutral aqueous solution of 5×10^{-4} M H_2O_2 purged with argon (oxygen content 0.1% as analyzed by chromatography). Gas samples taken during the reaction and after its completion showed no change in the oxygen content. Nitrite concentration analysis (Griess method) showed a yield equal to half the amount of NO_2 introduced, in quantitative agreement

---

* Radiation Research Dept.

with the yield in the $H_2O + NO_2$ reaction. These results indicate that under our experimental condition NO_2 reacts with H_2O (reaction 1) in preference to H_2O_2. As NO_2 reacts with water in a termolecular process involving the preequilibrium $2\ NO_2 \rightarrow N_2O_4$ it must be concluded that the $NO_2 + H_2O_2$ reaction is a relatively slow process, with $k_{NO_2 + H_2O_2} < 20\ M^{-1}\ sec^{-1}$.

H/D Isotope Effects in the Reduction of Water by Metals and Ions in Low States of Oxidation: M. Anbar*

Water undergoes reduction to hydrogen in neutral solutions by the action of alkali metals, alkaline earths and certain ions in low states of oxidation, such as Cr^{II} or Ti^{III}. In acid solutions the reduction reactions include all metals which are more electropositive than H^+. Some of these metals also reduce water in strongly alkaline solutions. The H/D isotope effects in the evolution of H_2 from many of these reactions have been interpreted in terms of the differences in the rates of cleavage of M-OH and MO-D bonds[1,2].

We have recently determined the H/D isotope effects in a number of reactions which have a strong bearing on the reduction of water, namely, $e^- + H_3O^+ \rightarrow H$, ($\alpha = 3.8 \pm 0.1$[3]), $e^-_{aq} + e^-_{aq} \rightarrow H_2$ ($\alpha = 4.7 \pm 0.2$[4]), and have shown that the reaction $e^-_{aq} + H$ produces H^- as its primary product[5]. In the present series of experiments, The H/D isotope effect in the reduction of water by Ti^{III} was determined both in neutral and alkaline solutions and found to be $\alpha = 4.65 \pm 0.1$. A similar isotope effect, $\alpha = 4.5$, was found for the Zn + Cu couple in acid solution. Isotope effects in the range 4.2 - 4.9 were reported for Zn, Al, Mn, Cr and Fe in acid solution[1,2]. It may be suggested that these reactions involve the formation of e^-_{aq}, which recombines to give H_2. This assumption is consistent with a recent report[6] on the effect of e^-_{aq} scavengers on the production of H_2 from sodium amalgam and water; e^-_{aq} was suggested as the primary intermediate in that reaction.

---

* Radiation Research Dept.

Another reaction investigated was the reduction of water by Cr^{II} chelated by tris-(β-aminoethyl)-amine, $N(CH_2CH_2NH_2)_3$. In this case $\alpha = 7.5 \pm 0.3$ was observed, which implies that the rate-determining step here does not involve the formation of e^-_{aq}. This isotope effect is comparable with that observed for pure Zn, pure Al and pure Fe[1,2] as well as for certain electrochemical processes in which the attachment of an H atom from water to the metal is assumed to be rate-determining[7]. This attachment is probably followed by a hydride ion transfer to water: $M\text{-}H + H_2O \rightarrow M + H_2 + OH^-$.

The isotope effect involved in the formation of H_2 by a hydride ion transfer to water was measured by Hughes, Ingold and Wilson[1] and found to be very close to unity. We have repeated this measurement studying the H/D isotope effect in the reaction of LiH with water, and found $\alpha = 1.03 + 0.03$. Moreover, the H_2 produced is a 1 : 1 combination of hydrogen atoms from the hydride ion and from the water: $LiH + D_2O \rightarrow HD$; the yield of H_2 and D_2 in this reaction is less than 1%.

References:

1. HUGHES, E.D., INGOLD, C.K. and WILSON, C.L., J. Chem. Soc., 493, (1934)
2. JOHNSTON, H.L. and DAVIS, G.O., J. Am. Chem. Soc., 64, 2613 (1942)
3. ANBAR, M. and MEYERSTEIN, D., J. Phys. Chem., 69, 698 (1965)
4. ANBAR, M. and MEYERSTEIN, D., This Report, p. 117, Chem. Commun., (in press)
5. ANBAR, M. and MEYERSTEIN, D., This Report, p. 119, Trans. Faraday Soc., (submitted)
6. HUGHES, G. and ROACH, R.J., Chem. Commun., 600, (1965)
7. BOCKRIS, B.E., Proc. Roy. Soc., Ser. A, 247, 400 (1958); 256, 128 (1960)

On the Mechanism of Deiodination of Iodoaromatic Compounds: M. Anbar*, S. Guttmann* and C. Friedman*.

In continuation of the investigation previously reported[1] kinetic studies have been carried out to clarify the mechanism of deiodination of iodoaromatic compounds.

Thin layer chromatography with an anion exchanger (Ecteola) was found to be very efficient and fast technique for the separation of organic and inorganic iodine. This procedure was applied for both preparative and analytical purposes.

No acid catalyzed deiodination of o-iodobenzoic acid was observed up to 1 M perchloric acid at 100°C. This precludes a simple electrophilic substitution mechanism for the deiodination reactions.

The possibility of formation of a transient iodonium ion was checked by following the formation of iodophenol from iodobenzoate + phenol, in the presence of copper ions and the reducing agents which were found to be effective in the deiodination reactions. No transiodinated product could be detected under these conditions.

The effect of substituents on the deiodination of o-iodobenzoate was examined. No marked changes in the rate of deiodination were found in the case of nitro substituted compounds. On the other hand, 2-iodo-3-hydroxy-benzoate was found to undergo much slower deiodination than the 2-iodo analogue.

Further experiments are in progress.

Reference:

1. ANBAR, M., GUTTMANN, S. and FRIEDMAN, C., Israel AEC Semi-Annual Report Jan.-June 1963, IA-900, p. 107.

---

* Radiation Research Dept.

LCAO-SCF Computation for Hydrogen Peroxide : U. Kaldor* and I. Shavitt**

The LCAO-SCF programs previously described[1] for calculating the properties of the H_2O_2 molecule were modified to permit the use of scaled wavefunctions in order to get better molecular energy values. Scaling of a function amounts to a uniform stretch of all vectors[2,3], and corresponds in our case to multiplying orbital exponents and dividing distances by a scale factor η . It is known[2] that the best scaled function automatically fulfills the virial theorem

$$\frac{-V}{2T} = 1 \qquad (1)$$

where V is the computed potential energy of the molecule and T is its kinetic energy.

We carried out computations for seven configurations of H_2O_2, differing only in the dihedral angles (Fig. 23a), and for a modified form of the molecule (Fig. 23b). The latter calculation was considered interesting because of the suggestion by Anbar[4] that an excited form of H_2O_2 might take part in photochemical decomposition, with the evolution of an oxygen radical.

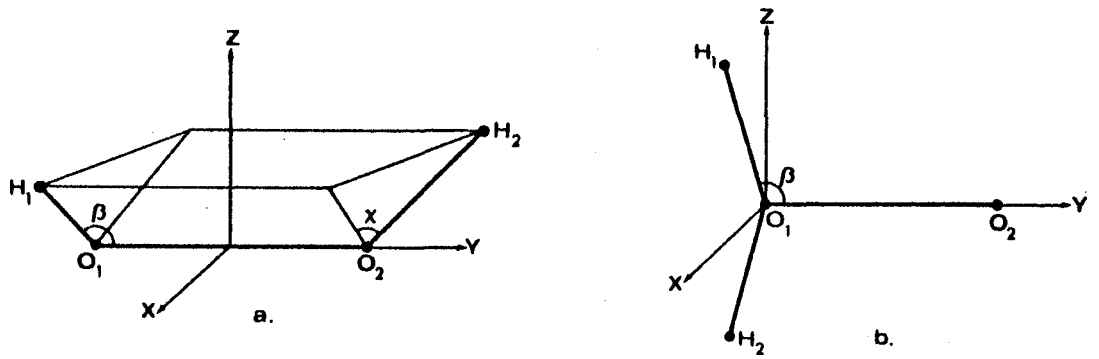

Fig. 23

Normal form (a) and modified form (b) of H_2O_2 molecule

* Soreq Radiation Research Dept.

** Technion - Israel Institute of Technology, Haifa

Computed energies, ionization potentials and dipole moments are given in Table 9

TABLE 9

Computed properties of H_2O_2

Form of H_2O_2	Dihedral angle	Total energy (au)	Ionization potential (eV)	Dipole moment (Debye)
Fig. 1a	0^o	-150.1375	10.40	2.236
	60^o	-150.1486	10.73	1.954
	100^o	-150.1549	11.08	1.493
	110^o	-150.1560	10.88	1.341
	120^o	-150.1565	10.65	1.161
	130^o	-150.1555	10.54	0.999
	180^o	-150.1528	10.18	0.000
Fig. 1b		-150.0019	5.69	3.219

The total energies were fitted by a least squares procedure to a series of the form $A_n \cos n\chi$, where χ is the dihedral angle. The best simple fit was obtained with the expression

$$\text{Energy (au)} = -150.14984 \pm 0.00765 \cos\chi + 0.00461 \cos 2\chi$$

for which the greatest deviation is 0.0006 au. A somewhat better fit, with a maximum deviation of 0.0004 au, was obtained with the expression

$$\text{Energy (au)} = -150.14992 \pm 0.00760 \cos\chi + 0.00444 \cos 2\chi + 0.00034 \cos 4\chi$$

The computed potential barriers to internal rotation are 2.2 kcal/mole for the transposition and 11.8 for the cis, compared with the experimental values[5] of 1.1 and 7.0 kcal/mole respectively. It should be noted that the barriers are obtained as differences of energy values of the order of 10^5 kcal/mole, and that the error in each of these values is of the order of 10^3 kcal/mole. The computed barriers are therefore in quite good agreement with experiment. The energy of the modified form H_2-O-O (Fig. 23b) is 4.2 eV higher than that of the normal form. This value should be regarded

as an upper limit, because the internuclear distances used are those found experimentally for normal H_2O_2, and it is unlikely that they are the best distances for the modified form.

References:

1. KALICH, U., Israel AEC Semi-Annual Reports, IA-900, Jan.-June (1963) p. 108; IA-920, July-Dec. (1963) p. 110; IA-984, Jan.-June (1964) p. 97; IA-1021, July-Dec. (1964) p. 89.
2. LOWDIN , P.O., Advances in Chemical Physics, Edited by I. Prigogine (Interscience Publishers, New York, 1959), Vol. 2, p. 207.
3. BOYS, S.F., and SHAVITT, I., University of Wisconsin Naval Research Laboratory, Report WIS-AF-13, March 4,(1962).
4. ANBAR, M.,Trans. Faraday Soc., 57, 971 (1961)
5. HUNT, R.H., LEACOCK, R.A., PETERS, C.W. and HECHT, K.H., J. Chem. Phys., 42, 1931 (1965).

LCAO- SCF Computations for Ammonia* : U. Kaldor** and I. Shavitt***

The LCAO-SCF method (see previous item) was used to obtain wavefunctions and energies for the ammonia molecule. The geometry of the molecule and coordinate system used are shown in Fig. 24 The geometrical parameters varied were the bond length R(N-H) and the angle θ between the threefold

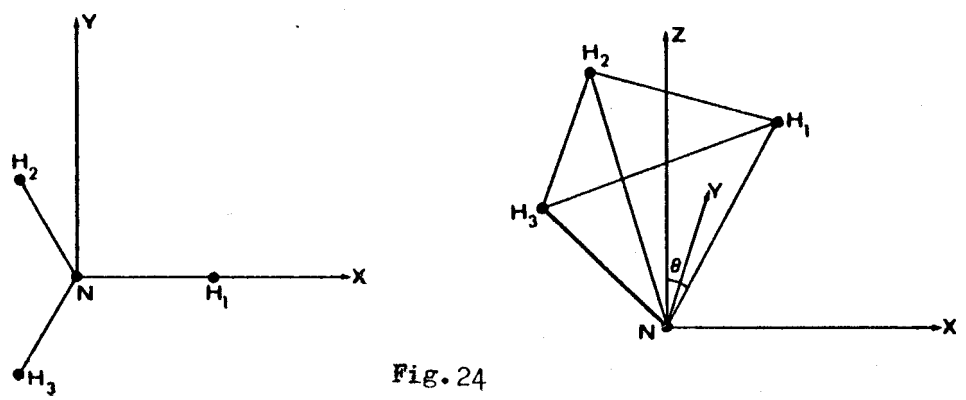

Fig. 24

Geometry of the NH_3 molecule and the coordinate system

* Part of a D.Sc. Thesis to be submitted by U. Kaldor to the Technion - Israel Institute of Technology, Haifa

** Soreq Radiation Research Dept.

*** Technion - Israel Institute of Technology, Haifa

rotation axis (Z axis) and the N-H bond. The basis set consisted of Slater orbitals. The exponents of the nitrogen orbitals were chosen according to Slater's rules: 6.7 for the 1s and 1.95 for the 2s and 2p orbitals. Two values, 1 and 1.2, were tried for the hydrogen 1s orbitals. The second value gave better results for all configurations investigated.

The computed quantities of the various configurations are given in Table 10. In Table 11 our results are compared with the experimental quantities and with the results of Moccia's one center expansion[1] in a basis set of 30 functions. Further computations with more basis functions centered on the nitrogen atom are now being carried out.

TABLE 10

Computed properties of NH_3

Bond length R(N-H) (au)	θ	Energy (au)	Ionization potential (eV)	Dipole moment (Debye)
1.9	60°	-55.99972	10.90	2.12
1.95	60°	-56.00367	10.83	2.08
2.0	60°	-56.00364	10.76	2.04
1.9	64°	-56.00434	10.47	1.97
1.95	64°	-56.00730	10.38	1.94
2.0	64°	-56.00633	10.31	1.91
1.96	65°	-56.00754	10.36	1.89
1.916	68°	-56.00584	10.03	1.78
1.95	68°	-56.00672	9.96	1.77
2.0	68°	-56.00480	9.88	1.75
1.9	72°	-56.00234	9.71	1.57
1.95	72°	-56.00334	9.59	1.56
2.0	72°	-56.00047	9.49	1.55
1.8	90°	-55.97836	9.31	0.00
1.9	90°	-55.98903	8.95	0.00
1.91	90°	-55.98911	8.92	0.00
2.0	90°	-55.98190	8.65	0.00

TABLE 11

Property	Experimental	One center expansion[1]	Present work
Total energy (au)	-56.578	-55.9748	-56.0076
Binding energy (au)	0.446	0.177	0.210
Inversion barrier (eV)	0.23[2]	0.0732	0.50
Dipole moment (Debye)	1.48	1.51	1.89
Bond length R(N-H) (au)	1.916	1.968	1.96
θ	68°	71.1°	65°
Ionization potentials (eV)	10.3[3] 11.0[4] 15.3[5] 17.0[4]	11.28 16.21	10.36 15.25

References:

1. MOCCIA, R., J. Chem. Phys., 40, 2176 (1964)
2. SWALEN, J.D., and IBERS, J.A., J. Chem. Phys., 36, 1914 (1962)
3. KISER, R.W. and GALLEGOS, E.J., J. Phys. Chem., 66, 947 (1962)
4. SUN, H. and WEISSLER, G.L., J. Chem. Phys., 23, 1160 (1955)
5. McDOWELL, C.A., J. Chem. Phys., 24, 618 (1956).

LCAO-SCF Computations for Ethylene : U. Kaldor* and I. Shavitt**

Our LCAO-SCF computer programs have been modified (see previous items) and they can now handle certain cases of open-shell electronic configurations[1]. The first molecule treated by the more flexible programs was ethylene, which is the simplest organic molecule having a double bond and is therefore useful for checking various approximations before applying them to bigger molecules. Most computations for the ethylene molecule

* Soreq Radiation Research Dept.
** Technion - Israel Institute of Technology, Haifa

hitherto carried out are of a semi-empirical nature, and one of the aims of this work was to check the validity of some of the assumptions made in these computations.

Computations were carried out for seven configurations, differing only in the angle between the planes of the two CH_2 groups (Fig.25). For each configuration we obtained the wavefunctions of the lowest singlet and triplet states and of the ground state of the cation and anion. The results are given in Table 12.

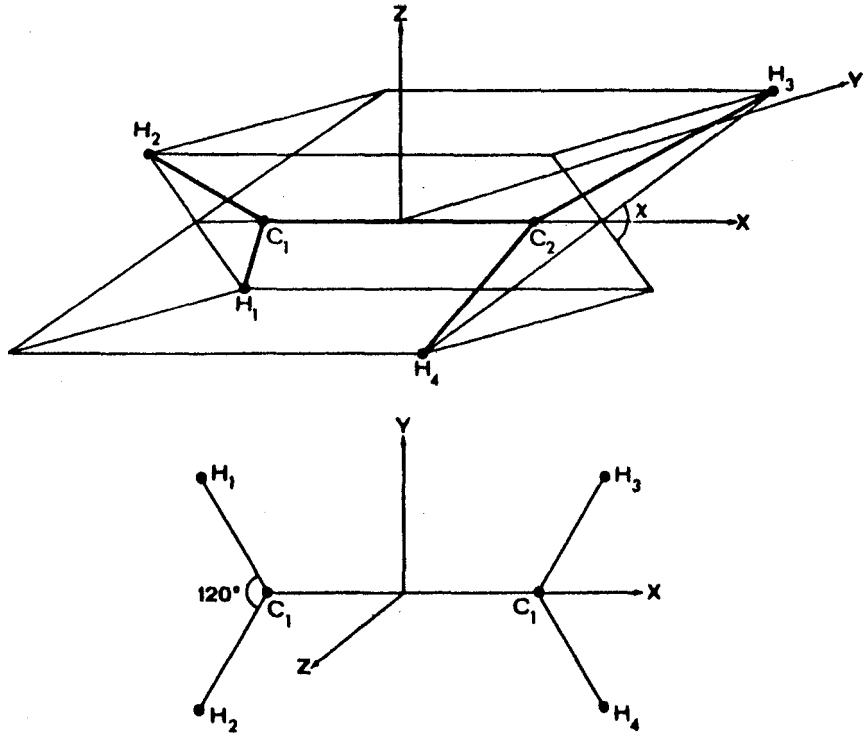

Fig. 25

Geometry of the ethylene molecule and the coordinate system

The computed wavefunctions are being analysed further in order to evaluate the effects of the sigma-pi separation usually assumed in semi-empirical calculations.

TABLE 12

Computed energy of ethylene (au)

Angle	Singlet	Triplet	Cation	Anion
0°	-77.83549	-77.71058	-77.49840	-77.63005
15°	-77.82962	-77.71421	-77.49832	-77.62977
30°	-77.81184	-77.72349	-77.49641	-77.62756
45°	-77.78251	-77.73536	-77.49007	-77.62128
60°	-77.74196	-77.74643	-77.47718	-77.60859
75°	-77.69082	-77.75409	-77.45678	-77.58807
90°		-77.75681		

Reference:

1. ROOTHAAN, C. C. J., Revs. Mod. Phys., 32, 179 (1960)

2. RADIATION CHEMISTRY

Mechanisms of Reactions of Hydrated Electrons[1] : M. Anbar

The reactions of solvated electrons are simply electron transfer processes, and as such they are the most elementary reduction reactions. With the discovery of radiolytically produced solvated electrons, it has become possible to study electron transfer processes directly and unambiguously. The rates of reactions of e^-_{aq} with a great number of different chemical species have been determined. These rates range from 16 M^{-1} sec^{-1} up to diffusion controlled processes.

The reactions of e^-_{aq} with any neutral chemical species may be expressed by the general formulation $e^-_{aq} + AB \rightarrow AB^- \rightarrow A + B^-$. The primary product AB^- may be stable and show up as the final product, or it may be unstable and dissociate to give a stable negative ion B^- and a free radical A, or a stable molecule A and a radical ion B^-. AB^- may react with water to give $ABH + OH^-$, and ABH may or may not undergo further chemical changes. When another reagent is present, AB^- may eventually transfer an electron to it: $AB^- + X \rightarrow AB + X^-$.

An extensive review of the reactions of hydrated electrons was published recently[1]. In this report we shall discuss some of the reactions of e^-_{aq} studied in our laboratory during 1965.

I. Metal Ion and Metal Ion Complexes

Alkali metal and alkaline earth ions (with the possible exception of Mg^{+2}) do not react with e^-_{aq}. This is expected in view of the redox potential of the hydrated electron, $E^o = + 2.7$ V. All other metal ions are liable to reduction by e^-_{aq}, the specific rates ranging from 7×10^{10} M^{-1} sec^{-1} for Tl^+ down to 7.7×10^7 M^{-1} sec^{-1} for Mn^{+2}_{aq} [2].

It has been suggested that the reactivity of metal ions is linearly correlated with their $M^{++} - M^{+}$ redox potentials, or with the related parameter of electron affinity[3]. Both correlations however have been shown to be open to serious criticism[1].

As an alternative mechanism we suggested that the availability of a vacant d orbital on the central atom and the gain in energy on addition of an electron into it are the major factors which determine the reactivity of transition metal ions. Taking the series Cr^{+2}, Mn^{+2}, Fe^{+2}, Co^{+2}, Ni^{+2}, Cu^{+2}, Zn^{+2} one sees that adding an electron to the $3d^4$ Cr^{+2} results in a maximum gain in exchange energy, since the electron spin is parallel to the four spins on the metal. This would explain the high reactivity of Cr^{+2} toward e^-_{aq} ($k = 4.2 \times 10^{10}$ M^{-1} sec^{-1})[2]. The next metal in this series is $3d^5$ Mn^{+2}. A sixth electron added must have its spin antiparallel to all the electrons already present, and so it is not stabilized at all. Moreover, it undergoes electrostatic repulsion in its paired orbital. This results in a relatively low reactivity toward e^-_{aq} ($k = 7.7 \times 10^{7}$ M^{-1} sec^{-1} see ref. 4). The addition of an electron to $3d^6$ Fe^{+2} results in some gain in exchange energy, which increases for $3d^7$ Co^{+2} and $3d^8$ Ni^{+2}. In the case of $3d^9$ Cu^{+2} the gain in exchange energy is maximal and comparable to that in Cr^{+2}, and indeed Cu^{+2} approaches Cr^{+2} in its specific rate (3.3×10^{10} M^{-1} sec^{-1} [5]). $3d^{10}$ Zn^{-2} is obviously expected to have a low reactivity, as all the 3d orbitals are filled and the extra electron has to be placed in the next outer shell[6].

The presence of ligands may affect the reactivity of the central atom in two ways: first, by changing the ligand field, and second, by acting as a bridge for electron transfer to the central atom. Ligands of high spectrochemical power, like CN^-, will exert their action by the first mechanism. This may explain the general tendency of cyano-complexes to be less reactive compared with halo complexes[2]. As cyanide ions induce a strong ligand field they will also change the spin distribution in the d orbitals. As expected from this scheme, ferrocyanide ions were found

quite unreactive toward e^-_{aq} ($k \ll 10^5$), owing to the fact that the additional electron has to enter a vacant e_g orbital with a high Δ. On the other hand, $Mn(CN)_6^{-4}$ was found to be much more reactive than Mn^{+2}_{aq} (2.5×10^{10} compared with 7.7×10^7 M^{-1} sec^{-1}) owing to the spin coupling which makes the accommodation of an additional electron in the low t_{2g} orbitals rather favorable. $Cr(CN)_6^{-4}$ was also found to be more reactive than Cr^{+2}_{aq}, in accord with this theory.

II. Aliphatic Compounds

Olefines show some reactivity toward e^-_{aq} ($k_{e^-_{aq} + CH_2:CH_2} = 7.6 \times 10^6$ M^{-1} sec^{-1} (11)). Conjugated olefines are more reactive, e.g. $k_{e^-_{aq} + \text{butadiene}} = 2.4 \times 10^8$ M^{-1} sec^{-1} (11). The accommodation of an electron on an olefine molecule may be looked upon as analogous to the addition of a nucleophilic reagent. In the latter case it has been shown(7) that if the carbon is activated by electron-withdrawing groups it can be directly attacked by nucleophils. e^-_{aq} is clearly a most efficient nucleophil, thus it may interact with a carbon atom adjacent to any double bond, provided this is not specially deactivated. Conjugation will obviously increase the chances of having the carbon positively polarized. The carbon on a carbonyl group is also positively polarized and may be attacked by e^-_{aq} - hence the fairly high reactivity of aldehydes and ketones. If this carbon is deactivated by an electron-donating group like a hydroxyl, alkoxy or amino group, its reactivity toward e^-_{aq} will be inhibited, as seen from the following comparative reactivities: the lower reactivity of acetic acid as compared with acetone ($k = 0.18$ and 5.6×10^9 M^{-1} sec^{-1} respectively (2)); the relatively low reactivity of acetamide and urea for which k is about 1.7×10^7 and 3×10^5 M^{-1} sec^{-1} respectively; the low reactivity of esters compared with aldehydes and ketones(8); and the even lower reactivities of lactic, citric and oxalic

as compared with that of acetic acid. Carboxylate ions are even less reactive toward e^-_{aq}, which is in accord with the fact that the carbon atom of the carboxylate is completely deactivated toward nucleophils.

Another group of aliphatic compounds which have been thoroughly investigated as to their reactivity toward e^-_{aq} are the haloaliphatic compounds . It was shown that neighboring groups which increase the positive polarization of the halogen increase the reactivity toward e^-_{aq} [9]. In other words, it may be assumed that the electron is accommodated on the halogen, forming RX^- as an intermediate. An alternative suggestion that has been advanced[8] is that the effect of near-by groups is due to the weakening of the C - X bond which undergoes cleavage in the rate determining step $RX + e^-_{aq} \rightarrow R + X^-$, and that RX^- is an activated complex and not an intermediate[3]. In order to decide between the two theories we investigated the reactivity of CF_3Cl. The C - Cl bond in this compound is of comparable strength to that in CH_3Cl, but the Cl atom is extremely polarized. It was found that CF_3Cl undergoes dechlorination by e^-_{aq} at a rate which is about two orders of magnitude faster than the reaction with RCH_2Cl, thus supporting the mechanism of accommodation of an electron on the halogen, forming RX^- as an intermediate.

III. Aromatic Compounds

The reactivity of aromatic compounds toward hydrated electrons has been extensively investigated[10] and this group of organic compounds is the largest for which a unified theory of reactivity could be developed. The reactivity of these compounds toward e^-_{aq} is a function of the electron density in the π orbitals of the aromatic rings, as expressed by Hammett's σ-function. This correlation holds over four orders of magnitude of specific rates, from phenol which reacts at 4×10^6 M^{-1} sec^{-1}, up to nitrobenzene with a rate constant of 3×10^{10} M^{-1} sec^{-1}, which is practically diffusion controlled. It is suggested that e^-_{aq} reacts with

aromatic compounds as a most reactive nucleophil which attacks a positive center on the ring. The probability of formation of such a center is inversely proportional to the density of the π electrons, just as the probability of an electrophilic attack is directly proportional to it.

References:

1. ANBAR, M., Solvated Electrons, Am. Chem. Soc., Advn. Chem. Ser. 50, 55 (1965)
2. ANBAR, M. and HART, E. J., J. Phys. Chem. 69, 973 (1965)
3. DORFMAN, L. M. and MATHESON, M. S., in Prog. in Reaction Kinetics, 3, 237 (1965)
4. BAXENDALE, J. H. et al., Nature 401, 468 (1964)
5. ANBAR, M. and NETA, P., Intern. J. Appl. Radiation and Isotopes 16, 227 (1965)
6. ANBAR, M. and THOMAS, J. K., J. Phys. Chem. 68, 3829 (1964)
7. HINE, J., Physical Organic Chemistry, 2nd ed. McGraw-Hill, New York (1962)
8. THOMAS, J. K., GORDON, S. and HART, E. J., J. Phys. Chem. 68, 1524 (1964)
9. ANBAR, M. and HART, E. J., J. Phys. Chem. 69, 271 (1965)
10. ANBAR, M. and HART, E. J., J. Am. Chem. Soc. 86, 1633 (1964)
11. HART, E. J., THOMAS, J. K. and GORDON, S., Radiation Res., Suppl. 4, 79 (1964)

Reactivity of Solvated Electrons in 2-Propanol : W. V. Sherman

The radiation-induced reactions occurring in propanol solutions have been studied. Particular attention was paid to the reactions of solvated electrons, since this species is known to be an important precursor of the final products. It has been shown[1] that the yield of molecular nitrogen in the radiolysis of solutions of nitrous oxide in 2-propanol is a measure of the solvated electrons scavenged by this solute. By allowing a second solute, S, to compete with nitrous oxide for solvated electrons we have determined the reactivities of a number of these solutes. The results are summarized in Table 13.

The reactions of solvated electrons with monosubstituted benzenes follow the general pattern of bimolecular nucleophilic substitution. This indicates that the rate determining step is the localized interaction of the solvated electron with the aromatic ring. There is a satisfactory

TABLE 13

Reactivity towards solvated electrons in 2-propanol

Solute S	$k_{e^-} + S / k_{e^-} + N_2O$
H^+	0.51
carbon tetrachloride	2.3
acetone	0.59
benzene	0.021
phenol	0.011
toluene	0.018
fluorobenzene	0.051
chlorobenzene	0.53
benzoic acid	0.97
acetophenone	1.7
benzophenone	1.3
benzonitrile	0.94
nitrobenzene	2.4

correlation between reactivity and the Hammett σ_{para} -functions. In this respect the reactions of electrons in 2-propanol qualitatively resemble those of the hydrated electron[2]. Quantitatively, however, the solvated electron in 2-propanol is less sensitive to substituent effects. This is reflected in the observed $\rho = 3.1$, which is significantly less than the value of 4.8 (ref.2) found for the hydrated electron.

References:

1. SHERMAN, W. V., J. Phys. Chem., (in press)

2. ANBAR, M. and HART, E. J., J. Am. Chem. Soc., 86, 5633 (1964)

Electron Scavenging Processes in Irradiated Cyclohexane Solutions : W. V. Sherman

The radiation chemistry of dilute solutions of nitrous oxide in cyclohexane has been studied. Evidence was found[1] to support the suggestion of

Scholes and Simic[2] that the electron is the precursor of the observed molecular nitrogen. The effect of potential electron acceptors on the nitrogen yield was examined; a correlation was observed between gas-phase electron affinities, as measured by Lovelock's method[3] and the ability of a particular electron acceptor to compete with nitrous oxide for the precursor of molecular nitrogen. The reactivity of monosubstituted benzenes towards electrons produced radiolytically in cyclohexane does not follow the pattern of bimolecular nucleophilic substitution. From this result it may be inferred that the rate determining step does not involve a localized interaction between the electron and the aromatic nucleus.

References:

1. SHERMAN, W. V., J. Chem. Soc., (in press)
2. SCHOLES, G. and SIMIC, M., Nature, 202, 895 (1964)
3. LOVELOCK, J. E., SIMMONDS, P. G. and Van den HEUVEL, Nature, 197, 249 (1963) and references therein

The H/D Isotope Effect in Hydrogen Generated Photolytically by the $e^-_{aq} + e^-_{aq}$ Reaction : M. Anbar and D. Meyerstein

The measurement of isotope effects in the radiolytic production of hydrogen from aqueous solutions has been shown to provide clues to the mechanism of this process. On the basis of the H/D isotope effect we suggested previously[1] that "molecular" hydrogen is not formed in the spur by the reaction $e^-_{aq} + e^-_{aq} \rightarrow H_2 + 2OH^-_{aq}$. As it has often been assumed that this reaction is responsible for the formation of a major part of the "molecular" hydrogen[2] we rechecked our conclusions by comparing the H/D isotope effect in the production of "molecular" hydrogen, α_M , with that of $e^-_{aq} + e^-_{aq}$ reaction, α_e .

Aquated electrons may be produced at a high rate by the photochemical process $OH^-_{aq} \xrightarrow{h\nu} OH + e^-_{aq}$ [3]. CD_3OH is added as an OH scavenger since it has little affinity for e^-_{aq} and H atoms.

Aquated electrons were produced by illuminating an alkaline solution (pH 14) containing 0.025 M CD_3OH with ultraviolet light (185 mμ) at 25°C. The light source was a mercury discharge tube with an output of the order of 10^{-6} einstein/cm^2.min. OH^-_{aq} has a high extinction coefficient at 185 mμ[4], so that 99% of the light was absorbed in a layer of less than 0.02 mm, giving a high steady state local concentration of e^-_{aq} (of the order of 10^{-6} M). Under the conditions of the experiment 2% of the hydrogen produced originated from D abstraction from CD_3OH, thus introducing a small systematic error which may however easily be corrected for (CD_3OH in H_2O gave $HD/H_2 = 0.02$).

The H/D isotope effect measured by this method was $\alpha_e = 3.9 \pm 0.2$, 4.7 ± 0.2 and 5.5 ± 0.2 for solutions containing 25, 50 and 75 atom percent deuterium respectively. The isotope effect in the "molecular" hydrogen, $\alpha_M = 2.2 \pm 0.1$, is significantly smaller than these values, confirming the conclusion that the major part of the "molecular" hydrogen does not arise from the $e^-_{aq} + e^-_{aq}$ reaction. This conclusion is further supported by the effect of scavengers on the yield of "molecular" hydrogen[5].

The isotope effect in the $e^-_{aq} + e^-_{aq}$ reaction may be of help in elucidating the mechanism of this process. One may assume that the two electrons form a transition state involving several water molecules with two diagonally opposed negatively charged centers and two stretched O - H bonds in the middle. This configuration is eventually transformed into a hydrogen molecule plus two receding OH^-_{aq} ions. Although the $e^-_{aq} + e^-_{aq}$ interaction is diffusion controlled as measured by pulsed radiolysis, the observed rate is that of the formation of the $(e^-_{aq})_2$ center which subsequently decomposes to give $H_2 + 2OH^-_{aq}$, with a preferential cleavage of H - O bonds. The involvement of several water molecules in the $(e^-_{aq})_2$ center may explain the change in α_e with the

deuterium concentration.

References:

1. ANBAR, M. and MEYERSTEIN, D., J. Phys. Chem., 69, 698 (1965)
2. See for example SCHWARZ, H. A., Radiation Res. Suppl.4, 89 (1964)
3. See for example, MATHESON, M. S., MULAC, W. A. and RABANI, J., J. Phys. Chem., 67, 2613 (1963)
4. JORTNER, J., RAZ, B. and STEIN, G., J. Chem. Phys., 34, 1455 (1961)
5. SWORSKI, T. J., J. Am. Chem. Soc., 86, 5034 (1964)

H/D Isotope Effects in the Formation of Hydrogen from the Combination of Two Radicals in Aqueous Solutions [1] : M. Anbar and D. Meyerstein

The "primary" products formed in the radiolysis of water include hydrated electrons, hydrogen atoms and molecular hydrogen[2]. Hydrogen molecules may be produced from hydrogen atoms and hydrated electrons by the combination reactions: $H + H \rightarrow H_2$, $H + e^-_{aq} \rightarrow H_2$ and $e^-_{aq} + e^-_{aq} \rightarrow H_2$. Two alternative explanations have been suggested for the fact that "molecular" hydrogen is produced even if e^-_{aq} and H atom scavengers are present in concentrations sufficient to eliminate any radical - radical combination. One is that the above combination reactions continue to occur in "spurs" inaccessible to scavengers at low concentrations[3-5]. The other is that "molecular" hydrogen is formed by a process such as $H_2O^* + H_2O \rightarrow H_2 + (2\ OH)$ [6].

The H/D isotope effects in the $e^-_{aq} + e^-_{aq}$ [7], $H^- + H_2O$ [8], and $H + RH$[9,10] reactions, as well as in the $e^-_{aq} + H_3O^+$ and $e^-_{aq} + NH_4^+$[11] reactions have been shown to cast some light on this problem. It has also been shown that the isotope effect in photolytically formed hydrogen from the $e^-_{aq} + e^-_{aq}$ reaction differs significantly from that in the formation of the radiolytic "molecular" hydrogen[7]. This finding has far-reaching implications for the interpretation of the mechanism of the primary reactions in the radiolysis of water. It thus seems that a systematic

study of the H/D isotope effects in the formation of hydrogen from radiolysed water would lead to a better understanding of this process.

In order to evaluate the isotope effect in the formation of hydrogen from radiolysed water one has to consider the following reactions:

$$H_2O \rightsquigarrow H_2 \text{ (molecular)} \qquad (1)$$

$$e^-_{aq} + e^-_{aq} \rightarrow H_2 \qquad (2)$$

$$e^-_{aq} + H \rightarrow H_2 \qquad (3)$$

$$H + H \rightarrow H_2 \qquad (4)$$

$$e^-_{aq} + OH \rightarrow OH^- \qquad (5)$$

$$H_2O \rightsquigarrow H \qquad (6)$$

$$e^-_{aq} + H_3O^+ \rightarrow H + H_2O \qquad (7)$$

$$e^-_{aq} + H_2O \rightarrow H + OH^- \qquad (8)$$

$$e^-_{aq} + H_2O_2 \rightarrow OH^- + OH \qquad (9)$$

$$H + OH^- \rightarrow e^-_{aq} \qquad (10)$$

$$OH + H_2 \rightarrow H + H_2O \qquad (11)$$

Hydrogen molecules are formed in reactions (1), (2), (3) and (4). The relative contributions of reaction (2), (3) and (4) depend on the acidity of the system, owing to reactions (7) and (10). Hydrogen is destroyed by OH radicals via reaction (11), which has a considerable H/D isotope effect. Reaction (11) thus affects the overall isotopic composition of the radiolytic hydrogen, in addition to reducing the hydrogen yield. It is evident, therefore, that in order to obtain meaningful results OH radicals must be eliminated by the addition of a scavenger. Such a scavenger should, as far as possible, be non-reactive toward e^-_{aq} and H atoms, and its oxidation products should be so too. Deuterated methanol, CD_3OH, approaches these requirements, being non-reactive toward e^-_{aq}, and reacting with H atoms at a specific rate of 8×10^4 M^{-1} sec^{-1}, compared with 2.3×10^8 M^{-1} sec^{-1} for OH radicals. When CD_3OH is added, one has to consider the reactions

$$OH + CD_3OH \rightarrow H_2O + CD_2OH \qquad (12)$$

$$H + CD_3OH \rightarrow HD + CD_2OH \qquad (13)$$

At appropriate CD_3OH concentrations reaction (12) will completely eliminate reaction (11). Reaction (5) will also be eliminated by CD_3OH to an extent depending on the $[CD_3OH] / [OH]$ concentration ratio, which is dose rate dependent. The concentration of CD_3OH should however be kept as low as possible to avoid reaction (13), which affects the overall isotopic composition of the radiolytic hydrogen. 0.1 M CD_3OH was used in our experiments, over the whole range of acidities. The contribution of reaction (13) to the formation of hydrogen was determined under our experimental conditions by measuring $G(HD) / G(H_2)$ for a solution of CD_3OH in H_2O.

The concentrations of the free radicals are dependent on the dose rate of irradiation. The yield of hydrogen from the radical - radical reactions (2), (3) and (4) in competition with the scavenging processes (9) and (13) is therefore dose rate dependent. Unless very high dose rates are applied, reaction (13) will eliminate reactions (3) and (4). The relative yields of reactions (2), (3) and (4) at any given acidity are also dose rate dependent because reactions (7), (8) and (10), which change the ratio e^-_{aq} / H, are first order in radical concentration. It is evident that in order to eliminate the interference of reactions (7), (8), (9), (10) and (13) with the radical - radical reactions, the highest possible concentration of radicals must be produced.

The Argonne Electron Linear Accelerator used in this study delivers 15 MeV electrons at a dose rate of 6×10^9 rad/sec [12]; 4 μsec pulses, at intervals of 1 msec were used in our study, producing radicals at initial concentrations of $\sim 10^{-4}$ M. The radicals recombine within less than 10 μsec. A Co^{60} gamma source with a dose rate of 110 rad/sec was used for the low dose rate irradiations.

The samples for irradiation were evacuated to 10^{-5} mm Hg and sealed under argon at a pressure of 100 mm Hg to facilitate the isotopic analysis[13]. The D_2O : H_2O solutions were prepared by weight, and the isotopic composition checked on aliquots by adding LiH and determining the HD/H_2 formed[8]. To the solutions at pH 1, 4, 7 and 10, iodide ions were added to give 2×10^{-3} M iodide; to the 1 N NaOH solutions, acetone was added to give 5×10^{-2} M acetone. Deuterated methanol (0.1 M) was added as an OH scavenger. The isotopic composition of the irradiated samples was determined with an accuracy of $\pm$ 0.5% in a CEC 21-401 mass spectrometer. The isotopic composition of the radiolytically generated hydrogen was determined with an accuracy of $\pm$ 1%.

I. H/D Isotope Effect in the $e^-_{aq} + e^-_{aq} \rightarrow H_2$ Reaction

Both hydrated electrons and hydrogen atoms are produced as primary products in the radiolysis of water ($G(e^-_{aq}) = 2.6$ [14], and $G(7) = G(H)$ from reaction (7) $= 0.6$ [10]. At pH 14 and the dose rates used, reactions (7) and (8) which convert e^-_{aq} to H atoms do not affect the concentration of e^-_{aq}. However, under our conditions > 95% of H atoms are converted to e^-_{aq} by reaction (10). On the other hand, a substantial fraction of hydrated electrons is eliminated by reaction (9). This leaves $G(2) = G(e^-_{aq} + e^-_{aq}) = \frac{1}{2}(G_{e^-_{aq}} + G_H - G_{H_2O_2}) = 1.2$. From the experimental H/D isotope effect in the hydrogen evolved, from the relative contributions of reactions (1) and (2), and from the isotope effect in reaction (1) $\alpha_1 = \alpha_M = 2.2 \pm 0.1$ (determined in the low dose rate experiments), $\alpha_2 = 4.6 \pm 0.1$ was calculated for reaction (2). This value is in good agreement with $\alpha_2 = 4.7 \pm 0.2$ determined by the photochemical decomposition of alkaline solutions[7].

II. H/D Isotope Effect in the $e^-_{aq} + H \rightarrow H_2$ Reaction

At pH 10 an overall H/D isotope effect = 2.7 $\pm$ 0.1 was observed. At this pH reaction (10) no longer contributes, and a substantial fraction of the hydrogen originates from reactions (3) and (4). Under these

conditions $G(e^-_{aq}) = G_{e^-_{aq}} - G_{H_2O_2} = 1.8$ and $G_H = 0.6$. A rough calculation shows that $G(H_2)$ consists of $G(1) = 0.45$, $G(2) = 0.70$, $G(3) = 0.40$ and $G(4) = 0.10$. From these values $\alpha_3 = 1.5 \pm 0.3$ was calculated.

Reaction (3) is characterized by a relatively small isotope effect which seems to be pH dependent. It has been suggested[15] that reaction (3), in accordance with the general behavior of e^-_{aq} reactions, produces a hydride ion as an intermediate:

$$e^-_{aq} + H \rightarrow H^- \qquad (14)$$

Under the conditions prevailing at pH 10, reaction (14) is not expected to modify the isotopic composition of the product, since practically all the hydrogen and deuterium atoms react by this reaction. Hydride ions were shown to react with water at a diffusion controlled rate, yielding H_2 with an isotope effect of unity[8]:

$$H^- + H_2O \rightarrow H_2 + OH^- \qquad (15)$$

Under our conditions at pH 10, the only route for the production of H atoms is via reaction (6) which involves an isotope effect of $\alpha_6 = 2.6$ [11]. Taking into account the hydride ion mechanism this would imply $\alpha_3 = 1.57$.

III. H/D Isotope Effect in the $H + H \rightarrow H_2$ Reaction

The overall isotope effect of reaction (4) was calculated from the measured overall H/D isotope effect in the hydrogen evolved at pH 1. At this pH reactions (2) and (3) do not contribute to the hydrogen formed, and all e^-_{aq} are converted to H atoms before having a chance to undergo reaction (9). With a correction for reaction (13), and using the known values of H_2 and α_1, α_4 was found to be 3.5 ± 0.2 . This is in good agreement with $\alpha_H = 3.6 \pm 0.1$ found in a study on the isotope effect in the formation of hydrogen atoms in acid solutions[11]. This is not surprising, since all the hydrogen and deuterium atoms are converted to hydrogen molecules by reaction (4).

IV. The Primary Processes in the Radiolysis of Water, in the Light of the H/D Isotope Effects

The diffusion model[4,5] which is at present the prevailing theory on the radiolysis of water, assumes that about 4 water molecules in clusters with a radius of less than 20 Å are decomposed coherently to give e^-_{aq}, OH and H_3O^+. These are believed to react with each other and with added solutes at the same specific rates observed for reactions in homogeneous systems, yielding the "primary" products H_2, H and H_2O_2. Major fractions of e^-_{aq} and OH radicals escape the radical - radical reactions and diffuse, according to this model, into the bulk of the solution. According to the diffusion model the $e^-_{aq} + e^-_{aq}$ reaction contributes about 80% of the "molecular" hydrogen[5]. The rest of the H_2 is presumably produced by the e^-_{aq} + H reaction, from H atoms formed via reaction (8)[4,5]. Taking the isotope effects for these two reactions as $\alpha_2 = 4.7$ and $\alpha_3 = 1.8$, and calculating the expected isotopic composition for the "molecular" hydrogen, one obtains $\alpha_{H_2} = 4.2$. This is in complete disagreement with the experimental value of $\alpha_1 = 2.2 \pm 0.1$ found throughout the whole pH range. It must be concluded that reaction (2) may contribute only a minor fraction to the "molecular" hydrogen. This is in accordance with our earlier conclusions[11] based on the observation that α_1 is independent of pH. Furthermore, experiments on the effect of different scavengers on G_{H_2} show that reaction (2) cannot be the main source of the "molecular" hydrogen[6].

It has been shown[16] that the "residual" hydrogen is not formed in the bulk from $e^-_{aq} + H_3O^+$, and it has been suggested[4,5,17] that it originates in the spurs from reaction (7). However the H/D isotope effect in the formation of the "residual" hydrogen, $\alpha_H = 2.6$, is significantly smaller than α_7[12]. It is therefore suggested that the "residual" hydrogen is the product of an independent process, namely the decomposition of excited H_2O to give H atoms[11].

To sum up our conclusions, it is likely that a major part of the molecular hydrogen, like the "residual" hydrogen, is not produced in reactions (2), (3) and (4). The similarity between α_1 and the "true" $\alpha_6 = 2.3 \pm 0.1$[12] suggests a common origin for both products.

The formation of the "molecular" and "residual" hydrogens and the molecular H_2O_2[18] by mechanisms not predicted by the diffusion model, implies that a revision of this model is called for.

References:

1. ANBAR, M. and MEYERSTEIN, D., Israel AEC Report IA-1074 (in press)
2. MATHESON, M.S., Radiation Res., Suppl. 4, 1 (1964)
3. KUPPERMANN, A., The Chemical and Biological Actions of Radiations, (Ed., M. Haissinski), Academic Press, (1961)
4. KUPPERMANN, A., Radiation Res., Suppl. 4, 69 (1964)
5. SCHWARZ, H.A., Radiation Res., Suppl. 4, 89 (1964)
6. SWORSKI, T.J., J. Am. Chem. Soc., 86, 5034 (1964) and in Solvated Electrons, Am. Chem. Soc., Advn. Chem. Ser., 50, 263 (1965)
7. ANBAR, M. and MEYERSTEIN, D., Chem. Commun. (submitted), this report, p. 115
8. HUGHES, E.D., INGOLD, C.K. and WILSON, C.L., J. Chem. Soc., 493 (1934)
9. LIFSHITZ, C. and STEIN, G., J. Chem. Soc., 3706 (1962)
10. ANBAR, M. and MEYERSTEIN, D., J. Phys. Chem., 68, 3184 (1964)
11. ANBAR, M. and MEYERSTEIN, D., J. Phys. Chem. 69, 698 (1965)
12. DORFMAN, L.M. and MATHESON, M.S., Reaction Kinetics, (Ed., G. Porter), Pergamon Press 3, 237 (1965)
13. ANBAR, M. and MEYERSTEIN, D., Israel AEC Report, IA-851 (1963)
14. RABANI, J., MULAC, W.A. and MATHESON, M.S., J. Phys. Chem. 69, 53 (1965)
15. ANBAR, M., Solvated Electrons, Am. Chem. Soc., Advn. Chem. Ser. 50, 55 (1965)
16. ALLAN, J.T. and SCHOLES, G., Nature 187, 218 (1960)
17. KUPPERMANN, A., Radiation Res. 25, 101 (1965)
18. ANBAR, M., PECHT, I. and STEIN, G., this report, p. 123

Formation of $H_2O_2^{18,18}$ and $H_2O_2^{16,18}$ in H_2O^{18} Solutions Containing $H_2O_2^{16,16}$:

M. Anbar, I. Pecht* and G. Stein**

Some time ago we reported[1] the results of experiments in which $H_2O_2^{16,16}$ was used as a scavenger in radiolysed H_2O^{18} and the formation of

* Weizmann Institute of Science, Rehovoth
** Hebrew University, Jerusalem

$H_2O_2^{16,18}$ and $H_2O_2^{18,18}$ was determined. The yield of $H_2O_2^{16,18}$ increased with $H_2O_2^{16,16}$ concentration whereas that of $H_2O_2^{18,18}$ decreased. The yield of $H_2O_2^{18,18}$ at low $H_2O_2^{16,16}$ concentrations (< 0.05 M) measures the so-called "molecular yield" of H_2O_2, $G(H_2O_2^{18,18}) = G_{H_2O_2} = 0.7$. As to the origin of this product, we suggested that part of it may be in the interaction of excited water molecules H_2O^* with their nearest neighbor non-excited water molecules. The formation of the $H_2O_2^{16,18}$ was interpreted as a result of the reaction of HO^{18} radicals with $H_2O_2^{16,16}$.

$$HO^{18} + H_2O_2^{16,16} \rightarrow H_2O_2^{16,18} + HO^{16} \qquad (1)$$

We have now extended our measurements of the yields of $H_2O_2^{18,18}$ and $H_2O_2^{16,18}$ over a wider range of $H_2O_2^{16,16}$ concentrations. The investigation was carried out at pH 5 to 6, at room temperature, using Co^{60} gamma rays (9000 rad/min). The analytical procedure was as previously described[1].

The results show that $G(H_2O_2^{18,18})$ decreases from 0.75 to 0.38 and $G(H_2O_2^{16,18})$ increases from 0.05 to 0.66 when $[H_2O_2^{16,16}]$ is increased from 0.01 to 5 M. Both changes show a fair agreement with a cube root dependence on $[H_2O_2]$. The differential of the change, $D = \Delta G(H_2O_2)/[H_2O_2]^{1/3}$ is 0.367 ± 0.027 for $G(H_2O_2^{16,18})$, which is about twice that for $G(H_2O_2^{18,18})$, 0.195 ± 0.026. The value of $G(O^{18}H)_{total} = G(H_2O_2^{16,18}) + 2\,G(H_2O_2^{18,18})$ is constant throughout the whole range of H_2O_2 concentrations, being 1.500 ± 0.048.

The cube root dependence implies that $H_2O_2^{16,18}$ is a product of the action of radiation on the solvent and not a result of "direct action" on $H_2O_2^{16,16}$. At $[H_2O_2^{16,16}] = 0.01$M, the value of $G(H_2O_2^{16,18})$ is only 0.05, whereas all the OH radicals in the bulk, which are formed with $G > 2.2$, are scavenged by the H_2O_2; thus the efficiency of reaction (1) is < 2% .

Thus, even if reaction (1) occurred in the spurs it could not account for the formation of $H_2O_2^{16,18}$.

If H_2O_2 originated from the recombination of OH radicals in the spurs, as has been generally assumed[2,3,4], the decrease in $G(H_2O_2^{18,18})$ could be attributed to the scavenging of OH radicals by the reaction $H_2O_2 + OH \rightarrow HO_2 + H^+ + OH^-$. In this case however a parallel decrease in $G(O^{18}H)_{total}$ would be expected. On the other hand, if H_2O_2 reached the spur where e^-_{aq} and OH radicals are assumed to recombine[3,4], it would scavenge e^-_{aq} by the reaction $H_2O_2^{16,16} + e^-_{aq} \rightarrow O^{16}H + OH^-$ and produce $O^{16}H$ radicals. At the same time, owing to the suppression of the $e^-_{aq} + O^{18}H$ reactions, $G(O^{18}H)_{total}$ should increase by 0.7 $O^{18}H$ radicals for each e^-_{aq} scavenged. In view of the difference between the specific rates of the $H_2O_2 + OH$ (4.5×10^7 M^{-1} sec^{-1}) and $H_2O_2 + e^-_{aq}$ (1.2×10^{10} M^{-1} sec^{-1}) reactions[4], it is highly unlikely that the decrease in $G(O^{18}H)_{total}$ owing to the former reaction is exactly compensated by the increase caused by the latter. It must be concluded, therefore, that H_2O_2 is not produced by the recombination of OH radicals in the spur, but by some other processes.

References:

1. ANBAR, M., GUTTMANN, S. and STEIN, G., J. Chem. Phys., 34, 703 (1961)
2. CZAPSKI, G., Disc. Faraday Soc., 36, 321 (1963)
3. ALLEN, A. O., Radiation Research Suppl. 4, 54 (1964)
4. MATHESON, M. S., Radiation Research Suppl. 4, 1 (1964)

Interaction of Chloride Ions with OH Radicals[1] : M. Anbar and J. K. Thomas*

The reaction of OH radicals with chloride ions was studied by the pulse radiolysis technique.

---

* Argonne National Laboratory, Illinois, U.S.A.

The spectrum observed in the radiolysis of dilute sodium chloride solutions (0.2 - 10 mM) showed a transient absorption if the pH was less than 3. In neutral solution transient absorption was observed only if the sodium chloride concentration was greater than 0.1 M. This absorption was unaffected by oxygen concentrations up to 1.1×10^{-3} M.

From the similarity in the spectra obtained by pulse radiolysis and flash photolysis we conclude that the species formed is Cl_2^- both in acid and in neutral solutions.

The optical density of the Cl_2^- at infinite time varied with pH and chloride ion concentration. The addition of methanol and potassium ferrocyanide reduced the optical density, the effect of potassium ferrocyanide being ten times greater than that of methanol. The decreased yield of Cl_2^- could not be accounted for in terms of reaction of the Cl_2^- with the added solutes, since the slow decay of the Cl_2^- was not affected by the solutes. It is possible that the Cl atoms may react with the solutes, lowering the Cl_2^- yield. Nevertheless the ten-fold difference in reactivity of the methanol and potassium ferrocyanide is curiously analogous to the reactivity of OH radicals.

The addition of hydrogen peroxide to acidified sodium chloride solutions results in a two-fold enhancement of the Cl_2^- absorption[2]. Here the H atoms produce more OH radicals via $H + H_2O_2 \rightarrow H_2O + OH$. From the above evidence we conclude that in acid solution Cl_2^- is produced by the reaction of OH radicals with chloride ions. The rate of appearance of the Cl_2^- is directly proportional to the chloride ion concentration and to the pH over the range 10^{-3} to 1 M perchloric acid:

$$\frac{d[Cl_2^-]}{dt} = k[Cl^-]\,[OH]\,[H_3O^+]$$

The effect of ionic strength on the rate of formation of Cl_2^- was investigated and a negative salt effect observed. At pH 2.65 the rate constant k decreased

nearly two-fold when the ionic strength increased from 0.012 to 1.00. The rate of Cl_2^- formation was not affected when D_2O was substituted for H_2O.

In neutral solution the formation of Cl_2^- was only observed at chloride ion concentrations of 0.1 M or greater, and then the rate of formation is extremely fast, the process being complete in less than the duration of the electron pulse (0.4 μsec). In aerated solution at pH 7 the yield of Cl_2^- increased with chloride ion concentration up to 3 M chloride. The yield was proportional to $[Cl^-]^{1/3}$. At 1 M chloride the yield of Cl_2^- was about one third of that in acid solution. Even at 3 M chloride the yield at pH 7 was less than at much lower chloride ion concentrations in acid solution. Making the solution 10^{-3} M in hydrogen peroxide produced no change in the yield of Cl_2^-. At this concentration of hydrogen peroxide all the hydrated electrons should have reacted to produce OH radicals: $e_{aq}^- + H_2O_2 \rightarrow OH^- + OH$ ($k = 1.1 \times 10^{10}$ M^{-1} sec^{-1}, half-life $< 10^{-7}$ sec) . It would appear that at pH 7, OH radicals formed in the bulk of the solution do not produce Cl_2^-. The above facts suggest that at neutral pH the origin of the Cl_2^- is in the spur regions.

The yield of Cl_2^- decreased progressively when sodium hydroxide was added to the solution. Above pH 12 increasing the hydroxyl ion concentration ten-fold decreased the yield of Cl_2^- by a factor of 2. Thus the scavenging action of the OH^- depends roughly on $[OH^-]^{1/3}$.

References:

1. ANBAR, M. and THOMAS, J. K., J. Phys. Chem., 68, 3829 (1964)
2. SWEET, J. and THOMAS, J. K., J. Phys. Chem., 68, 1363 (1964)

Reactivity of Aromatic Compounds Toward Hydroxyl Radicals[1] : M. Anbar, D. Meyerstein and P. Neta

The reaction of benzene and substituted benzenes with hydroxyl radicals has been the subject of several recent studies[2-5]. It was

suggested that this reaction involves the addition of the OH radical to the aromatic ring. We have carried out an extensive investigation of the way in which substituents affect the reaction, in order to infer its nature by comparison with the reactions of conventional electrophilic and nucleophilic reactants. The specific rates for a series of substituted benzenes and benzoate ions were derived from competition kinetics using the method developed by Kraljic and Trumbore[6]. The rate constants range from 1.17×10^9 M^{-1} sec^{-1} for p-nitrobenzoate ion, up to 5.3×10^9 M^{-1} sec^{-1} for aniline. The relative rates of the reaction are in good agreement with Hammett's $\sigma\rho$ relation for electrophilic substitution with $\rho = -0.41$. The electrophilic behavior of the OH radical is not surprising in view of its high electron affinity. The absolute value of ρ is small compared with the values for other electrophilic substitutions[7], probably because of the high reactivity of OH radicals.

References:

1. ANBAR, M., MEYERSTEIN, D. and NETA, P., J. Phys. Chem. (in press)
2. DORFMAN, L. M., TAUB, I. A. and HARTER, D. A., J. Chem. Phys., 41, 2954 (1964)
3. MATTHEWS, R. W. and SANGSTER, D. F., J. Phys. Chem., 69, 1938 (1965)
4. DIXON, W. T. and NORMAN, R. O. C., Proc. Chem. Soc., 97 (1963)
5. ADAMS, G. A., BOAG, J. W., CURRANT, J. and MICHAEL, B. D., Pulse Radiolysis (Ed. M. Ebert), Academic Press, p.131, 1965
6. KRALJIC, I. and TRUMBORE, C. N., J. Am. Chem. Soc., 87, 2547 (1965)
7. STOCK, L. M. and BROWN, H. C.,Advn. Phys. Org. Chem., 1, 36 (1963)

Reactivity of Aliphatic Compounds Toward Hydroxyl Radicals : M. Anbar, D. Meyerstein and P. Neta

The rate constants for the reaction of hydroxyl radicals with some aliphatic compounds have recently been determined by competition kinetics[1-5], and it has been suggested that the RH + OH reaction proceeds by hydrogen

abstraction[5-7]. We have investigated the effect of structure and substituents on the reaction rates, in order to gain more information on the mechanism of these reactions. The specific rates were determined using the methods developed by Hummel and Allen[1] and by Kraljic and Trumbore[4]. The results confirm that abstraction of a hydrogen atom occurs as the rate determining step. The reactivities of aliphatic compounds toward OH radicals were found to be dependent on both inductive and resonance effects, as expressed by Hammett's σ function. This was examined in a series of substituted methanes and acetate ions. The specific rate constants range from 2.1×10^{6} M^{-1} sec^{-1} for CH_3CN up to 1.4×10^{9} M^{-1} sec^{-1} for CH_3NH_2. The reactivities of long chained compounds were shown to be the sum of the partial reactivities of C - H bonds at different positions in the molecule.. The following partial specific reactivities were derived ($\times 10^{-8}$ M^{-1} sec^{-1} per hydrogen atom):

$CH_4 = 0.36$; $RCH_3 = 0.36$; $R_2CH_2 = 3.0$; $R_3CH = 8.4$; $CH_3COO^- = 0.14$; $RCH_2COO^- = 1.75$; $CH_2(COO^-)_2 = 0.16$; $R_2CHCOO^- = 5.3$; $CH_3OH = 1.8$; $RCH_2OH = 5.0$; $R_2CHOH = 8.8$; $CH_3OR = 0.6$; $RCH_2OR = 1.4$; $(RO)_2CH_2 = 0.5$; $(RO)_2CHR = 0.9$; $ROCR_2CH_2OH = 1.65$; $HOCR_2CH_2OH = 2.25$; $HOCR_2CH_2CR_2OH = 2.25$; $HOCR_2CH(OH)R = 4.2$.

References:

1. HUMMEL, A. and ALLEN, A. O., Radiation Res., 17, 302 (1962)
2. ADAMS, G. A., BOAG, J. W., CURRANT, J. and MICHAEL, B. D., Pulse Radiolysis (Ed. M. Ebert), Academic Press, p.131, 1965
3. MATTHEWS, R. W. and SANGSTER, D. F., J. Phys. Chem., 69, 1943 (1965)
4. KRALJIC, I. and TRUMBORE, C. N., J. Am. Chem. Soc., 87, 2547 (1965)
5. THOMAS, J. K., Trans. Faraday Soc., 61, 702 (1965)
6. FUJIMATO, M. and INGRAM, D. J. E., Trans. Faraday Soc., 54, 1304 (1958)
7. LIFSHITZ, C. and STEIN, G., J. Chem. Soc., 3706 (1962)

Reactivity of Aromatic Compounds Toward Hydrogen Atoms : M. Anbar, D. Meyerstein and P. Neta

The reaction of OH radicals with aromatic compounds has been shown to be analogous to electrophilic aromatic substitution (see p.127). A similar investigation of the reactivity of aromatic compounds towards hydrogen atoms has been carried out in order to elucidate the nature of the PhX + H reaction.

The specific rate constants for the reaction of monosubstituted benzenes with H atoms were determined by competition kinetics, using isopropanol as the competing compound. Deaerated solutions containing 5×10^{-2} M isopropanol, 1×10^{-3} M acetone and different concentrations of PhX at pH 8 to 9, were irradiated in a Co^{60} gamma source. The hydrogen evolved was determined by gas chromatography.

Under our experimental conditions e^-_{aq} reacts with acetone and OH radicals react with isopropanol. H atoms react both with isopropanol and with PhX, but only in the case of isopropanol is H_2 formed (see p.132). Taking into account the values of G_{H_2} (determined in KBr solution), $G_{H_2} + G_H$ (determined in isopropanol solution) and $k_{H + \text{isopropanol}} = 5.0 \times 10^7\ M^{-1}\ sec^{-1}$ (ref.1), the rate constants of the PhX + H reactions were found to be: $PhNO_2$ = 16.6, PhCN = 4.53, $PhCOCH_3$ = 12.6, $PhSO_3^-$ = 4.30, $PhNHCOCH_3$ = 6.70, $PhCH_2COO^-$ = 7.70, $PhCOO^-$ = 8.70, PhOH = 42.0, $PhNH_2 = 17.6 \times 10^8\ M^{-1}\ sec^{-1}$. These values were correlated with Hammett's σ function and it was concluded that the attack of H atoms on aromatic compounds is analogous to electrophilic aromatic substitution. Nitrobenzene and acetophenone were found to be more reactive than expected from their σ values, probably owing to an additional reaction between their functional groups and the H atoms.

References:

1. APPLEBY, A., SCHOLES, G. and SIMIC, M., J. Am. Chem. Soc., 85, 3891 (1963)

Reduction of Cobalt(III) Complexes by Hydrogen Atoms : M. Anbar and D. Meyerstein

Aquated electrons and hydrogen atoms are the most elementary reducing agents in aqueous solutions, but it has been found that they react differently in many reactions[1]. The reduction of transition metal complexes by hydrated electrons has recently been investigated, and it was found that the ligand affects the rate of reaction[2]. As this reduction is obviously an outer sphere process[3] the effect of different ligands is a measure of their efficacy in transferring an electron to the central atom. It was of interest to examine the effect of ligands on the rate of reaction of hydrogen atoms with metal complexes in order to compare the mechanism of this reduction with that of e^-_{aq}.

The rate of reaction of radiolytically produced hydrogen atoms with $Co^{III}(NH_3)_5X$ complexes was determined. The measurements were carried out using competition kinetics, the competing process being hydrogen abstraction from 2-D-isopropanol or CD_3OH[4].

A comparison of the results[5] with the corresponding rates of reaction for aquated electrons reveals a significant difference in the effects of ligands on the reactivity. In the case of electrons the order of reactivity is:

$$OH^- > CN^- > NH_3 > H_2O > F^- > Cl^- > I^-$$

as opposed to the order measured for hydrogen atoms:

$$H_2O > F^- > NH_3 > OH^- > CN^- > Cl^- > N_3^- > Br^- > I^-$$

This may indicate a difference in the mechanism of reduction. As the aquated electrons undoubtedly react via an electron transfer mechanism, hydrogen atoms probably react via an atom transfer

$$(NH_3)_5\ CoX^{+2} + H \rightarrow (NH_3)_5\ Co^{+2} + XH$$

The difference in the efficacy of H_2O and OH^- as bridging ligands would require an increase in the reactivity of aquo complexes with increasing pH, as opposed to the decrease observed for e^-_{aq} (ref.1). This has actually been observed for Fe^{+3} (ref.6), Cu^{+2} (refs.7 and 8), and Cr^{+3} (ref.9).

The rates of reduction of cobalt complexes by hydrogen atoms are several orders of magnitude slower than the corresponding reactions with hydrated electrons. This effect is most conspicuous for the aquo and fluoro complexes, where the reactions with e^-_{aq} are close to the limit of diffusion controlled processes. This is in accord with the differences observed between atom and electron transfer reductions of the same complexes.

References:

1. MATHESON, M. S., Ann. Rev. Phys. Chem., 13, 77 (1962)
2. ANBAR, M. and HART, E. J., J. Phys. Chem., 69, 973 (1965)
3. SUTIN, N., Ann. Rev. Nucl. Sci., 12, 285 (1962)
4. ANBAR, M. and MEYERSTEIN, D., J. Phys. Chem., 68, 3184 (1964)
5. ANBAR, M. and MEYERSTEIN, D., Nature, 206, 818 (1965)
6. ROTHSCHILD, W. G. and ALLEN, A. O., Radiation Res., 8, 101 (1958)
7. ALLEN, A. O., Radiation Res., Suppl.4, 54 (1964)
8. ANBAR, M. and NETA, P., Intern. J. Appl. Radiation Isotopes, 16, 227 (1965)
9. ANBAR, M. and MEYERSTEIN, D. (unpublished results)

On the Mode of Reaction of H Atoms and OH Radicals with Benzoate Ions :

M. Anbar

Benzoate ions were shown to react very rapidly with hydrated electrons[1], H atoms[2] and OH radicals[3]. The reactions proceed via different intermediates and yield different final products. The most

likely pathways include the following initial steps :

$$\text{(i)} \quad C_6H_5COO^- + e^-_{aq} \rightarrow C_6H_5COO^{-2}$$

$$\text{(ii)} \quad C_6H_5COO^- + H \rightarrow C_6H_6COO^-$$

$$\text{(iii)} \quad C_6H_5COO^- + H \rightarrow C_6H_4COO^- + H_2$$

$$\text{(iv)} \quad C_6H_5COO^- + OH \rightarrow C_6H_5(OH)COO^-$$

$$\text{(v)} \quad C_6H_5COO^- + OH \rightarrow C_6H_4COO^- + H_2O$$

To decide whether the reactions with H and OH proceed both by hydrogen abstraction (iii and v) and by addition (ii and iv), the final products were examined by using tritiated $C_6H_4TCOO^-$. Reaction (iii) should result in the production of gaseous HT, and action (v) in the formation of tritiated H_2O. $C_6H_5TCOO^-$ (80 mc/mmol) 2×10^{-2} M was irradiated at pH 5 with a Co^{60} gamma source. The dose rate was 6×10^3 r/min and the total dose 2 Mrad. The H_2 produced was collected and analyzed in an internal gas counter. The water was distilled, carrier BzOH was added and precipitated and the water redistilled. This procedure was repeated twice, after which an aliquot of the water was assayed for tritium in a liquid scintillation counter, with an efficiency of 7%. The tritium activities detected both in the gas phase and in the solvent were extremely low. $G(H_2)_{abstraction} < 0.01$ and $G(H_2O)_{abstraction} < 0.005$. The results imply that both H atoms and OH radicals react with benzoate ions by addition reactions and not by abstraction. The adduct of $C_6H_5COO^-$ + OH has also been observed by pulse radiolysis.

References:

1. ANBAR, M. and HART, E. J., J. Am. Chem. Soc., 86, 5633 (1964)
2. ANBAR, M., MEYERSTEIN, D. and NETA, P., Nature (in press)
3. ANBAR, M., MEYERSTEIN, D. and NETA, P., J. Phys. Chem. (in press)

Reactivity of Aliphatic Compounds Toward Bromine and H Atoms in Aqueous Solution[1] : M. Anbar, D. Meyerstein and P. Neta

Relative rate constants for the reactions of hydrogen atoms with saturated aliphatic compounds were determined by competition kinetics using 2-D-2-propanol as a reference compound and analysing the isotopic composition of the hydrogen evolved during radiolysis. The reactivity of bromine atoms toward aliphatic compounds was examined by following the radiolytic bromination of the latter in aqueous solutions containing molecular bromine. A comparison of the reactivities of bromine atoms and hydrogen atoms shows an analogy in the behaviour of the two reagents. The effect of branching of the aliphatic chain as well as the effect of functional groups is similar. The order of reactivity of C - H bonds is primary < secondary < tertiary, including hydrogens which are in the alpha positions of alcohol and carboxylate ions. It seems that Br atoms do not attack certain groups (e.g. CH_3 in acetate and CH_2 in dioxane) which react slowly with H atoms (the absence of any reaction at all is probably due to the lower reactivity of Br atoms). It is concluded that the mechanisms of reaction of both H and Br atoms with saturated aliphatic compounds are similar and involve hydrogen abstraction.

Reference :

1. ANBAR, M., MEYERSTEIN, D. and NETA, P., J. Chem. Soc. (in press)

Radiolysis of Alkali Halides in Aqueous Solutions Saturated with CO_2 : M. Anbar and P. Neta

The radiolysis of iodide and bromide ions in aqueous solutions saturated with CO_2 has been investigated and the results compared with those in solutions saturated with N_2O or N_2 (see Table14). $G(I_2)$ in CO_2-saturated solution at pH 5 was lower than in N_2O-saturated solution[1], but higher than in N_2-saturated solution. $G(I_2)$ increased when the pH was

TABLE 14

$G(I_2)$ for iodine formation from irradiated iodide solutions

pH →	pH 6	pH 5	pH 6	pH 3.5		pH 2.5		
Satd. with → / KI (M)	N_2O	CO_2	N_2	N_2O	CO_2	N_2O	CO_2	N_2
1×10^{-3}	1.60	0.16	0.00	3.25	1.40	3.25	2.10	-
5×10^{-3}	1.83	0.38	0.05	3.27	1.45	-	2.40	-
1×10^{-2}	2.16	0.49	0.25	3.28	1.55	3.40	2.45	0.5
5×10^{-2}	2.30	0.85	0.35	3.48	1.80	3.45	2.86	-
1×10^{-1}	2.86	1.27	0.55	3.58	1.94	3.55	3.02	0.8
5×10^{-1}	3.66	2.06	0.75	-	-	4.40	4.05	1.5

lowered to 2.5 . In acid solution the increase in $G(I_2)$ with iodide concentration was much higher in CO_2-saturated solution than in N_2O- or N_2-saturated solutions. $G(Br_2)$ was similar in CO_2- and N_2-saturated Br^- solution at pH 2.5 ($G(Br_2) = 0.15$ to 0.64). Analysis of the results led to the following conclusions: CO_2^- reduces I_2, Br_2 and H_2O_2; CO_2^- in acid solution is in equilibrium with CO_2H [2]; CO_2H oxidizes I^- and H_2O_2 but reduces Br_2; and $k_{(CO_2^- + I_2)} / k_{(CO_2^- + H_2O_2)} < k_{(e^-_{aq} + I_2)} / k_{(e^-_{aq} + H_2O_2)} = 4$ [3] .

References:

1. ANBAR, M., MEYERSTEIN, D. and NETA, P., J. Phys. Chem., 68, 2967 (1964)
2. HUSAIN, A. and HART, E. J., J. Am. Chem. Soc., 87, 1180 (1965)
3. ANBAR, M. and NETA, P., Intern. J. Appl. Radiation Isotopes, 16, 227 (1965)

Radiolytic Debromination of 2-Bromopropionate Ions in Aqueous Solutions Saturated with CO_2 [1] : M. Anbar and P. Neta

The radiolytic debromination of 2-bromopropionate ions has been investigated. It has been shown that hydrated electrons debrominate RBr quantitatively, whereas H atoms on interaction with RBr form either Br^- or H_2. OH radicals do not debrominate RBr directly.

$$CH_3CHBrCOO^- + e^-_{aq} \rightarrow CH_3CHCOO^- + Br^-$$
$$CH_3CHBrCOO^- + H \rightarrow CH_3CHCOO^- + HBr$$
$$CH_3CHBrCOO^- + H \rightarrow CH_3CBrCOO^- \text{ (or } CH_2CHBrCOO^-) + H_2$$
$$CH_3CHBrCOO^- + OH \rightarrow CH_3CBrCOO^- \text{(or } CH_2CHBrCOO^-) + H_2O$$

The organic radicals $CH_2CHBrCOO^-$ and $CH_3CBrCOO^-$ formed by hydrogen abstraction by H atoms and OH radicals were shown to produce Br^- by reaction with H_2O_2 or RBr:

$$CH_3CBrCOO^- + H_2O_2 \rightarrow CH_3COCOO^- + HBr + OH$$
$$CH_3CBrCOO^- + RBr \rightarrow (CH_3CBrCOO^-)^+ + R + Br^-$$
$$(CH_3CBrCOO^-)^+ + OH^- \rightarrow CH_3COCOO^- + HBr$$

Carbon dioxide is a very efficient e^-_{aq} scavenger ($k_{e^-_{aq} + CO_2} = 7.67 \times 10^9\ M^{-1}\ sec^{-1}$) [2], forming CO_2^-. It has been shown that CO_2^- reduces I_2, Br_2 [3] and H_2O_2 [4], and it was thus of interest to study the behavior of CO_2^- toward RBr and RCl. $G(Br^-)$ was the same for N_2- and CO_2-saturated solutions of bromopropionate (Table 15). On the other hand, $G(Cl^-)$ from chloroacetate solution decreased on addition of CO_2. It is thus concluded that CO_2^- reduces RBr, but does not react with RCl:

$$CO_2^- + RBr \rightarrow CO_2 + R + Br^-$$

$G(Br^-)$ was also determined in RBr solutions containing Cu^{++} or NO_3^- ions and saturated with N_2 or CO_2 (Table 15). The lowering of $G(Br^-)$ by Cu^{++} and NO_3^- in deaerated RBr solution is consistent with their specific reaction rates with e^-_{aq}. In CO_2-saturated solution containing 10^{-3} M RBr and 10^{-3} M $CuSO_4$ or $NaNO_3$, 90 - 95% of the e^-_{aq} reacts with CO_2.

TABLE 15

Radiolytic debromination of 2-bromopropionate

Added solute	Concentration of added solute (M)	$G(Br^-)$	
		N_2-saturated	CO_2-saturated
-	-	4.2	4.2
$CuSO_4$	10^{-3}	1.9	1.7
$NaNO_3$	10^{-3}	2.9	3.6

Therefore in these solutions RBr competes with Cu^{++} or NO_3^- for the CO_2^- radicals. From Table 15 it is seen that the effect of CO_2 on $G(Br^-)$ is different in the presence of Cu^{++} or NO_3^-. A qualitative comparison shows that

$$k_{(CO_2^- + Cu^{++})} / k_{(CO_2^- + RBr)} > k_{(e_{aq}^- + Cu^{++})} / k_{(e_{aq}^- + RBr)}$$

whereas

$$k_{CO_2^- + NO_3^-)} / k_{(CO_2^- + RBr)} < k_{(e_{aq}^- + NO_3^-)} / k_{(e_{aq}^- + RBr)}$$

It is likely that the charge of the added ion has a different effect on the rate of reaction with e_{aq}^- and CO_2^-. The separation of the charges on the activated complex are expected to be smaller in the CO_2^- - X reaction than in the e_{aq}^- - X reaction, and thus the former processes are expected to be more strongly affected by the electrostatic factors.

References:

1. NETA, P., Ph.D. thesis, Weizmann Institute of Science, Rehovoth (1965)
2. GORDON, S., HART, E.J., MATHESON, M.S., RABANI, J. and THOMAS, J.K;, Discussions Faraday Soc., 36, 193 (1963)
3. ANBAR, M. and NETA, P., this report, p. 134
4. HUSAIN, A. and HART, E.J., J. Am. Chem. Soc. 87, 1180 (1965)

Radiolytic Formation of Tetravalent Bromine and its Reactions with Halide Ions and Halogens[1,2] : M. Anbar and P. Neta

The formation of tetravalent bromine as a result of the reduction of bromate ions by radiolytically produced hydrated electrons and hydrogen atoms has been investigated in the iodide-bromate and bromide-bromate systems. $BrO_3^=$ (or BrO_2) may react both as an oxidant or as a reductant. It oxidizes iodide and bromide in an acid catalyzed reaction, and reduces iodine and bromine to give I_2^- and Br_2^-. A quantitative estimate of the results yields $k_{(BrO_3^= + I_2)} / k_{(BrO_3^= + I^-)} = 10 \pm 5$ in neutral solution and 0.2 in acid solution (0.1 M $H_2PO_4^-$), while $k_{(BrO_3^= + Br_2)}/k_{(BrO_3^= + Br^-)} \approx 100$ in acid solution. It is concluded that the reaction of $BrO_3^=$ with bromide ions is much slower than that with iodide ions. The addition of $MnSO_4$ to the iodide-bromate system increases $G(I_2)$, pointing to the reactions $BrO_3^= + MN^{++} \rightarrow BrO_2^- + Mn^{+3}$ and $Mn^{+3} + I^- \rightarrow Mn^{++} + I$. The results indicate that $k_{BrO_3^= + MN^{++}}$ and $k_{BrO_3^= + I^-}$ are approximately equal.

References:

1. ANBAR, M. and NETA, P., J. Inorg. Nucl. Chem., (in press)
2. ANBAR, M. and NETA, P., Israel AEC Semi-Annual Report, July-December, 1964, IA-1021, p.83

Radiolytic Isotopic Exchange between Bromopropionate and Bromide Ions : M. Anbar and P. Neta

In the radiolytic isotopic exchange of chlorine between chloride ions and trichloroacetic acid[1], it has been suggested that the first step is the reaction of trichloroacetic acid with hydrated electrons, forming chloride ions and CCl_2COOH. The back-reaction leading to isotopic exchange has not been fully elucidated. It was therefore decided to

investigate the related process of radiolytic isotopic exchange between bromopropionate and Br^-. Br^{82} was used as a tracer and the analyses were performed by anion exchange and counting of the radioactivity. The results are summarized in Table 16 .

TABLE 16

Radiolytic isotopic exchange between Br^- and bromopropionate or tribromoacetate ions

RBr	[RBr] (M)	[Br^-] (M)	$G_{exch.}$	
			N_2O-satd.	N_2-satd.
$CH_3CHBrCOO^-$	10^{-1}	1×10^{-3}	0.13	-
$CH_3CHBrCOO^-$	10^{-3}	1×10^{-2}	0.06	-
$CH_3CHBrCOO^-$	10^{-2}	1×10^{-2}	0.26	0.65
$CH_3CHBrCOO^-$	10^{-1}	1×10^{-2}	0.48	0.42
$CH_3CHBrCOO^-$	10^{-2}	3×10^{-2}	0.5	-
$CH_3CHBrCOO^-$	10^{-1}	3×10^{-2}	1.15	-
$CH_3CHBrCOO^-$	10^{-1}	1×10^{-1}	1.45	-
$CH_2BrCH_2COO^-$	10^{-2}	3×10^{-2}	0.55	-
$CH_2BrCH_2COO^-$	10^{-1}	3×10^{-2}	1.25	-
CBR_3COO^-	10^{-3}	1×10^{-2}	0.05	0.47

In deaerated (N_2-saturated) solutions, e^-_{aq} reacts with RBr to yield $R + Br^-$, and H atoms react with RBr to yield either Br^- or H_2. OH radicals react with Br^-, to produce Br_2, and with RBr to produce organic radicals ($CH_3CBrCOO^-$, $CH_2CHBrCOO^-$). The exchange process may proceed by the reaction $R + Br_2 \rightarrow RBr + Br$. Each of the three different organic radicals, namely CH_3CHCOO^-, $CH_3CBrCOO^-$ and $CH_2CHBrCOO^-$ will yield different products.

In the N_2O-saturated solutions N_2O competes with RBr for the hydrated electrons, and thus the increase in G(exchange) with RBr concentration is due to an increase in G(debromination). At 10^{-2} M RBr N_2O scavenges about 70% of the e^-_{aq} and the Br^- ions react with almost all the oxidizing radicals; under these conditions G(R) limits G(exchange). This is corroborated by the fact that when G(R) is higher, an increase in G(exchange) is observed.

In the exchange of tribromoacetate the organic radicals can be formed only by debromination. At low substrate concentrations in N_2O-saturated solutions most of the electrons react with N_2O and G(R) is small; G(exchange) is thus also small. In N_2-saturated solution all the e^-_{aq} debrominate tribromoacetate and G(exchange) is higher by an order of magnitude.

The fact that G(R) may limit G(exchange) implies that under the experimental conditions used no direct exchange takes place between RBr and the radiolytically formed Br_2, Br or Br^-_2. This is in agreement with the conclusions of Noyes et al.[2,3] on the exchange of iodine with iodo-aliphatic compounds.

Further evidence for the suggested mechanism was obtained by analysing the exchange products to determine the position of the radioactive bromine atom. The analysis was performed by following the kinetics of the alkaline hydrolysis of the bromopropionate[4]. The results show that in 2-bromopropionate, in addition to the occurrence of isotopic exchange, some 3-bromopropionate ($\sim$ 10%) is formed, while when 3-bromopropionate undergoes exchange, about an equal amount of the alpha bromo isomer is produced. Taking into account the thermal exchange, it was concluded that in the latter case only a third of the isotopically labeled organic product carries the radiobromine in the beta position. The results indicate that hydrogen abstraction from bromopropionate ions

by OH radicals takes place mainly at the alpha position.

References:

1. BORIE, R. D., Jr., and JOHNSTON, F. J., Radiation Res., 15, 724 (1961)
2. ZIMMERMAN, J. and NOYES, R. M., J. Chem. Phys., 18, 656, 658 (1950)
3. NOYES, R. M. and SIBBETT, D. J., J. Am. Chem. Soc., 75, 767 (1953)
4. LANE, J. F. and HEINE, H. W., J. Am. Chem. Soc., 73, 1348 (1951)

Dehalogenation of Organic Halogen Compounds on Reaction with Aliphatic Free Radicals : M. Anbar and P. Neta

Organic halogen compounds undergo dehalogenation when radiolysed in dilute aqueous solutions, forming halide ions and organic radicals[1,2]. It has been shown that the reaction of the hydrated electrons with chloroacetate ions quantitatively produces Cl^- ions, whereas the reaction of the H atoms may follow two pathways, namely halogen abstraction or hydrogen abstraction. The reaction of organic halogen compounds with OH radicals seems to produce no halide ions[3,4].

The radiolytic debromination of 2-bromopropionate ions has recently been investigated[5] and it was suggested that the organic radicals formed by the reaction of bromopropionate with H atoms and OH radicals may react with RBr to yield Br^-. In order to check this point organic radicals were produced in the presence of bromopropionate and bromoacetate ions, by reacting CH_3OH, C_2H_5OH, $(CH_3)_2CHOH$, CH_3COOH and CH_3COCH_3 with the primary radicals. The organic radicals were found to yield Br^- with a high efficiency. On the other hand, they did not produce Cl^- from chloroacetate ions. It is suggested that the reaction of organic radicals with RBr may lead to debromination by a charge-transfer mechanism, e.g. $CH_2OH + RBr \rightarrow CH_2OH^+ + R + Br^-$.

References:

1. HAYON, E. and ALLEN, A. O., J. Phys. Chem., 65, 2181 (1961)

2. JORTNER, J. and RABANI, J., J. Am. Chem. Soc., 83, 4868 (1961)

3. HAYON, E. and WEISS, J., Proc. 2nd Intern. Conf. Peaceful Uses Atomic Energy, Geneva, 1958, 29, 80 (1959)

4. TEPLY, J. and BEDNAR, J., Proc. 2nd Intern. Conf. Peaceful Uses Atomic Energy, Geneva, 1958, 29, 71 (1959)

5. NETA, P., Ph.D. thesis, Weizmann Institute of Science, Rehovoth (1965)

Radiolysis of Nitrate and Nitric Acid Aqueous Solutions : M. Anbar, M. Faraggi and D. Zehavi

Several studies have been carried out on the effects produced by ionizing radiation in aqueous solutions of nitric acid[1,2] and nitrate ions[1,3-6]. The experimental data of different investigators are in disagreement and have led to conflicting conclusions as to the participation of excited water molecules, the reactivity of the OH radical toward the nitrate ion and the validity of extrapolation of the radiolytic behavior of water to concentrated electrolyte solutions.

It has been established that the main radiolytic products in these systems are hydrogem peroxide, nitrite ion, hydrogen and oxygen. In dilute solutions hydrogen atoms and hydrated electrons reduce nitrate to nitrite ions[3-5]. Hydroxyl radicals oxidize the nitrite to nitrate ions[4], and it has also been suggested that they react with NO_3^- [2]. In concentrated solutions various mechanisms have been proposed, e.g. the direct effect of radiation on the solute[1], or energy transfer to the nitrate ion via its sphere of hydration[5].

The aim of our investigation was to determine the kinetics of the reactions involved in the radiolysis of nitrate ions in aqueous solutions.

I. Radiolysis of Aqueous Nitrate Solutions

Sodium nitrate in neutral solutions was irradiated with Co^{60} gamma rays, under aerated and deaerated conditions. The nitrate concentration ranged from 10^{-3} to 6.5 M, and the dose from $5 \times 10^{17} - 10^{19}$ ev/g. The yield of nitrite and hydrogen peroxide was measured and found to increase linearly with dose. The results under aerated and deaerated conditions were the same, showing that oxygen has no effect on the radiolysed system. Nitrite yields increased from 0.32 at 10^{-3} M to 1.70 at 6.5 M. Hydrogen peroxide was formed at a constant yield of $G = 0.75 \pm 0.02$ over the whole range of concentrations.

From these data and from the yields of gaseous products reported by others and confirmed in this laboratory, the radiolysis of the nitrate ion was interpreted as follows. In the dilute concentration range up to 10^{-1} M, the results are accounted for in terms of the conventional "primary" species e^-_{aq}, OH and H atoms. Hydrated electrons and hydrogen atoms reduce the nitrate ions, while OH radicals react with the nitrite to reform nitrate. Taking the appropriate values for these radicals, $G(NO_2^-) = \frac{1}{2}(G_{e^-_{aq}} + G_H - G_{OH})$ is found to be 0.32 . In concentrated solutions from 10^{-1} to 6.5 M, two other effects are involved in addition to the indirect effect of radiation: (a) energy transfer from the excited water molecules to the nitrate ion, (b) direct effect of radiation on the nitrate ion. These two effects produce nitrite ions and oxygen atoms, the latter probably reacting with the water to give H_2O_2. The experimental results are in good agreement with the calculated values, based on this mechanism.

II. Radiolysis of Hydrogen Peroxide in Aqueous Nitric Acid Solutions

One of the fundamental problems in the radiation chemistry of aqueous solutions is the formation of the so-called "molecular" hydrogen peroxide and hydrogen, and the radiolytic behavior of these products.

The radiolytic decomposition of hydrogen peroxide in our system was therefore investigated quantitatively. Solutions of 10^{-3} - 10^{-1} M hydrogen peroxide in 0.5 - 6.5 M nitric acid were irradiated in aerated and deaerated solutions. The decomposition of H_2O_2 was found to be linear with dose and to increase with the nitric acid concentration. The results are summarized in Table 17.

TABLE 17

Radiolytic decomposition of hydrogen peroxide in nitric acid

	$G(-H_2O_2)$ in air-saturated solutions			$G(-H_2O_2)$ in air-free solutions		
$[HNO_3]$ M \ $[H_2O_2]$ →	10^{-3}M	10^{-2}M	10^{-1}M	10^{-3}M	10^{-2}M	10^{-1}M
0.5	3.10	3.10	3.30	3.20	3.25	3.25
1.0	3.25	3.30	3.45	3.40	3.45	3.50
1.5	3.40	3.40	3.60	3.55	3.60	3.70
2.5	3.70	3.70	3.90	3.80	3.75	3.90
4.0	4.15	4.15	4.35	4.20	4.25	4.35
6.0	4.75	4.75	4.90	4.85	4.80	5.00

The results at low concentrations of nitric acid may be attributed to the following reactions:

a) reduction of nitric acid to nitrite

$$HNO_3 + H \rightarrow NO_2 + H_2O \qquad (1)$$

and

$$2\ NO_2 + H_2O \rightarrow NO_2^- + NO_3^- + 2\ H^+ \qquad (2)$$

followed by

$$NO_2^- + H_2O_2 \rightarrow NO_3^- + H_2O \qquad (3)$$

b) reaction of the OH radical with H_2O_2

$$H_2O_2 + OH \rightarrow HO_2 + H_2O \qquad (4)$$

followed by

$$HO_2 + HO_2 \rightarrow H_2O_2 + O_2 \qquad (5)$$

In addition it might be expected that H_2O_2 and HO_2 would react according to

$$HO_2 + H_2O_2 \rightarrow H_2O + OH + O_2 \qquad (6)$$

which would lead to a chain reaction, but this phenomenon is not reflected in the measured $G(-H_2O_2)$ which is almost independent of H_2O_2 concentration.

According to this mechanism hydrogen peroxide decomposition yields would be $G(-H_2O_2) = \frac{1}{2}G_H + \frac{1}{2}G_{OH} - G_{H_2O_2} = 2.50$, but even at low acid concentration the $G(-H_2O_2)$ values are higher than this. This may be due to an additional yield of NO_2^- from the reaction of nitric acid in the "spurs" with the precursors of "molecular" hydrogen, it being well known that HNO_3 reduces G_{H_2} [1,7]. Thus an additional term $0.45 - G_{H_2}$ has to be added to $G(-H_2O_2)$:

$$G(-H_2O_2) = \tfrac{1}{2}G_H + \tfrac{1}{2}G_{OH} - G_{H_2O_2} + (0.45 - G_{H_2}) = 2.80$$

In addition the reaction of H_2O^* with HNO_3 would give NO_2 and OH via the reaction

$$H_2O^* + HNO_3 \rightarrow NO_2 + OH + H_2O \qquad (7)$$

thus increasing the decomposition yield of H_2O_2. Similar behavior has been found in the radiolysis of halide ions[8].

At higher concentrations of nitric acid the increase in $G(-H_2O_2)$ may be attributed to direct action of radiation on the acid:

$$HNO_3 \rightarrow OH + NO_2 \qquad (8)$$

References:

1. MAHLMAN, H. A., J. Chem. Phys., 35, 936 (1961)
2. CHALLENGER, G. E. and MASTERS, B. J., J. Am. Chem. Soc., 77, 1036 (1955)
3. HYDER, M. L., J. Phys. Chem., 69, 1858 (1965)
4. ERSHOV, B. G. et al., Dokl. Akad. Nauk S.S.S.R., 159, 431 (1964)
5. MAHLMAN, H. A. and SCHWEITZER, G. K., J. Inorg. Nucl. Chem., 5, 213 (1958)
6. BEDNAR, J. and LUKAC, S., Coll. Czechoslov. Chem. Commun., 29, 341 (1964)
7. SWORSKI, T. J., J. Am. Chem. Soc., 86, 5034 (1964)
8. ANBAR, M., MEYERSTEIN, D. and NETA, P., J. Phys. Chem., 68, 2967 (1964)

Radiolysis of Dichromate Ions in Nitric Acid Solutions : M. Anbar, M. Faraggi and D. Zehavi

Dichromate ions in acid solutions are reduced by gamma irradiation according to the following reactions:

$$Cr^{6+} + H \rightarrow Cr^{5+} + H^+ \qquad (1)$$

$$Cr^{6+} + H_2O_2 \rightarrow Cr^{5+} + HO_2 + H^+ \qquad (2)$$

$$Cr^{6+} + HO_2 \rightarrow Cr^{5+} + O_2 + H^+ \qquad (3)$$

$$2\ Cr^{+5} \rightleftarrows Cr^{+6} + Cr^{+4} \qquad (4)$$

$$2\ Cr^{+4} \rightleftarrows Cr^{+5} + Cr^{+3} \qquad (5)$$

OH radicals, on the other hand oxidize Cr^{+3}

$$Cr^{3+} + OH \rightarrow Cr^{4+} + OH^- \qquad (6)$$

In the presence of nitric acid, the nitrite ions formed also reduce Cr^{6+}:

$$Cr^{6+} + NO_2^- + H_2O \rightarrow Cr^{4+} + NO_3^- + 2\ H^+ \qquad (7)$$

(i) Chromate Ion Effect

Solutions of 3×10^{-4} to 10^{-2} M $K_2Cr_2O_7$ in 10^{-2} to 8 M nitric acid were irradiated. Cr^{3+} formation (determined spectroscopically) was found to be linear with dose for solutions in the range 10^{-3} - 10^{-2} M $K_2Cr_2O_7$. However, in 3×10^{-4} M $K_2Cr_2O_7$ the yield of Cr^{3+} decreased with dose. Moreover, Cr^{6+} continued to be reduced after the end of the irradiation, indicating the formation of some unstable peroxide. Figure 26 gives the Cr^{3+} yield as a function of nitric acid concentration. These yields were calculated from the linear dependence of Cr^{3+} on dose. No oxygen effect was found in this system.

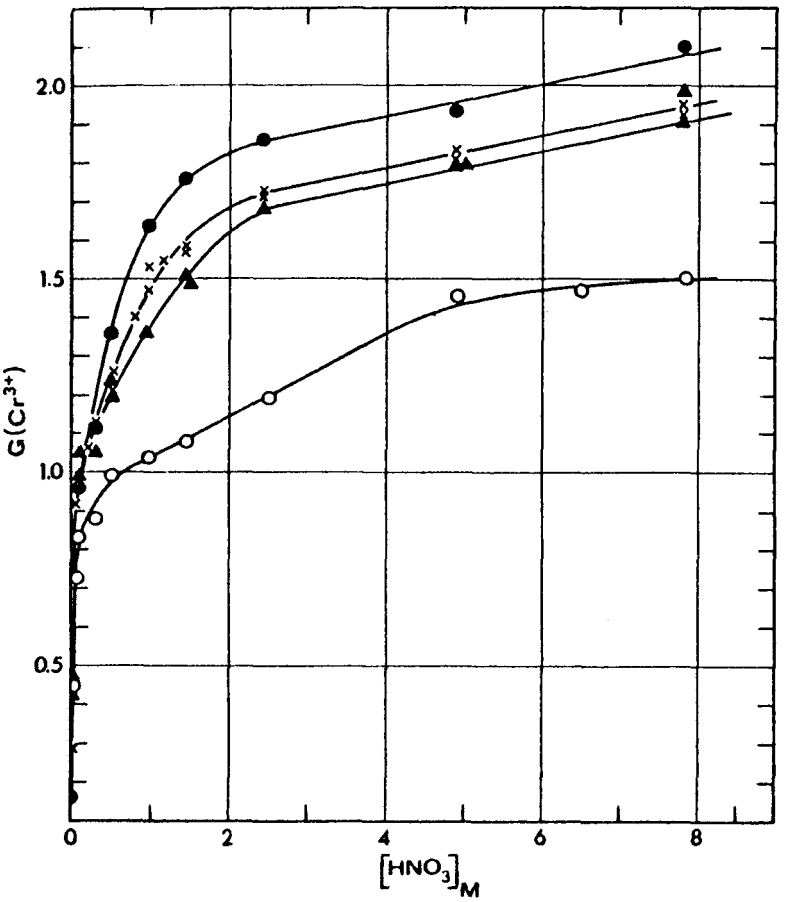

Fig. 26

Yield of Cr^{3+} as a function of $[HNO_3]$ and $[Cr^{6+}]$

● - 10^{2} M $K_2Cr_2O_7$ X - 6×10^{-3} M $K_2Cr_2O_7$

▲ - 3×10^{-3} M $K_2Cr_2O_7$ O - 10^{-3} M $K_2Cr_2O_7$

(ii) Dose Rate Effect

Lowering the dose rate from 5×10^{17} eV/g/min (the value used in this study) to 8×10^{16} eV/g/min, increased $G(Cr^{3+})$ by 10%. This dose rate dependence is attributed to competition between reactions (2) and (7) on the one hand, and the reaction between H_2O_2 and NO_2^- on the other:

$$NO_2^- + H_2O_2 \rightarrow NO_3^- + H_2O \qquad (8)$$

(iii) Effect of Nitrate Concentration

Table 18 shows the Cr^{3+} yield for 3×10^{-3} M $K_2Cr_2O_7$ at various concentrations of nitric acid and nitrate ion. The decrease in $G(Cr^{3+})$ at low acid and high nitrate concentrations is also due to competition between reaction (8) and reactions (2) and (7). Moreover, it seems very likely that reactions (2) and (7) are dependent on $[H^+]^2$, while reaction (8) is known to be a first order reaction[1].

TABLE 18

Radiolytic yield of Cr^{3+}

	$G(Cr^{3+})$						
$[NO_3^-]_M$ \ $[HNO_3]_M$	0.01	0.1	0.5	1.0	1.5	2.5	5.0
0.0	0.47	0.99	1.21	1.38	1.52	1.68	1.79
0.4	-	0.84	-	-	-	-	-
0.49	0.30	-	-	-	-	-	-
0.5	-	-	1.21	1.41	-	-	-
1.0	-	-	-	-	1.51	-	-
1.4	-	0.52	-	-	-	-	-
1.49	0.19	-	-	-	-	-	-
2.0	-	-	1.20	-	-	-	1.83
2.5	-	-	-	-	-	1.78	-
3.5	-	-	-	-	1.66	-	-
4.0	-	-	-	1.45	-	-	-
4.5	-	-	-	-	-	1.77	-
4.9	-	0.38	-	-	-	-	-
4.99	0.13	-	-	-	-	-	-
5.5	-	-	-	-	1.66	-	-
6.0	-	-	-	1.52	-	-	-
6.5	-	-	1.17	-	-	-	-

(iv) Effects of Cr^{3+}, H_2 and Tl^+

These experiments were carried out to investigate the role of hydroxyl radicals and their yield in our system. It was found that the addition of Cr^{3+} (up to 6×10^{-2} M) has no effect on $G(Cr^{3+})$. Hydrogen at atmospheric pressure increased $G(Cr^{3+})$ from 0.47 to 0.99 at 10^{-2} M HNO_3. At higher acid concentrations no significant hydrogen effect was detected. Experiments with Tl^+ were possible only at high acid concentrations because of the low solubility of the chromate thalium complex at low acid concentrations. G(OH) was found to be 4.5 at 8 M HNO_3 indicating the direct production of OH radicals from the acid by the reaction

$$HNO_3 \rightarrow NO_2 + OH \qquad (7)$$

in agreement with ref.2.

References:

1. ANBAR, M. and TAUBE, H., J. Am. Chem. Soc., 76, 6243 (1954)
2. MAHLMAN, H. A., J. Chem. Phys., 35, 936 (1961)

Gamma Induced Reactions in Solutions of Tetrachloroethylene in n-Pentane:

A. Horowitz and A. Rajbenbach

Solutions of tetrachloroethylene in n-pentane were irradiated and the products analysed. The solute was found to cause a marked decrease in the radiolytic hydrogen yield, $G(H_2)$ dropping from 5.17 in pure pentane to 3.36 in 3×10^{-3} M tetrachloroethylene . HCl was formed in high yields, the yields being higher than the decrease in hydrogen yields. G(HCl) rose from 3.5 to 18.5 when the concentration of the solute was increased from 1.5×10^{-2} M to 5×10^{-1} M. These high G values strongly suggest that HCl is formed in a chain reaction. The same applies to trichloroheptene-1, which was formed in comparable yields. The structure of this compound was established by combustion analysis and from the infra-red spectrum. Its G values plotted against the concentration of tetrachloroethylene gave a straight line through the origin. A similar plot for HCl yielded a

straight line of slightly different slope, the intercept being at $G \approx 2.8$. A third major product identified was trichloroethylene, the G value of which was 1.3 and 3.5 at tetrachloroethylene concentrations of 3×10^{-2} and 5×10^{-1} M respectively.

These results indicate that HCl is formed in two distinct processes, one accompanied by the production of trichloroheptene, the other by the formation of trichloroethylene. The formation of the last product is probably due to a large extent to some form of energy transfer from solvent to solute. Hydrogen scavenging by tetrachloroethylene followed by ejection of a chlorine atom would not appear to be a plausible reaction in the liquid phase. Neither could the disproportionation reaction between a pentyl and chloroethyl radical (viz. $C_5H_{11}' + C_2Cl_4H' \rightarrow C_5H_{11}Cl + C_2Cl_3H$) account for the formation of most of the C_2Cl_3H since its yields were consistently higher than those of chloropentane, and furthermore no products of the combination of tetrachloroheptane radicals were found.

Other products detected include hexachloroethane. The chlorine balance based on the products found was fairly satisfactory proving that the most important radiolytic products have been identified. Further study is in progress to elucidate the chain reaction resulting in the very high yields of HCl and trichloroheptene-1.

Electron Scavenging Processes in Irradiated Alkane-Perfluorocarbon Solutions:
A. Rajbenbach

It has been suggested that low concentrations of N_2O in alkanes scavenge electrons[1], the reaction resulting in the formation of molecular nitrogen. In our previous work[2] we found that small amounts of perfluorocyclobutane, and to a lesser degree perfluorocyclopentane, reduce the yield of molecular hydrogen, an effect which was assumed to be due to interaction

between a precursor of molecular hydrogen, presumably an electron, and the fluorocarbon. To test this assumption further we have studied the radiation chemistry of dilute solutions of nitrous oxide and several perfluorocarbons in n-hexane. The yields of hydrogen, nitrogen, methane, and in some isolated cases hexenes, were measured. It was found that the lower perfluoroalkanes from CF_4 to C_4F_{10} had no effect on the formation of N_2. The higher fluoroalkanes, and especially some of the cyclic perfluorocarbons, reduced the nitrogen yield markedly.

A kinetic study based on the assumption that the higher perfluorocarbons and nitrous oxide compete for electrons showed that some of the perfluorocarbons had a rate constant for electron capture of the same order of magnitude as nitrous oxide.

In the radiolysis of n-hexane perfluoroalkane solutions in the absence of nitrous oxide a decrease in hydrogen yields was observed. The effectiveness of the various fluorocarbons in suppressing the hydrogen yield follows the same order as manifested in nitrogen reduction in the first set of experiments.

References:

1. SCHOLES, G. and SIMIC, M., Nature, 202, 895 (1964)
2. RAJBENBACH, A., Israel AEC Semi-Annual Report, January-June 1964, IA-984, p.91

Gamma Radiolysis of the n-Hexane-Perfluorocyclobutane System : A. Rajbenbach

In previous work[1] it was established that the presence of a low concentration of perfluorocyclobutane markedly decreases the radiolytic yields of hydrogen and unsaturates from n-hexane. This effect was attributed to an interaction between the fluorocarbon and the common precursor of part of the hydrogen and the hexenes. With a view to elucidating the mechanism of this reaction, similar studies of the effects of tetrafluoroethylene and

perfluoropropene, the major products in the radiolysis of pure perfluorocyclobutane, were carried out. These compounds were generated by pyrolysis of teflon. The effectiveness of both these fluorocarbons in reducing the hydrogen yield was lower than that of perfluorocyclobutane, confirming the assumption that the effect of the latter is not due to secondary reactions of its radiolysis products with hydrogen atoms from n-hexane.

In the search for new products not identified previously SiF_4 and HF were found. SiF_4 is presumably produced by a secondary reaction between HF and the walls of the glass vessel. The G values for the formation of HF both in its original form and as SiF_4 were found to correspond rather closely to the G values for disappearance of perfluorocyclobutane in the concentration range from 0.08 to 3 moles perfluorocarbon in n-hexane. Another significant finding was that the sum of the G values for hydrogen and HF was equal to the G value for hydrogen in pure n-hexane. Addition of hydrogen scavnegers such as hexene-1 and benzene had a very small effect on either the disappearance of perfluorocyclobutane or the formation of HF, further confirming the assumption that hydrogen atoms are not involved in the attack on perfluorocyclobutane.

Reference:

1. RAJBENBACH, A., Israel AEC Semi-Annual Report, January-June 1964, IA-984, p.91

Radiation-Induced Reduction of Benzophenone in 2-Propanol : W. V. Sherman

The gamma radiolysis of dilute solutions of benzophenone in 2-propanol has been studied further. It was previously found[1] that benzophenone is quantitatively reduced to benzpinacol, and that a precursor of this product is the benzophenone ketyl radical $(C_6H_5)_2COH$. It was shown that this radical is not formed via the triplet benzophenone responsible for the reduction induced by ultraviolet light, and it was suggested that it might be produced via a hydrogen atom scavenging process or an electron scavenging process.

To test the first possibility, a careful study was made of the hydrogen yields in the radiolysis of 2-propanol solutions containing benzophenone in the concentration range 1 x 10^{-3} to 1 x 10^{-1} M. It was found that while G(-benzophenone) remained constant at about 6, the value of $\Delta G(H_2)$, the decrease in hydrogen yield compared with the pure solvent, was never greater than approximately 1.5 . Hence a process involving solely hydrogen atom scavenging cannot account for the observed yields of benzpinacol.

To test the possibility of an electron scavenging process the radiolysis of benzophenone solutions containing nitrous oxide was studied. The presence of benzophenone was found to decrease the nitrogen yield, which indicates that benzophenone was successfully competing for electrons. However, G(-benzophenone) was not significantly affected by the presence of nitrous oxide and it must be concluded that the benzophenone anion, which is undoubtedly formed, is not a precursor of benzpinacol.

Reference:

1. SHERMAN, W. V. and COHEN, S. G., J. Am. Chem. Soc., 86, 2390 (1964)

On the Radiolytic Isotopic Exchange of Gaseous Nitrogen : M. Anbar and P. Perlstein

Some time ago[1] we investigated the isotopic exchange of nitrogen between N_2^{1414} and N_2^{1515} in the gas phase under radiolytic conditions. We found a surprisingly high value for G_{exch}, namely 9.5 $\pm$ 0.25 in the pressure range 33 - 440 mm Hg. A major part of this exchange was attributed to the dissociation of excited nitrogen molecules formed by processes other than the recombination of $N_2^+ + e^-$. In a recent study Dawes and Back[2], reported a value of 7.3 $\pm$ 0.5 for G_{exch} and offered a completely different mechanism for the radiolysis of nitrogen, based on the participation of N_4^+ in the exchange process. These results prompted us to reinvestigate the system experimentally and to reconsider the interpretation of the observations.

Several series of experiments were conducted[3] using X-rays, gamma rays, mixed reactor radiations (see next item) and beta particles from Kr^{85} as an internal source of radiation. The dose rates ranged from 0.2 to 60 Mrad/h and the total dose from 10 to 800 Mrads. A nitrous oxide gaseous dosimeter ($G(-N_2O) = 12$) was used, as well as a Fricke dosimeter with the appropriate corrections. G_{exch} was again found to be 9.5 ± 0.5 . It is hard therefore to account for the discrepancy of about 20% between our results and those of Dawes and Back.

Dawes and Back carried out two series of experiments using nitric oxide as a scavenger for the intermediate in the exchange process. In the $N^{15}O + N_2^{1414}$ series $G(N_2^{1415})$ was 2.57 whereas the $N^{15}O + N^{14}O + N_2^{1414} + N_2^{1515}$ series $G(N_2^{1415})$ was 2.85 .

We have repeated the NO experiments using first a mixture of 98.4% N_2^{1515} + 1.6% $N^{14}O$. The value obtained for $G(N_2^{1415})$ was 2.5 ± 0.13, in excellent agreement with Dawes and Back. The results indicate that NO is an extremely effective scavenger of the intermediates in the exchange process, and that the discrepancy in G_{exch} between our results and those of Dawes and Back can hardly be attributed to dosimetry as good agreement is obtained when a scavenger is deliberately added. It should be noted that identical results were also obtained in both studies[1,2] in the presence of small amounts of oxygen. It is suggested therefore, that the lower value for G_{exch} reported by Dawes and Back for "pure" nitrogen is due to a trace impurity in their system.

Regarding the mechanism of the exchange reaction proposed by us[1] certain points require revision. First, our value of G_{exch} can hardly be accounted for by a purely dissociative process in view of the high dissociation energy of N_2. Second, our conclusion that excited nitrogen molecules do not undergo isotopic exchange with N_2 molecules in their ground state, is open to criticism. This conclusion, which was reached on the basis of the results of Back and Mui[4], is not valid if N_2^* is too

short-lived to be found outside of the discharge tube used in their study. In fact the reaction

$$N_2^{1414}\ (\text{excited}) + N_2^{1515} \rightarrow 2\ N_2^{1415} \qquad (1)$$

is energetically feasible even for the lower excitation levels of N_2 down to 6 eV above ground level.

It appears therefore that neither of the exchange mechanisms proposed so far[1,2] is satisfactory.

A quantitative evaluation of the exchange reaction suggests that it may proceed via ionic species. Reaction (2), suggested by Dawes and Back,

$$N_4^+ + e^- \rightarrow {}^xN_2 + 2\ N \qquad (2)$$

where ${}^xN_2$ is exchanged nitrogen, can account at most for $G_{exch} = 4.3$, and thus one has to consider other reactions of ionic species which lead to isotopic exchange. The most plausible assumption is that the two nitrogen atoms formed on neutralization of N_4^+, each carrying a kinetic or electronic excitation energy of $(14.3 - 9.8) / 2 = 2.2$ eV (corresponding to 50 kcal/mol), undergo isotopic exchange with a nitrogen molecule:

$$N_{hot}^{14} + N_2^{1515} \rightarrow N_2^{1415} + N^{15} \qquad (3)$$

Reaction (3) has a low activation energy, and it seems reasonable to suppose that "hot" nitrogen atoms with rather high kinetic energy such as are produced in reaction (2) will undergo reaction (3) on their first collision with N_2. According to our suggested mechanism, reaction (2) contributes 1/2 an exchanged nitrogen molecule for each neutralized N_4^+, reaction (3) adds 2 x 2/3 exchanged nitrogens, and the recombination of the thermalized N atoms adds another 1/2 an exchanged N_2. Thus for each of the 2.88 N_2^+ produced per 100 eV one obtains $2\frac{1}{3}$ exchanged nitrogens, resulting in $G_{exch} = 6.7$ for the ionic contribution. This requires $2.88 \times 15.6 = 44.9$ eV (15.6 eV being the ionization potential of N_2).

Adding G_{exch} = 3.0 for the exchange proceeding via excited species (a value derived from the effect of nitric oxide on G_{exch}) a total G_{exch} = 9.7 is obtained, in excellent agreement with the experimental value.

It should be pointed out however that the agreement between the calculated G_{exch} and the experimental value may be fortuitous or even due to errors, and that the radiolysis of nitrogen still calls for further study.

References:

1. ANBAR, M. and PERLSTEIN, P., J. Phys. Chem., 68, 1234 (1964)
2. DAWES, D. H. and BACK, R. A., J. Phys. Chem., 69, 2385 (1965)
3. ANBAR, M. and PERLSTEIN, P., Israel AEC Semi-Annual Report, January-June 1964, IA-984, p.88
4. BACK, R.A. and MUI, J.Y.P., J. Phys. Chem. 66, 1362 (1962)

Radiosensitization of Enolase by Copper Ions : M. Anbar and A. Levitzki

Previous work has demonstrated the effect of cupric ions in sensitizing α-amylase and catalase to radiation damage[1]. It has also been shown that other metal ions do not have a comparable sensitizing effect. The copper binding site was not identified, but the sensitization induced by cupric ions suggests that they are bound in the vicinity of the active site of the enzymes. Since it has been shown that cupric ions bind to the active site of enolase[2], radiosensitization of this enzyme by cupric ions was expected.

Purified rabbit liver enolase was dialyzed at 0° for 24 hours against 0.01 M phosphate buffer pH 7.4, containing 0.01 M EDTA. Sulphates of the metals listed in Table 19(Analar grade) were dissolved in 0.01 M phosphate buffer pH 7.4, and added to the enzyme. Triple distilled water was used throughout. The samples were irradiated at room temperature with

a Co^{60} gamma source at a dose rate of 6300 rad/min. The irradiations were performed under an argon or N_2O atmosphere as previously described. The enzyme activity towards the disodium salt of 2-phosphoglyceric acid was then measured spectrophotometrically according to Westhead and McLain[3], using the Zeiss PMQ-II spectrophotometer.

Table 19 gives the results for the N_2O-saturated solutions. The solutions contained 2 x 10^{-6} M of the enzyme, plus the metal sulphate at molar ratios of 5 or 15. As in the case of α-amylase and catalase, Cu^{++} was the only ion which induced radiosensitization of the enzyme.

TABLE 19

D_{37} of rabbit liver enolase in the presence of various metal ions under N_2O (in rads)

Metal ion added	Molar ratio metal/enzyme	
	5	15
None	14,200	13,900
Cu^{++}	8,500	6,900
Zn^{++}	13,800	14,900
Mg^{++}	13,600	14,900
Mn^{++}	14,000	13,800
Fe^{++}	13,800	13,500
Co^{++}	14,250	14,200

The degree of radiosensitization of enolase as a function of the Cu/Enzyme molar ratio is presented in Table 20.

From the behavior of the system under N_2O and A it was inferred that OH radicals are the main reactive species responsible for the radiation damage under our experimental conditions. These radicals most probably oxidize copper to the unstable tervalent state, which in turn

oxidizes the groups adjacent to its binding site, resulting in irreversible radiolytic damage. The results corroborate previous suggestions that copper ions may have a specific role in radiobiological damage[4].

TABLE 20

D_{37} of rabbit liver enolase as a function of the Cu/Enzyme ratio

Molar ratio $\frac{Cu}{enolase}$	N_2O	A
0	14,200	17,200
3	10,400	12,500
5	8,500	10,100
10	7,900	9,200
15	6,900	7,500
20	5,800	4,300
50	2000-3000	6,300

The solutions contained 2×10^{-6} M of enzyme in 0.001 M phosphate buffer pH7.4 . The irradiations were performed at room temperature, with a Co^{60} gamma source at a dose rate of 6300 rad/min. Enzyme activity was measured according to Westhead and McLain[3].

References:

1. ANBAR, M. and LEVITZKI, A., Radiation Res., 27, 32 (1966), Israel AEC Semi-Annual Reports, January-June, 1964, IA-984, p.120 and July-December, 1964, IA-1021, p.91

2. MALMSTRON, B. G., Arch. Biochem. Biophys., 46, 345 (1953)

3. WETSHEAD, E. W. and McLAIN, M., J. Biol. Chem., 239, 246 (1964)

4. ANBAR, M., Nature, 200, 376 (1963)

3. NUCLEAR CHEMISTRY

(See also Activation Analysis (p.196), Radioisotope Production (p.21), Reactor Operation pp.4-12, Biology p.217)

A Triplet at 2.8 MeV in Ne^{21} (1)*: A. L. Catz and S. Amiel

The low lying levels of Ne^{21} as populated by the $O^{18}(\alpha,n)Ne^{21}$ reactions taking place in a Po^{210}-H_2O^{18} mixture were studied using high resolution gamma ray spectroscopy.

The spectrometer used was a Ge(Li) diode of 4 cm^2 x 2.5 mm with a resolution (FWHM) of 4 keV at 122 keV and 8 keV at 3 MeV.

The previously reported Ne^{21} level at 2.8 MeV was found to be in fact a triplet of levels located at 2779 ± 5, 2791 ± 5 and 2812 ± 5 keV (Fig. 27). A revised level scheme of Ne^{21} is given in Fig. 28 .

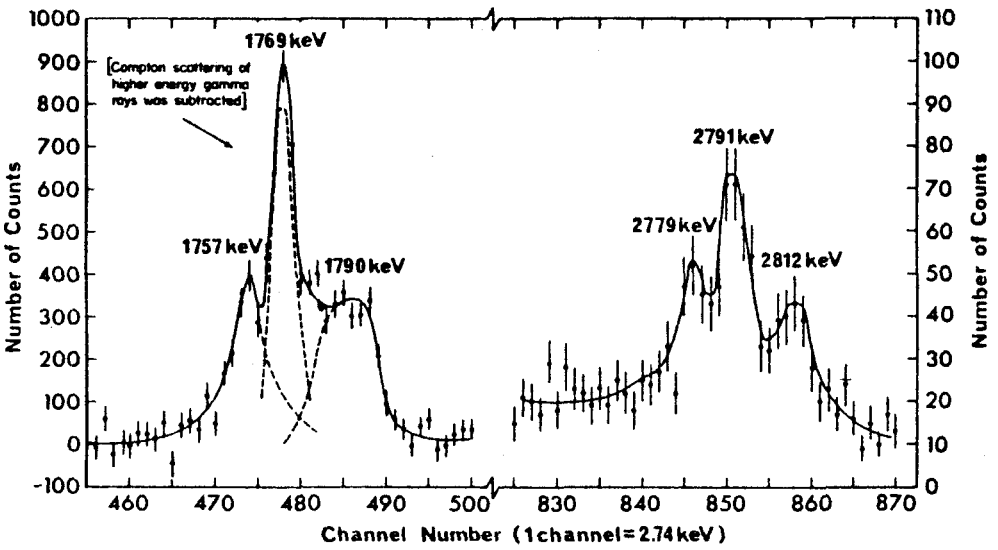

Fig. 27

Shape of the 2.8 MeV triplet and its second escape peaks

* Part of a Ph.D. thesis to be presented by A. L. Catz

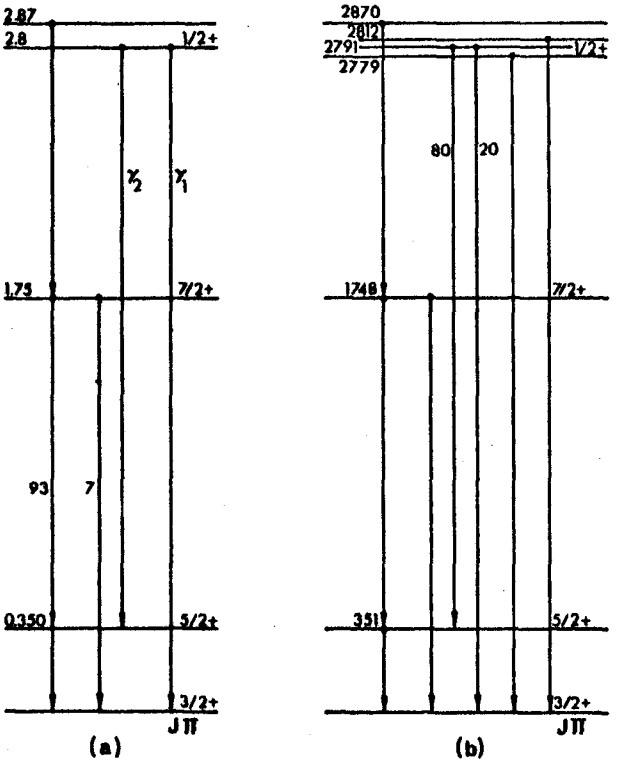

Fig. 28

De-excitation scheme of low lying levels of Ne^{21}
a) prior to present data, b) revised according to present data including the 2.8 MeV triplet

The present results clarify the discrepancies in the branching ratio of the γ transitions from the 2.8 MeV level of Ne^{21} as reported by various investigators using different reactions.

Reference:

1. CATZ, A.L. and AMIEL, S., Phys. Letters, 1966 (in press)

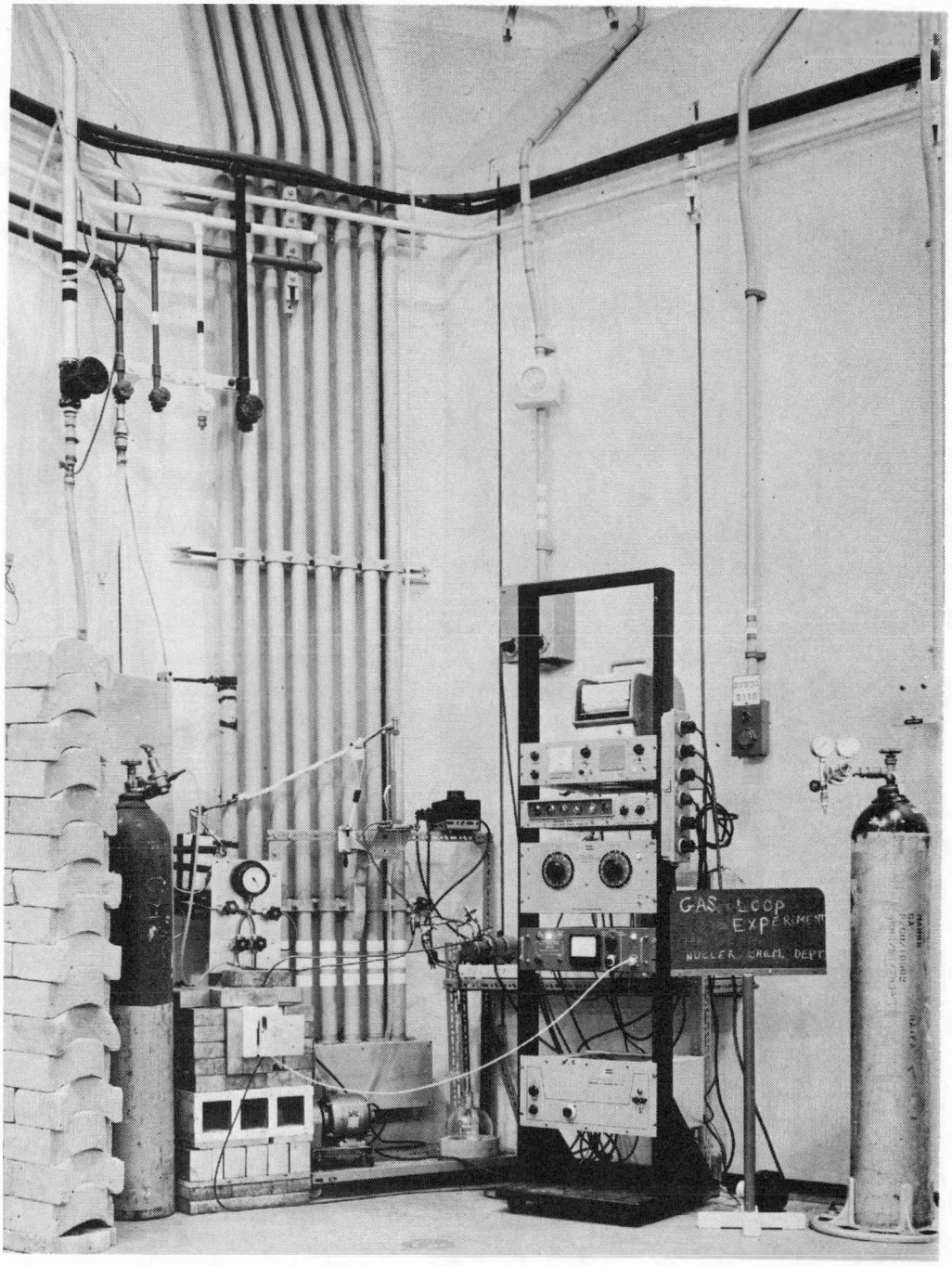

Gas loop experiment in the reactor hall

Lifetime Measurements Using the Doppler-Broadening Attenuation Technique*:

A. L. Catz

The high resolution of the Ge(Li) solid state gamma ray spectrometer permits detection of the small shifts in gamma ray energies caused by the Doppler effect which arises from the motion of the photon-emitting nucleus.

When the gamma rays which reach the detector are emitted not at a definite angle relative to the direction of motion of the nucleus but at random, i.e. isotropically, the Doppler effect, when present, will be observed as a broadening of the original line while its mean remains unchanged.

The exact shape of the line is determined by the velocity distribution of the emitting nuclei at the time of their de-excitation. This spectrum is determined in turn by the initial velocity distribution and by the ratio between the lifetime of the nuclear energy state and the stopping time of the moving nuclei in the surrounding medium. Both these factors have to be known in order to obtain information on the life-time of a specific nuclear energy state from the observed broadening of the emitted gamma ray.

This method was used to measure the lifetimes of the 477 keV level of Li^7 and the 4436 keV level of C^{12}, the latter by studying the broadened spectrum of the gamma ray of this energy emitted in the $Be^9(\alpha,n)C^{12*} \rightarrow C^{12} + \gamma$(4436 keV) reaction which takes place in a Po-Be mixture.

The velocity distribution of the excited C^{12} nuclei at time t = 0, i.e. at the time of their formation, was calculated using known data on the excitation function of the $Be^9(\alpha,n)C^{12*}$ reaction and assuming that the neutrons and C^{12} recoils are emitted isotropically in the centre-of-mass system. The stopping of the C^{12} recoils in the beryllium was calculated assuming that it is governed by the relation[1] $\frac{dE}{dx} = KV$. K was estimated from data reported in ref.1.

---

* Part of a Ph.D. thesis to be presented by A. L. Catz

The lifetime of the Li^7 level was measured from the shape of the 477 keV gamma ray peak emitted in the reaction $B^{10}(n,\alpha)Li^{7*} \rightarrow Li^7 + \gamma$ (477 keV) induced by thermal neutrons in boron. The velocity distribution of the excited nuclei at time t = 0 is very simple in this particular case, since the Li^7 recoils are monoenergetic. The stopping of the recoils was calculated with the same assumptions as in the preceding case.

The results obtained are:

4436 keV level of C^{12} $T_{\frac{1}{2}} = 4.21 \pm 0.76 \times 10^{-14}$ sec

477 keV level of Li^7 $T_{\frac{1}{2}} = 1.04 \pm 0.21 \times 10^{-13}$ sec

Both results are in agreement with previously reported measurements [2,3].

The gamma rays emitted from Ne^{21} levels as populated by the $O^{18}(\alpha,n)Ne^{21*}$ reaction (from a Po^{210}-H_2O^{18}) source were also studied, and the broadening of the peaks is now being analysed in an attempt to obtain the corresponding lifetimes.

References:

1. PORAT, D. I. and RAMAVATARAM, R., Proc. Phys. Soc. 77, 97 (1960)
2. MOUTON, W.L., SELLSCHOP, J.P.F. and WIECHERS, G., Phys.Rev. 129, 361 (1963)
3. Nuclear Data Sheets (National Academy of Sciences, Washington, D.C.)

Evaluation of Fast Neutron Spectroscopy by the Time-of-Flight Technique[1]:

A. Notea

A detailed evaluation was made of a general method for measuring neutron energy by the time-of-flight technique. In this method neutrons are scattered by hydrogen in one scintillator (the "scatterer") and detected by a second scintillator after traversing a known distance; the recoil photon energy and the scattered neutron energy are measured simultaneously by the "scatterer" and the "time-analyzer" respectively. The results are analyzed as a p' x n' matrix in a two-dimensional pulse height multi-channel analyzer. The sum of the recoil photon and scattered neutron energies gives the energy of the primary neutron emitted by the source.

The resolution, efficiency and effective energy range were calculated as functions of the spectrometer characteristics. Two sources of error were taken into account in the calculation of the resolution, namely the measurement of the recoil proton energies and the measurement of the scattered neutron energies. Fast electronics may reduce the error in the scattered neutron energy, so that the main contribution to the error will be the uncertainty in the flight path. The error in the recoil proton energy cannot be reduced since it arises from the low intrinsic efficiency of the available scintillators and from the imperfect collection of the emitted photons.

The probability functions for each process during the measurement were calculated for the case of finite dimension scintillators placed close together. Multiplication of these functions gives the spectrometer efficiency. The main limitation to the efficiency derives from the fact that only a small portion of the scattered neutrons are detected.

The most suitable scintillators available at present are the plastic scintillators of the NE102 type for which graphs and tables necessary for deriving the spectra were calculated. The sensitivity threshold of the scintillator determines the low energy limit which can be measured (about 600 keV for NE102). It was concluded that by using scintillators of special shape and appropriate electronic equipment, 10^{-3} of the neutrons which fall on the "scatterer" will be counted. With the combination of fast electronics, efficient scintillators and good optical transfer of light, results with a resolution (FWHM) of 3 - 5% can be obtained.

Different calibration methods were discussed, as well as background problems and the means of eliminating them. Data processing was given in an analytical form suitable for use in a computer program.

As an example, the neutron energies in the range of 1.5 - 7 MeV from a Pu-Be source were measured using a system whose components are

currently available. The spectrum obtained is identical to that reported for other methods.

Reference:

1. NOTEA, A., M.Sc. thesis submitted to the Technion - Israel Institute of Technology, Haifa. Also Israel AEC Report IA-1025 (1965) in Hebrew

N^{17} Delayed Neutron Spectrum Measured by a He^3 Spectrometer*: A. Notea and S. Amiel

In order to investigate the use of a He^3 neutron spectrometer for measuring delayed neutron emission from fission products, the neutrons emitted in the decay of 4.1 sec N^{17} were measured.

The decay scheme of N^{17} proposed recently[1,2] indicates that 95% of the beta decays are followed by neutron emission. Using proton recoil[3] and time-of-flight spectrometry, three distinct neutron groups were observed, viz. at 0.385, 1.163 and 1.683 MeV, with abundances of about 45%, 45% and 5% respectively.

Sources of N^{17} were prepared by neutron irradiation of Li_2CO_3 enriched to 99.3% Li^6 and 98% O^{18}. The irradiations were carried out in the IRR-1 fast pneumatic rabbit system set to operate automatically for shuttling the sample between the irradiation and measurement positions.

A commercial counter** filled with 4 atm He^3 and 2 atm. krypton was used as a neutron spectrometer. A typical spectrum obtained with a multichannel pulse height analyser is shown in Fig. 29. Neutrons with energies above 1 MeV cause a "background" due to recoils of He^3 nuclei from scattering processes. This background was corrected for using the spectra obtained with the same spectrometer for the monoenergetic neutrons from the reactions $Li^7(p,n)Be^7$ and $B^{11}(\alpha,n)N^{14}$ produced in a Van de Graaf generator[4].

---

* Part of a Ph.D. thesis to be presented by A. Notea

** Texlium model 9341, Texas Nuclear Corp., U.S.A.

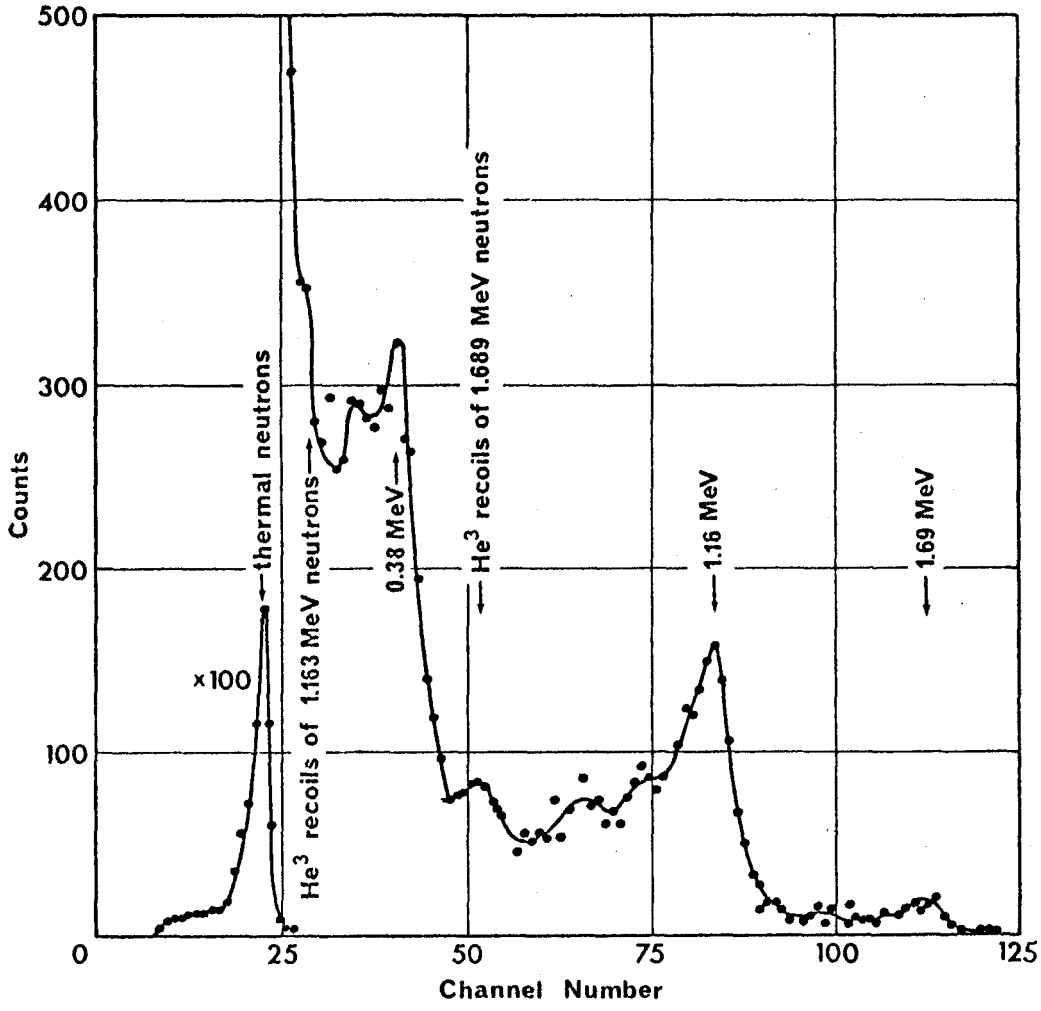

Fig.29

Energy spectrum of N^{17} delayed neutrons measured with a He^3 spectrometer

The measured energies of the three neutron groups and their relative abundances corrected for the variations of $He^3(n,p)H^3$ cross section[5] are in good agreement with the published data.

A statistically significant spectrum of the two main groups and the thermal peak was obtained in about one hour (a cycle consisted of 4 sec irradiation, 2 sec delay and 10 sec count), when a source of 43 mg of Li_2CO_3 was irradiated in a thermal neutron flux of 10^{13} $n/cm^2.sec$.

This suggests the use of N^{17} as an energy reference source for studies carried out near reactors (when no accelerator is available).

References :

1. GILAT, J., O'KELLY, G.D. and EICHLER, E., ORNL-3488 p.4 (1963)
2. SILBERT, M.G. and HOPKINS, J.C., Phys. Rev. 134B, 16 (1964)
3. PERLOW, G.J., RAMLER, W.G., STEHNEY, A.F. and YINTEMA, J.L., Phys. Rev. 122, 899 (1961)
4. NOTEA, A. and CUTTLER, J., unpublished results, 1965
5. BATCHELOR, R. and PARKER, K., AWRE O-78/65 (1964)

Measurement of (n,γ) Cross Sections of the Products of (n,2n) Reactions :

E. Yellin and H.L. Finston*

In these experiments an attempt was made to measure the thermal neutron capture cross sections of neutron deficient nuclides produced by fast neutrons through the (n,2n) reactions. Since the nuclides are produced by fast neutrons while the burn-up is through thermal neutrons, a comparison of the activity in two samples, one covered with Cd and the other bare, will yield the rate of burn-up. A measurement of the thermal flux will then give the desired cross section. Another method of obtaining the neutron absorption cross section of such nuclides would be to irradiate carrier-free samples, but in most cases these are impossible to obtain.

Attempts were made to measure the absorption cross section of 108 d Y^{88}, 13.2 d I^{126}, and 100y Tb^{158}. These were chosen because their cross sections were expected to be high, and the natural abundance of the target is 100% in each case; furthermore the activities of the products are easy to measure.

Preliminary results indicate that the present irradiation facilities in the reactor do not provide sufficiently reproducible fluxes or equal fluxes over large areas. It was therefore decided to discontinue this work until suitable facilities become available.

---

* Israel AEC Fellow. Permanent address: N.Y. City University, Brooklyn College, N.Y.

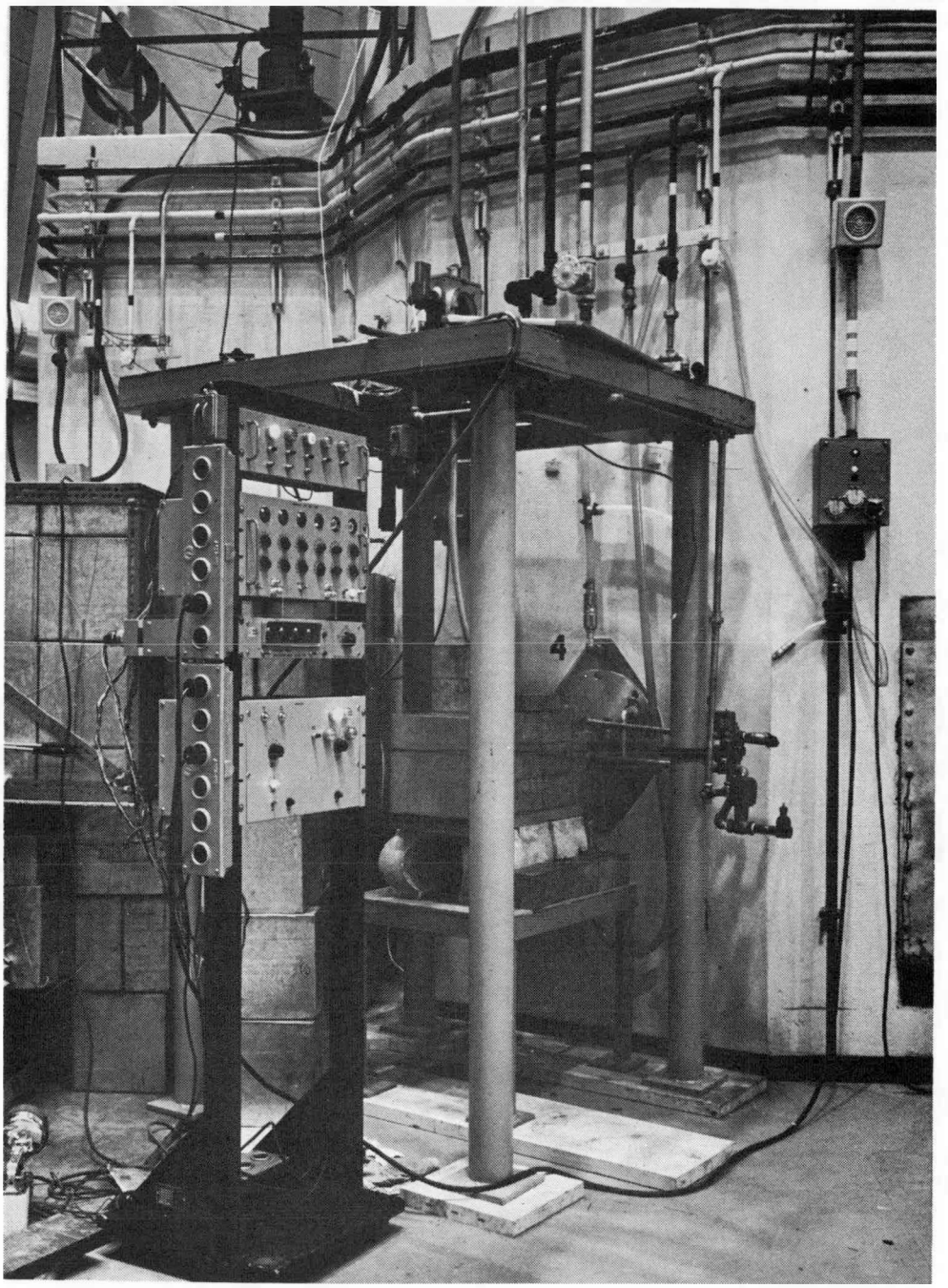

Fast shuttle rabbit facility

Photoneutron Emission from U-235 Thermal Fission Products in Heavy Water:
Jose O. Juliano* and S. Amiel

The gross photoneutron activity produced after thermal fission by U^{235} fission products in D_2O was analysed. Agreement within ± 5% was obtained between calculated and experimental data for times of ~ 1 h after the end of irradiation. Computer calculations were based on the best known data for fission and charge distribution, gamma ray energies and abundances, the excitation function for deuterium photodisintegretion, counting efficiencies, etc.

For shorter periods, nuclear data (mainly decay scheme details) are incomplete and the discrepancies between the calculated and experimental values are considerable.

The fission product chains responsible for photoneutron emission in D_2O were found to be (in each case the contributing nuclides are underlined):

$$\underline{12.8\ \text{d}\ Br^{140}} \rightarrow \underline{40.2\ \text{h}\ La^{140}} \rightarrow Ce^{140};$$

$$\underline{77\ \text{h}\ Te^{132}} \rightarrow \underline{2.3\ \text{h}\ I^{132}} \rightarrow Xe^{132};$$

$$\underline{17\ \text{h}\ Zr^{97}} \rightarrow 73\ \text{m}\ Nb^{97};$$

$$\underline{10.3\ \text{h}\ Y^{93}} \rightarrow 10^6\ \text{y}\ Zr^{93};$$

$$\underline{2.8\ \text{h}\ Kr^{88}} \rightarrow \underline{17.8\ \text{m}\ Rb^{88}} \rightarrow Sr^{88};$$

$$\underline{92\ \text{m}\ La^{142}} \rightarrow Ce^{142};$$

$$\underline{78\ \text{m}\ Kr^{87}} \rightarrow 4.7 \times 10^{10}\ \text{y}\ Rb^{87};$$

$$\underline{32.2\ \text{m}\ Cs^{138}} \rightarrow Ba^{138};$$

$$\underline{31.8\ \text{m}\ Br^{84}} \rightarrow Kr^{84};$$

$$\underline{15.4\ \text{m}\ Rb^{89}} \rightarrow 50.5\ \text{d}\ Sr^{89}.$$

Three shorter lived photoneutron activities of 8.3 m, 2.5 m and ~ 40s were observed. The latter two were tentatively assigned to the ($33\ \text{s}\ Kr^{90} \rightarrow 2.7\ \text{m}\ Rb^{90}$) and ($17\ \text{s}\ Se^{87} \rightarrow 55\ \text{s}\ Br^{87}$) chains.

* Philippine Atomic Research Center, Diliman, Quezon City, Philippines.

Half-Life Measurements of Short-Lived Selenium Isotopes* : A. Notea and E. Yellin

In connection with a study of delayed neutron emitters, experiments are in progress to determine the half-lives of the delayed neutron precursors Se^{86} and Se^{87}.

The half-lives of the short selenium isotopes were measured by Sattizahn et al.[1] who found a 16 sec activity which could be assigned to either Se^{86} or Se^{87}. Using the same chemical procedures as in ref. 1 we have distinguished between mass chains 86 and 87 by measuring the delayed neutron activity of 54 sec Br^{87} as a function of selenium separation time.

The shortest time for the separation of selenium from fission products was 20 sec from the end of irradiation. Preliminary measurements gave an upper limit of about 8 sec for the half-life of Se^{87}. The work is being continued in order to determine exactly the half-lives of both Se^{86} and Se^{87}.

Reference :

1. SATTIZAHN, J.E., KNIGHT, J.D. and KAHN, M., J. Inorg. Nucl. Chem. 12, 206 (1960)

Criteria for Selectivity in Recoil Labelling[1]** : S. Amiel and Y. Paiss

Atoms formed in different types of nuclear processes often differ in their major physical properties. For example the initial kinetic energy and charge state of a nuclide formed as a fragment in a nuclear reaction differ from those of the same nuclide produced in radioactive decay. These properties were examined with the aim of finding parameters leading to selectivity in "hot" displacement reactions, when atoms produced by different nuclear processes recoil into appropriate stopping media. Different probabilities of labelling were inferred from revised versions of the billiard-ball collision model and from scavenging effects. The conclusions

---

* Part of a Ph.D. thesis to be presented by A. Notea

** Part of a Ph.D. thesis to be presented by Y. Paiss

were examined in the light of the experimental results obtained for the displacement reaction : $I^{*}+CH_4 \rightarrow CH_3I^{*}+H$, where the labelling atom is a fission fragment, an atom recoiling after neutron capture, or a beta decay product. Possible applications of selective labelling for the separation of primary nuclear reaction products from the same nuclides produced by radioactive decay, were considered.

Reference:

1. AMIEL, S. and PAISS, Y., Radiochimica Acta 4, 157 (1965)

The Influence of Noble Gases on the Selectivity of Recoil Labelling of CH_3I by Fission Iodine* : Y. Paiss and S. Amiel

In continuation of the study of selectivity effects in recoil labelling in the gaseous phase[1,2] the effect of added noble gases on the labelling yield and on the selectivity were examined.

The addition of noble gases as diluents for CH_3I exposed to fission fragments affected the labelling by "hot" iodine as follows:

a) The labelling efficiency decreased with increasing atomic mass of the noble gas (Fig. 30).

b) As the diluting gas was changed from He through Ne, Ar, Kr to Xe, the selectivity dropped from He to the medium weight gases, then increased again for Xe (Fig. 31).

These results suggest three roles for the noble gases:

(i) As moderator for the "hot" iodine : The moderating efficiency of noble gases for iodine increases from He to the heavier gases, reaching a maximum in Xe. In "thick" targets of CH_3I, where practically no competing reactants for hot iodine exist, the moderation is of less importance because iodine itself, present as CH_3I, is a good moderator.

* Part of a Ph.D. thesis to be presented by Y. Paiss

(ii) As "cushion" for "hot" methyl iodide : The molecule CH_3I^* formed by a hot reaction between CH_3I+I^* will, in general, have a high kinetic energy, sufficient to undergo decomposition upon the first collision with a heavy neighbouring molecule. The dilution of the CH_3I medium with light atoms such as helium will increase the probability of a collision with a light mass M_L. In such a collision the CH_3I^*, of mass M_H and kinetic energy E_0, can acquire an internal energy E_i of not more than $E_i = E_0 \{ M_L / (M_L + M_H) \}$. On the other hand it may impart energy to M_L. If M_L is small compared with M_H, and the time between collisions is long compared with the redistribution time of energy in the methyl iodide molecule, the latter may lose large fractions of its kinetic energy without undergoing decomposition even after many collisions. Fig.30 illustrates this effect, where the labelling efficiency of CH_3I is at a maximum in the presence of He as diluent and decreases with increasing atomic weight of the diluent.

(iii) As scavenger: The scavenging effect of Xe atoms for iodine ions is well known[3]. The Xe serves as scavenger for the secondary iodine and may thus be effective in increasing the selectivity(Fig.31).

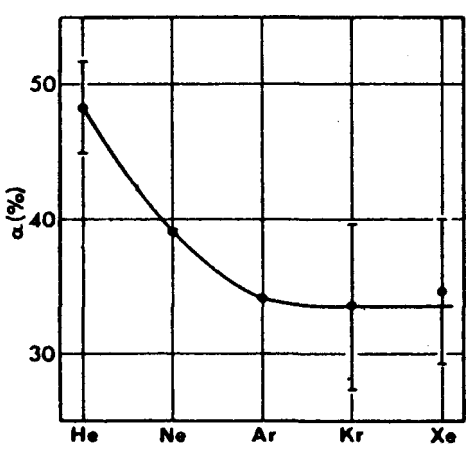

Fig.30

Yield of labelling of CH_3I by primary fission iodine (α) in presence of noble gases

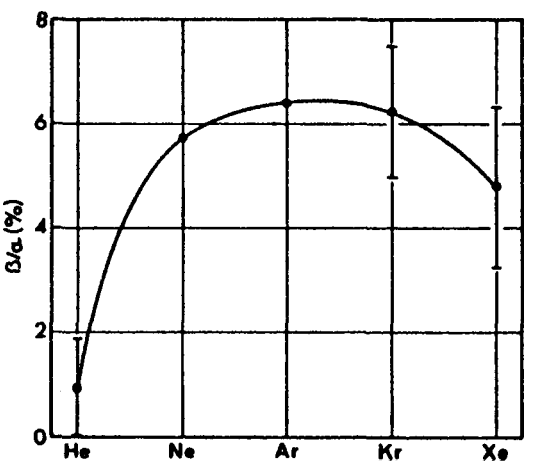

Fig.31

Ratio of labelling by secondary (β) and primary (α) iodine in the presence of noble gases

The selectivity effect discussed here is merely an alternative way of looking at high energy chemical interactions where the efficiency-determining parameter is the energy at which the reaction takes place. In our case this leads to selectivity as regards the origin of the hot iodine isotope.

References:

1. PAISS, Y. and AMIEL, S., J. Am. Chem. Soc. 86, 2332 (1964)
2. AMIEL, S. and PAISS, Y., Radiochim. Acta 4, 157 (1965)
3. RACK, E. P. and GORDUS, A. A., J. Chem. Phys. 43, 1855 (1961)

Energy Distribution of Hot Atoms in a Gaseous Medium : Elastic Scattering by Spherical Potentials of the Form $V(r) = A_1/r^{S1} + A_2/r^{S2}$: M. Baer and S. Amiel

Atoms recoiling from nuclear processes are generally slowed down by successive collisions until they reach thermal equilibrium. Some of the recoiling atoms, however, may undergo chemical interaction while still at high energies. It was recently shown[1,2] that chemical processes such as $RY + X \rightarrow RX + Y$ may occur in the gaseous phase with atoms of translational energy much greater than 10 eV. Products of such processes with fission fragments were shown to be formed in substantial yields. When the process takes place inside a "thick" target, the yield y will depend on both the excitation function of the reaction, p(E) and the energy distribution of the energetic atoms in the target, the relation being:

$$y = \int_{E_1}^{E_o} f\, p(E)n(E)dE$$

Here E_1 and E_o are respectively the threshold energy of the reaction and the initial energy of the hot atom, p(E) is the probability of a certain reaction at an energy in the interval E...E + dE, n(E)dE is the probability

that the hot atom will collide in a unit of time when its translational energy is within the interval E...E + dE, and f is the probability of meeting a target molecule of type RY in the medium.

An attempt was made to obtain the energy distribution, n(E), of the hot atoms in a "noble" homogeneous gaseous medium. The treatment was essentially based on neutron thermalization calculations[3]. Since the rigid sphere potential used for the case of neutron moderation is in fact a first approximation to the real potential governing the scattering of hot atoms, Estrup[4] and Hsiung and Gordus[5,6] modified the treatment by introducing more realistic potentials. The present computation is based on a spherical potential of the general form $V(r) = A_1/r^{S1} + A_2/r^{S2}$, where A_i and S_i $(i = 1,2)$ are the parameters determining the potential in question.

For a general potential function the energy distribution, n(E), cannot be obtained in an analytical form; therefore a program was prepared, based on the classical formulae of scattering[7], for computing n(E) for such potentials. Since the four general parameters appearing in this way in the potential function are sufficient to describe the short-range forces[8] which, actually, are the only ones that govern the scattering of the hot atom, this program may be used as a general tool for computing the distribution function n(E) of hot atoms in a gaseous phase in the steady state under the influence of spherical potentials.

As the parameters of the potential have not yet been determined for the various cases, we intend to measure them experimentally, in order to obtain at least their order of magnitude for energies below a few keV.

References:

1. PAISS, Y. and AMIEL, S., J. Am. Chem. Soc. 86, 2332 (1964)
2. AMIEL, S. and PAISS, Y., Radiochim. Acta 4, 157 (1965)
3. PLACZEK, G., Phys. Rev. 69, 423 (1946)
4. ESTRUP, P. J., J. Chem. Phys. 41, 164 (1964)

5. HSIUNG, C. and GORDUS, A. A., J. Am. Chem. Soc. 86, 2782 (1964)

6. HSIUNG, C., VEROSUB, K. L. and GORDUS, A. A., J. Chem. Phys. 41, 1595 (1964)

7. LANDAU, L. D. and LIFSHITZ, E. M., Mechanics, Pergamon Press (1960)

8. BUCKINGHAM, R. A., Planet-Space Sci. 4, 205 (1961)

Production of Tritium in the Reaction $N^{14}(n,t)C^{12}$ with 14 MeV Neutrons :

T. Sonnino, S. Kruger* and A. Nir*

The tritium produced in the atmosphere by the reaction $N^{14}(n,t)C^{12}$ accounts for a considerable part of the tritium produced in nature. The cross section and the excitation function for this reaction are not sufficiently known to permit calculation of the tritium cycle in the atmosphere. Cross section measurements with 14 MeV and 19 MeV neutrons will contribute to an understanding of this reaction.

Preliminary calculations were made of the experimental yield under various conditions of irradiation on the basis of the break-up model described by Gradsztajn et al(1).

A procedure was worked out for separating the tritium produced. The method is based on introduction of H_2 carrier before irradiation of the N_2 gas target. After reaction, the active hydrogen is reacted with ethylene on palladium as catalyst to form ethane, which is counted in a low level gas proportional counter.

Reference:

1. GRADSZTAJN, E., YIOU, F., KLAPISCH, R. and BERNAS, R., Phys. Rev. Letters 14, 436 (1965)

* Weizmann Institute of Science, Rehovoth

Cm^{244} as an Alpha-Emitter for Analytical Uses of the Reaction $O^{18}(\alpha,n)Ne^{21}$:

T. Sonnino and H. Peres*

In a search for better alpha emitters to be used in analytical applications of the reaction $O^{18}(\alpha,n)Ne^{21}$ (1), the isotope Cm^{244} was investigated.

A 2 mc deposited source, prepared as curium oxide by the Lawrence Radiation Laboratory, Berkeley, was used. Two kinds of O^{18} targets were used - gaseous CO_2 and solid KNO_3 deposited on paper. The neutron count, gamma spectra and gamma spectra in coincidence with neutrons were investigated. The aim was to get a maximum signal-to-noise ratio and a good sensitivity for O^{18}.

Under the present conditions of operation, neutron counting provides better signal-to-background ratio than either neutron-gamma coincidence or gamma counting of the 350 keV gamma rays of Ne^{21}. However, this is due in part to the high background of spontaneous fission of Cm^{244}. Cm^{242} is therefore recommended as a possible source, although limited by its shorter half-life (163 d).

Source stability was also investigated, being a critical factor in the radiation hazard to the user and the reproducibility of the measurements. Stability and freedom from contamination were satisfactory during the first year of storage. In the second year there was a discontinuity which has yet to be investigated.

The possibility of scanning paper chromatograms of compounds labelled with O^{18} was also studied.

Reference:

1. AMIEL, S. and NIR, A., Proc. of IAEA Symposium, Vienna, Oct.1964, Vol.I, p.287

---

* Weizmann Institute of Science, Rehovoth

QMGAMA, A Program for the Analysis of Gamma Spectra : M. Baer

A program for the analysis of gamma spectra[1,2] on the Philco-2000 computer was prepared. The program fits an experimental spectrum to a function of the form

$$S(c) = \sum_{k=1}^{m} J_k S(E_k, c)$$

where $S(c)$ is the given experimental spectrum as a function of the channel number c, m is the number of components in the spectrum, J_k is the intensity of the k-th component, and $S(E_k,c)$ is the normalised spectrum of the k-th component of energy E_k. $S(E_k,c)$ is obtained from a series of standard spectra stored in the computer memory. The program computes best fit values for J_k and E_k ($k = 1,...m$), using a combination of least squares and iterative procedures.

An attempt was made to use Heath's catalog of standard spectra[1,2] for the analysis of data obtained in our laboratory. The poor quality of the resulting fits showed that, due to differences in the experimental set-ups, the Heath set of standard spectra cannot serve as a basis for analysis and a new set will have to be prepared.

References:

1. HEATH, R. L., Data Analysis Techniques for Gamma-Ray Scintillation Spectrometry, IDO-16784 (1962)

2. HELMER, R. G., HEATH, R. L., METCALF, D. D. and CAZIER, G. A., A Linear Least Squares Fitting Program for the Analysis of Gamma-ray Spectra including a Gain-shift Routine. IDO-17015 (1964)

QMBLSQ, A Program for the Analysis of Multicomponent Exponential Decay Curves[1] : M. Baer

A program was prepared for the analysis of multicomponent exponential decay curves. The program was coded in the ALTAC III language for the Philco-2000 computer, with one sub-routine (for solving a system of linear equations and for inverting a matrix) coded in the TAC language.

The aim of the program is to compute A_k and λ_k, $k = 1...m$, which are the parameters in the function

$$f(t) = \sum_{k=1}^{m} A_k e^{-\lambda_k t}$$

The method used was essentially the method of least squares[1]. Since some of the unknowns do not enter the equation linearly, an iterative procedure was adopted until convergence was attained.

As convergence is attained only rarely in cases where the number of unknown λ_k's is greater than 2, two modifications were introduced which yielded convergence in a majority of cases.

The program offers the advantage of relatively high precision in solving the system of linear equations and in the inversion of the matrix, and also permits considerable flexibility in using the input data.

References:

1. BAER, M., Israel AEC Report IA-1047 (1965)

2. LIETZKE, M.H., General Least Squares and the Inversion of Symmetric Positive Matrices, Proc. of a Symp. on Application of Computers in Nuclear and Radiochemistry, Gatlingburg, Tennessee

   NERVIK, W.E., BRUNHILDE - A Code for Analyzing Multicomponent Radioactive Decay Curves. ibid

   CUMMING, J.B., CLSQ - The Brookhaven Decay Curve Analysis Program, ibid

4. BIOCHEMISTRY

(see also p.156)

The Poly-L-Histidine Copper (II) Complex as an Oxidase : A. Levitzki*, I. Pecht** and M. Anbar*

Synthetic polyamino acids have been shown to be instructive protein models[1], and it seemed possible that in combination with metal ions they might exhibit some resemblance to metalo-proteins. This possibility was investigated by examining the catalytic activity of complexes of copper with polyamino acids. It was reported earlier[2,3] that poly-L-histidine is the only polyamino acid which increases the oxidase activity of copper.

Some physical properties of the copper-polyhistidine complex were measured (Table 21). The complex has a negative Cotton effect within the region of the chromophore absorption, with an inflection at 5.45 mμ. It should be pointed out that no optical activity of the blue band in ceruloplasmin was observed. Thus the resemblance between the kinetic properties of the Cu-PLH complex and ceruloplasmin[2,3] does not extend to their physical properties. However, it should be noted that the absorption band at 320 mμ exists in both the Cu-PLH complex and the natural copper-protein. This suggests that histidine participates in copper binding in ceruloplasmin.

TABLE 21

Optical properties of the Cu-PLH complex compared with human ceruloplasmin

Substance	λ max (mμ)	$\epsilon(M^{-1}\ cm^{-1})$	λ max (mμ)	$\epsilon\ (M^{-1}\ cm^{-1})$ †
Cu-PLH	545	55	320	160
ceruloplasmin	605	1000	320	-

† Calculated on the basis of copper

References:

1. KATCHALSKI, E., SELA, M., SILMAN, H.I. and BERGER, A., The Proteins, Ed. H. Neurath, Academic Press,Inc., New York, 1964, Vol.2, p.405
2. LEVITZKI, A., PECHT, I. and ANBAR, M., Israel AEC Semi-Annual Report July-Dec. 1964, IA-1021, p.121
3. LEVITZKI, A., PECHT, I. and ANBAR, M., Nature 207, 1386 (1965)

* Soreq Radiation Research Dept.
** Weizmann Institute of Science, Rehovoth

Substrate Specificity of Ceruloplasmin : A. Levitski*

It was recently demonstrated by Frieden et al[1,2] that contrary to previous reports[3] ceruloplasmin does catalyze the oxidation of L-ascorbic acid. As ceruloplasmin exhibits other oxidase activities, for example toward epinephrine, serotonin and paraphenylenediamine, the question arises whether ceruloplasmin is a mammalian ascorbic acid oxidase. It was thus of interest to investigate whether it has different catalytic efficiencies toward L-ascorbate and D-isoascorbate.

The oxidase activity of purified human ceruloplasmin toward D-isoascorbate and L-ascorbate was measured by the method described by Frieden et al. The results are shown in Table 22.

The kinetic parameters of the two isomers are seen to be identical, within the experimental error. The oxidation of neither of the isomers was inhibited by neocuproine or serum albumin. It may be concluded that the protein does not distinguish between the two isomers and its specificity is determined by the existence of the enediol group which is present in both substrates. This is in agreement with the finding that catechol is also oxidized by ceruloplasmin[4]. Although the existence of ascorbic acid oxidase in plants, fungi and bacteria is unequivocal, contradictory findings concerning its specificity for L and D isomers were reported. Rosenberg reported that ascorbic acid oxidase catalyzes the oxidation of L-ascorbic acid more rapidly than its analogues[5], while McCarthy et al.[6] found that cucumber ascorbic acid oxidase oxidizes D-isoascorbic acid as rapidly as L-ascorbic acid. Other oxidase activities of ascorbic acid oxidase were also reported, for example the oxidation of various hydroquinones[7]. The similarity in the oxidase activity of plant ascorbic acid oxidase and ceruloplasmin suggests that ceruloplasmin, in spite of its broad specificity, may be considered a mammalian ascorbic acid oxidase. Although it may be argued that the turnover number of ceruloplasmin compared with ascorbic acid oxidase is low (see Table 22), it has already been pointed out that

---

* Radiation Research Dept.

ceruloplasmin is present in the blood at high concentrations[2], in order to induce rapid oxidation of serotonin or epinephrine which are present in the serum.

TABLE 22

Kinetic parameters of the ceruloplasmin catalyzed oxidation of L-ascorbate and D-isoascorbate

Parameter measured	Ceruloplasmin		Ascorbic acid oxidase	
	L-ascorbate	D-isoascorbate	L-ascorbate	D-isoascorbate
K_m (μM)	5.0	4.5	39 (ref. 8)	not determined
Turnover number (moles substrate/ moles enzyme/min)	10.5	9.4	6.5×10^5 (ref. 9)	not determined

The reaction mixture contained 1.40×10^{-7} M human ceruloplasmin purified according to the method of ref. 1, 0.2 M ascorbate buffer pH 5.5, 16 μM neocuproine and 8.0×10^{-5} M L-ascorbate or D-isoascorbate in a final volume of 3.0 ml. The solution was saturated with pure oxygen before addition of the enzyme and substrate. The disappearance of the L-ascorbate or D-isoascorbate was followed at 2.65 mμ in a thermostated Zeiss PMQ II spectrophotometer, at 30°.

References:

1. OSAKI, S., WALTER, C. and FRIEDEN, E., Biochim. Biophys. Res. Com., 12, 1 (1963)
2. OSAKI, S., McDERMOTT, A. and FRIEDEN, E., J. Biol. Chem., 239, 3570 (1964)
3. MORELL, A.G., AISEN, P. and SCHEINBERG, I.H., J. Biol. Chem., 237, 3455 (1962)
4. PEISACH, J. and LEVINE, W.G., J. Biol. Chem., 240, 2284 (1965)
5. ROSENBERG, H., Skand. Arch. Physiol., 76, 119 (1937)
6. McCARTHY, J.F., GREEN, L.F. and KING, C.G., J. Biol. Chem., 128, 455 (1939)
7. DAYAN, J., Ph.D. thesis, Columbia University, 1960
8. FRIEDEN, E. and MAGGIOLO, I.W., Biochim. Biophys. Acta, 24, 42 (1957)
9. COHEN, G., Ph. D. thesis, Columbia University, 1964

5. ANALYTICAL LABORATORIES

A. ANALYTICAL CHEMISTRY

Determination of Dissolved Gases in Natural Waters by Gas Chromatography : M. Wiernik and M. Mantel

In his study of the radon and radium content of some water sources in Israel, E. Mazor[1] pointed out the importance of dissolved gas analysis. A study of the dissolved gas content of natural waters has been started in cooperation with Dr. E. Mazor of the Isotope Department of the Weizmann Institute of Science.

Preliminary experiments to find a suitable method of analysis were conducted on artificial mixtures of gases (H_2, O_2, Ar, CH_4, CO, CO_2 and SH_2) using a Perkin Elmer 116E chromatograph. The method chosen was similar to that published by Manka[3]. The apparatus (Fig.32) consists basically of two columns and two detector cells arranged alternately in series.

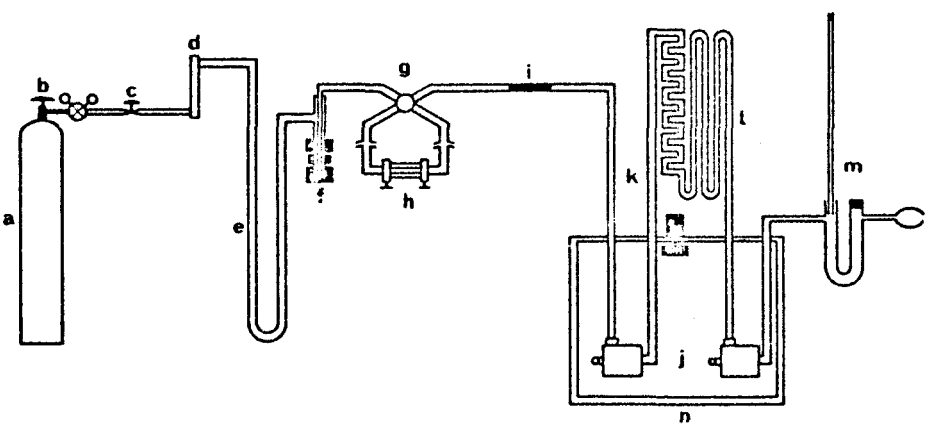

Fig. 32

Apparatus for gas chromatography

a- carrier gas supply; b- two stage regulator; c- fine valve; d- rotameter; e- desiccant tube; f- home made injection port for syringes; g- four-way valve; h- calibration gas pipette; i- first column (10 cm × 1/4 inch O.D., silica gel 20-80 mesh); j- thermistor bead detectors (only the "sample" side was used); k- delay tube (13 m. Tygon tube 1/4 inch O.D.); l- second column (2 m × 1/4 inch O.D., molecular sieve 5A 30-60 mesh); m- soap film flowmeter; n- thermostatic oven with fan.

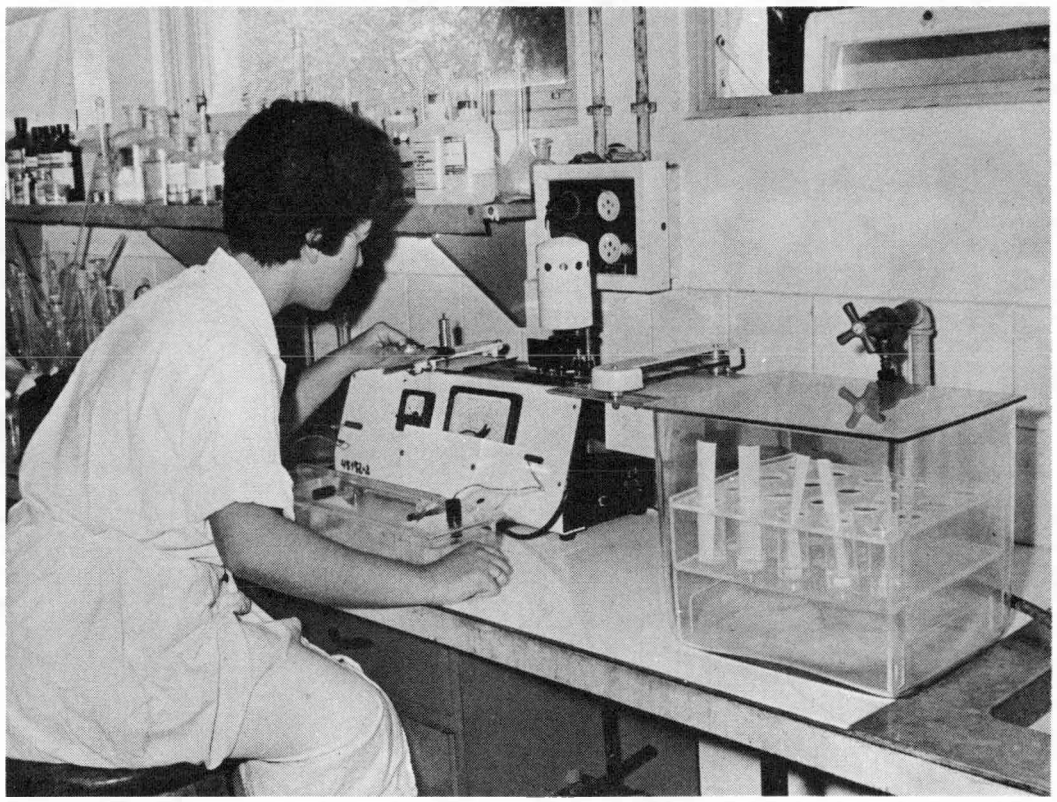

Analytical laboratory

The detectors were the measuring cells of two Perkin Elmer detectors, the reference cells of the latter being disconnected. This arrangement was necessary since the reference cell of the Perkin Elmer detector gives very broad overlapping peaks, so that it was not possible to use a single complete detector. A delay tube was added in order to avoid overlapping of signals from the two detectors.

Fig.33 shows a typical chromatogram obtained. In order to determine the range for which the detector response is linear, different quantities of pure gases were injected. Both the peak height and peak area were found to be linear up to at least 2 ml in the case of SH_2 and O_2 + 5% Ar, and up to at least 1 ml for CH_4 and CO. The peak area was linear up to at least 8 ml for N_2 and 1 ml for CO_2 and H_2, the respective peak heights being linear up to 0.8 ml CO_2, and nonlinear for H_2.

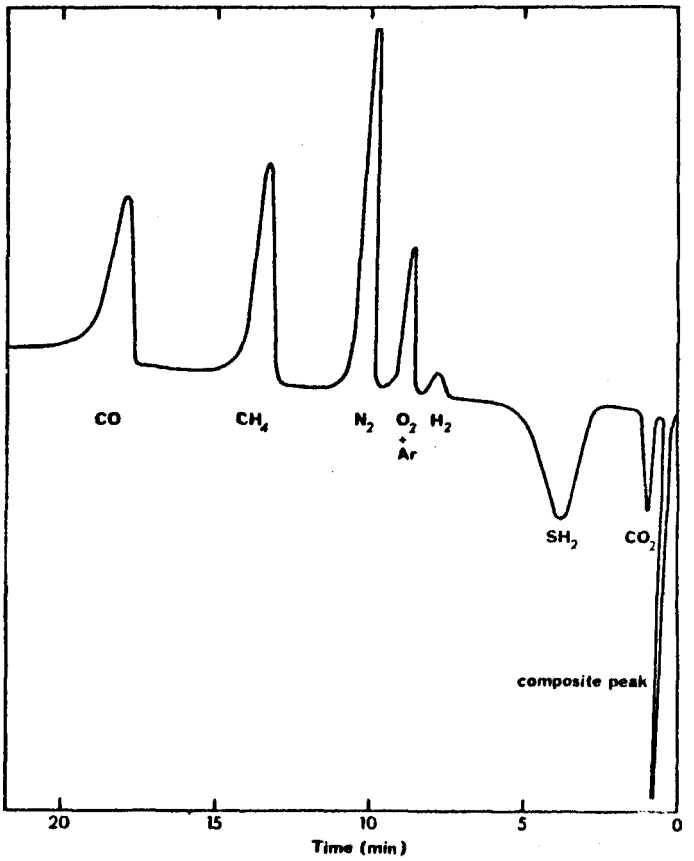

Fig. 33

Typical chromatogram. Temperature of columns 28°C (room temperature); detector temperature 42°C; carrier gas - helium, 58 ml/min

In view of the success of the preliminary experiments attempts will be made to increase the response, sensitivity and baseline stability of the apparatus. For this purpose a Gow-Mac Ice Bath thermistor detector with symmetrically shaped cells was acquired, as well as a Gow-Mac power supply and a 1 mV Honeywell potentiometric recorder.

A vacuum network for the extraction and treatment of dissolved gases has been designed and partially constructed. A titanium oven is included in this system for the isolation and concentration of the noble gases prior to their determination. Analysis of natural water samples from different parts of the country will be started soon.

References:

1. MAZOR, E., Geochim. et Cosmochim. Acta, 26, 765 (1962)
2. WIERNIK, M., Israel AEC Report, IA-1066 (in press)
3. MANKA, D.P., Anal. Chem., 36, 480 (1964)

Determination of Caesium in Sea Water: M. Mantel and A. Padova

The mean concentration of caesium in sea water has for many years been accepted to be 2 µg/l. More recent works report values of 0.5 µg/l in the North Atlantic and 0.3-0.4 µg/l on the United States Eastern Shores[1]. Variations of concentration with depth are also reported.

The main problem in the determination of caesium in sea water is its low concentration, coupled with the presence of high concentrations of other alkali metals. Even the most sensitive methods necessitate preconcentration to bring the caesium into the detectable range. Most of the published methods are laborious and require large quantities of sea water (2-200 liters). A new method is therefore being worked out in our laboratory and it is hoped to use it to determine caesium in the Mediterranean, Red and Dead Seas.

The proposed method consists of three stages:

a) Preconcentration and at the same time separation from the bulk of the salts, by solvent extraction with tetraphenylboron[2].

b) Separation from rubidium, potassium and ammonium ions by the use of thallous phosphotungstate (TPT) as cation exchanger[3] and thallous nitrate as eluent.

c) Determination of caesium in the now pure solution by atomic absorption spectrophotometry.

The first step, namely extraction with tetraphenylboron, was studied and the optimum conditions for maximum recovery of caesium (95%) from 500 ml sea water were established by the use of Cs^{137}. The TPT separation step is now being studied using Rb^{86} and Cs^{137} as tracers.

References:

1. YAMAGATA, N., Bull. Inst. Publ. Health, 14, 59 (1965)
2. FINSTON, H.L. and KINSLEY, M.T., The Radiochemistry of Caesium , NAS-NS-3035(1961)
3. CARON, L.H. and SUGIHARA, T.T., Anal. Chem., 34, 1082 (1962)

Determination of Natural Thorium in Urine: M. Mantel and H. Brown*

A convenient method for detecting thorium poisoning was developed, for use in the routine check of workers who are in contact with natural thorium.

The method is based on measurement of the delayed neutrons emitted after the fission of thorium[1]. Since uranium and plutonium also emit delayed neutrons after fission, a complete separation from these two elements is necessary. This is achieved by extracting the thorium from 1 liter urine with 0.2 M 2-thenoyltrifluoroacetone (TTA) in chloroform in the presence of acetate buffer at pH 4.5[2]. The thorium is back-extracted into nitric acid, the solution introduced into a polyethylene container and irradiated for 1 min (using the pneumatic transfer tube) in the IRR-1 reactor operating at 2 MW power. Since only neutrons of energy 1 MeV or more cause fission in thorium a cadmium shield was used to eliminate neutrons of lower energy and increase the sensitivity for thorium.

The recovery of thorium during the extraction step was 90%, as found by the use of carrier free Th^{234} tracer prepared from uranyl nitrate

* IAEA Fellow. This work is part of an M.Sc. Thesis.

hexahydrate in 9.6 M HCl (ref. 3) by ion-exchange on a Dowex-1-x 4 column. The separation from uranium was checked by analysing the chloroform extract by the fluorometric method.

Accurate and reproducible results were obtained down to 4 μg thorium per liter urine. Since the maximum permissible dose for thorium is considered to be 10-20 μg thorium per liter urine the method is suitable for the detection of thorium poisoning.

References:
1. AMIEL, S., Anal. Chem., 34, 1683 (1963).
2. RAINS, T.C., FERGUSON, M. and HOUSE, H.P., Anal. Chem., 33, 1645 (1961).
3. SILL, C.W., Anal. Chem., 36, 675 (1964).

Improved Method for the Determination of Iodine in Urine[1]: M. Mantel

The determination of iodine in urine is of great value in thyroid metabolism studies. An improved method of analysis was developed which gives accurate and reliable results and is at the same time rapid and easy to perform.

Like other methods, the present analysis is based on destruction of the organic matter followed by spectrophotometric determination of the liberated iodine by its catalytic action on the oxidation-reduction reaction between Ce^{IV} and As^{III}. By using I^{131} as a tracer it was possible to study the losses of iodine during the destruction of organic matter. Zinc sulphate and sodium hydroxide (Folin Wu's reagent) followed by dry-ashing with potassium carbonate were found to give the best results. The maximum overall loss was 5%. This error was eliminated by using a calibration graph based on standards subjected to the whole procedure.

The error arising from the nature of the catalytic reaction itself, namely instability of the color with time, were overcome by stopping the reaction by the addition of a known amount of ferrous ions[2] which are

oxidized by the Ce^{IV} ions remaining from the catalytic reaction. The ferric ions formed are determined spectrophotometrically by measuring the absorption of the thyocyanate complex at 460 mμ. An accuracy of ± 4% was obtained calculated from 10 determinations of the same sample.

References:

1. MANTEL, M., Analyt. Chem. (submitted).
2. DUBRAVCIC, M., Analyst, 78, 494 (1953).

Microcoulometric Determination of Chloride Ions: M. Wiernik and A. Glezer

The sensitivity of silver anode - constant current coulometric methods for the determination of chloride ions has been improved from the cited value of 0.2 mg chloride in 50 ml support electrolyte[1] to microgram quantities. At the same time this modern technique was introduced into the routine work of the analytical laboratory.

A lower current was used, down to 0.1 mA, provided by a Model E211 Metrohm coulometer, and a PHM 25 SE Radiometer pH meter with scale expender in order to increase the reading sensitivity. The size of the titration cell was reduced to a minimum compatible with the available electrodes of the pH meter.

The titration cell, shown in Fig.34, is a 5 ml glass beaker. A closed sintered glass tube contains the platinum cathode, isolated from the rest of the solution in order to avoid discharge of the silver ions. The silver generator anode is coiled around this tube, and both electrodes are connected to the coulometer. The potentiometric electrodes, a P401 silver indicator electrode and a K601 saturated mercurous sulfate reference electrode, are inserted beside the tube and connected to the pH meter. A micro spin bar is placed at the bottom of the cell and the whole assembly stands on a magnetic stirrer.

The general procedure is as follows. A 3 ml portion of support electrolyte (80% v/v ethanol in water, 0.05 M in perchloric acid and saturated

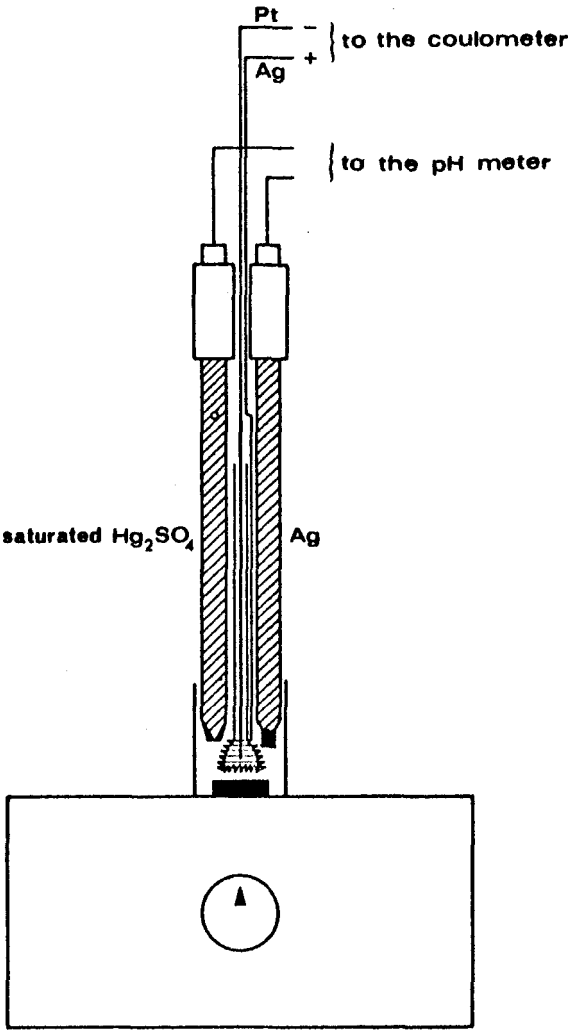

Fig. 34

Arrangement for microcoulometric determination of Cl^-

with sodium nitrate) is introduced into the cell, 1 ml of sample is added and the solution is titrated stepwise, with stirring, using a known constant current. The readings are recorded till the endpoint is passed. From the known electrolysis current and the measured time required to reach the equivalence point, the quantity of silver ion generated and thus of halide ion precipitated is computed by Faraday's Law.

For samples down to 10^{-3} M the sharp inflection of the curve permits easy detection of the endpoint (Fig.35, curve a), but for 10^{-4} M samples there is no inflection (Fig.35, curve b) and the curve obtained must be compared with calibration curves obtained for standard solutions.

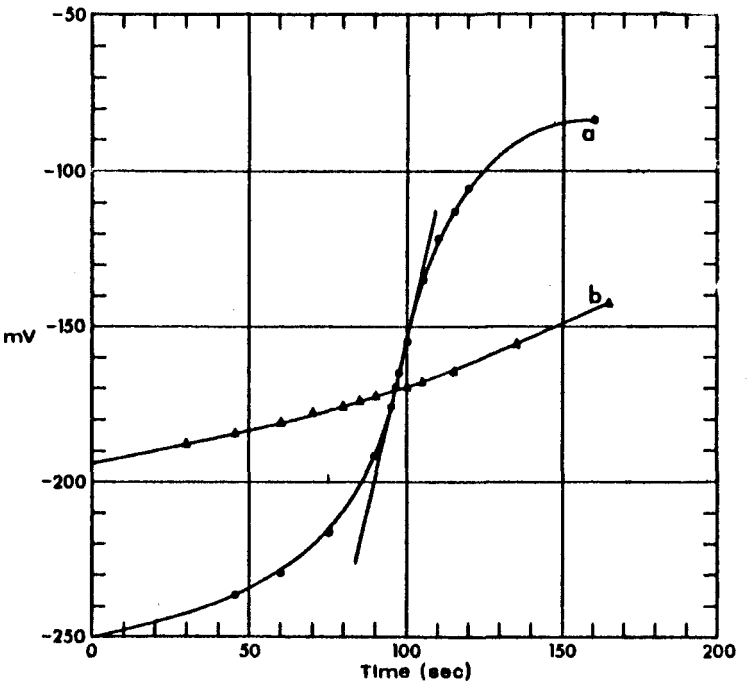

Fig. 35

Titration curves

a) 1 ml 10^{-3} M NaCl titrated with 1 mA
b) 1 ml 10^{-4} M NaCl titrated with 0.1 mA

A saturated mercurous sulfate electrode was preferred to the reference glass electrode suggested by Lingane[1], since with samples of very different pH the endpoint may be different, and for the 10^{-4} M level a special calibration may be needed in each case.

At the 10^{-3} M level, measurements are accurate to within $\pm$ 1%. With 10^{-4} M solutions, the relative standard deviation of nine determinations was $\pm$ 3.8%, which means that the method is comparable in accuracy and sensitivity to the spectrophotometric methods[2], with the advantage that it is more rapid (one determination takes 5 - 10 minutes), needs no standards

but only a simple calculation based on the Faraday Law, and requires no reagents except silver wire and the support electrolyte.

References:

1. LINGANE, J. J., Anal. Chem., 26, 622 (1954)
2. BOLTZ, D. T., Colorimetric Determination of Non-Metals, Interscience, New York, p.161-180, 1958

B. SPECTROSCOPY

Spectrochemical Determination of Alkali Metals in Reactor Waters :
Irena Schoenfeld

A spectrochemical method has been worked out for determining alkali metals in reactor waters. The work is a continuation of that reported previously for the analysis of trace elements in reactor waters[1].

The experimental conditions used are given in Table 23.

TABLE 23

Experimental conditions

Spectrograph	Jarrell Ash Grating Spectrograph, Ebert mounting, 3.4 m focal distance, grating 15000 grooves/inch, first order. Corning 3-70 filter to cut out overlapping orders.
Spectral range	6350 A - 8850 A
Slit width	15 μ
Mode of illumination	The image of the source on the collimator mirror
Source	DC arc, 7.5 amp., Jarrell Ash Standard Varisource
Electrodes	UCP ultra purity graphite. Upper - 3 mm diameter with pointed end, lower - 4.5 mm diameter with a hole of 1 mm diameter and 3 mm depth
Analytical gap	2 mm
Exposure time	15 sec
Photographic plates	Kodak IN
Developing	D-19, 3 min, 20°C

Samples for analysis were taken from the reactor pool during six months under normal conditions. Standards were prepared by dissolving suitable amounts of alkali chlorides or carbonates (Johnson Matthey, Specpure) in demineralized water. In view of the suppressing influence of alkali earth elements on the intensity of alkali metal lines appropriate small

quantities of barium and calcium were added to the standards if these elements were found in the spectrum of the sample to be analysed. Pure graphite (4 mg per charge) was added to the standards and samples, after which they were evaporated to dryness in platinum dishes under the infrared lamp. The residue was loaded in specially prepared electrodes (see Table 23). The depth of the electrodes proved critical for the sensitivity and reproducibility of the results. Although evaporation of standards was time-consuming, this technique prevented errors which might arise from losses during concentration of the sample.

An attempt was made to concentrate the traces of alkali metals by absorption on activated carbon, which could be taken for excitation directly after decantation. However measurements performed with the aid of radioactive isotopes (Na^{22}, $T_{\frac{1}{2}}$ - 2,6y and Cs^{137}, $T_{\frac{1}{2}}$ - 33y) showed insufficient absorption coefficients.

Table 24 gives the analytical lines used and limits of detection

TABLE 24

Limits of detection

(Concentration factor - 500)

Element	Analytical line A	Absolute sensitivity 10^{-6} g	Limit of detection ppb
Li	6707.844	0.05	0.1
Na	8183.270	0.05	0.1
K	7664.907	0.05	0.1
Rb	7800.227	0.5	1.0
Cs	8521.10	5.0	10.0

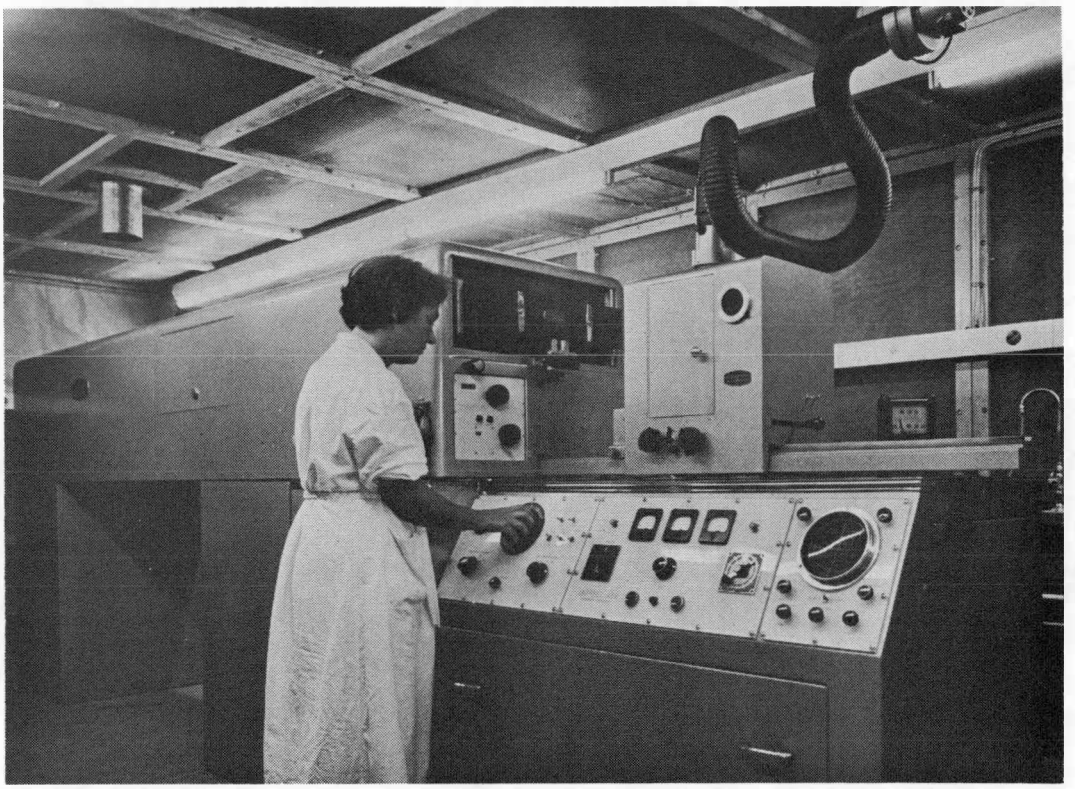

The Jarrel-Ash spectograph - the main tool of the spectroscopic group

obtained for the various alkali metals. The concentrations were evaluated by visual comparison of the intensity of the analytical lines for samples and standards. This was sufficient for purity monitoring of the reactor water . The differences in the concentration of alkali metals in all the samples analyzed were small. The potassium content varied from 5 to 10 ppb and sodium from 20 to 50 ppb. Lithium, rubidium and caesium were not detected.

The sensitivity of the present method is similar to that obtained by flame photometry[2,3].

References :

1. SCHOENFELD, I., Israel J. Chem. 3, 47 (1965)
2. JOHNSON, G., AB Atomenergi, Sweden, AE-105, 1963
3. FERRARIS, M.M., Comitato Nazionale Energia Nucleare, Roma, RT/PROT 13, 1963

Influence of Alkali Metals on the Intensity of Boron and Strontium Lines Obtained by Copper Spark Excitation : Irena Schoenfeld

In the course of work on the determination of boron and strontium in reactor waters by the copper spark technique[1] a strong influence of foreign elements on the line intensities was observed.

In the present work the influence of alkali metal cations on the analytical lines of interest was investigated. To solutions containing 5 ppm boron and 2.5 ppm strontium, pure alkali metal cations were added in concentrations calculated according to their atomic weights (50 ppm Li, 165 ppm Na, 280 ppm K, 615 ppm Rb, 960 ppm Cs). The spectra of these solutions were obtained under experimental conditions similar to those in ref. 1. The exposure time was shortened to 15 sec, since it was observed that the influence was most marked in the first period of sparking.

The relation between the ionization potential of the alkali metals and the intensity of the boron and strontium lines is given in Fig. 36.

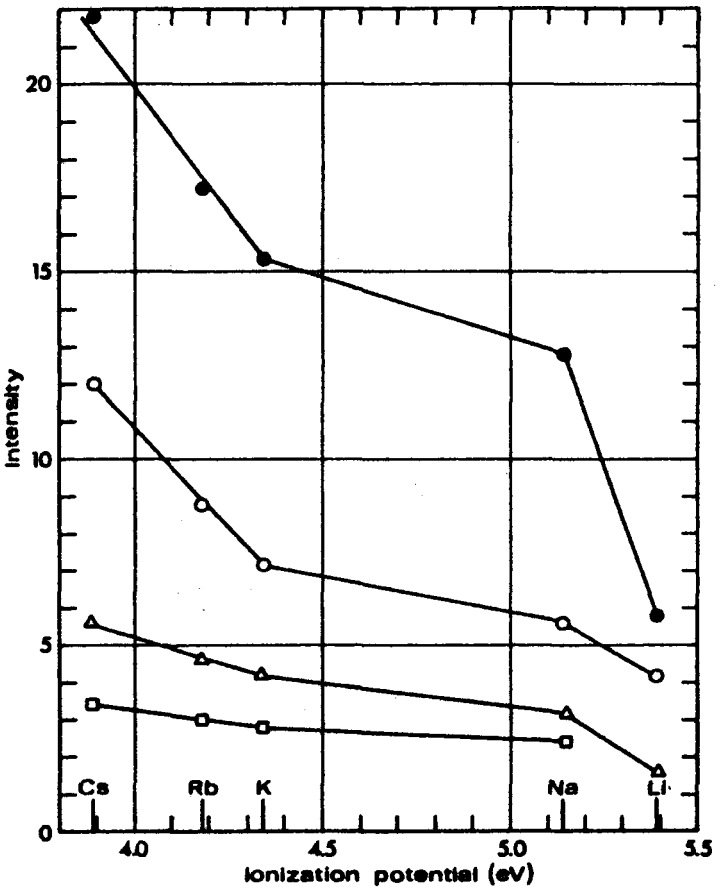

Fig. 36

Intensity of boron and strontium lines as a function of the ionization potential of the alkali metals. Each point represents the mean of eight measurements taken from two photographic plates

● SrII - 4077.7 ○ SrII - 4215.5 △ BI - 2497.7 □ BII - 3451.4

These preliminary results show that both the atomic and ionic lines of boron and the two ionic lines of strontium investigated are suppressed in a similar way in the presence of alkali metals, the influence being greater for strontium.

Further experiments will be carried out to see if the observed shape of the graphs is related to irregularities in any of the physical constants of the alkali metal chlorides, such as heat of formation or boiling point.

Reference:

1. SCHOENFELD, I., Israel J. Chem. 3, 47 (1965)

Spectrochemical Determination of Gallium in Uranium-Gallium Alloys :

I. Schoenfeld and S. Held

The "copper spark" technique described for the determination of In in U-In alloys[1] was applied to the analysis of Ga in U-Ga alloys. The method is suitable for the concentration range 0.05 - 2 wt percent Ga.

The entire procedure was identical to that described in ref. 1. In order to check the influence of the pH of the solutions used, two series of standards were prepared, one with 0.02M HCl and the other with 0.2M HCl. Although the intensity of the analytical lines (Ga 4172.05 A and U 4171.59 A) was higher at the lower acid concentration, the intensity ratio as measured photometrically remained constant.

The analytical curve was based on the measurement of 6 photographic plates (Table 25). The coefficient of variation of a single determination was about 15%. The concentration of Ga in the sample under investigation was read from the analytical curve, the confidence interval being ± 15% as calculated for the mean value of 6 determinations at 95 percent probability level. The accuracy of the method was further verified by use of additional standards containing 0.25, 0.30 and 0.40 wt percent Ga.

The limit of detection established visually was found to be 0.02 wt percent Ga using the 0.02M HCl solution.

The same analytical curve could be used for samples containing more than 2 wt percent Ga if they are diluted with uranium standard solution to the required concentration range.

TABLE 25

Determination of Gallium in Uranium-Gallium alloys

C wt % Ga	n	$\overline{\Delta Y}$	$S_{\Delta Y}$	$\bar{S}_{\Delta Y} = \frac{S_{\Delta Y}}{\sqrt{n}}$	$\overline{\Delta Y} \pm t\bar{S}_{\Delta Y}$	$\frac{S_c}{\bar{C}}$ %
0.05	15	-0.82	0.065	0.018	-0.82 ± 0.039	16.2
0.10	22	-0.61	0.057	0.012	-0.61 ± 0.025	14.2
0.20	23	-0.30	0.039	0.009	-0.30 ± 0.019	9.8
0.50	24	+0.08	0.058	0.012	+0.08 ± 0.025	14.5
1.00	21	+0.35	0.053	0.012	+0.35 ± 0.025	13.2
2.00	20	+0.58	0.049	0.011	+0.58 ± 0.023	12.2

n - number of measurements

ΔY - logarithm of the intensity ratio of the analytical lines

$$S_{\Delta Y} = \sqrt{\frac{\Sigma (\Delta Y - \overline{\Delta Y})^2}{n - 1}}$$

t - a constant depending on the number of degrees of freedom on which $\bar{S}_{\Delta Y}$ is based. The confidence interval is computed for 95 per cent probability level.

$\frac{S_c}{\bar{C}} = 2.3 \frac{1}{b} S_{\Delta Y} \times 100$ - coefficient of variation for a single determination.

b - the slope of the analytical curve. In the present work b = 0.93

Reference:

1. HELD, S. and SHOENFELD, I., Israel J. Chem., 1, 86 (1963)

Spectrochemical Determination of Boron, Barium, Lithium and Rubidium in Mediterranean and Dead Sea Water[1] : I. Schoenfeld and S. Held

Spectrochemical methods based on the technique of addition were worked out for determining boron, barium, lithium and rubidium in Mediterranean and Dead Sea waters.

The rotating disc - spark excitation technique was used in the case of boron in Mediterranean and Dead Sea water, and barium in Dead Sea water. The relative mean standard deviation was about 13%. The limit of detection was 2 and 20 mg B/liter in Mediterranean and Dead Sea water respectively, and 3 mg Ba/liter in Dead Sea water. For barium in the Mediterranean Sea, only the order of magnitude obtained by DC arc excitation of the dry residue was determined.

Lithium was determined by the solution-impregnated electrode technique, using DC arc excitation. The relative mean standard deviation was about 13% for Mediterranean and 6% for Dead Sea water, and the limit of detection 0.05 mg Li/liter.

Rubidium was determined by DC arc excitation of the dry residue mixed with Ag_2O as a buffer. The relative mean standard deviation was about 15% and the limit of detection 0.1 mg Rb/liter.

The concentrations found for boron, barium, lithium and rubidium in Mediterranean Sea water are close to the published values for other sea samples. The concentration of boron found in Dead Sea water is in agreement with the results obtained in other laboratories. The results for lithium are close to those obtained by flame photometry[2].

Reference :

1. SCHOENFELD, I. and HELD, S., Israel AEC Report IA-1061, 1965

2. YOFFE, I. and STILLER, M., Bull. Res. Counc. of Israel 11 A2, 132 (1962)

C. ACTIVATION ANALYSIS (Nuclear Chemistry Department)

Determination of Iron-58 in Blood by Activation Analysis* : C. Schenberg

Stable Fe^{58} was used as a tracer in ferrokinetic studies in babies up to the age of 10 weeks. Iron nitrate enriched to 78% Fe^{58} was injected intravenously, and its rate of disappearance studied by sampling the blood for 2 hours after injection.

The dried and ashed plasma samples (0.4 - 1.2 cc fresh plasma per sample) were sealed in quartz ampoules and irradiated for 24 hours in the reactor core, at a flux of 2.5×10^{13} $n/cm^2.sec$, together with standards of pure iron solutions.

After a cooling period of about two weeks the samples were dissolved in concentrated HNO_3, with about 10 mg iron carrier. The solution was then treated with H_2O_2, and $Fe(OH)_3$ was precipitated with NH_4OH and filtered. Fe^{59} activity in the precipitate was determined by gamma ray spectrometry. After counting, the chemical yield was determined by redissolution of the precipitate in H_2SO_4, reduction with metallic Zn, and permanganate titration of the resulting Fe^{++}.

On the average, the chemical yield was over 90%. The overall precision of the procedure was 3 - 7%, and the sensitivity better than 10^{-8} g Fe^{58}. More than 150 samples were analysed. The Fe^{58} content varied between 0.02 and 0.4 μg over a natural Fe^{58} background of about 0.01 μg.

The medical aspects of this study will be published elsewhere.

---

* Project carried out in cooperation with Drs. Matot and Illian of the Sharon Hospital, Petah-Tikva

Uranium Assay in Meteorites : J. Gilat and S. Amiel

The high sensitivity and specificity of delayed neutron counting for the nondestructive activation analysis of uranium[1] make this method especially suitable for the analysis of meteorites. In a conventional 4π counting system, 1 μg of natural uranium irradiated for 60 seconds in a thermal neutron flux of about 4×10^{12} $n/cm^2.sec$ (the flux now available in the pneumatic tube facility) yields about 400 neutron counts over a background of about 10 counts, when counted for one minute with a 20 sec delay after the end of irradiation. Since meteorites usually contain a few tens of ppb of uranium, a precision of 5-15% can easily be obtained by repeated irradiations of samples weighing a few grams. Interference from fast fission of Th^{232} is negligible, since the thorium content of meteorites is usually of the same order of magnitude as that of uranium, and the sensitivity is much lower. In chondrites, which have high oxygen and low uranium concentrations, some interference was found from 4 sec N^{17}, produced by the $O^{17}(n,p)N^{17}$ reaction with the fast neutrons in the irradiation flux. This source of error was eliminated by increasing to 30 sec the delay period between the end of irradiation and counting.

Seventeen samples of chondrites obtained from Prof. E. Anders and Dr. D. Heyman of the University of Chicago were analysed, with the following results:

Meteorite	Uranium 10^{-8} g/g sample	Meteorite	Uranium 10^{-8} g/g sample
Arapahoe (I)	2.11 ± 0.27	Wickenburg	2.56 ± 0.23
Bruderheim	1.80 ± 0.21	Kingfisher (I)	2.63 ± 0.21
Ramsdorf	1.80 ± 0.27	Barreta (I)	1.91 ± 0.16
Harleton	1.18 ± 0.15	Kingfisher (II)	2.03 ± 0.17
Goodland	1.88 ± 0.18	Hayes Centre	2.32 ± 0.30
Arapahoe (II)	1.57 ± 0.16	McKinney	1.61 ± 0.19
Farmington	1.91 ± 0.19	Lubbock	3.27 ± 0.22
Potter	1.91 ± 0.15	Barreta (II)	3.23 ± 0.27
		Richardton	1.51 ± 0.20

Reference:

1. AMIEL, S., Anal. Chem. 34, 1683 (1962)

Determination of Bromine by X-Ray Counting : H.L. Finston, J. Gilat and C. Schenberg

Determination of bromine by activation and X-ray counting or spectroscopy of 4.5 h Br^{80} was attempted. This technique should in principle be less susceptible to interferences by the common radioactive contaminants than assay of the 36 h Br^{82} by gamma ray spectrometry. Preliminary results with a thin window proportional counter filled with P-10 gas indicate that a sensitivity of at least 1 μg is attainable, and that bromine can be determined nondestructively in the presence of up to 100 times as much Na and K. Mn^{56} when present is a source of interference. Further experiments with a detector of improved resolution (the present one is about 20%) are in progress.

Manganese Content of Soils and Plants as Determined by Activation Analysis[1]: A. Nilubol * and U. Kafkafi**

The effect of the parent material on the manganese content of the soil formed from it and of the plants grown in this soil was studied. A rapid procedure based on neutron activation analysis was used. Soils formed from basaltic rocks had very high concentrations of manganese (3300 and 1300 ppm). Alluvial soil influenced by desert aeolian deposits contained 750 ppm manganese. Soils developed on dolomite rocks and sand dunes contained 227 and 159 ppm respectively. No correlation was found between the concentration of manganese in plants and that in the soils on which they were grown. Possible mechanisms to explain the experimental observations were considered.

Reference:

1. NILUBOL, A. and KAFKAFI, U., Paper SM-65/26, presented at the IAEA Symposium on the Use of Isotopes and Radiation in Soil-Plant Nutrition Studies, June 1965, Ankara, Turkey

---

* IAEA Fellow. Permanent address: Thai Atomic Energy Commission for Peace, Bangkok, Thailand

** Volcani Institute of Agricultural Research, Rehovoth

Miscellaneous Determinations

(i) Determination of Oxygen in Steel :

Oxygen traces in steel samples were determined by activation analysis, using the $O^{16}(n,p)N^{16}$ reaction with 14 MeV neutrons and measuring the 6.13 MeV gamma rays of N^{16}.

An argon-actuated pneumatic transfer system was used to place the samples next to a neutron generator target, in a flux of about 5×10^8 n/cm^2. sec. With a cycle of 10 sec irradiation, 3 sec delay and 30 sec counting, the yield was approximately 50 counts per milligram oxygen. Background could be kept negligible. In samples of low oxygen content, counts from 10 consecutive irradiation cycles were usually collected. The detection limit was about 1 mg (or 100 ppm for 10 g samples) and the precision 5-15%, the main sources of error being counting statistics and the 1.6 ± 0.1 mg natural oxygen content of the polyethylene ampoules used as sample containers.

Ten steel samples obtained from Arbed Ltd., Luxembourg (through Euratom) were analysed. The oxygen concentrations found varied from about 100 to about 800 ppm. (J. Gilat and Y. Eden)

(ii) Precision and Accuracy of Routine Uranium Analyses by Delayed Neutron Counting :

Routine determinations of uranium in solid and liquid samples were continued. Over 150 samples were analysed.

The precision of these analyses was found to be about ±3%, even though in some cases the error due to counting statistics was less than 1%. The error can be attributed to neutron flux fluctuations in the reactor. A procedure is being worked out whereby uranium standards will be irradiated together with the sample and counted simultaneously with it in a separate neutron counter. Use of these internal standards will enable us to correct for the flux fluctuations.

The accuracy of our analyses suffers from the lack of an absolute dilute standard for powdered samples. The standard in use at present is a dunite-pitchblende mixture with a nominal uranium content of 10 ppm (obtained through the U.S. National Bureau of Standards). In view of a recent comparison with samples obtained from the IAEA (two samples of Torbenite of different origins, analysed at several other laboratories), this concentration has been revised to 12.5 ppm. All our results will be based on this value, which is accurate to better than 5%. (J. Gilat, Y. Eden and J. Latti*)

(iii) Use of Activation Analysis in Forensic Investigations :

Samples of paint smears on metal, wood and textiles, steel samples, firearm ammunition, grease smears, metal depositions and plastics sent in by the Criminal Investigation Department of the Police, were activated in the pneumatic tube of the IRR-1 reactor and the characteristic gamma ray spectra were analysed and used for identification purposes. This work is being done on a routine basis.(Y. Tamir**)

(iv) Rapid Determination of Au, Pt, Ag and Pd in Precious Metal Scraps by Activation Analysis :

Quantitative analyses were carried out for the determination of Au, Pt, Ag and Pd in metals, by activation in the IRR-1. The (n,γ) reaction products (Ag^{108}, Au^{198}, Pd^{109}, Pd^{111}, Pt^{193}, Pt^{197}, Pt^{195m}) were identified by their gamma energies and half-lives. A 3" NaI crystal was used for most of the determinations. The 13.6 h Pd^{109} was detected by measuring the 22 keV X-ray radiation with a thin NaI(Tl) crystal. Errors were of the order of a few percent. (H.L. Finston*** and C. Schenberg)

---

* Summer student

** Israel Police Central Laboratory

*** Israel AEC Fellow. Permanent address: N.Y. City University, Brooklyn College, N. Y.

(v) Determination of Exchangeable Body Electrolytes by Isotope Dilution* :

Body electrolytes (Na,K,Cl) were determined by standard isotope dilution techniques, using Na^{24}, K^{42} and Br^{82} (as tracer for chlorine). The use of gamma spectroscopy was proposed for the simultaneous determination of a mixture of the three isotopes in urine and plasma samples. In an extensive series of tests on different mixtures of the three isotopes, it was found that the presence of Br^{82} interferes strongly with the determination of K^{42}. At optimum ratio between the three isotopes, Na^{24} can be determined with an accuracy of $\pm 3\%$ in urine, and K^{42} and Br^{82} with an accuracy of $\pm 10\%$. In plasma, K^{42} cannot be determined in the presence of either of the other isotopes due to the high Na/K ratio (about 35) in plasma.

An alternative method based on chemical separation of the three isotopes is being worked out. (Y. Eden, J. Gilat and C. Schenberg)

(vi) Quantitative Determination of Trace Amounts of K, Na and Cl in Human Tissue by Activation Analysis** :

Several preliminary experiments were run in order to establish a routine procedure for the determination of Na, K and Cl in human heart tissues. Difficulties were encountered due to the high concentration of Na with respect to K, the ratio being about 100/1. Because of the insufficient resolution of the scintillation detectors, the photopeak of K^{42} (1.51 MeV) is masked by the predominant Na^{24} 1.37 MeV photopeak and the escape and Compton background of the 2.75 MeV gamma ray. Experiments using a high resolution Ge(Li) solid state detector are in progress. (C. Schenberg, Y. Eden and H. L. Finston***)

---

* Work carried out for the Heart Institute, Beilinson Hospital

** Project carried out in collaboration with Prof. Tur and Dr. J. Agmon of the Heart Institute, Beilinson Hospital

*** Israel AEC Fellow. Permanent address: N.Y. City University, Brooklyn College, N.Y.

(vii) Qualitative Determination of Silicon in Oil Samples :

A comparison method was used to determine whether given oil traces were based on silicon or carbon. The procedure for the detection of Si was based on the $Si^{28}(n,p)\ Al^{28}$ reaction with 14 MeV neutrons from a neutron generator. The Al^{28} was assayed by its gamma ray and by following its decay. The detection limit was about 6 μg. The presence of Si was affirmed in two samples, but there was no detectable amount in the third. (C. Schenberg and Y. Eden)

(viii) Determination of Traces of Na in KCl by Activation Analysis* :

Sodium was determined in samples of analytical grade potassium chloride. The analysis was carried out by irradiation of the samples for 10 minutes in a neutron flux of 7×10^{12} $n/cm^2.sec$ and measurement of the 2.75 MeV gamma ray of Na^{24}. $NaNO_3$ (600 μg) and Na_2CO_3 (800 μg) were used as standards. The sensitivity of the analysis was about 1 μg. Two samples of about 3 mg were analysed and the presence of a few hundred ppm Na ($\pm$ 7-10%) was detected. (Y. Eden and C. Schenberg)

* Work carried out for Prof. A. Glasner of the Hebrew University, Jerusalem

BIOLOGY AND MEDICINE

Dynamic Study of Thyroxine Deiodination in Humans†: M. Anbar*, S. Guttmann**, G. A. Rodan*** and J. A. Stein***

Attention was drawn recently to the peripheral metabolism of thyroxine as a parameter of thyroid function in man. The main process of thyroid hormone degradation is deiodination. The rate of deiodination may be estimated using radioactive hormone and following the plasma, urinary and fecal radioactivity for about two weeks(1). However, this method is rather elaborate. The direct determination of the rate of deiodination by following the accumulation of iodide originating from thyroxine is practically impossible owing to the complexity of the pathways of iodide metabolism. To cope with this problem a double tracer method was devised, by which the rate of build-up of iodide that originates from thyroxine is followed simultaneously with the aid of two different radioisotopes of iodine(2). This relatively expedient method made it possible to study a sufficient number of human subjects to establish a normal range for the rate of deiodination as well as its variation with age, thyroid pathology and other conditions.

L-thyroxine labeled with iodine-125 (50 μc in 50% propylene glycol solution) was injected intravenously into the subjects, 48 hours prior to an injection of iodide-131. During this period complete equilibration of the thyroxine within its pool of distribution is attained, while any labeled impurities are excreted. On the day of the examination 10 μc of carrier-free iodide-131 was injected intravenously. Urine and blood samples were collected simultaneously at 4, 6 and 8 hours following the injection, while the subjects continued their daily routine.

The radioactivities of I^{125} and I^{131} were determined simultaneously in a well-type NaI scintillation detector connected to two single channel pulse height analyzers and two scalers. One analyzer was set with a channel

† IAEA Project, Contract No.RB/R2/78
* Soreq Radiation Research Dept.
** Weizmann Institute of Science, Rehovoth
*** Hadassah Municipal Hospital, Tel-Aviv

between 20-40 keV to count I^{125} and the other between 100-400 keV to count I^{131} only. In order to determine the contribution of I^{131} in the I^{125} channel a standard sample of I^{131} was measured and the ratio (R) of the count rates in the two channels was calculated. The instruments were set to give a ratio R of 0.05 or less. From the radioactivity measurements in plasma and urine the rate of deiodination of thyroxine was calculated on the basis of the following considerations: a) When iodide-131 is administered and allowed to equilibrate with the minute amount of iodide-125 which originates from the deiodination of thyroxine-I^{125}, the two radioisotopes will be excreted in the urine at a rate which is proportional to their relative concentrations in the plasma. Thus the level of free circulating iodide-I^{125} in the plasma can be calculated. b) The rate of disappearance of iodide-I^{131} from the plasma is equal to that of iodide-I^{125}. c) I^{125} plasma radioactivity is at least 98% due to thyroxine, thus to a first approximation it is equal to that of PBI^{125}. The rate of deiodination can thus be evaluated from the rate of iodide removal and from the ratio of the concentrations of the labelled thyroxine to the iodide which originates from it, under equilibrium conditions.

Using this method, female and male human subjects aged 18 to 86 years were examined. The following results were obtained :

(i) Normal Subjects

The normal rate of deiodination of thyroxine was determined in 220 euthyroid subjects who were in good health. No difference between females and males was observed, but changes with age were found. The half-time of deiodination was found to change linearly with age. A high significance of the coefficient of correlation was obtained for the data for ages 18 to 60 ($r = + 0.71$, $p < 0.01$), and a somewhat lower significance when the age group over 60 was included ($r = 0.60$, $p < 0.01$). The mean half-time of thyroxine in humans increases from 8.5 days in the third decade to 13.1 days in the sixth decade, beyond which no significant increase is observed.

(ii) Thyroidal Disorders

The thyroxine deiodination rate was determined in 50 patients with thyroidal diseases diagnosed by the usual methods. In the hyperthyroid cases the rate of deiodination was higher by a factor of two to three, and in the hypothyroid patients it was lower than normal, with half-lives as long as 28 days.

(iii) Medications

A group of subjects undergoing acute or chronic treatment with different drugs known to affect either thyroid function or thyroxine metabolism were examined. Thyroid hormones, when administered to subjects for a few days, induced an increase in the rate of deiodination without causing clinical manifestations. Propylthiouracil administered to hyperthyroid patients lengthened the half-time of deiodination markedly before clinical improvement was observed. Radioopaque substances containing iodine did not affect the normal deiodination rate, although the 24 hour I^{131} uptake in the thyroid was decreased. Corticosteroid treatment increased the rate of deiodination, whereas estrogen decreased it.

(iv) Malignant Diseases

Eighty two patients with various malignant diseases at different stages of advancement were examined. No correlation could be made between specific malignant diseases and the rate of deiodination. In all cases when deviations from the normal were observed it was a decrease in the rate of deiodination, which was most pronounced in the severe cases examined.

(v) Comparison of Thyroxine Deiodination with Thyroxine Protein Binding

These two parameters were measured in parallel in 75 patients and an inverse correlation was established, i.e. a decrease in protein binding of thyroxine was invariably accompanied by an enhanced rate of deiodination. Moreover, substances which alter the binding capacity of

the serum proteins for thyroxine also affect the rate of deiodination of thyroxine.

References:

1. INGBAR, S.H. and FREINKEL, N., J. Clin. Invest., 34 808 (1955)
2. ANBAR, M., GUTTMANN, S., RODAN, G.A. and STEIN, J.A., J. Clin. Invest., 44, 1986 (1965)

Thyroxine Metabolism in Tumor Bearing Rats : M. Anbar*, S. Guttmann** and G. A. Rodan***

It was previously demonstrated that there is an increase in the rate of peripheral deiodination of l-thyroxine-I^{131} in rats inoculated with certain transplantable tumors(1). Experiments performed *in vivo* showed that the phenomenon persists after surgical removal of the tumor, and that there is an induced increase in deiodination in normal rats kept in parabiosis with tumor-bearing ones(2). The thyroxine deiodinating activity of muscle extracts was not significantly different in controls and tumorous rats(3). A substantial increase was found in the ratio of free to protein-bound thyroxine in the plasma of tumorous rats, which was thought to be due to a decrease in the binding capacity of the plasma proteins(4).

It was suggested(5) that the level of circulating free thyroxine is one of the main factors regulating its peripheral deiodination. The observations on tumor-bearing rats strongly support this hypothesis. A high level of free thyroxine and an accompanying high rate of thyroxine deiodination is observed in the hyperthyroid state. In the tumor bearing rats, however, no thyroidal abnormalities could be detected(2). Therefore it was of interest to determine the rate of deiodination simultaneously with the rate of other processes of thyroxine degradation.

Tumor bearing and normal rats were injected intravenously with l-thyroxine-I^{131}, 48 hours after thyroidectomy. The animals were kept in

* Soreq Radiation Research Dept.
** Weizmann Institute of Science, Rehovoth
*** Hadassah Municipal Hospital, Tel Aviv

Collection of a blood sample from a rat

metabolic cages and the daily PBI^{131} and urinary and fecal radioactivity excretion were assessed. No significant difference was found in the rate of disappearance of trichloroacetic-acid-precipitable radioactivity in the plasma. The daily iodide radioactivity excreted in the urine was three times higher in the tumor bearing animals, indicating an increase in the rate of deiodination. On the other hand, the tumorous animals had a markedly lower fecal excretion of radioactivity, pointing to a disturbance in the enterohepatic metabolization of thyroxine. It may be suggested, therefore, that the presence of tumor affects primarily the hepatic phase of thyroxine metabolism, and the increase in the rate of deiodination is a compensatory regulating process, brought about by a higher level of circulating free thyroxine[4], which tends to maintain a constant plasma thyroxine concentration.

References:

1. STEIN, J.A., ANBAR, M., GUTTMANN, S. and ERNST, N., Nature, 192, 1303 (1961)
2. ANBAR, M., GUTTMANN, S., RODAN, G.A. and STEIN, J.A., Israel AEC Report IA-847 (1963)
3. ANBAR, M., GUTTMANN, S., LEVITZKI, A., STEIN, J.A. and TATA, J.R., Israel AEC Semi-Annual Report, January-June 1963, IA-900, p.134
4. ANBAR, M., GUTTMANN, S. and LEVITZKI, A., Israel AEC Semi-Annual Report, July-December 1964, IA-1021, p.107-108
5. ANBAR, M., GUTTMANN, S., RODAN, G.A. and STEIN, J.A., J. of Clin. Invest., 44, 1986 (1965)

Effect of Cortisol on Calcium Metabolism in the Rat : G. A. Rodan*, M. Paran** and M. Anbar***

Clinical experience has drawn attention to the action of Adrenocortical Steroids (ACS) on bone and calcium metabolism. Osteoporosis, which is one of the features of Cushing's disease (hyperfunction of the adrenal cortex), is a frequent complication of intense ACS treatment. Senile osteoporosis was also attributed to hormonal imbalance resulting in a relative preponderance of adrenocortical hormones[1].

* Hadassah Municipal Hospital, Tel Aviv
** Israel AEC Fellow
*** Soreq Radiation Research Dept.

ACS's have been successfully used to lower the blood calcium level in hypercalcemia, other than due to hyperparathyroidism[2], and even in the latter disease high doses of steroids have been reported to be effective[3].

The mode of action of ACS has been the subject of many investigations. The ACS's have been found to cause increased urinary[4,5,6] and gastro-intestinal[6,7] excretion of calcium, inhibition of intestinal absorption of calcium[8,11] shrinkage of the fast equilibrating calcium pool in the organism, and a decrease in the calculated kinetic constants representing bone growth (calcium accretion), bone resorption and rates of equilibration between equilibrating Ca pools[10,11]. There are some conflicting findings in the literature with regard to the effect of ACS on the blood calcium level. No lowering of a normal blood calcium level was found in humans[12,13]. A significant hypercalcemia was described in dogs[10] and hypocalcemia was induced in normal rats by high doses of hydrocortisone[14]. These differences might be species specific. The action of ACS on the kidney, gut and skeleton were considered by inference to be distinct and independent of each other[14]. These effects have been interpreted along the lines of the known effects of ACS on mineral metabolism and protein synthesis. The mode of action, however, remains obscure.

In the present investigations the action of ACS on the calcium metabolism was studied, with special reference to the effect on the mineral phase of bone.

In all the experiments a single high dose of 25 mg hydrocortisone per animal was administered. In the first experiment radiocalcium was injected intravenously in four young rats, two hours after the hydrocortisone administration. Four animals served as controls. The animals were kept in metabolic cages for five hours. Sequential blood radioactivities and total radioactivity in urine were assessed, and at the end of the experiment as well the radiocalcium uptake in diaphyses and epiphyses of the tibia was determined.

The total radioactivity excreted in the urine was markedly higher in the hydrocortisone treated animals. The radiocalcium uptake in the diaphyses and epiphyses of the treated rats was lower than in the control animals. The disappearance curves of radiocalcium in the blood were different. In the treated animals, the level of radiocalcium decreased more rapidly than in the controls during the first four hours, and then more slowly than in the controls.

In another experiment two groups of 7 animals each, one group treated and one not,were kept in metabolic cages for 24 hours. The urinary calcium excretion, determined in urine collected over 6-hour periods, varied with the amount of urine passed, and was higher for any period in the hydrocortisone treated animals. The plasma disappearance curves of Ca^{45} in these animals, three months older than those of the previous experiment, was similar in the treated and untreated groups. It was concluded that hydrocortisone enhances the calcium clearance in the kidney of the rat.

The total radioactivity excreted in the feces during twenty-four hours was also higher in the hydrocortisone treated animals. The uptake of radioactivity in the tibia epiphyses was 19% lower and in the tibia diaphyses 10% lower than in the untreated animals.

In a third experiment the kinetics of the radiocalcium uptake in bone was examined. Forty animals were given an intraperitoneal injection of hydrocortisone, and the radioisotope (Ca^{47}) was administered at the same time. Forty animals served as controls. Groups of treated and untreated animals were sacrificed after various intervals, and the radioactivity in epiphyses and diaphyses of the tibia and in the blood were measured. Maximum uptake, 50% higher than in the controls, was found in the tibia of the treated animals two hours after hydrocortisone administration. At three hours the radiocalcium uptake fell below that of the controls and remained lower during the whole experiment, which lasted twenty-four hours. The plasma kinetics appeared to reflect the fate of radiocalcium in bone. As in the first experiment, the plasma radioactivity

in the treated animals was markedly lower during the first two hours, followed by a very slight change during the next two hours, after which the curve was comparable with that of the controls.

The above findings are consistent with those reported in the literature with regard to the effect of hydrocortisone on urinary and fecal excretion of calcium, which are both increased. It was shown, moreover, that a single high dose of hydrocortisone exerts this action in the rat a few hours after administration. The low uptake of bone, comparable to the calcium pool shrinkage observed in kinetic studies, was manifest three hours after the hydrocortisone administration, and seems to be due to a direct action on bone. The preceding markedly increased radiocalcium uptake in bone is a hitherto unreported finding, possibly related to the mode of action of ACS on bone. This problem is being investigated by comparing the action of hydrocortisone on S^{35} and Ca^{47} uptake, and also on bone uniformly labeled with Ca^{45}.

References :

1. REIFENSTEIN, E.C., Jr., Clin. Orthop. 10, 206 (1957)
2. SHULMAN, L.E. et al., The effects of ACTH and cortisone on sarcoidosis. Bull. Johns Hopkins Hosp., 91, 371, 1952
3. JACKSON, W.P., Lancet, 1, 893, (1961)
4. CLARK, I. and GEOFFREY, R.F., Fed. Proc., 16, 65 (1957)
5. GROLLMAN, A., Proc. Soc. Exp. Biol., N.Y., 85, 582, (1954)
6. COLLINS, E.J. et al., Acta Endocr., Copenhagen, 42, 348, (1963)
7. SOFFER, L.J. et al., Clin. Endocr., Vol. 10, 594 (1950)
8. HARRISON, H.E., Amer. Phys., Vol. 199, 265 (1960)
9. GARRET, E.R. et al., J. Pharm. Sci., 52, (7) 668 : 78, (1963)
10. GARRET, E.R. et al., J.Pharmac. Exp. Ther. 145/3, 357, (1964)
11. MILHAUD, G.W. et al., Etude du metabolisme du calcium chez le rat à l'aide de la cortisone. Rev. Franc. Etud. Clin. Biol., 5, 354 (1960)
12. CONNOR, T.B. et al., Unpublished observations, 1956
13. CONNOR, T.B. et al., The use of cortisone and ACTH in hypercalcemic states. J. Clin. Endocr., 16, 945, 1956
14. RODAN, G.A., M.D. Thesis, 1964

Transfer of Ce^{144} via Placenta and During Lactation to Offspring in Mice : A. Neharin and E. Lubin

This investigation is a continuation of a similar study on the transfer of Eu^{152-4} to the offspring in mice[1]. Our main interest is the case of an acute contamination occurring a long time before the pregnancy. The question is whether the radioisotope that has already been fixed in the bone, is removed during pregnancy or lactation, and if so, in what quantities in relation to the time elapsed since contamination.

Four experimental groups, each of 12 female mice, were injected with 3 μc/0.2 ml of Ce^{144}-citrate. An additional group was held as controls. The groups were mated to untreated males by the harem method.

Group A was mated, and the isotope administered on the 18th day of gestation. The animals were sacrified on the 20th day (the total period of gestation being 21 days) and the Ce^{144} content determined in the whole litter, uterus and placenta, blood (0.5 ml), liver, femur and remaining carcass.

These measurements showed the transfer of the contaminant to the fetus through the placenta, very shortly after the contamination has occurred, and also the distribution of the isotope in the various organs.

Group B was mated immediately after dose administration. The offspring were whole-body counted for body burden soon after delivery. Thereafter, the lactating litter was counted in the same manner twice a week until weaning, after which 3 more counts were taken during the next 5 weeks. From this group mainly the transfer of the contaminant through the milk was determined.

Groups C and D were mated 4 and 8 weeks respectively after injection of the isotope. The offspring were counted for body burden as in Group B, to indicate the effect of the time elapsed since contamination on the transfer to the offspring during pregnancy and lactation.

Group E was injected with the same dose of the isotope but was not mated. Periodical whole-body counts were taken to show the mean body burden and the biological half-life of the isotope in virgin females, for comparison with the lactating mothers.

The results are summed up below.

a) The transfer of the contaminant through the placenta expressed as percent of the mother's body burden at the time of delivery was clearly related to the time elapsed since the date of contamination (Fig.37).

b) The transfer of the contaminant through the milk was considerable. Lactating litters showed a gradually rising body burden which reached

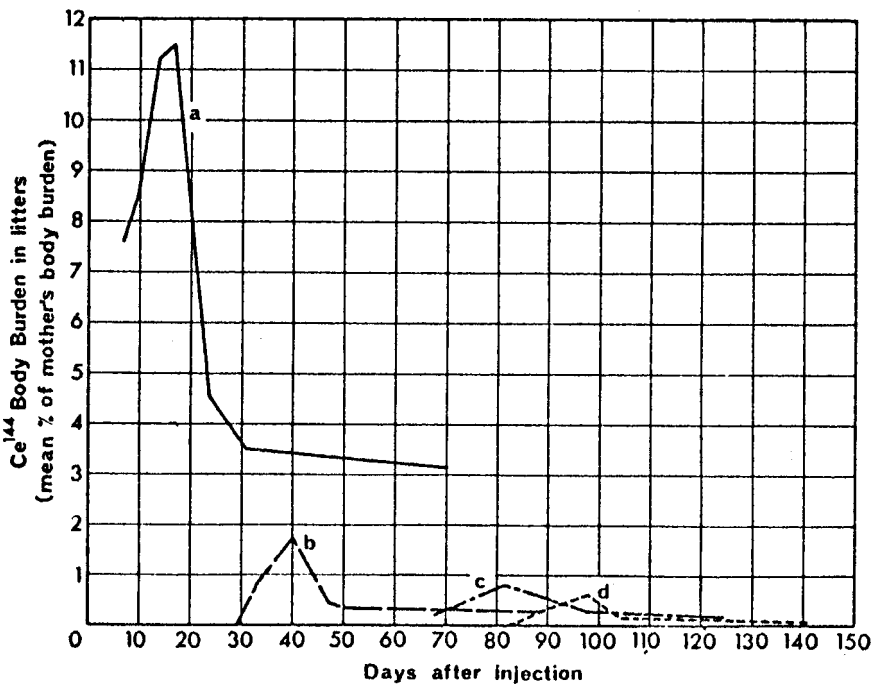

Fig. 37

Transfer of Ce^{144} to offspring in mice. Each curve represents one litter

a - Ce^{144} injected 2 days before delivery
b - Mated immediately after injection
c - Mated 4 weeks after injection
d - mated 8 weeks after injection

a peak on the 11th to 14th day and then dropped rapidly till the weaning day. Three more counts taken during the next 5 weeks showed a very small and gradual decrease (Fig. 37).

c) The transfer of Ce^{144} to the lactating litters was higher the closer the gestation period was to the day of administration of the isotope (Fig. 37).

d) The body-burden of the contaminant showed a somewhat quicker decrease in the lactating mothers than in the virgin females.

e) The distribution of Ce^{144} in the offspring was measured in the period of maximal activity and found to be mainly in the digestive tract.

Reference:

1. LUBIN, E. and NEHARIN, N., Israel AEC Semi-Annual Report July-Dec.1964, IA-1021, p.111

Trace Element Composition of Snake Venoms : A. Ar*, S. Gitter** and S. Amiel***

In previous work(1) it was demonstrated that trace elements in snake venoms can in principle be used as internal tracers. Further, it was shown that copper and zinc are coherent with the various fractions of the venom.

Progress has now been made with regard to the possibility of changing the natural Cu^{65}/Cu^{63} ratio by in vivo administration of Cu^{65} to Vipera palestinae specimens. The limiting factors in these experiments are the minute amounts of venom which can be obtained per snake specimen and the relatively low concentration of copper incorporated in the venom. Attempts to label venom in vitro by radioactive Cu^{64} yielded only low results (0.03%).

---

* Tel-Aviv University
** Rogoff Medical Research Center, Beilinson Hospital
*** Soreq Nuclear Chemistry Dept.

Further studies have been made to establish the correlation between the amounts of Cu administered to the snakes and the concentration of Cu in the venom. The results seem to indicate that the body pool of copper is higher in venomous snakes than in mammals, although it may vary greatly under different conditions. It is probable that an equilibrium exists between body and venom copper, as no significant difference could be found between the copper content of venom in snakes treated with Cu^{64} before and after extraction of the venom.

More data about the copper pool will be obtained by studying the Cu content of various snake tissues.

Reference:

1. MOAV, B., GITTER, S., WELLWART, J. and AMIEL, S., Proceedings of Radiochemical Methods of Analysis, Vol. 1, p.205, IAEA, Vienna (1965)

Reverse Transpiration in Plants : I. Gindel* and M. Kanter**

In continuation of the work reported previously(1), experiments were carried out using tritiated water to investigate the transport of moisture deposited on plant foliage to the soil and to the surrounding vegetation.

Maize seedlings were grown in pairs in small pots and the condition and water content of the soil carefully controlled. The leaves of one of the seedlings were immersed in tritiated water for periods varying from 30 minutes to 4 hours. At the end of the immersion samples were taken from the roots of the immersed plant, from the soil, and from the leaves of the untreated plant. The moisture was extracted by vacuum distillation, collected in a cold trap and its activity measured in a Tri-Carb scintillation detector with an efficiency of 8%. A sample of the original tritiated water in which the plants were dipped was used as a standard.

---

* Volcani Institute of Agricultural Research
** Soreq Radioisotope Training Centre

In all cases the presence of tritiated water was detected in the roots of the immersed plant and in the soil surrounding the roots, but no activity was found in the leaves of the second plant. The concentrations reached a saturation value after about 2 h. The fact that there was no further increase might be due to the fast exchange of tritium with the hydrogen in atmospheric water vapour.

Reference:

1. GINDEL, I. and KANTER, M., Israel AEC Semi-Annual Report, July-Dec.1964, IA-1021, p.120

Blank Page

N U C L E A R S A F E T Y

In addition to the investigations reported on more fully below, various topics were studied on behalf of and in collaboration with the Israel Nuclear Hazards Evaluation Committee (INHEC). These are mentioned briefly here.

Nuclear safety and hazards evaluation studies connected with the proposed dual purpose nuclear reactor for sea water desalination and electricity production were continued, including:

a) Specification of the nuclear safety requirements concerning siting and construction of nuclear reactors in Israel.

b) Site selection studies for the proposed dual purpose nuclear reactor.

c) Compilation of the INHEC requirements concerning the prior survey of environmental data (meteorological, hydro-geological, seismological, oceanographic, demographic, etc.) at a site considered for a nuclear reactor.

A study of the weighting factors of nuclear radiation doses (external and internal) according to the number of people affected by these doses, was initiated. The first phase of this study consisted in the computation of the environmental hazards resulting from a hypothetical accident occurring in a nuclear reactor located at different sites in Israel, and selection of the typical consequences to be analysed.

A set of isopleths indicating the radiation doses in the vicinity of the IRR-1 reactor following a major accident, was prepared for different release conditions (height of release, atmospheric conditions etc.). These isopleths are intended to serve as a "canned" computation for rapid evaluation of the consequences to the environment in case of an emergency.

A guide was issued for the submission of periodical reports to the compliance committee, concerning the safety of a nuclear reactor or chemo-nuclear installation. The pertinent data to be included in these reports were set out.

Background studies were started for the preparation of safety regulations for nuclear installations, and for the drawing up of standards and criteria related to licensing, safe operation, etc. The following items are in preparation:

a) Licensing and compliance regulations for nuclear installations.
b) Criteria for radioactive waste disposal.
c) Standards for establishing a radioactivity monitoring network in the vicinity of nuclear installations.
d) Standards for testing safety systems in nuclear installations.
e) Standards for the environmental surveys required for licensing a nuclear installation.
f) Standards for the emergency network required in a nuclear installation.

Radiation Doses from a Radioactive Cloud and from Deposition of Fission Products, as a Function of Distance from Release Point, for Various Atmospheric Conditions: J. Tadmor and H. Galron

In the evaluation of the hazards to the environment resulting from an accident in a nuclear reactor, diffusion of the fission products released from the reactor during inversion conditions and their deposition by rain are generally taken as representative of the most hazardous conditions[1-3]. However, it was shown in a previous report[4,5] that for small distances

from the release point and for inversion conditions, the radiation doses from dry deposition are greater than those from rainout deposition, the situation being reversed at larger distances.

In the present work the radiation doses from a radioactive cloud and from dry and rainout deposition of fission products were investigated as a function of distance from release point for different atmospheric conditions. The computations were made for a point source (1 curie) released instantaneously at zero height. The dry deposition velocity was taken as 10^{-2} m/sec for the halogens and 10^{-3} m/sec for other fission products[6]. The fraction deposited from the cloud by rain was considered to be 10^{-4} for the halogens and 2×10^{-4} for the other fission products[7]. Sutton's diffusion equation and Chamberlain's correction for deposition[8] were used. Both lapse and inversion conditions were investigated, for different wind velocities (1, 2, 3 m/sec for inversion conditions and 5 and 10 m/sec for lapse conditions). The atmospheric diffusion parameters were identical to those assumed in a previous report[9].

The Total Integrated Concentration (TIC) in the radioactive cloud, as a function of distance from release point under various atmospheric conditions, is shown in Fig. 38 for the iodines and in Fig. 39 for the other fission products released. It is seen that in the latter case the TIC is higher during inversion conditions than during lapse conditions over the whole range of distances investigated. The situation is different for the iodines. These have a relatively high velocity of deposition (10^{-2} m/sec), and during inversion conditions, when deposition is higher, they are depleted from the radioactive cloud. Thus, beyond a certain distance from the release point, the TIC during lapse conditions is greater than during inversion conditions.

The point of intersection between the TIC of the iodines for inversion and lapse conditions varies with the wind velocity, reflecting the influence of this factor on the dilution of the cloud; higher wind

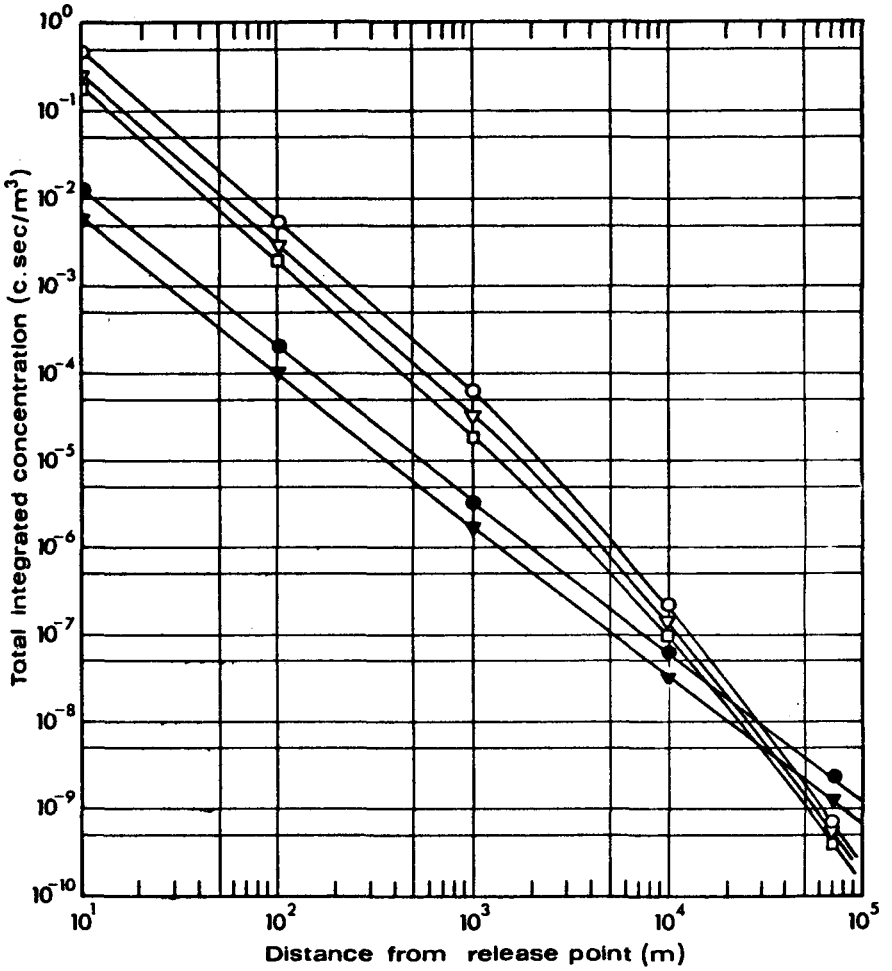

Fig. 38

Total integrated concentration (TIC) of the iodines in the radioactive cloud, as a function of distance from release point, for various atmospheric conditions and wind velocities (u)

○ inversion, u = 1 m/sec
▽ inversion, u = 2 m/sec
□ inversion, u = 3 m/sec
● lapse, u = 5 m/sec
▼ lapse, u = 10 m/sec

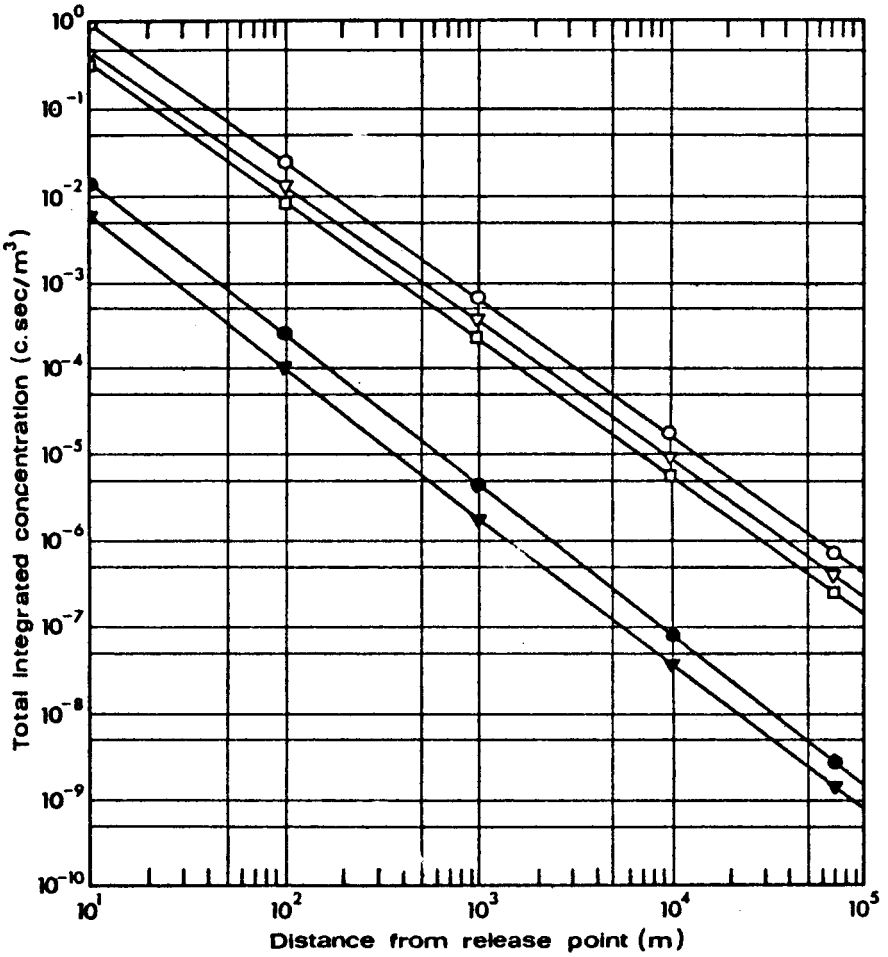

Fig. 39

Total integrated concentration (TIC) of fission products, excluding iodines, in the radioactive cloud, as a function of distance from release point, for various atmospheric conditions and wind velocities (u)

○ inversion, u = 1 m/sec
▽ inversion, u = 2 m/sec
□ inversion, u = 3 m/sec
● lapse , u = 5 m/sec
▼ lapse, u = 10 m/sec

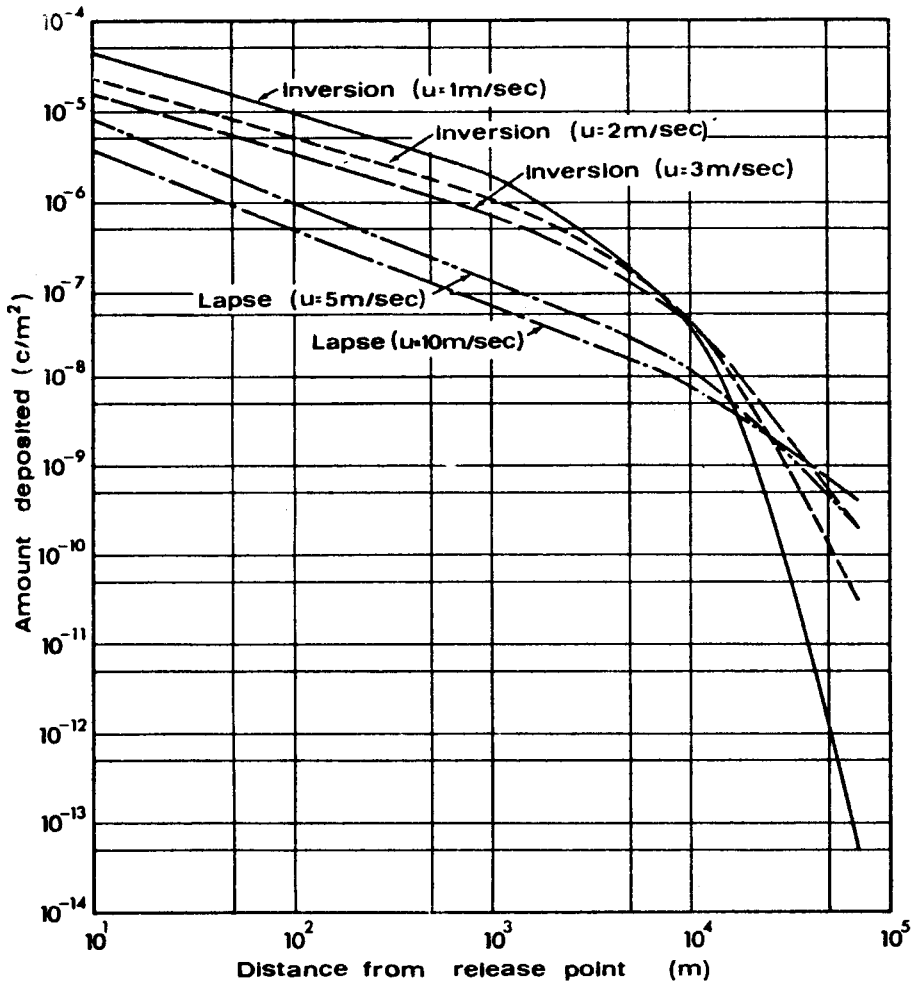

Fig. 40

Rainout deposition of fission products, excluding iodines, from the radioactive cloud, as a function of distance from release point, for various atmospheric conditions and wind velocities

velocities during inversion conditions and lower wind velocities during lapse conditions cause the intersection point to move closer to the point of release. For the conditions studied the intersection point was 15 to 45 km from the release point.

A similar picture is obtained for the iodines deposited on the ground during dry atmospheric conditions. For rainout conditions both the iodines and the other fission products, show this behaviour due to the relatively high fraction of all fission products deposited by rainout (see Fig. 40).

An intersection point between dry and rainout deposition as a function of distance, as found previously[4,5] for inversion conditions, was found in the present work also for lapse conditions.

The existence of the intersection points discussed above indicates that in the hazards evaluation of nuclear installations, all atmospheric conditions have to be considered, since for certain distances from the release point, at which highly populated centers may exist, consideration of inversion and rainout conditions only may lead to underestimation of the hazards.

References:

1. Final Hazards Summary Report for Big Rock Point Plant; Big Rock Nuclear Plant Consumers Power Company (Nov.14, 1961) Vol.I, Section 13
2. USAEC Report, ACNP-60573 (1962)
3. USAEC Report, ACNP-62574 (1962)
4. TADMOR, J. and GILAAD, Y., Israel AEC Semi-Annual Report, January-June 1964, IA-984, p.131
5. TADMOR, J. and GILAAD, Y., Israel AEC Semi-Annual Report, July-December 1964, IA-1021, p.134
6. USAEC Report, WASH-740; p.50
7. EISENBUD, M., Environmental Radioactivity, McGraw-Hill Book Company Inc. (1963), p.91
8. CHAMBERLAIN, A. C., UKAEA Report AERE HP/R 1261 (1953)
9. TADMOR, J., Israel AEC Report, IA-689, p.132

QJHAZ - A Code for Environmental Hazards Evaluation : Y. Milmann and J. Tadmor

The first version of this code[1] has now past the debugging phase. The code performs the following calculations:

a) For a given reactor power, irradiation time and cooling time, it calculates the fission products inventory for 27 isotopes which constitute the major environmental hazards[2].

b) Using Sutton's diffusion equation it calculates external and internal doses for instantaneous point and volume sources at various heights. The virtual distance concept[3] is introduced. The external dose is taken as the sum of the dose from the cloud passing overhead at a given distance, and the dose from radio-isotopes deposited on the ground. External doses are computed as a function of distance, time of exposure and meteorological parameters. Internal doses to the thyroid and bones as the critical organs are calculated as a function of distance and meteorological parameters.

c) Isopleth widths as a function of distance are calculated for both types of exposure, from which a quick estimate of damage can be made.

A second version of the QJHAZ code is being developed. It has the additional feature that it provides for continuous release of fission products to the atmosphere, allowing a stepwise time dependence of the release function (the fraction of radioisotopes released from the containment as a function of time). Two types of accidents are considered: explosion type and fire type.

The basic equations were formulated by Alonso[4]. They are simple material balance equations for the growth and decay of radioisotopes, but the source and sink terms contain information about the type of accident and the nature of the safeguards of the reactor. The "explosion type" accident is represented by a source term of the form

$$S_{j,i}(T) = F_{j,i}\, N_{j,i}(\tau,\ t,\ P_o)\, \delta(T)$$

where the indices j,i denote the i-th isotope in the j-th radioactive decay chain. $S_{j,i}(T)$ is the source term as a function of time, $F_{j,i}$ is the fraction of the particular radioisotope released from the core, $N_{j,i}$ is the number of atoms produced in the core as a function of irradiation time τ, cooling time t and power P_o, and $\delta(T)$ is the Dirac impulse function.

The "fire type" accident is represented by a source term of the form

$$S_{j,i}(T) = \begin{cases} KF_{j,i}\, N_{j,i}(\tau, t+T, P_o) & 0 < T \leq K^{-1} \\ 0 & T > K^{-1} \end{cases}$$

that is, the source term is assumed to be proportional to the number of atoms existing at time T for the period $0 < T \leq K^{-1}$, and zero for $T > K^{-1}$, so that K^{-1} is the time needed to extinguish the fire.

The sink term includes expressions for double and single containment, and for engineered safeguards such as emergency sprays, forced plating out, retention systems and delay systems.

The solutions of the equations turn out to be cumbersome. As an example, we reproduce here the solution for one of the simple cases, namely a fire type accident, with single containment, a delay system, and only two radioisotopes in every radioactive decay chain. Let $A_i(T)$ denote the activity of the parent isotope in chain i, and $B_i(T)$ that of the daughter isotope. ϕ is the sink term, τ' the delay time of the retention system, V the ventilation constant and D the decontamination factor.

$$A_i(T) = \begin{cases} VDA_i(0)\exp(-\lambda_{A_i}\tau') \dfrac{1-\exp(KF_{A_i}-\phi_{A_i})T}{\phi_{A_i}-KF_{A_i}} & \text{for } 0 < T < K^{-1} \\ VDA_i(0)\exp(F_{A_i}-\phi_{A_i}\tau') \dfrac{\exp(-F_{A_i})-\exp(K^{-1}\phi_{A_i})}{\phi_{A_i}-KF_{A_i}} + & \\ + \dfrac{\exp(K^{-1}\phi_{A_i})-\exp(\phi_{A_i}T)}{\phi_{A_i}} & \text{for } T > K^{-1} \end{cases}$$

$$B_i(T) = \begin{cases} VD\exp(-\lambda_{B_i}\tau') \; {}_{B}B_i(0) \dfrac{1-\exp(KF_{B_i}-\phi_{B_i})T}{\phi_{B_i}-KF_{B_i}} + & \\ + {}_{A}B_i(0) \dfrac{1-\exp(KF_{A_i}-\phi_{A_i})K^{-1}}{\phi_{A_i}-KF_{A_i}} & \text{for } 0 < T < K^{-1} \\ VD\exp(-\lambda_{B_i}\tau') \; {}_{B}B_i(0) \dfrac{1-\exp(KF_{B_i}-\phi_{B_i})K^{-1}}{\phi_{B_i}-KF_{B_i}} + & \\ + {}_{A}B_i(0) \dfrac{1-\exp(KF_{A_i}-\phi_{A_i})K^{-1}}{\phi_{A_i}-KF_{A_i}} + & \end{cases}$$

$$+ {}_{C}B_i(0)\,\frac{\exp(-K^{-1}\phi_{A_i})-\exp(-\phi_{A_i}T)}{\phi_{A_i}} +$$

$$+ {}_{D}B_i(0)\,\frac{\exp(-K^{-1}\phi_{B_i})-\exp(-\phi_{B_i}T)}{\phi_{B_i}} \qquad \text{for } T > K^{-1}$$

where

$${}_{A}B_i(0) = \frac{\lambda_{A_i}\,A_i(0)}{\phi_{B_i}-KF_{B_i}-(\phi_{A_i}-KF_{A_i})}$$

$${}_{B}B_i(0) = B_i(0)-{}_{A}B_i(0)$$

$${}_{C}B_i(0) = \exp(F_{A_i})\,\frac{\lambda_{A_i}\,A_i(0)}{\phi_{B_i}-\phi_{A_i}}$$

$${}_{D}B_i(0) = {}_{B}B_i(0)\exp(F_{B_i}) + {}_{A}B_i(0)\exp(F_{A_i}-K^{-1}\phi_{A_i}+K^{-1}\phi_{B_i})$$

$$- {}_{C}B_i(0)\exp(K^{-1}\phi_{B_i}-K^{-1}\phi_{A_i})$$

Similar results have been obtained for a variety of other cases and the equations are included in the program.

Other features included in the code are Chamberlain's correction term for deposition when the height of release is greater than zero[5] ,

and calculation of the direct radiation from the reactor building (considering build-up and attenuation factors).

References:

1. MILMANN, Y. and TADMOR, J., Israel AEC Semi-Annual Report July-Dec. 1964, IA-1021, p.132
2. GALRON, H. and TADMOR, J., Proceedings of the Second National Health Physics Meeting, Nahal Soreq, 6 May 1964, p.17
3. HOLLAND, J. Z., USAEC Report ORO-99
4. ALONSO, A., "NUBE" - A Digital Code to Evaluate the Hazards of Different Types of Reactor Accidents
5. CHAMBERLAIN, A. C., UKAEA Report AERE HP/R 1261

Relative Hazards of Fission Products in the Environmental Hazards Evaluation of Nuclear Reactors : H. Galron and J. Tadmor

In continuation of the study reported previously[1-3], the relative hazards of the fission products which may be released in an accident at a nuclear reactor were evaluated for rain conditions.

The infinite time radiation dose caused by contamination of the ground was considered. This varies with distance. At relatively short distances from the release point (a few km), the sequence of importance of the fission products arranged according to magnitude of radiation dose is

$$Ru^{103},\ Cs^{137} - Ba^{137},\ Ru^{106} - Rh^{106},\ I^{131},\ Zr^{95}\ \text{etc.} \qquad (1)$$

This sequence is determined by the fission yield, gamma energy, percentage of release from molten fuel, and radioactive decay of the various fission products. At distances of a few tens of kilometers, the sequence is different, the radioactive iodines being the main contributors to the radiation dose. This change is caused by the fact that during rainout conditions the depletion of the iodines from the travelling cloud is relatively lower as compared with the other fission products.

It is interesting to note that the sequence of importance of the fission products deposited during dry weather conditions (for which the halogens have the highest velocity of deposition), is similar to (1) over the whole range of distances studied, up to 70 km.

If we consider the radiation doses from contaminated ground as a function of time since deposition, the sequence of importance of the fission products varies, owing to the differences in the radioactive decay of the products. Figure 41 illustrates this for the case of deposition at a distance of 7 km, during rainout conditions.

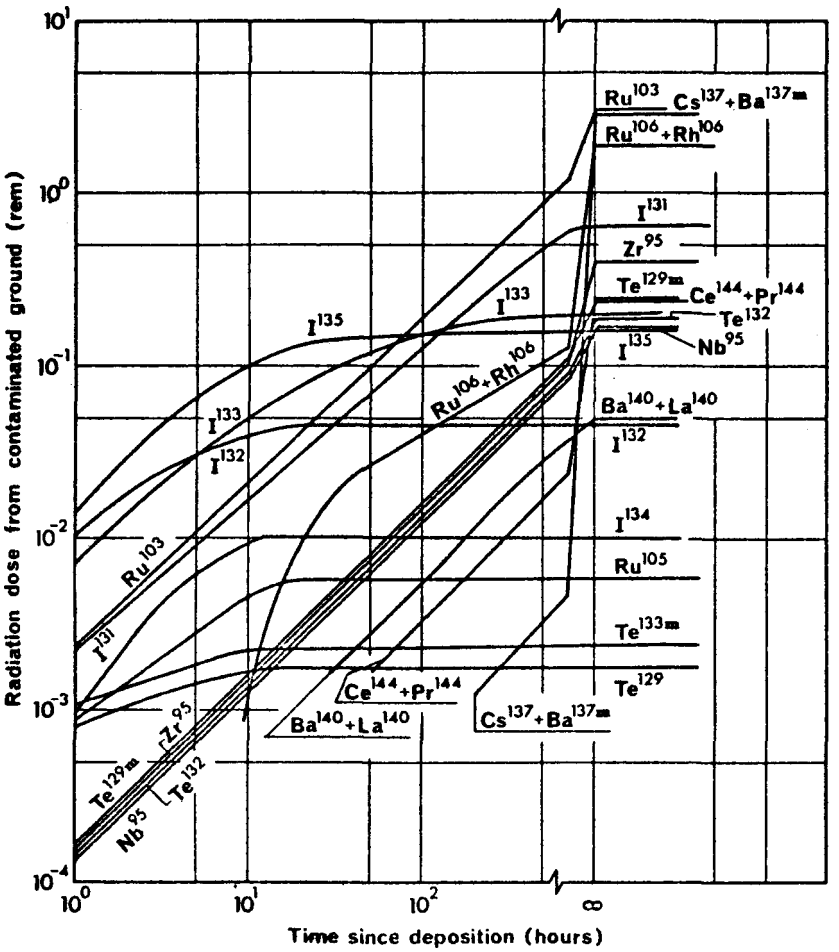

Fig. 41

Radiation doses from fission products deposited during rainout conditions, as a function of time since deposition

References:

1. GALRON, H. and TADMOR, J., Israel AEC Semi-Annual Report Jan.-June 1964 IA-984, p.128
2. GALRON, H. and TADMOR, J., Israel AEC Semi-Annual Report July-Dec.1964 IA-1021, p.135
3. GALRON, H. and TADMOR, J., Proceedings of the Second National Health Physics Meeting, Nahal Soreq, 6 May 1964, p.17

Turbulent Diffusion from an Instantaneous Plane Source : Y. Milmann and J. Tadmor

In a previous work[1] the concentration of diffusing matter in a turbulent medium was computed numerically using Joseph's expression extended to the case of a plane source, with initial conditions governed by Sutton's diffusion formula[1]. In continuation of this work, a more general solution of the problem has been developed.

The basic equation governing diffusion is

$$\frac{\partial c}{\partial t} = \text{div } (D \text{ grad } c)$$

where c is the concentration of diffusing matter, t is the time variable and D the diffusion coefficient. In a turbulent medium D is not constant. On the basis of experimental investigations, it is best given by the relation

$$D = K\sigma^{n} \qquad (1)$$

where σ is the standard deviation of the physical dimensions of the diffusing spot, K is a proportionality constant and n is an exponent determined experimentally.

Since the standard deviation is a rather difficult quantity to deal with in diffusion phenomena, we tried to find a relation with more convenient variables. The usual approach[2] is to regard D as a function of the

coordinates, $D = D(x(t), y(t), z(t))$, and proceed to solve the diffusion equation by an iterative procedure. The approach which we used was to find an equation with t as the (only) explicit variable

$$D = D(t) \tag{2}$$

The advantage of this lies in the fact that the divergence operates only on the spatial coordinates, so that the basic equation can be written

$$\frac{\partial c}{\partial t} = D(t)\, \nabla^2 c \tag{3}$$

The particular problem on which this method was tried was that of an instantaneous plane source which is introduced into an infinite medium with axial symmetry. The diffusion equation is

$$\frac{\partial c}{\partial t} = D(t)\, \frac{\partial^2 c}{\partial r^2} + \frac{1}{r}\, \frac{\partial c}{\partial r} \tag{4}$$

The initial condition is

$$c(r,0) = c_o \exp\left(-\frac{r^2}{\sigma_o^2}\right) \tag{5}$$

and conservation of matter gives:

$$\int_0^\infty \int_0^{2\pi} c(r,t)\, r\, dr\, d\phi = M \tag{6}$$

where M is the total amount of diffusing matter introduced into the medium at time $t = 0$. Let us introduce another time variable, t^*, defined by

$$t^* = \int_0^t D(t)\, dt \tag{7}$$

The equation will now be

$$\frac{\partial c}{\partial t^*} = \frac{\partial^2 c}{\partial r^2} + \frac{1}{r}\, \frac{\partial c}{\partial r} \tag{8}$$

which can be solved easily:

$$c(r,t^*) = c_o \frac{r_o^2}{\sigma_o^2+4t^*} \exp\left(-\frac{r^2}{\sigma_o^2+4t^*}\right) \tag{9}$$

The square of the standard deviation is

$$\sigma^2 = \frac{\iint c(r,t^*) r^3 \, dr \, d\phi}{\iint c(r,t^*) \, r \, dr \, d\phi} = \sigma_o^2 + 4t^* \tag{10}$$

so that we can write the following integral equation for $D(t)$:

$$D(t) = K\left(r_o^2 + 4\int_o^t D(t)\, dt\right)^{n/2} \tag{11}$$

The solution of this equation is

$$D(t) = \left[2(2-n)\, K^{2/n} t + D_o^{2/n-1}\right]^{n/(2-n)} \tag{12}$$

where $D_o = D(0)$.

Let us now derive the expression for $\sigma = \sigma(t)$:

$$\int_o^t D(t)\, dt = \frac{1}{2\left(\frac{n}{2-n}+1\right)\left(2-n\right) K^{2/n}} \left[\left\{2(2-n)K^{2/n} t + D_o^{2/n-1}\right\}^{n/(2-n)+1}\right]_o^t$$

$$\sigma^2 = \sigma_o^2 + 4\int_o^t D(t)\, dt = \sigma_o^2 + \left[\left\{2(2-n)\, Kt + \left(\frac{D_o}{K}\right)^{2/n-1}\right\}^{2/(2-n)}\right]_o^t$$

from which

$$\sigma^2(t) = \left[2(2-n)\, Kt + \sigma_o^{2-n}\right]^{2/(2-n)} \tag{13}$$

An expression very similar to eq.13 was derived in Ref.2 by an entirely different method - making an assumption about the form of D and separating the variables. The expression (in our notation) is

$$\sigma^2(t) = \left[(2-n)\ K(t-t_o)\right]^{2/(2-n)} \qquad (14)$$

The slight difference may stem from different initial conditions assumed in these methods.

In continuation of the present work, the diffusion coefficient and standard deviation as a function of time will be found for various initial distributions, and conclusions will be drawn regarding the Lagrangian auto-correlation function and spectrum of turbulence.

References:

1. MILMANN, Y. and TADMOR, J., Israel AEC Semi-Annual Report, July-December 1964, IA-1021, p.127
2. Radioactive Waste Disposal into the Sea. International Atomic Energy Agency - Safety Series No.5 (Vienna 1961)

Maxima of Sutton's Equation Corrected for Deposition : Y. Milmann and J. Tadmor

Sutton's equations for the ground level concentration of a diffusing cloud and for the distance of maximum concentration[1] do not take into account depletion of the cloud by deposition. Chamberlain introduced a correction for Sutton's equation in order to take into account this depletion[2].

A study is being carried out to find:

a) the distance from the release point which maximizes Chamberlain's equation for a particular height of release.
b) the height of release which produces the maximum concentration at a given distance from the release point.

This problem is of importance in the design of the height of stack release in a nuclear installation, mainly when release of particles of high velocity of deposition is involved. It turns out that for a given distance from the source, an increase in the height of release, within certain limits, may cause an increase in the ground concentration at this distance.

References:

1. Meteorology and Atomic Energy - USAEC Report AECU-3066
2. CHAMBERLAIN, A. C., UKAEA Report AERE HP/R-1261

HEALTH PHYSICS

Air Radioactivity and Fallout Deposition Monitoring : Y. Prulov, M. Stiller, Y. Feige and E. Shalmon.

Fallout monitoring during 1965 included the following measurements:

(i) Gross beta activity of dust samples and gummed tapes at Nahal Soreq.

(ii) Sr^{90}, Cs^{137} and gross beta activity of fallout collected in water-containing pots at four stations, and of dust samples obtained from air monitors at three stations.

(iii) As in (ii) for rain samples collected at two stations.

(iv) Gamma spectra of various fallout samples.

(v) I^{131} in air dust, milk and thyroid samples (see p.247), during the period following the Chinese nuclear test of May 14.

The gross beta activity of the dust samples collected at Nahal Soreq is shown in Fig.42. The low values obtained during the latter part of 1964 (0.2 - 0.35 pc/m^3) continued till March 1965, when a "spring peak" of 0.5 - 0.8 pc/m^3 was observed. The radioactive fallout from the second Chinese nuclear test on May 14, was observed at the beginning of June 1965, when the air activity rose to 1.7 pc/m^3 with a corresponding rise in the short-lived radioisotopes I^{131}, Zr^{95}-Nb^{95}, and Ba-La^{140}. These values dropped gradually during the summer of 1965. The air activity during Oct.-Nov. 1965 ranged between 0.03 and 0.14 pc/m^3, values which are far below those recorded since 1960/61.

The gross beta activity on gummed tapes ranged between 0.003 and 0.9 mc/km^2/day during 1965 (see Fig. 43). At the beginning of 1965 and on rainy days fallout values were usually above 0.1 mc/km^2/day. On dry days the values were always below 0.1 mc/km^2/day except for the "spring peak" during March-April 1965, and after the Chinese nuclear test. The latter

was reflected in the peak in deposited beta activity during the first half of June 1965 (0.8 mc/km^2/day). During the summer of 1965, the beta deposited activity was below 0.01 mc/km^2/day.

Deposition of Sr^{90} and Cs^{137} collected in water-containing pots is summarized in Table 26. The deposition at all four collection stations was higher during the rainy months, the rise being related to the amount of rain. For the first three stations shown in the table the average pot-collected activity ranged from 6.3 to 8.8 pc Sr^{90}/m^2/mm rain and from 9.8 to 12.2 pc Cs^{137}/m^2/mm rain. These values are about one half to one quarter of those obtained during the previous year[1]. At Eilat the activity per mm of rain was much higher than at the other three stations, but the total deposition was lower, owing to the very low rainfall.

Table 27 summarizes the results for air dust samples. At Nahal Soreq and Beersheba the concentrations are about the same, while at Eilat they are lower.

Analyses of rain samples for the winter of 1964/65 (Table 28) showed lower activities than those of the previous two years.

Figure 44 shows a typical gamma spectrum of an air dust sample collected and counted shortly after the second Chinese detonation. Fresh fallout isotopes are clearly distinguished (Ba^{140}-La^{140}; Zr^{95}-Nb^{95}). The I^{131} is less clearly seen, being masked by the 0.33 MeV peak of La^{140}. Fig. 45 is the gamma spectrum of a rain sample collected at the reactor site on October 7, 1965, and counted two weeks later. At that time the contribution of fresh fallout activity had almost disappeared, and the spectrum has the same pattern as before the Chinese detonation, except for the presence of a very low activity of Zr^{95}-Nb^{95}.

Reference:

1. STILLER, M., PRULOV, J. and FEIGE, Y., Israel AEC Semi-Annual Report, Jan.-June 1964, IA-984, p. 139

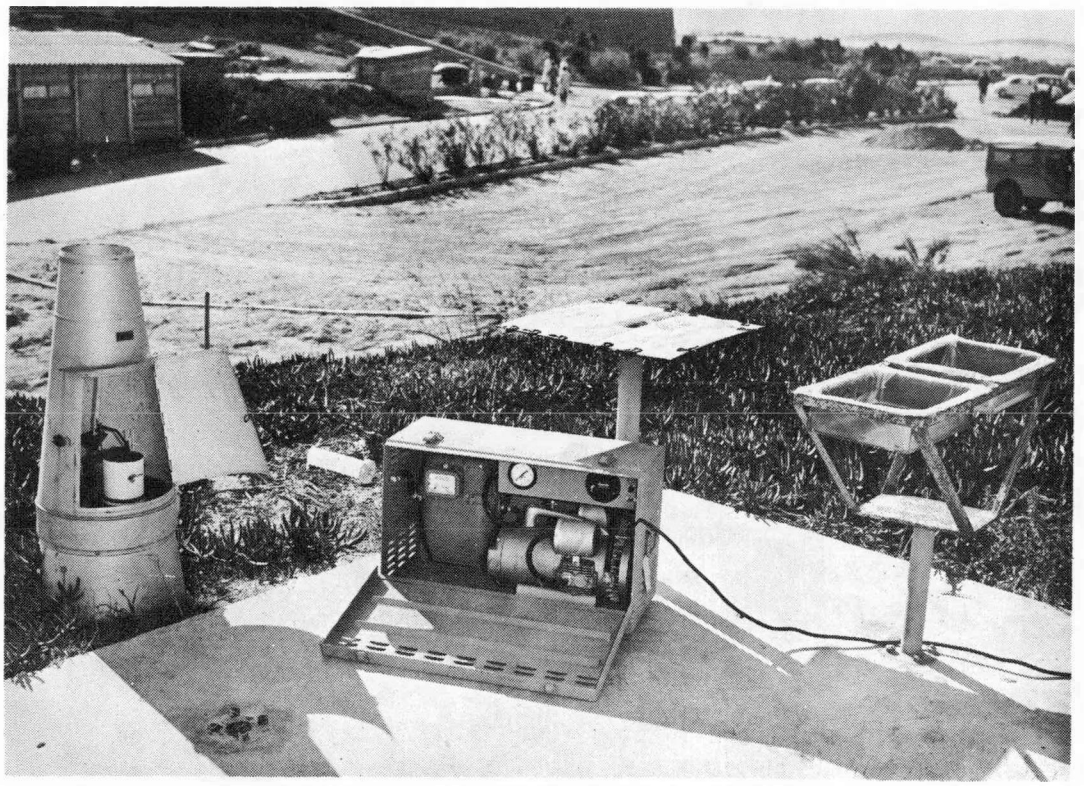

Fallout monitoring

TABLE 26

Monthly Sr^{90} and Cs^{137} deposition during 1965 (analysis of water-containing pot collectors)

Month	Nahal Soreq			Tirat Yael			Beersheba			Eilat		
	mm rain	mc/km²		mm rain	mc/km²		mm rain	mc/km²		mm rain	mc/km²	
		Sr^{90}	Cs^{137}		Sr^{90}	Cs^{137}		Sr^{90}	Cs^{137}		Sr^{90}	Cs^{137}
January	180.0	0.50	1.00	427.4	1.33	0.90	186.4	0.29	0.73	22.8	0.33	0.56
February	88.0	0.81	0.65	76.9	0.80	0.92	3.7	0.13	0.21	-	0.15	0.15
March	72.6	0.32	0.64	76.5	0.46	1.27	34.5	0.22	0.58	0.9	0.20	0.07
April	10.5	0.51	0.47	120.0	0.94	1.21	30.0	0.55	0.83	0.9	0.07	0.15
May	-	0.11	0.15	-	1.39	0.48	-	0.10	0.27	-	0.05	0.20
June	-	0.06	0.14	-	0.30	0.73	-	0.05	0.25	-	0.05	0.20
July	3.3	0.12	0.13	-	0.18	1.16	-	0.21	0.14	-	0.05	0.12
August	-	0.04	0.14	-	0.12	0.71	-	0.04	0.08	-	0.04	0.16
September	-	0.07	0.15	-	0.69	0.20	-			-	0.04	0.10
Total	354.4	2.59	3.47	700.8	6.21	7.58	254.6	1.59	3.09	24.6	0.98	1.71
$\frac{\text{pc } Sr^{90}/m^2}{\text{mm rain}}$ (ave.)	7.3			8.8			6.3			40.0		
$\frac{\text{pc } Cs^{137}/m^2}{\text{mm rain}}$ (ave.)	9.8			10.8			12.2			70.0		
average ratio Cs^{173}/Sr^{90}	1.3			1.2			1.9			1.8		

TABLE 27

Average monthly air concentrations of gross beta, Sr^{90} and Cs^{137} activities (pc/m^3)

Month 1965	Nahal Soreq			Beersheba			Eilat		
	Gross	Sr^{90}	Cs^{137}	Gross	Sr^{90}	Cs^{137}	Gross	Sr^{90}	Cs^{137}
January	0.155	lost	0.027	no sample collected			0.15	0.011	0.012
February	0.14	0.012	0.018	0.18	0.030	0.024	0.17	lost	0.008
March	0.25	0.042	0.027	0.31	0.024	0.047	0.09	0.011	0.009
April	0.26	0.017	0.037	0.33	0.018	0.035	0.095	0.006	0.016
May	0.19	0.015	0.035	0.39	0.021	0.027	0.11	0.005	0.013
June	0.29	0.027	0.035	0.33	0.032	0.028	lost	lost	lost
July	0.23	0.034	0.037	0.18	0.034	0.033	no sample collected		
August	0.10	0.012	0.014	lost	0.021		no sample collected		
September	0.08	0.011	0.011				no sample collected		
Cs^{137}/Sr^{90}	1.3			1.2			1.4		

TABLE 28

Comparison of Sr^{90} and Cs^{137} fallout in rain during the seasons of 1962 to 1965

Rainy season	Site	Rain (mm)	Sr^{90} mc/km^2	Cs^{137} mc/km^2
1962/63	Tirat Yael	786.8	21.4	-
	Nahal Soreq	274.3	13.7	-
1963/64	Tirat Yael	1081.3	29.5	43.7
	Nahal Soreq	586.9	14.2	21.1
1964/65	Tirat Yael	1238	7.8	9.4
	Nahal Soreq	724.4	3.9	>4.1

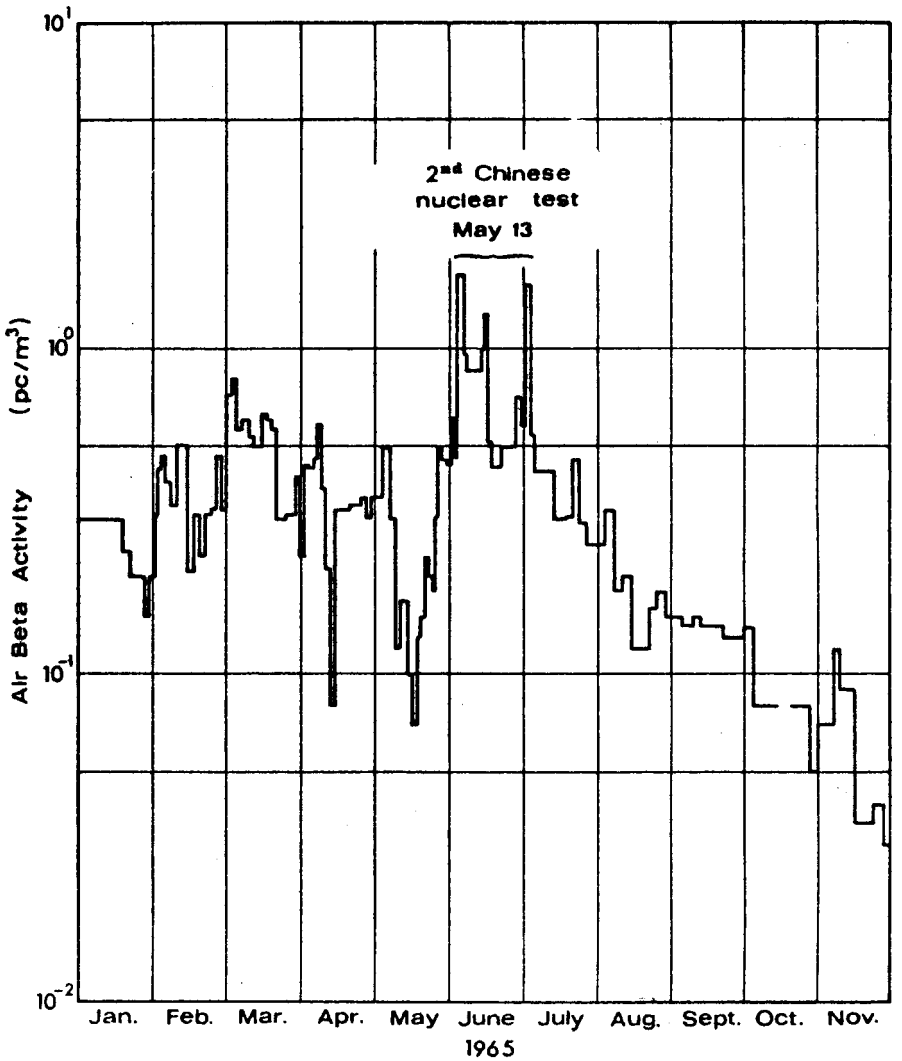

Fig. 42

Daily gross beta activity in air at Nahal Soreq during Jan.-Dec.1965.
Activity is measured 7 days after collection.

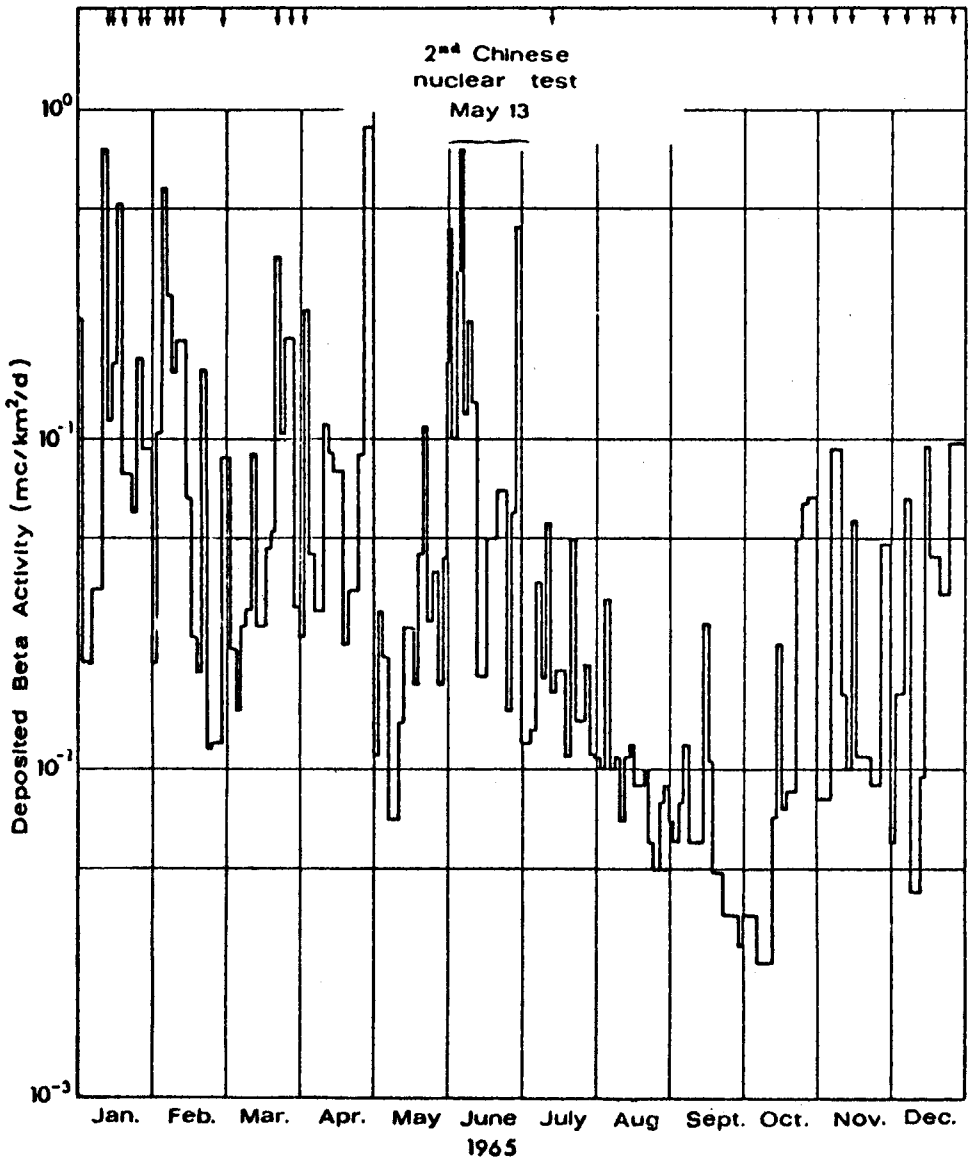

Fig. 43

Daily gross beta activity deposited at Nahal Soreq during Jan.-Dec. 1965.
The samples were measured 7 days after collection.
Rain days are indicated by arrows.

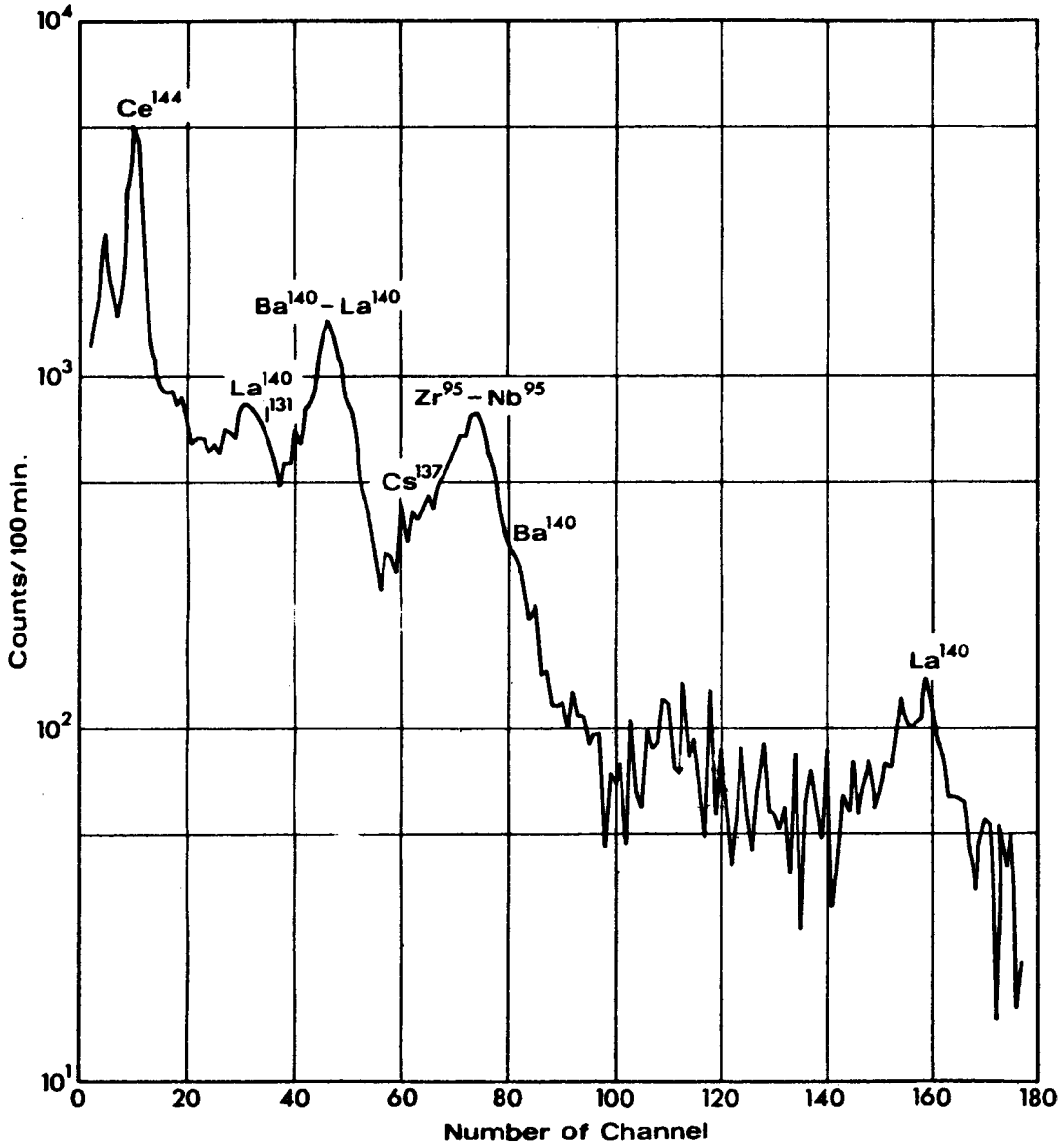

Fig. 44

Gamma spectrum of air dust sample from Palmachim. The sample was counted 6 days after collection.

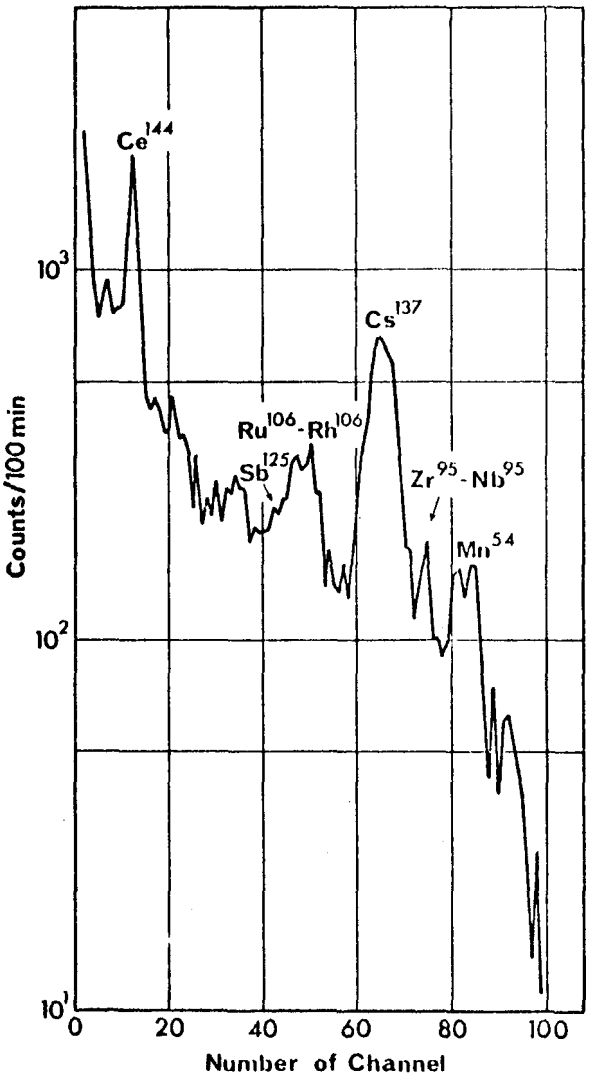

Fig.45

Gamma spectrum of a rain sample collected at the reactor site . The sample was counted 2 weeks after collection.

Sr^{90} and Cs^{137} Concentrations in Milk: Y. Prulov and M. Stiller

During 1965, about 70 milk samples from different parts of the country were analysed for Sr^{90} and Cs^{137}. The results are summarized in Table 29. During the first half of the year the average Sr^{90} concentration was about 5 pc/l, with values ranging from 1.0 to 10.9 pc/l. The average Cs^{137} concentration was about 30 pc/l, the values ranging from 10.6 to 73.0 pc/l. Most of the values were clustered around the mean values.

TABLE 29

Sr^{90} and Cs^{137} concentration in milk during 1965

Mean values

Period	Sr^{90} pc/l	Cs^{137} pc/l	Cs^{137}/Sr^{90}
Jan. - June 1965	4.9	30.9	6.3
July - Dec. 1965 (sheep excluded)	2.9	19.5	6.7

In the second half of the year there was a general decrease in the concentrations. Thus Sr^{90} averaged 3 pc/l and ranged between 1.0 - 6.5 pc/l, and Cs^{137} averaged 18 pc/l and ranged between 8.6 - 29.0 pc/l. Again most concentrations were near the mean values.

The significant difference in the concentrations of Sr^{90} and Cs^{137} during the first and second halves of 1965 may largely be explained by the methods of feeding the cattle. Thus during the first half of 1965 the main feed was green pasture, which contained higher concentrations of Sr^{90} and Cs^{137} due to washout of nuclear debris from the air. On the other hand, during the summer months stored feed, which is less contaminated, was used.

Milk in Israel contains lower concentrations of Sr^{90} and Cs^{137} than the milk in America and Europe (20-50 pc/l Sr^{90} and 100-250 pc/l Cs^{137} in Belgium[1] and about the same concentrations in Italy[2]). The average Sr^{90} and Cs^{137} concentrations were far below the maximum permissible concentrations for

the population at large. (The M.P.C. values for drinking water are 1,000 pc/l for Sr^{90} and 200,000 pc/l for Cs^{137} (3).)

References:

1. La Retombée Radioactive Mesurée à Mol - R - 2348, 1964
2. Data on Environmental Radioactivity in Italy - B10/08/64, 1964
3. National Bureau of Standards Handbook 69, U.S. Department of Commerce, 1959

Sr^{90} and Cs^{137} in Food: Y. Prulov and M. Stiller

During April-October 1965, over 100 food samples were analysed at the request of the Ministry of Health. The Ministry provided the samples, which consisted of packages containing representative daily food consumed by five adults. Each package was divided into seven components according to the type of food, and each sample was analysed separately for Sr^{90} and Cs^{137}. Foods which are usually consumed in small quantities, such as coffee, tea, etc., were not included in the packages but were analysed separately once every three months.

Table 30 gives the mean Sr^{90} and Cs^{137} contents found in the more common foods. From these values the total daily intake per adult was estimated to be 22 pc of Sr^{90}, and 92 pc of Cs^{137}.

TABLE 30

Mean Sr^{90} and Cs^{137} contents of the more common foods

Type of food	Concentration in pc/kg	
	Cs^{137}	Sr^{90}
Bread	45	16
Meat and eggs	52	4.6
Vegetables	6	6.4
Fats	15	3
Milk products	257	70
Fruits and jams	16	2.5
Miscellaneous	75	19
Cocoa	213	21
Coffee	142	44
Tea	388	375
Sugar	1.1	14
Salt	3.7	10

Sr^{90} in Soil: Y. Prulov and M. Stiller

Soil may be expected to accumulate Sr^{90} deposited from nuclear test debris. In fact the Sr^{90} content of soil can serve as a measure of the integrated Sr^{90} fallout, provided a location of minimum runoff is chosen and the sample is taken deep enough to include all the Sr^{90} in the soil.

The depth of penetration of Sr^{90} in soil depends on the type of soil and amount of rainfall. Thus heavy soils (high specific gravity and low permeability) retain most of the Sr^{90} in the upper 10-15 cm, while light soils allow deeper penetration. Soils having high exchangeable calcium values tend to retain Sr^{90} in the upper layers.

It has been observed and widely accepted that the total amount of Sr^{90} in soil at a particular site is very close to the total amount of it deposited by rain at that site. This is to be expected since rain is the principal mechanism by which Sr^{90} is deposited. Table 31 presents the expected amounts of Sr^{90} in soil at 7 sampling sites, and compares them with the observed values. These expected values were obtained by adding the amount of Sr^{90} in the soil in 1958[1] to the total amount deposited by rain since October 1958. The rain data were obtained from the Meteorological Service. Sr^{90} concentrations in rain were obtained from analyses of rain samples at Nahal Soreq and Tirat Yael. These two stations are representative for the major part of Israel (except the southernmost part).

There is close agreement between the expected and observed values of Sr^{90} in soil at Ruhama, Tirat Yael and Taoz. At Beit Guvrin and Mishmar Haemek the agreement is somewhat less close, and at Hanita and Regavim there are wide discrepancies which are probably due to insufficient depth of sampling.

Reference:

1. GAT, J. R., GILAT, J., Israel AEC Report IA-572 (1960)

TABLE 31

Expected and observed concentrations of Sr^{90} in soil

Rainy Season	Mean Seasonal Specific Activity mc Sr^{90}/km^2 / mm rain	Mishmar Haemek		Hanita		Regavim		Tirat Yael		Taoz		Beit Guvrin		Ruhama	
		$\frac{Sr^{90}}{km^2}$ (mc)	rain (mm)	$\frac{Sr^{90}}{km^2}$ (mc)	rain (mm)	$\frac{Sr^{90}}{km^2}$ (mc)	rain (mm)	$\frac{Sr^{90}}{km^2}$ (mc)	rain (mm)	$\frac{Sr^{90}}{km^2}$ (mc)	rain (mm)	$\frac{Sr^{90}}{km^2}$ (mc)	rain (mm)	$\frac{Sr^{90}}{km^2}$ (mc)	rain (mm)
Oct.1958 - Sept.1959	0.015	6.9	459.4	10.3	686.5	8.56	570.8	10.6	708.1	5.36	358.6	5.5	365.6	4.76	317.7
Oct.1959 - Sept.1960	0.015	7.05	470.0	9.3	619.1	6.75	449.5	13.1	877.5	2.35	156.7	2.67	178.5	2.39	159.5
Oct.1960 - Sept.1961	0.001	0.66	665.4	0.67	674.7	0.58	586.7	0.84	844.7	0.5	501.1	0.43	432.8	0.39	399.9
Oct.1961 - Sept.1962	0.022	17.6	801.0	13.3	606.6	16.9	769.4	23.6	1071.7	9.1	413.5	6.62	300.8	0.88	222.4
Oct.1962 - Sept.1963	0.022	12.0	546.6	15.8	719.7	12.7	567.7	22.2	1011.2	4.86	222.0	3.52	160.1	3.07	139.6
Oct.1963 - Sept.1964	0.022	17.1	776.6	16.9	766.6	15.9	724.4	23.8	1083.8	16.0	726.0	12.6	572.1	11.7	530.3
Subtotal		61.3		57.2		61.4		94.1		38.1		31.3		27.2	
From soil analyses till October 1958		5.6		12.1		13.6				22.5		14.6		4.4	
Total expected mc Sr^{90}/km^2		66.9		69.3		75.0		>94		61.6		45.9		31.6	
Observed mc Sr^{90}/km^2		41.5		31.4		23.5		89		62.0		36.8		31.4	

Fresh Fallout in Israel from the Second Chinese Nuclear Test : A. Donagi*, A. Eisenberg**, Y. Feige, Y. Prulov, E. Shalmon

Fallout from the Chinese nuclear test of May 14, 1965 was first detected in Israel in air samples taken on May 28, 1965. Gamma-spectrometric analysis showed the presence of I^{131} but no Ba^{140}-La^{140} or Zr^{95}-Nb^{95}. These appeared in air samples only three days later. This fractionation effect was probably due to differences in the transport mechanism of gaseous fission products as compared with particulate debris. During the week of 28.5.1965 to 3.6.1965 the I^{131} concentrations in surface air were 0.05 to 0.18 pc/m^3.

In milk samples, I^{131} was first detected about three weeks after its appearance in the atmosphere and could still be discerned as late as the second half of August. The mean concentration was about 10 pc/l. High levels of I^{131} activity were also found in the thyroid glands of sheep, and persisted for about 3 months. The highest activity observed was about 7 pc/g, in a sample collected in the early part of July.

Radioactivity of Wild Fruits in the Vicinity of the IRR-1 Reactor : A. Tal and E. Shalmon

Samples of wild fruits (grapes and figs) were collected at a distance of about 1 km from the reactor, and also near the waste disposal pit. The fruits were ashed at 400°C and the ashes analysed by gross beta counting and gamma spectrometric analysis. All the samples contained only traces of Cs^{137} and K^{40}. Their concentrations ranged from 3×10^{-5} to 9×10^{-5} µc/kg for Cs^{137} and 3×10^{-4} to 8×10^{-4} µc/kg for K^{40}. In the figs, a gamma peak was also observed at 0.75 MeV. This peak appears to be due to trace activity of Zr-Nb^{95}.

The trace activities of fission products observed in the fruits are far below the maximum permissible levels. From a comparison with controls

---

* Tel-Hashomer Hospital

** Ministry of Health, Jerusalem

it is concluded that the activities are due to deposition of fallout from nuclear detonations rather than to contamination from the IRR-1 reactor.

Evaluation of Some Procedures for Sizing Atmospheric Aerosols : E. Shalmon and A. Donagi*

The behaviour of an aerosol is largely determined by its particle size distribution. The commonly employed measurements of total airborne mass concentration of dust do not give reliable estimates of potential hazards, since they fail to make allowance for the retentions of the various portions of the respiratory system which are highly size dependent and vary over wide ranges. Accordingly, it has become accepted that the particle size distribution of an atmospheric aerosol must be evaluated before the potential hazard associated with its inhalation can be estimated.

A review of the literature on the size distribution of atmospheric dust reveals large discrepancies in the results reported by the different investigators. Some of these results are presented in Table 32.

TABLE 32

Particle size distribution characteristics reported in the literature

Location	Count median diameter (micron)	Mass or Volume median diameter (micron)	Standard geometric deviation	Refs.
14 U.S. cities (average)	0.54	0.97	1.56	3,4,5,6
Knolls Atomic Power Laboratory	0.028	1.12	3.05	7
University of Minnesota (indoor air)	0.46 - 0.95	1.8 - 7.9 (range for eight samples)	1.66-3.36	8
4 U.S. cities (40 samples)				
Range	up to 0.2	0.8 - 8	1.74-3.16	9
Average	0.03	3.56		

* Tel-Hashomer Hospital

Aerosol samples were collected on membrane filters, using a positive displacement pump as the air mover. Membrane filters were chosen because they have high surface retention and uniformly high efficiencies greater than 99% for particles larger than 0.01 micron in diameter[1]. Particles larger than 1 micron in diameter were sized by light microscopy, and sub-micron particles by electron microscopy. Photographs were made of the dust samples as viewed through the microscopes. Best results were generally obtained at 430 magnification with the light microscope, and between 2,000 and 10,000 with the electron microscope.

The micrographs were projected on a vertical screen and the sizing carried out on the projections. Each sizing involved about 5,000 dust particle. A log-normal distribution of particle sizes was expected[1] and the size intervals were selected accordingly.

The size data were converted to cumulative percentages, which were plotted on logarithmic probability paper as a function of the diameter corresponding to the upper limit of each size interval.

Surface area and volume distributions were plotted not from the direct measurements obtained with the light microscope, but from a plot of log frequency versus the square of the logarithm of the diameter of the particles.

Table 33 summarizes the results obtained for various dust samples. The following points were noted:

(i) The light and electron micrographs indicate no sharp cutoff in the sizes of particles retained by the filters. Particles down to about 0.001 micron were observed.

(ii) The reproducibility of the results by this method was good, as indicated by duplicate sizings of the same dust sample by different people. It was found that the use of a projected micrograph yielded more reproducible results than the commonly accepted technique of sizing directly through a microscope.

(iii) Sizing of dust particles by horizontal and by mean geometric diameters were found to give essentially the same distributions, and thus, the easier method of measuring only the horizontal projected diameter of the particles would be acceptable.

(iv) Almost all (above 99.9%) tropospheric aerosol particles are smaller than 1 micron in diameter.

(v) Almost all (over 97%) of the surface area and volume of tropospheric aerosols aerosols are associated with particles larger than 1 micron.

TABLE 33

Summary of count, surface area, and volume median diameters of various dust samples

Designation of Sample	Count median diameter (micron)	Standard geometric deviation	Surface area median diameter (micron)	Standard geometric deviation	Volume median diameter (micron)	Standard geometric deviation
TAS-A	0.045	3.56	5.4	2.08	9.0	1.86
TAS-C,D,E (combined)	-	-	-	-	6.5	1.96
TAS-A to F (combined)	-	-	3.8	2.21	7.4	1.92
TAS-A to F (combined)[a]	-	-	-	-	6.9	1.92
TAS-A to F (combined)[b]	-	-	-	-	7.6	1.91
T - 1	0.012	2.22	6.6	2.25	14.9	2.02
T - 2-4 (combined)	0.011	2.32	6.0	2.21	12.2	2.00
I - 1-5 (combined)	0.010	2.36	6.2	2.28	14.8	2.06

a - measured by observer A b - measured by observer B

References:

1. SHALMON, E., Deposition of Some Radionuclides on Tropospheric Aerosols, Thesis, University of Michigan, Ann Arbor, Michigan, 1964
2. AITCHISON, J. and BROWN, J.A.C., The Log-Normal Distribution, Cambridge University Press, 1957
3. BLATZ, H., ed., Radiation Hygiene Handbook, McGraw-Hill, 1959
4. FRIEDLANDER, S.K., et al., Handbook on Air Cleaning, AECD-3361, Harvard University, School of Public Health, 1952
5. IVES, J.E., et al., Atmospheric Pollution of American Cities for the Years 1931 to 1933, Pub. Health Bull., 224 U.S. Gvt. Print. Office, 1936.
6. MAGILL, P.L., HOLDEN, F.R. and ACKLEY, C., eds., Air Pollution Handbook, McGraw-Hill, 1956
7. FITZGERALD, J.J. and DETWILER, C.G., Am. Ind. Hyg. Assoc. Quart., 16 123, 1955
8. WHITBY, K.T., ALEGERN, A.B., and JORDAN, R.C., Size Distribution and Concentration of Airborne Dust, Presented at the Semi-Annual Meeting of the American Society of Heating and Air Conditioning Engineers, San Francisco, Calif., June 1955
9. WHITBY, K.T., et al., The ASHAE Airborne Dust Survey, Heating Piping and Air Conditioning, November 1957.

A Survey of the Operation of Dental X-Ray Apparatus in Israel : A. Donagi*, E. Shalmon and D. Fishel**

A survey was conducted to determine the safety of operation of dental X-ray machines in Israel, with a view to establishing routine country wide supervision of these machines. Unfortunately, a considerable number of the machines in use are relatively old and in bad condition, emitting excessive radiation which affects both patient and operator. It was found that radiation exposure from dental X-ray machines accounts for an appreciable fraction of the total population dose.

* Ministry of Health, Jerusalem

** Hadassah School of Dentistry, Jerusalem

A five percent random sample of dentists and dental practitioners was investigated. Details of the physical characteristics of the machines and the practices of the operators were recorded, according to the pattern adopted by the U.S. Public Health Service[1,2,3]. The following are the more important parameters investigated:

Make, model, age and usage of apparatus
Professional age of operator
Work load of the apparatus
Normal operating control settings
Presence of collimator and filtration
Diameter of central beam
Radiation output of central beam
Scattered radiation around the apparatus
Radiation shielding and protective devices
Type of film used and techniques of film developing

The findings of the survey are listed below:

(i) There are about 1,200 dental X-ray machines in Israel, corresponding to about 65% of all the practitioners.

(ii) The average professional age of the dentists is 25 years and of the dental practitioners 31 years. These professional ages are considerably higher than those in the U.S.A., and may account for the lack of awareness of radiation hazards and control which are revealed in this survey.

(iii) The professional age of practitioners is inversely related to the number of X-ray examinations performed by them.

(iv) The age of X-ray apparatus in Israel and the diversity of makes are considerably greater than those in the U.S.A. The mean age of foreign made machines, which account for about 69% of all machines, is 16.7 years, against 5.3 years for the Israeli makes.

(v) Although most of the X-ray machines have a connecting cable between timer and apparatus, in 77% of the cases this cable is too short, thus causing an unnecessary radiation exposure to the operator.

(vi) Only about 38% of all X-ray apparatus and 5% of the Israeli made machines have filtration. Such filtration considerably reduces the radiation exposure of the patient.

(vii) Only 46% of X-ray machines had collimators and 29% have central beams diameters of less than 7.6 cm factors which reduce the radiation dose to the patient.

(viii) The occupational radiation exposure of the operators is below the maximum permissible doses, but is high considering the low working load of the machines.

(iv) Radiation exposure of patients tends to be considerably higher than that found in other countries, and results mainly from scattered radiation.

References:

1. Physical Survey Manual - Dental X-Ray. U.S. Public Health Service, 1960.
2. YALE, S.H. and HAUPTFURER, J.D., J.A.D.A. 58, 49-54, April 1963.
3. Medical X-Ray Protection up to Three Million Volts, National Bureau of Standards Handbook 76, U.S. Department of Commerce, 1961.

Blank Page

APPLICATIONS

During the year under review the use of radioisotopes as well as of Soreq's large Co^{60} radiation source for applications in both industry and agriculture has been greatly extended. Most of the work was carried out within the framework of contracts with private and public institutions.

A new company, "ISORAD" Ltd., was set up to promote the use of radiation in industry. ISORAD is a private company owned jointly by the Israel Government and NUMEC - Nuclear Materials and Equipment Corporation, Apollo, Pennsylvania. Two meetings of the company took place, in June and October 1965.

The National Research Council has set up a steering committee to coordinate a national irradiation program. An extensive program has been drawn up, in cooperation with the Ministry of Agriculture and the Ministry of Commerce, for the irradiation of foods and agricultural products and for the use of irradiation in pest control.

The scope and versatility of the Co^{60} facility used in the above irradiation programs have been greatly increased by the incorporation of several improvements (see p. 311).

Steps have been taken to obtain official authorization for the use of irradiated food products for human consumption. As a test case, an application has been submitted to the Israel Ministry of Health for authorization to use radiation for sprouting control of potatoes and onions, and for insect eradication in wheat. The application was based mainly on

the corresponding petitions submitted in the U.S. and Canada to the respective Food and Drug Administrations, as well as on the permission granted in the Soviet Union to use irradiated potatoes, and on the report of the working group of the U.K. Ministry of Health on food irradiation.

In a campaign to promote the use of radiation and radioisotopes, numerous lectures were delivered at many institutions, and a number of seminars were held at Soreq for administrative and technical directors in the food, wood, plastics and ceramics industries, as well as for scientists, technicians and agriculturalists.

Dr. Ch. Miller of Applied Nucleonics Consultants, Los Angeles, U.S., joined the Department at the beginning of August 1965, on an Israel A.E.C. fellowship for the academic year 1965/66.

A. INDUSTRIAL APPLICATIONS OF RADIOISOTOPES

A Laboratory Apparatus for the Study of Reactions in Sprays[1]*

: E. Foa M. Konigsbuch**, S. Lask, O. Schächter** and Z. Stuhl

In the studies already reported[2] on the reactions occurring in an Aman Spray Reactor, a laboratory apparatus specially built for the purpose was used. The apparatus has been modified and improved over the past three years, and its present form and characteristics are described in this report[1]. A schematic representation is given in Fig. 46.

---

* Work performed under a grant from the Ministry of Development

** Bar Ilan University

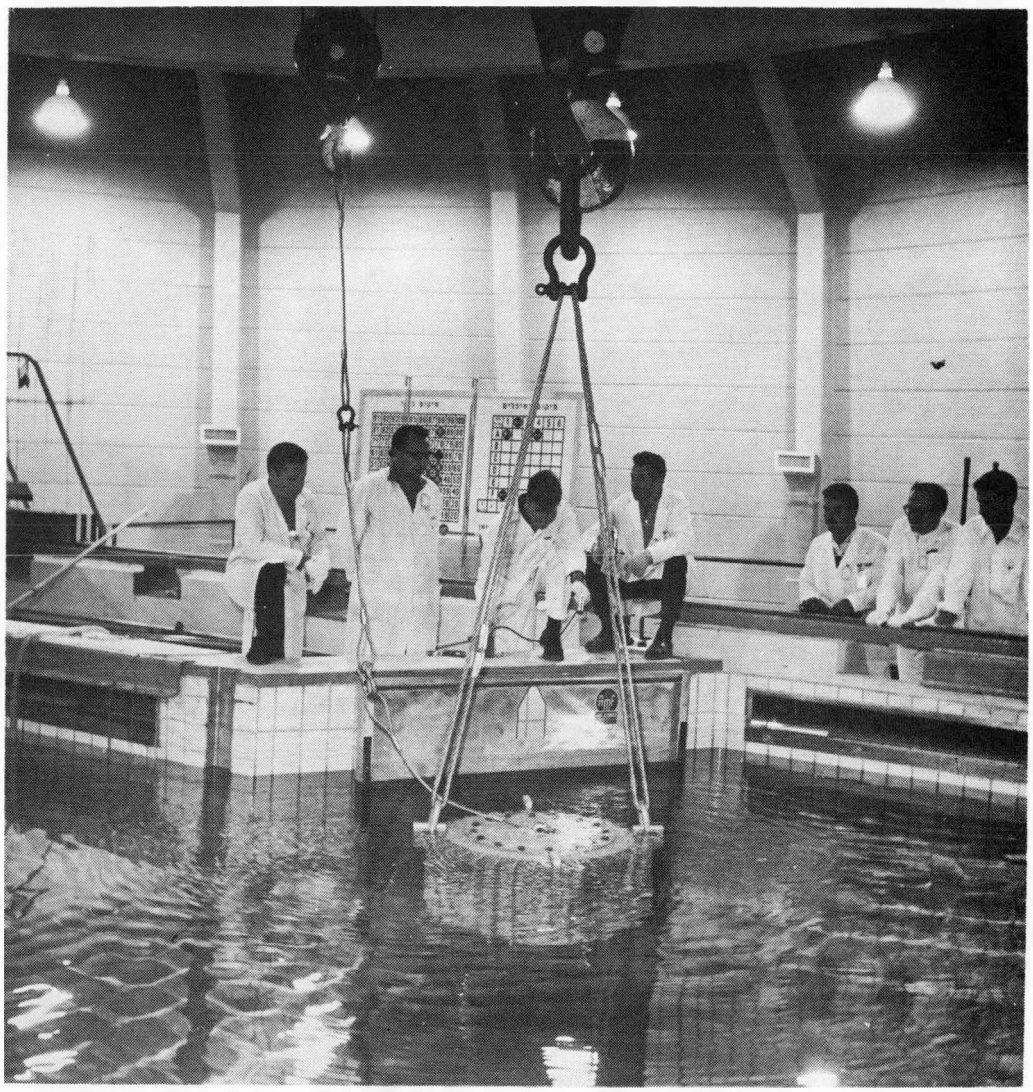

Co^{60} source in its cask being lowered into the reactor swimming pool

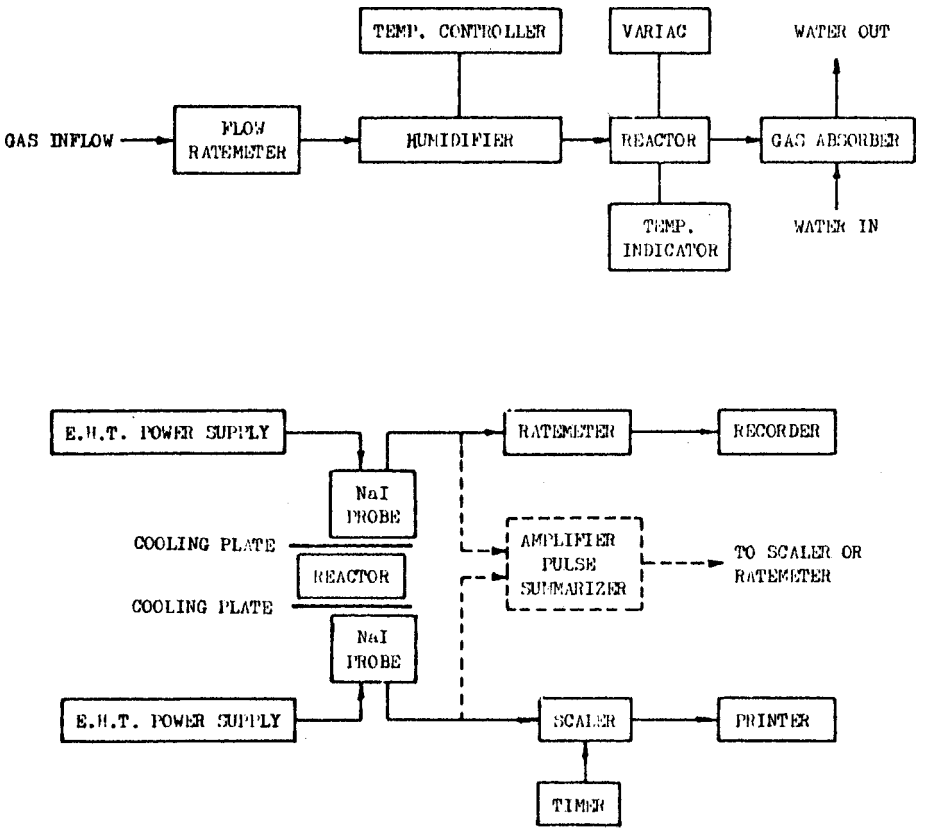

b

Fig. 46

Scheme of laboratory apparatus for studying reactions in sprays
a) the reactor b) the detection apparatus

The apparatus was designed to simulate as closely as possible the conditions prevailing in the commercial reactor. An important feature is that the detection system, which is based on the use of radioactive tracers, can record the concentrations of the radioactive species continuously. Reactions are studied by examining what occurs in a stationary drop. In particular, reactions in which hydrogen chloride is formed as a product have been investigated. The technique is based on the use of Cl^{38}-labelled chlorides which are heated in the form of a single droplet in a current of gas. Changes in activity are measured both in the droplet and in the escaping gases, which are absorbed in a filter impregnated with alkali. This arrangement permits the study of the influence of the most

important variables: temperature, drop size, rate of flow and composition of gas, and concentration of the solutions.

The apparatus is composed of two main parts:

a) The reactor proper, with provision for heating, temperature control and measurement, thermal insulation, and gas flow control.

b) Detecting apparatus, which includes two crystal scintillation counters, a ratemeter and automatic recorder unit, a scaler and printer system, and an attachment for measuring the activity of the gaseous reaction products.

The temperature can be controlled to within ± 1%. The size of the droplets investigated is between 0.5 and 5 microliters and the radioactivity from 1 to 5 microcuries.

References:

1. FOA, E., KONIGSBUCH, M., LASK, S., SCHACHTER, O. and STUHL, Z., Israel AEC Report, IA-1078 (in press)
2. FOA, E., KONIGSBUCH, M., LASK, S., SCHACHTER, O. and STUHL, Z., Israel AEC Semi-Annual Reports, Jan.-June 1963, IA-900, p.131; July-Dec. 1963, IA-920, p.134; Jan.-June 1964, IA-984, p.155; July-Dec.1964, IA-1021, p.144

Determination of Polyelectrolyte Residuals after Flocculation, Using a Radioactive Tracer[1]: Z. Stuhl and Ch. Gilath

Flocculation with polyelectrolytes is widely used in processes of solid-liquid separation and is finding application in the field of water treatment. One of the problems in this technique is to determine the polyelectrolyte residuals after completion of the flocculation process and separation of the flocs. In the case of treatment of water for drinking purposes, data on residuals is of great importance from the point of view

of public health. Also, a better understanding of the mechanism of flocculation, such as its relation to absorption, could be gained from this data.

Flocculation experiments with polyectrolytes are being carried out at the Sanitary Engineering Laboratories of the Technion, Israel Institute of Technology. Existing methods for determining polyelectrolyte concentrations[2] are not suitable for the very low residual concentrations encountered in water treatment. Experiments were thus carried out with a C^{14}-labelled cationic polyelectrolyte, namely cationic quaternized polyvinylpyridonium polymer. An easy way of preparing the labelled polymer was found to be the use of C^{14}-labelled CH_3I for quaternization of inactive polyvinylpyridonium. 100 microcuries of $C^{14}H_3I$ (specific activity 5 mc/millimole), contained in a glass ampoule, were cooled with a dry-ice acetone mixture. 1 cc of a solution of polyvinylpyridonium in nitromethane, containing 20 mg of the polymer, was added. An excess of inactive CH_3I was added and the quaternized polymer precipitated. The precipitate was separated by filtration, yielding 30 mg of active polymer of a specific activity of 1.2 μc/mg.

In the flocculation experiments the residual concentration of the polymer was determined by measuring the activity of the solution by the liquid scintillation technique (in dioxane solution). As is known, quenching problems arise when working in aqueous solutions; a mixture of 3.5 ml of the solution to be analysed and 16.5 ml of scintillator was found to give the best conditions for the measurements. No quenching was found due to the polymer itself. The system was calibrated at a known concentration of active polymer.

By this easy and rapid method residual labelled polymer could be determined down to a concentration of 0.005 mg/ml.

Reference :

1. Paper Presented at the XXXV Meeting of the Israel Chem. Soc., Feb.1966
2. FUOSS, R. M. and SADEK, H., Science 110, 552 (1949)

Studies of Sand Movement on the Sea Bed Using Radioactive Tracers* :

Z. Stuhl, Ch. Gilath and P. Pfeffer

There is today considerable interest in sand movement studies. Geologists and oceanographists need experimental methods for checking theories and models of sand transport, and information is required on the rates at which harbours fill with sand. Sand for building is dug from the sea bottom and the holes formed are expected to fill in again. It is important to avoid shore erosion and therefore to know the mechanism of hole filling.

In Israel several authorities such as the Geological Institute, the Ports Authority and the Committee for Shore Preservation are interested in sand movement studies along the Mediterranean coast. Lately work in this field was undertaken jointly by the Israel AEC and the Geological Institute. The immediate aim of the project is to develop a method for tracing sand movement by using radioactively tagged sand. A sample of labelled sand is introduced at a known place on the sea bed, and the spread of the activity is mapped after various time intervals.

(i) Labelling of the sand

The choice of the radioisotope to be used was governed by the requirement that the half-life should be of the order of a few days or longer and the energy of the emitted gamma rays sufficiently high for effective detection.

Activities of a few curies must be injected in order to allow for a detectable activity of 1 $\mu c/m^2$ after dispersal of the active grains over an area of about 1 km^2. About 100 active grains/m^2 are necessary for a reliable measurement. The grain size in our case is in the range of 100-200 microns, requiring the use of a few kg of labelled sand.

---

* Work performed in collaboration with the Israel Geological Institute, the Ports Authority and the Committee for Shore Preservation, under a grant from the Ministry of Development.

Several methods of labelling the sand were considered. Activation of the sand by irradiation in the IRR-1 reactor at a flux of 2.5×10^{13} n/cm^2.sec for 1 - 24 h was found to give inadequate specific activities and half-lives. The use of irradiated glass particles was rejected because of recent publications mentioning the great difference in the hydrodynamic behaviour of glass and sand grains. The method finally chosen was surface labelling with Au^{198} or Cr^{51}.

The sand is first treated with 10% nitric acid to decompose carbonates and any organic materials. It is neutralized and then boiled with NaOH (30%) for 1.5 h and washed with water. The sand surface is then ready for labelling by one of the following methods:

a) Redox System. The sand is treated with an acidic (HCl) solution of $SnCl_2$, then washed to remove unadsorbed $SnCl_2$, and treated with $AgNO_3$ solution. A solution containing hydrazine sulphate and pyridine is added while stirring. The silver-coated sand is washed to remove traces of Ag^+. Up to this stage only non-radioactive substances are handled. The prepared sand is now ready for reduction of gold on it. This is easily done by addition of an acidic (HCl) $Au^{198}Cl_3$ solution and labelling is complete within a few minutes. The yield is higher than 95%. The great advantage of this method lies in the fate that all preliminary work can be done in the laboratory and the final work with radioactive gold in the injection container itself. Specific activities of 1 curie/kg and higher are easily obtained.

b) Formation of sesquioxides. Activated chromium powder is dissolved in HCl (1:3), and an excess of NaOH is added to obtain a chromite solution. The sand is boiled with the chromite solution for 1.5 h. After washing, the activity is fixed on the surface by drying at 200°C for 12 h. The maximum labelling yield was 50% at a chromium-to-sand weight ratio of 0.1%. With the available flux of 2.5×10^{13} n/cm^2.sec and irradiation for 4 weeks, a specific activity of about 2 curies/kg sand could be produced. The idea of labelling with non-radioactive chromium and irradiating the labelled sand is also being considered.

(ii) Injection of the labelled sand.

An injection vessel was designed in the Technical Services Department, by Mr. Ch. Gavish. The vessel has a volume of about 15 liters, which allows about 5 kg labelled sand to be prepared at a time. The injection vessel is lowered to about 1.5 meters below the surface of the sea (for shielding purposes) and is partly filled with water. A glass ampoule containing 20 cc of the $Au^{198}Cl_3$ solution is dropped into the vessel and crushed. Air is bubbled into the solution and the sand sample poured in gradually. This labelling can be done conveniently in a harbour. The vessel opens upon contact with the sea bottom and the labelled sand pours out of it.

(iii) Mapping the activity on the sea bed

The detector is towed along the sea bed behind a boat, and thus it must be robust and stable, as well as well as highly sensitive. Its hydrodynamic properties must be such that it does not rise from the bottom when towed at a velocity of 1 m/sec. The Littoral Drift Probe made by the Danish Isotope Centre was chosen. The count rate at the sea bottom will be continuously recorded and the location of the boat determined at different times by navigational measurements.

The results obtained will be converted into isoactivity curves, as a function of time, from which it will be possible to determine the direction and velocity of the sand movement under the given experimental conditions (winds, currents and wave direction, strength and frequency).

The first experiments will be conducted with Au^{198}-labelled sand, but if the half-life proves too short, work will continue with Cr^{51}.

References:

1. CURTOIS, G., private communication
2. PETERSEN, B.R., Ingeniøren International Edition, 4, 3, 99 (1960)

Method for Determining Movement of Silt in a Wadi : Z. Stuhl and Ch. Gilath

During rain periods the wadis (dry watercourses) suddenly fill up with flood waters which bring down large amounts of silt. If reservoirs are built to catch the rain water the silt will be deposited in them, gradually filling them up. It is thus of great practical importance to estimate the amount of silt brought down by floods. Recently the Geomorphological Laboratory of the Geography Department of the Hebrew University began measurements of silt movement along the Nahal Soreq Wadi, using dyed particles. However particles of less than 500 microns cannot be traced in this way, and it is just this fraction of particles that is of greatest importance in the determination of silt movement. The problem can be solved by radioactive labelling.

Labelling of the silt was carried out by using the cation exchange properties of clay. Cr^{51} with a half-life of 27.8 days was chosen. A well defined fraction of silt (88 - 120 microns) was treated with HNO_3 to destroy the carbonates and organic materials present. This treatment also replaced the exchangeable cations with H^+. After washing the residue to pH 7, a solution of $Cr^{51}Cl_3$ was added to the silt suspension, with shaking. The exchange was complete in a few minutes and a specific activity of 1 curie/kg silt was obtained. Three kilograms of labelled silt was divided into 20 portions and the portions buried along a 10 meter length of the wadi bed. The aim of such a distribution was to get a good average picture of the movement and to reduce any insignificant displacement. The rate of silt movement will be investigated as a function of the flooding conditions.

Mixing Conditions in Pulp Chests in a Paper Mill : Ch. Gilath, S. Lask, Z. Stuhl, E. Foa, M. Finkel*, D. Schiffer*

Experiments were performed to check the effectiveness of pulp mixing in chests at the American-Israel Paper Mill, Hadera. The

---

* American-Israel Paper Mill, Hadera.

technological process in this mill starts with a batch operation, namely slushing of the dry pulp with water. Batches are discharged into a chest and the process becomes continuous from there on. The pulp is pumped through two additional chests, connected in series, and finally to the paper machine.

The chests are agitated, but a certain amount of channeling, which interferes with homogenisation of the pulp, was suspected. The matter had been investigated by using dyed pulp to trace the movement of material through the chests. These tests showed qualitatively that the mixing conditions were fairly good under the particular flow conditions of the test. However, this type of test is not entirely satisfactory. Each grade of paper requires different flow conditions, and the mixing must be examined for each case. Since most grades of paper are spoiled by adding dye, the production losses would be considerable. A better tracing method, which would also give more quantitative results, was thus needed.

The residence time distribution technique, using a radioactive tracer, was employed to determine the mixing conditions in one of the mixing chests. A pulse of Na^{24} (as an aqueous solution of Na_2CO_3) was injected into the feed stream to the chest. The activity of the outlet stream was measured with a scintillation detector placed in contact with the exit pipe and connected to a ratemeter and recorder. The curve obtained was corrected for recirculated activity (determined by means of a detector placed at the inlet stream to the chest), and thus the concentration versus time curve was obtained.

The function $F(t/\theta)$ representing the residence time distribution gives the fraction of the injected tracer activity which leaves the system up to the time t/θ . Here θ is the mean residence time, obtained by dividing the volume of the vessel by the flow rate; t/θ is the reduced time. If S^* is the whole area beneath the activity concentration curve, and S the area up to a certain time t/θ, when $F(t/\theta) = \frac{S}{S^*}$.

A mathematical model of the chest as a vessel composed of three regions - dead volume, plug flow and perfect mixing - connected in series, was considered. According to Ref.2, for this case

$$1 - F = e - \frac{1}{(1-p)(1-m)} \left[\frac{t}{\theta} - p(1-m) \right]$$

where p is the fraction of the vessel volume which acts as an ideal plug flow region, m is the fraction acting as dead volume, and 1 - (p+m) is the fraction working in ideal mixing conditions.

The parameters p, m and 1 - (p+m) were determined by plotting (1-F) against t/θ. In the experiment performed there was found to be 12% dead volume, 5% plug flow and 83% perfect mixing. No channeling was found in the system.

The use of radioactive tracers to obtain residence time distribution curves of flow systems provides valuable continuous information about the system, in an easy way, without disturbing the normal production process.

References:

1. Paper presented at the XXXV Meeting of the Israel Chemical Society, Feb. 1966
2. REBHUN, M. and ARGAMAN, A., Technion Report C V 106, 1963

Use of Radioactive Tracers for Corrosion Studies: S. Lask and Ch. Gilath

A study of the mechanism of halogen ion migration through passivation layers on stainless steel is being undertaken at the Corrosion Laboratories of the Israel Metal Institute. Preliminary experiments were performed to evaluate the use of radioactive tracers for this study. Two kinds of information can be obtained by radioisotope tracer techniques:
a) the general surface concentration of the halogen ions,
b) a microscopic picture of the halogen concentration distribution on the surface, as obtained from autoradiographs.

Chlorine-38, produced by irradiating NH_4Cl in the IRR-1 reactor, was used for the first experiments. Aqueous solutions of HCl^{38} (obtained by decomposition of NH_4Cl^{38}) were used to establish the sensitivity of the above techniques. At a maximum concentration of 3000 ppm Cl^-, the specific activity of the HCl solution was about 700 μc/ml.

Counting for 1 min on a 1 cm^2 surface using a GM counter, the sensitivity was about 0.1 mμc/cm^2 (based on twice the standard deviation). This corresponds to 3×10^{-2} micrograms of Cl^-/cm^2 for a solution of the above specific activity.

Autoradiographs were taken with a medium grain size Kodak X-ray microtex film and exposures of a few hours, up to practically complete decay of the Cl^{38}. Satisfactory darkening was obtained for a specific activity of about 1 mμc Cl^{38}/cm^2, but the resolution obtained was not better than 30 microns. A much better resolution of about 2 microns was obtained with Kodalith Ortho film, but the very low sensitivity of this film necessitates the use of specific activities of about 100 mμc/cm^2. Experiments will be continued with the Kodirex X-ray film, which is expected to give a good resolution at a reasonably low specific activity.

Thus, both counting and autoradiography are suitable for use in the corrosion study.

Radioactive Tracer Method for Determining the Weight Distribution of Carbon Black in Rubber: Z. Stuhl and Ch. Gilath

In the making of rubber, the carbon black incorporated is dispersed in the form of grains of submicron dimensions. However these grains may coalesce to form agglomerates, which impairs the quality of the rubber. It is accepted practice to check the degree of agglomeration by counting the number of agglomerates larger than 6 × 6 microns, under the microscope.

The present work was undertaken to ascertain if there is any detectable inhomogeneity in the weight distribution of the carbon black, and if so, whether this is related to the degree of agglomeration. There are no simple chemical methods for this determination and thus a radioactive tracer method was tried. A 150 g quantity of carbon black (IPC, type FIAF) was irradiated for 5 minutes in the IRR-1 reactor at a flux of 7×10^{12} n/cm^2 sec. The trace amount (about 0.1%) of sodium present was converted to radioactive Na^{24} (half-life 15 h). The irradiated carbon black was used to make a batch of 500 g of rubber. Prior to vulcanizing the rubber sheet, three samples - of 10, 100 and 1000 mg - were taken from each of 24 points on the sheet. The activity of the samples was measured with a scintillation counter. The count rates were corrected for the decay of radioactivity and the results converted into the weight of carbon black per sample.

The standard deviation of the counts was calculated separately for the 10, 100 and 1000 mg sample groups. There was no significant difference between the standard deviations of the three groups, it being less than $\pm$ 2.5% in all cases. Of this, the standard error due to counting statistics (square root of the count) was about $\pm$ 1%, leaving an error of less than $\pm$ 2% from all other sources including changes in counting geometry and inhomogeneity of the neutron flux. Thus it can be stated that the weight distribution of carbon black has a standard deviation which does not exceed $\pm$ 2%, i.e. no significant inhomogeneity was detected.

The method described above is simple, fast and reliable, and can be used on samples down to 1 mg.

Investigation of the Flow of a Submerged Radioactive Spring (Radioisotope Training Center): C. Braudo, E. Mazor*, F. Mero**

A considerable part of the salinity of Lake Kinereth arises from springs flowing up through the bed of the lake. Many of these highly

* Isotope Department, Weizmann Institute of Science
** Tahal, Water Planning for Israel Ltd.

saline springs are also radioactive and it has been suggested that the radioactivity of the water might be used as a sensitive indicator to aid in the location of such sources, the final purpose being either to contain the water or to pump it away.

The water issuing from the springs is diluted almost immediately in the large volume of lake water, and thus any measurement of salinity, temperature or radioactivity must be carried out in the immediate vicinity of the source with submersible detectors. A submersible probe was designed containing a scintillation detector consisting of a 2" dia × 4" NaI crystal viewed by a type 6292 photomultiplier. The signal was conducted via a 50 meter coaxial cable to a portable battery-operated scaler ratemeter. Attenuation in the cable was compensated by a preamplifier operating in a mixed current and voltage mode, as suggested by Miwa and Tohyama[1] and suitably modified in our electronic workshop.

The preliminary tests were conducted at a spring whose characteristics are well known, not far from the inlet to the National Water Carrier. The increased salinity and higher temperature associated with the spring water were accompanied by activity about 100 times the normal background activity of the water measured some distance from the spring. The mud on the bed of the lake in the vicinity of the spring was even more active (more than 150 times the background activity). This preliminary series of tests was brought to an end by a fault in the cable to the probe.

Subsequently a further series of tests was carried out at a spring (Ma'agan 2) which has the physical form of a conical crater some 20 meters deep in the lake bed. At this point the bed is covered by 21 meters of water. The activity profiles measured are shown in Fig. 47. Simultaneous measurements of temperature and conductivity showed that the radioactivity correlated fairly well with the salinity and temperature of the water, and visual observation by a diver established that the water of the spring (high activity and salinity) also carried with it a large quantity of suspended solids.

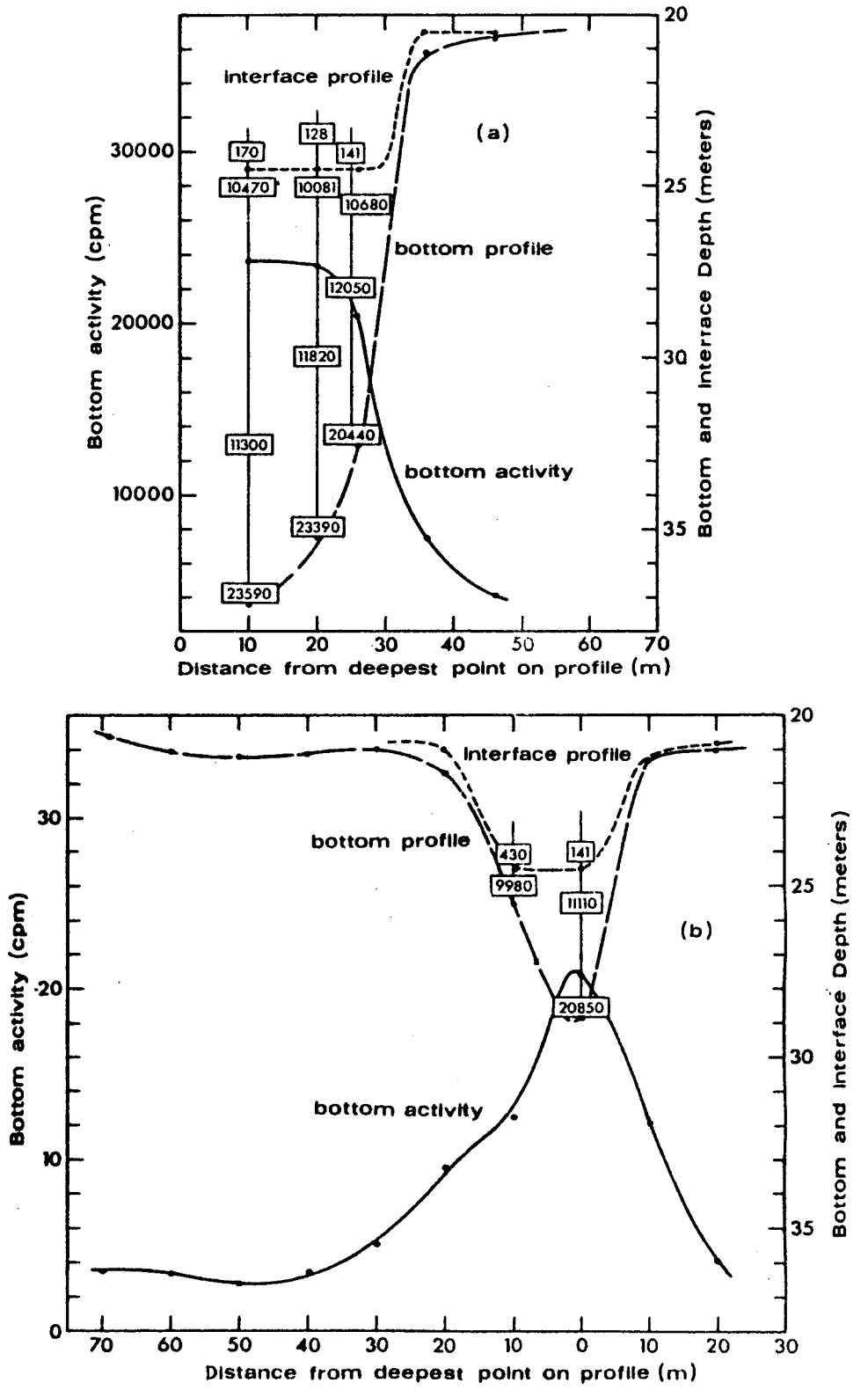

Fig. 47

Radioactivity of Ma'agan II. Figures in boxes give the activity at the particular location in c.p.m.

a) East-West profile b) North-South profile.

Inspection of the activity profiles shows that there is a well defined lake - spring interface. The activity is constant below the interface and negligible above it, arguing fast and thorough dilution. The activity of the mud on the bed of the lake seems to rise as one approaches the throat of the crater. Further tests are being carried out to investigate the speed and mechanism of dilution of the spring water.

Reference:

1. MIWA, H. and TOHYAMA, T., Nuclear Electronics II, p.421, I.A.E.A., Vienna 1962

B. IRRADIATION OF AGRICULTURAL PRODUCTS

Effect of Irradiation in Delaying Sucrose Decomposition in Sugar Beets:

E. Eisenberg, R. S. Kahan, A. Heller* and A. Perlman*

This experiment was planned in collaboration with the Sugar Beet Growers Association and the sugar factory "Sugat Ltd".

One of the problems of the local industry is the need to store sugar beets for one to three days in order to permit continuous plant operation on Saturdays (no crops are harvested on Saturdays). When the green top is removed and the beet stored, the sugar concentration diminishes, the loss increasing with temperature.

A preliminary experiment was carried out to test the effect of different radiation doses on sucrose concentration during storage under normal plant conditions. The beet was treated with doses in the range 1 - 100 krad, applied during the first 24 hours of storage. The batch size was about 25 kg. The sugar content was measured after storage for 1 - 13 days. A single analysis was performed per batch, under normal industrial analytical conditions at the sugar factory.

---

* Sugar Beet Growers Association

The sugar content in the irradiated samples appeared to be 10% - 20% higher than in the controls during the whole period of storage. The lowest dose tested (1 krad) seemed to give the best results. However it should be noted that the sugar content of beets harvested in the same field may vary by the amounts observed, and that our results are based on analyses of single batches only. Nevertheless the results obtained justify further investigation during the 1966 harvest season.

Extension of the Ripening Period of Stored Avocado Pears : R. S. Kahan, G. Zaubermann*, E. Eisenberg

Several varieties of avocado pears are grown in Israel. The fruit is picked while still green and then allowed to ripen. The ripening period is fairly short, and towards the end of it the fruit becomes discoloured and a fungal growth (colletotrichum) develops.

Preliminary experiments during the 1964/65 season showed that the ripening period of the main variety grown (Fuerte) could be extended by relatively low radiation doses. Doses in the 5-200 krad range were tested at 2 dose rates (250 krads/h and 430 krads/h) using the Gamma Cell-200 source. In one experiment, 20 krads extended the ripening period from 7 days (control) to 12-18 days. Similar results have been reported recently from California[1].

Experiments on this and other varieties are being carried out during the 1965/66 season.

Reference:

1. YOUNG, R. E., Nature 205, 1113-14 (1965)

---

* Dept. of Fruit and Vegetable Storage - Volcani Institute of Agricultural Research

Inhibition of Sprouting in Stored Potatoes: R.S. Kahan, N. Temkin-Gorodeiski* and E. Eisenberg

Experiments conducted abroad have demonstrated the efficacy of irradiation in inhibiting sprouting and extending the storage life of potatoes. It has also been shown that such irradiated potatoes retain their wholesomeness, and in Canada, the U.S.A. and U.S.S.R. the use of these potatoes for human consumption has been approved.

The present experiments were conducted to confirm the results obtained abroad for the local varieties of potatoes. The project was planned in cooperation with the Vegetable Crops Dept. of the Ministry of Agriculture and is being executed in collaboration with the Volcani Institute of Agricultural Research.

Tests are being carried out on the "Up-to-Date" variety of potatoes, which is the main type grown in Israel. Some work on this variety has been reported from India[1,2]. In the present experiments, potatoes harvested during May-June 1965 from fields that had not been treated with chemical sprays were irradiated. After storage for 3 months under ambient conditions, non-irradiated controls were shrivelled and soft and had sprouts 10-30 mm long. Batches that had been irradiated with 7.5 - 15 krads showed very little sprouting (1-2 mm sprouts), while those irradiated with 15 krads gave sprouts 3-5 mm long. All the irradiated lots were of good appearance and firm.

A large scale experiment is now being conducted to investigate the effect of temperature on the storage life of irradiated potatoes. Loss in weight, losses due to rot, chemical changes, and the culinary quality of the stored potatoes will be observed over a period of 12 months. The potatoes taken for the experiment are of commercial origin and had been in storage at 8° for several weeks. They were thus close to the end of their natural dormancy period. They were kept for a further

---

* Volcani Institute of Agricultural Research

10 days at ambient conditions and then irradiated, without regrading. Part were treated in their original commercial 45 kg sacks; the rest were transferred to small containers for irradiation and returned to sacks for storage. A total of about 6 tons were irradiated.

Doses of 6, 10 and 14 krads (± 17%) were applied at 2 dose rates (20 and 100 krads/h). The irradiated potatoes and controls are being stored at 4 temperatures: at 4° and 8°C in commercial storage, and at 14° and ambient temperature in darkened rooms. The effect of irradiation is being compared with that of 2 chemical treatments for sprouting control. Sample sacks are withdrawn from storage every 4-8 weeks, and after preliminary evaluation are stored for a further 4 weeks under ambient conditions to simulate marketing and consumer handling.

References:

1. MATHUR , P.B., Nature 198, 99 (1963)
2. MATHUR , P.B., Nature 199, 1007 (1963

Comparison of the Effects of Gamma Radiation and other Treatments on the Storage Qualities of "Lassen" Strawberries

It has been reported from abroad that irradiation is effective in delaying spoilage in strawberries. Experiments were conducted* to check the response of the local variety and to compare the results with those of other treatments of commercial interest. The treatments tested were:

a) irradiation with 100 and 200 krads, at a dose rate of 100 krads/h.
b) keeping at 10°-15° from the time of picking until irradiated after 18 hours ("precooling").
c) dipping in 0.1% Captan

The fruit was picked towards the end of the season, at two stages of ripening, namely pinkish-red and red-ripe. Except in the case of

---

* By S. Ben-Yehoshua (Volcani Inst. of Agricultural Research), R. S. Kahan and E. Eisenberg

treatment b) above it was kept at ambient conditions (26-27°C) for 18 hours before treatment and storage. The experimental unit was 100 fruits, packed in 4 commercial plastic baskets. The storage temperatures tested were 2°-3° and 20°C.

Table 34 gives the incidence of rot for storage at 20°. Irradiation with 200 krads was the best single treatment (16% and 45% rot in pink-hard and red-ripe fruits respectively, versus 76% and 96% for the controls). A combination of immediate precooling, dipping in Captan and 100 krads reduced rot to zero for pink-hard fruits. Table 35 shows that storage at 2°-3° after irradiation gave a marked improvement for fruit stored for 2-7 days, but had little or no effect on fruit stored for 14 days, especially if it was kept for an additional day at 23°C. The effect of storing at 2°-3° was less marked for the other types of treatment.

The fruit picked at the pink-hard stage did not ripen uniformly, the stem end frequently remaining pink and hard while the bulk of the strawberry became red and ripe. Irradiation intensified the red colour of the pulp.

Organoleptic tests, based on triangular comparison by a panel of 5 persons, showed a distinct reduction in the aroma of the pulp of fruit treated with 200 krads. The flavour and texture of the fruit were not affected.

The effects of precooling were poor, possibly because the portable equipment used was inadequate. In preliminary experiments it was found that increasing the CO_2 content to 10% of the atmosphere during precooling gave greatly improved storage qualities.

In another series of tests* the effect of dipping the fruit in 0.2% dehydroacetic acid (DHA) was compared with that of irradiation. These experiments were conducted under rather unfavourable weather conditions, the day of picking being a sharav (hot and dry). After treatment the fruit was stored at 0° or 17°C. The red-ripe fruit spoiled immediately.

* By N. Temkin-Gorodeiski (Volcani Inst. of Agricultural Research), E. Eisenberg and R. S. Kahan

TABLE 34

Effect of various treatments on the spoilage of strawberries stored for 2 days at 20°C

Treatment \ State at picking	% Spoilage	
	Pink-hard	Red-ripe
none	76	96
0.1% Captan	45	61
precooling to 10-15°C	35	60
100 krads	30	90
200 krads	16	45
precooling + 0.1% Captan + 100 krads	0	30

TABLE 35

Effect of irradiation on spoilage of fruit stored at 2°-3°C

Storage time →	2 days		7 days		14 days		14 days plus 1 day at 23°C	
Treatment \ State at picking	Pink-hard	Red-ripe	Pink-hard	Red-ripe	Pink-hard	Red-ripe	Pink-hard	Red-ripe
none	0	25	13	43	49	66	67	84
100 krads	0	15	10	17	25	75	52	75
200 krads	0	10	6	15	36	58	60	89

The pink-hard responded as follows. With 100 krads (dose rate 217 krads/h) spoilage after 4 days at 17° was 17%, versus 65% for the untreated controls. The spoilage increased to 35% on the 5th day. For storage at 0° the spoilage was 18% after 7 days, compared with 33% for the controls. However after storage for an additional day at 17° there was as much spoilage in the irradiated as in the control fruit. Essentially the same results were obtained with 200 krads. The action of DHA was rather similar. Fruit treated with DHA and stored at 17° had the better appearance. On the other hand, for fruit stored at 0°, 100 krads irradiation gave better results.

Effect of Co^{60} Radiation in Extending the Storage Life of Shamouti Oranges Inoculated with Fungal Spores of Penicillium Digitatum and Penicillium Italicum[1] : R. S. Kahan and R. Barkai-Golan *

Radiation was found to delay the appearance of rot in Shamouti oranges inoculated with fungi. However the radiation caused peel damage.

Fruit picked at the beginning of the main Shamouti harvest season was cleaned and inoculated with suspensions containing either P.digitatum or P.italicum spores. Three concentrations were used for each pathogen (100, 1000 and 10,000 spores per inoculum). The inoculated fruits were irradiated with doses of 50-250 krads, applied at 390 krads/h, and then stored for 80 days at 23°C. The experimental unit was 20 oranges.

The results are given in Table 36 . Doses above 50 krads delayed the appearance of rot, the effect being more marked when the initial spore concentration was lower. A dose of 200 krads was usually sufficient to delay rot for at least a month, while 250 krads usually prevented development of the pathogen entirely.

---

* Dept. of Fruit and Vegetable Storage, Volcani Inst. of Agricultural Research

TABLE 36

Effect of radiation in delaying the appearance of visible rot in inoculated oranges stored at 23°C

Fungus	Dose (krads)	Days before appearance of rot		
		100 spores per inoculum	1000 spores per inoculum	100,000 spores per inoculum
P. digitatum	0	3	3	3
	50	3	4	3
	100	5	4	3.5
	150	23	-	10
	200	27	-	26
	250	no rot	no rot	30
P. italicum	0	3	3	3
	50	8	5	4
	100	20	9	5
	150	29	-	23
	200	no rot	35	40
	250	no rot	no rot	no rot

Slight radiation damage to the peel was observed in some of the fruit treated with 50 and 100 krads. All the fruit receiving 150 krads or more showed marked peel damage, in the form of surface pitting which appeared 3 days after irradiation and darkened and spread with time. Similar peel damage has been observed in non-inoculated Shamouti fruits[2].

References:

1. BARKAI-GOLAN, Rivka, and KAHAN, R.S., Volcani Inst. of Agr. Research Bulletin No. 91, p.19 (1965) (in Hebrew)

2. KAHAN, R.S., Israel AEC Semi-Annual Report July-Dec. 1964, IA-1021, p.149

Effects of Gamma Irradiation on Valencia-Type (Jaffa Late) Oranges :

R.S. Kahan, S.P. Monselise*, E. Eisenberg and C. Satchy

Studies on the effects of radiation on Shamouti oranges[1] were extended to the Valencia variety. The Co^{60} plate source was used, and the effects of 4 doses (50, 100, 150, 200 krads) at 4 dose rates in the range 50-300 krads/h were investigated. External damage and chemical and enzymatic changes were examined in fruit stored in a cellar at ambient conditions (20-30°) for 13 and 90 days. Only a limited number of replicate analyses were performed so that the results must be regarded as preliminary.

Visible damage to the peel was far less marked than in the case of Shamouti oranges. The damage appeared 5-10 days after irradiation and spread during the next 20-30 days to an area 2-3 times as large as that initially affected. After this there was no spread of the damage up to the end of the 90-days storage period. The extent of visible peel damage appeared to be affected by the dose rate (least damage at 200 krads/h and most at 50 krads/h). Such effects were also observed in regard to weight loss during storage (least loss at 200 krads/h in most cases, and most loss at 300 krads/h). There were no clear cut effects of the dose rate on the chemical constituents and enzymatic activity of the skin. These factors were in any case not greatly influenced by radiation.

The increased damage observed at low rates may have been due not so much to the dose rate itself as to ozone in the irradiation chamber during the prolonged exposure.

Reference:

1. KAHAN, R.S., Israel AEC Semi-Annual Report, July-Dec. 1964 IA-1021, p.149

---

* Dept. of Citriculture, Hebrew University, Rehovoth

Determination of the Radiation Required for 90% - 100% Lethality in Penicillium Italicum Spore Suspensions[1] : R S. Kahan and R. Barkai-Golan*

P. italicum amd P. digitatum are the common rot-causing fungi attacking stored citrus fruit in Israel. The need to combat these fungi is of special importance in the export of citrus, since the fruit takes several weeks to reach its destination. An in vitro study was made to determine the radiation dose required for 100% destruction of the spores in various spore populations. Beraha et al.[2] determined some sublethal and supra-lethal doses for these fungi, and Sommer and Maxie[3] determined the C.I.D.80 (the dose required to inactivate 80% of the spore population) for various populations. However these doses cannot be extrapolated since the response to radiation is not linear.

P. italicum spores were prepared in suspensions containing 10^2, 10^3, 10^4, 10^5, and 10^6 spores per ml. The suspensions were irradiated with doses of 100-300 krads, and after suitable dilution they were incubated on normal potato-dextrose agar medium at 23°C. The number of spores which formed colonies are given in Fig. 48 . All the doses used inactivated over 99% of all the spore populations tested, but the dose required for 100% lethality varied with the initial spore concentration. 100 krads did not cause 100% lethality even in the smallest population tested (100 spores/ml); 150 and 200 krads gave 100% lethality in populations of 100 spores/ml; 300 krads caused 100% lethality in populations of 10^2 - 10^5 spores/ml. Doses of 150 krads or higher inactivated at least 99.95% of all the populations tested.

It seems probable that doses of 100 krads would be adequate for commercially packed fruit in which the residual spore concentrations are far less than those used in this experiment. Similar experiments will be carried out for P. digitatum.

---

* Dept. of Fruit and Vegetable Storage, Volcani Inst. of Agricultural Research

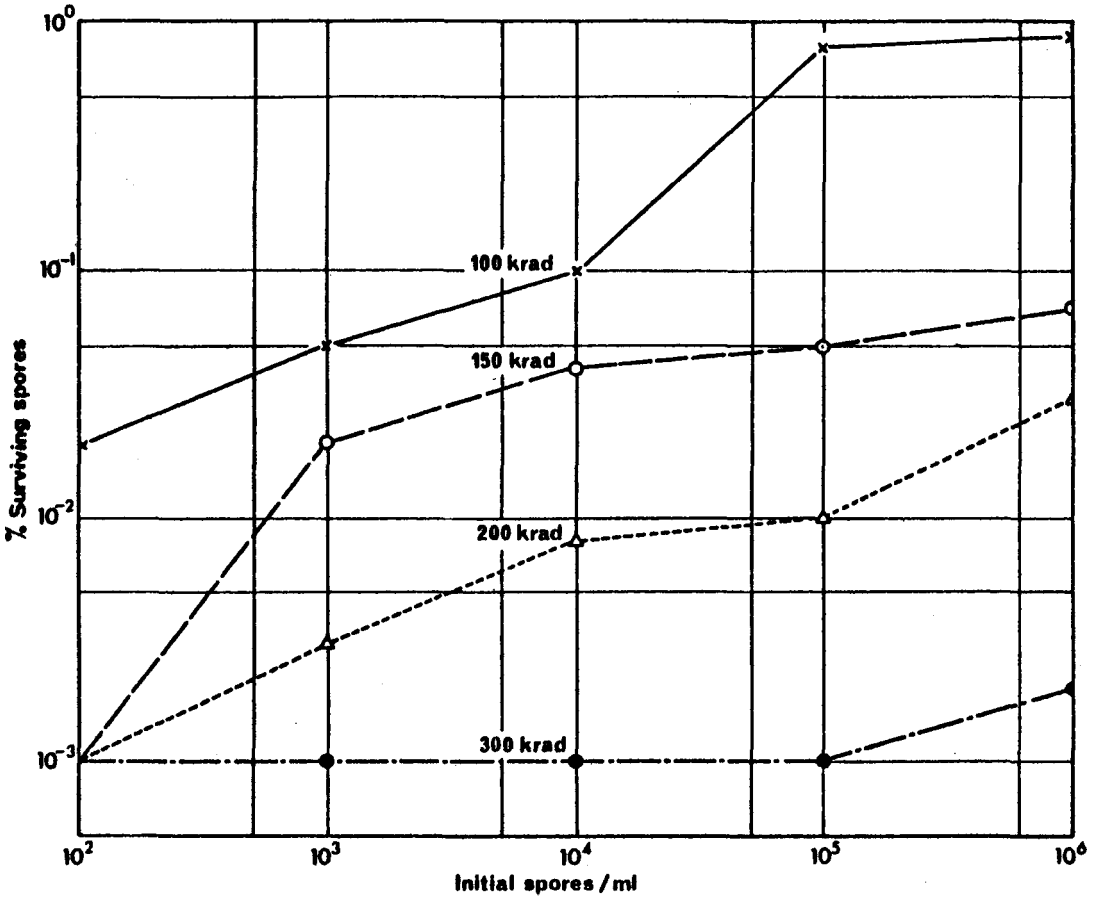

Fig. 48

Effect of gamma radiation on the percentage of viable spores surviving from various initial concentrations

——— 100 krad — — — — 150 krad
- - - - 200 krad —·—·— 300 krad

References:

1. BARKAI-GOLAN, Rivka and KAHAN, R.S., Inst. of Agricultural Res. Bull. No. 91, 27-28 (1965) in Hebrew

2. BERAHA, L., RAMSEY, G.B., SMITH, M.A. and WRIGHT, W.R., Phytopathology 49, 91 (1959); 56 474-(1960)

Control of the Mediterranean Fruit Fly (C. Capita Wied) by Mass Irradiation Sterilisation of Laboratory-Bred Flies: I. Cohen*, D. Nadel**, B.A. Peleg**, R.S. Kahan and E. Eisenberg

Tests are being carried out under field conditions in three selected areas in order to evaluate the efficacy of fly control by the release of large numbers of laboratory-bred flies sterilised by irradiation. The flies, which are bred at the Biological Control Institute, Rehovoth, are irradiated during the pupal stage, on the last day before emergence of the adults. The dose is 5-8 krads, which produces a lethal mutant in the spermatozoa of the mature male flies, and renders the mature female sterile and unable to ovipósit and damage fruit. Currently about 7 million pupae are being irradiated and released per week. A total of 80 million pupae have been treated since the project was begun in April 1965.

This large-scale project is based on the results of successful small-scale experiments which solved the following problems:

a) Determination of the dose which would produce a lethal mutant in the males but leave them sufficiently active to compete effectively with wild-type males.

b) Determination of the optimum stage at which to irradiate the pupae.

c) Development of a suitable container for irradiating liter quantities of pupae (60,000 pupae per liter).

d) Development of a rapid method for confirming the sterility of both male and female flies before their release.

e) Testing of various methods of release under field conditions.

f) Investigation of the efficacy of the treatment under field conditions.

---

* Agro-Technical Division, Citrus Marketing Board, Tel Aviv
** Biological Control Institute (C.M.B.) Rehovoth

Radiation Susceptibility of Various Developmental Stages of the Mediterranean Fruit Fly (Ceratitis Capita Wied) : R. S. Kahan, B. A. Peleg* and E. Eisenberg

An experiment is being carried out to determine the lethal dose of gamma radiation for laboratory-bred flies at various stages of the development cycle. The insects are dispersed in a suitable synthetic food medium and irradiated with the Co^{60} plate source. A dose of 10 krads was found to kill all immature stages of the fly. This dose also rendered the adult fly sterile. Thus 10 krads may be sufficient for quarantine control of citrus and other fruits against this fly.

Tests are now being carried out with lower doses and in vivo conditions, and eventually the wild type flies will be studied.

Preliminary Experiments on the Use of Radiation in Agriculture and Related Fields

Several experiments have been carried out or are in progress to explore new applications of irradiation. These experiments have been undertaken in collaboration with various other institutions and will be reported on at a later stage. The following topics are being studied:

a) Delay of sprouting in stored gladiolus bulbs. (R. Shiloh, Dept. of Floriculture, Volcani Institute of Agricultural Research).

b) Control of growth of microflora in experimental soils used in soil studies. (A. Geron, Dept. of Soil Science, Volcani Institute of Agricultural Research).

c) Control of rots in "Hayani" soft dates. (S. Ben-Yehoshua, Volcani Institute of Agricultural Research).

d) Preliminary tests on Beit-Alpha variety of winter-harvested onion bulbs. (M. Avidov, Dept. of Vegetable Crops, Ministry of Agriculture and N. Temkin - Gorodeiski, Volcani Institute of Agricultural Research).

e) Changing the time required for onion bulbs to reach maturity. (M. Avidov, Dept. of Vegetable Crops, Ministry of Agriculture).

---

* Biological Control Institute, Agrotechnical Division, Citrus Marketing Board of Israel, Rehovoth

f) Control of ticks causing cave-fever and disease-bearing mosquitoes (R. Galon, Israel Institute for Biological Research, Ness Ziona).

g) Formation of visible mutants in plants from irradiated potato tubers. (Y. Natav (Reves) Dept. of Vegetable Crops, Ministry of Agriculture).

h) The effect of irradiation on the phytotoxic fungi attacking table-grape varieties (Queen of the Vineyards, Alphonse Levallec, and Sultanina) and on rot-causing pathogens in grapes. (R. Barkai-Golan and S. Reich, Dept. of Fruit and Vegetable Storage, Volcani Institute of Agricultural Research).

i) Disinfection of dried egg albumin against Salmonella (Tomaz Ltd.,Hedera).

j) Disinfestation and disinfection of bran. (D. Nadel Biological Control Institute of Citrus Marketing Board, Rehovoth).

k) Disinfestation of contaminated filled chocolate confectionery. (D. Mor, Ministry of Commerce and M. Calderon, Ministry of Agriculture).

l) The effect of irradiation on stored melon pathogens. (R. Barkai-Golan, Dept. of Fruit and Vegetable Storage, Volcani Institute of Agricultural Research).

m) Preservation of peeled sliced grapefruit in plastic packages. (R. Beck, Dept. of Food Technology, Technion, Haifa).

n) The effect of irradiation on the pathogen Phytophtera citrophthora causing brown rot in citrus fruit. (M. Shiffmann - Nadel and E. Cohen, Dept. of Fruit and Vegetable Storage, Volcani Inst. of Agricultural Research).

o) Effects on the development of rot-causing pathogens in strawberries. (R. Barkai-Golan, Dept. of Fruit and Vegetable Storage, Volcani Institute of Agricultural Research).

p) Preliminary experiments to compare the effects of diphenyl and gamma radiation on artificially inoculated Shamouti oranges. (R. Barkai-Golan, Dept. of Fruit and Vegetable Storage, Volcani Inst. of Agricultural Research).

Determination of Ozone in the Gamma Cell : M. Lapidot and A. Algave

Measurements were carried out to calibrate the "Ozonomat" apparatus which has been installed for continuous monitoring of the ozone concentration in the air of the gamma cell. For the calibration the air was absorbed into an alkaline solution of fluoresceine (zinc-reduced fluorescine)[1] and the ozone present determined from the change in colour

produced by the oxidation of the fluoresceine. The amount of fluoerescine obtained was measured spectrophotometrically at 4900 Å, and the ozone concentration calculated by the method of Egorow[2].

Air was pumped from the gamma cell, at a spot about 20 cm from the source, and passed successively through two absorption bottles containing the fluoresceine solution. The following table gives the ozone concentration in the gamma cell as a function of irradiation time for a dose of rate of 200 krads/h.

TABLE 37

Ozone concentration in gamma cell

Time of irradiation hours	Ozone concentration ppm (by wt)
0.5	0.644
1	0.752
2	1.17
3	6.12

References:

1. WALTHER Deckert, Z. Annl. Chemie 150, 421 (1956)
2. KERTESZ, Z.I. and PARSONS, Grace F., Science, 142, 1289 (1963)

Calibration of the Gamma Cell and Dosimetric Development Work :

Carmela Satchy

Measurements were made to map the radiation field in the gamma cell when the 30,000 curie Co^{60} source is in operating position. Silver phosphate glass dosimeters were used. These were calibrated at different wavelengths, against the Fricke $FeSO_4$ dosimeter, using the Gamma-Cell 200 source at a flux of 400 krad/h. Fading curves of the glass dosimeter were prepared and conditions of accelerated fading were established. The additivity of fractionated doses was determined and the accuracy and reproducibility of calibration by the dosimeter established. For the mapping

measurements dosimeters were positioned on plastic sheets stretched on wooden frames and arranged at different distances from the source. The depth-dose curves obtained are shown in Figs. 49, 50 and 51.

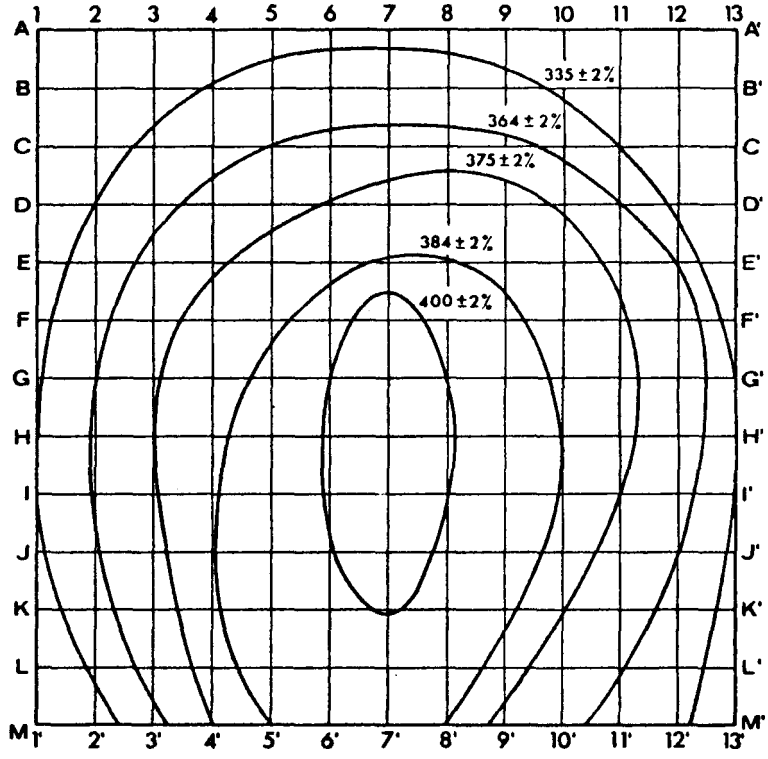

Fig. 49

Isodose curves at the window of the gamma cell, with the 30,000 curie Co^{60} source in operating position. Dose rates are given in krads/h. A vertical section is shown, representing a quarter of the cell. The doses are symmetrical upon reflection about M-M' and 13-13'

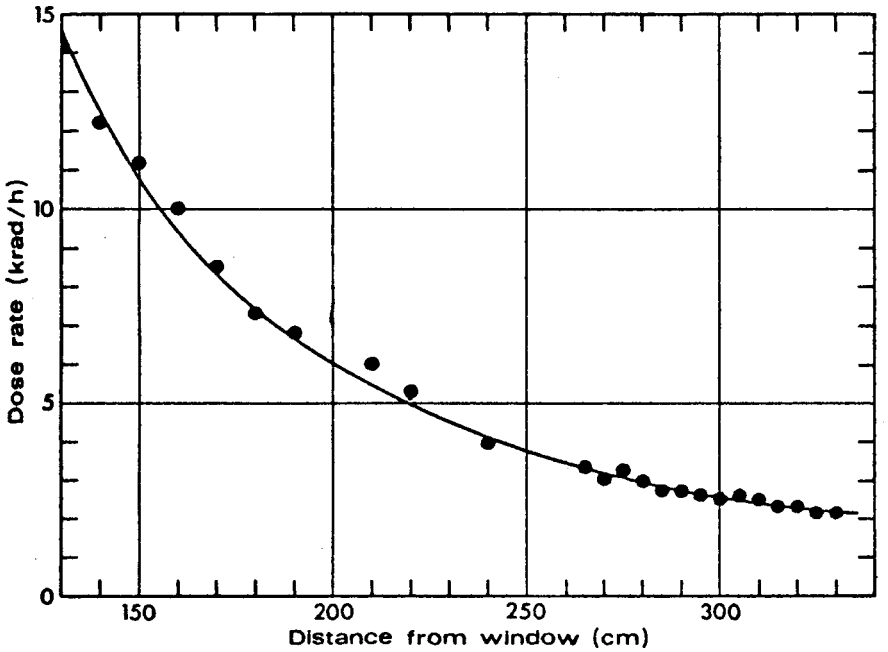

Fig. 50

Dose rate as a function of distance from the window. Location K13, at a height of 37 cms above the floor.

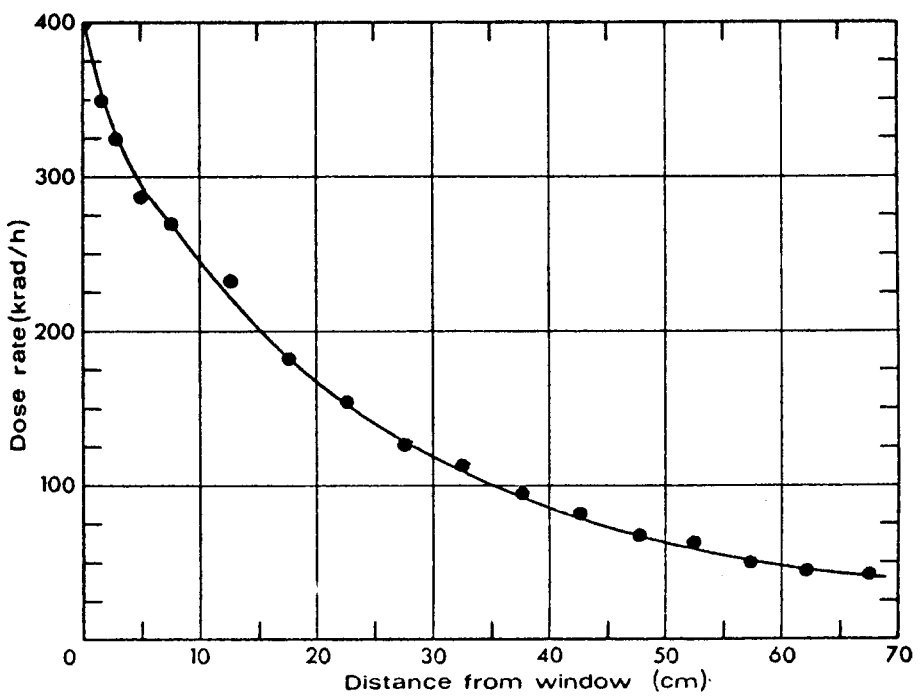

Fig. 51

Dose rate as a function of distance from the window. Location Q7, at a height of 37 cms above the floor.

Routine dosimetry was performed in order to determine the following factors for items of different densities and geometries:

a) The appropriate location and time of irradiation for various dose-rates and doses.

b) The distribution of the absorbed dose.

Various dosimeters were compared, namely Fricke ampoules[2,8], silver metaphosphate activated glass plates[1,3,5] and cobalt glass plates[4]. The glass dosimeters, which are too expensive for routine work, were regenerated by heating at 470° for 15 minutes[1,5]; this results in the disappearance of the colour centers. Both kinds of glass were subjected to 5 successive identical exposure-regeneration cycles, with doses over the range 120-180 krad and dose-rates of 160-250 krad/h. One hour after each irradiation the optical density at 400 mμ was measured with a Spectronic 20 Colourimeter. The response of the glass was found to remain essentially constant over the whole treatment. The error was ± 12% for the cobalt glass and ± 10% for the silver metaphosphate glass.

Some specimens of glass were found to retain a certain amount of colouration after the thermal regeneration procedure. Those having an optical density of over 0.1 (about 15-20% of the cases) were chemically treated to ensure complete bleaching. Several processes were tried, the most efficient for silver metaphosphate glass being soaking in NaOH solution (4 min in 10% NaOH or 10 min in 5% NaOH) followed by rinsing in water and reheating. The chemically treated specimens were irradiated in parallel with new specimens and their response was found to be similar to that of heat-regenerated glasses.

The modified Fricke dosimeter[2,6,7] (based on cupric-ferrous sulphate) was chosen for the higher range of doses, up to 10^6 rads.

A review of world literature on new dosimeters was prepared. Photographic films, print-out-papers, X-ray films, cellophane dyes, chlorinated hydrocarbons and similar materials were investigated as possible cheap dosimeters.

Research has started on the development of new dosimeters based on the decrease in the fluorescence of organic compounds. Azo or diazo compounds dissolved in solvents like benzene (for the lower dose range) or polystyrene (for the higher dose range) will be irradiated and the changes measured by gasometric or fluorimetric means.

References:

1. PROCTOR, B.E., GOLBLITH, S.A. and DAVISON, S., NYO 3345 (1955)
2. JARRET, R. and HALLIDAY, J., U.S. Army Natick Lab.
3. SCHULMAN, J.H., NRL Memorandum Report 266, Feb. 1954
4. JOHNSON, W.T.K., IEEE Tran. Nuc. Sci. NS - 10(4), 23-9 (1963)
5. DAVISON, S., GOLDBLITH, S.A. and PROCTOR, B.E., Nucleonics 14, 34 (1956)
6. HART, E.J. and WALSH, P.D., Radiation Research 1, 342 (1954)
7. Radiation Research, 2, 33 (1955)
8. FRICKE, H. and STERNE, M., Am. J. Roentgenol, Radium Therapy, 18 430-32 (1927)

I N S T R U M E N T A T I O N

Electrostatic Analysers : H. Z. Sar-El *

Two new types of electrostatic analysers were developed. The first is a cylindrical type, as shown in cross section in Fig.52 . It was developed in an attempt to get a higher beam intensity, for a given resolution, than can be achieved with a parallel plate analyser[1,2]. Two factors pointed to the choice of the cylindrical condenser for the investigation - the law that conservative fields of axial symmetry have the property of image formation, and the fact that the parallel plate condenser is the limiting case of the cylindrical condenser.

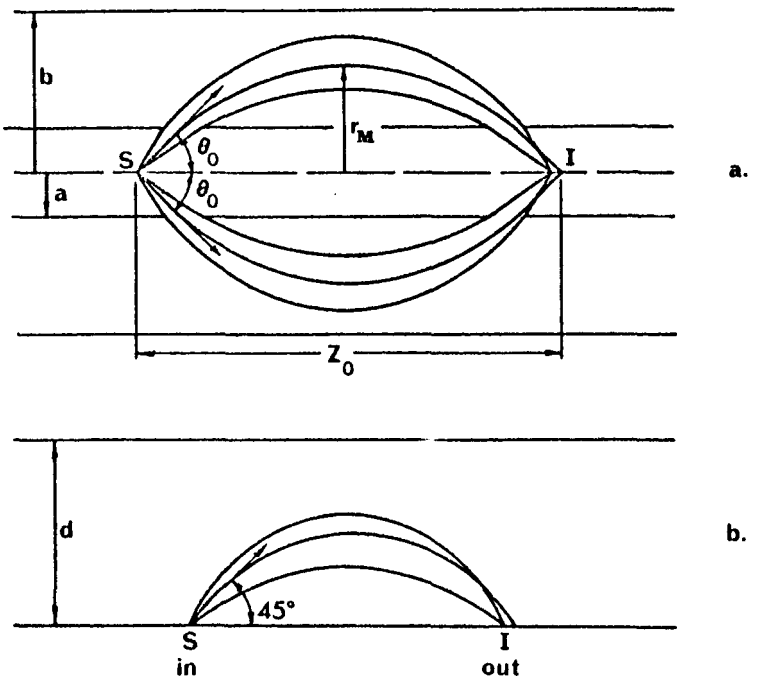

Fig. 52

Cross sectional scheme of a) the cylindrical analyser, and b) the parallel plate analyser, which is the limiting case of a) .

* Solid State Physics Dept.

Particles of energy $E = eV_o$ emitted from a point source S (Fig. 52) about an angle θ_o enter the field through a slot in the inner cylinder. They are deflected back by a suitable voltage V_p and come to a first order focus on the common axis at a point I . The distance $Z_o = SI$ is given by

$$Z_o = 2a \cot \theta_o \left(1 + Ke^{0.5K^2} \int_o^K e^{-(u^2/2)}\, du\right) \qquad (1)$$

where

$$K = 2 \frac{V_o}{V_p} \cdot \log\left(\frac{b}{a}\right) \cdot \sin^2 \theta_o \qquad (2)$$

and a,b are the radii of the inner and outer cylinders respectively.

The essential features of this analyser are the following:

a) It has a space focusing property.

b) A first order focus exists for monoenergetic particles emitted about an angle θ_o where $0^\circ < \theta_o < 90^\circ$. To every θ_o there corresponds a single value of K, and both determine the value of Z_o for predetermined values of a and b.

c) For $\theta_o = 42^\circ\ 18.5'$ there exists a third order focus for monoenergetic particles. The dispersion is finite.

To check the theory, an analyser for $\theta_o = \pi/4$ was built. The slots were covered with W wires of 0.05 mm diameter to prevent distortion of the field. The source S was a hole in a diaphragm through which the beam of an electron gun passed. Another perforated diaphragm was placed at the focus, followed by a Faraday cup as a collector. Fig. 53 shows the shape of the peak obtained by sweeping the voltage V_p of the analyser for 100 eV electrons.

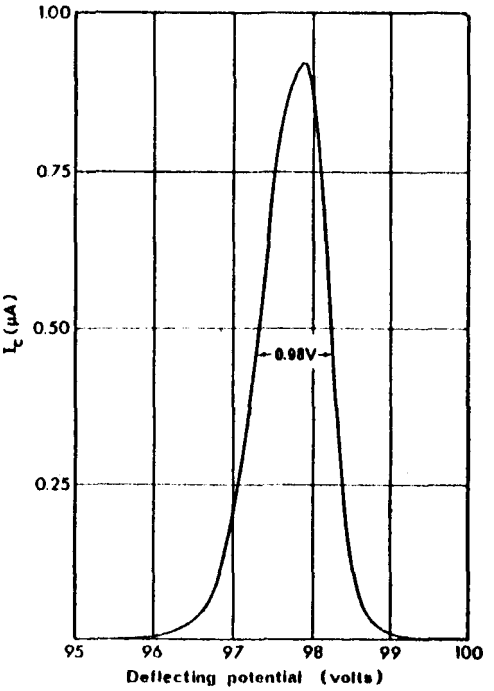

Fig. 53

Collector current as a function of the deflecting voltage in the cylindrical analyser

The second analyser makes use of the spherical condenser[4], as shown in cross section in Fig. 54. The source S and its image I lie in the hollow inner sphere of the condenser.

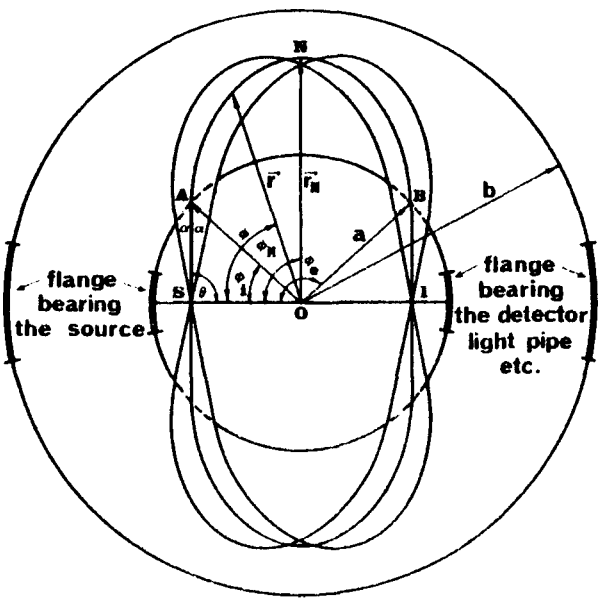

Fig. 54

Cross sectional scheme of the spherical analyser, showing trajectories of monoenergetic particles and the 2 places of focus, N and I

This analyser has the following features:

a) For particles which obey the relation

$$\frac{V_p}{V_o} \cdot \frac{b}{b-a} = 2 \qquad (3)$$

the distance Z = SI between the source and its image does not depend on θ_o. Thus we have a case of perfect focusing for 100% transmission. The dispersion is then zero. By sacrificing transmission in favour of dispersion, an analyser can be obtained.

b) For $\varphi_M = \pi/2$ there exists a first order focus for particles which obey eq.3, irrespective of the source location along the radius of the inner sphere (φ_M is the value of φ corresponding to r_M, the maximum value of r for particles emitted at $\theta_o = \pi/2$ and obeying eq.3.).

c) If the distance between the source S and the common center of the spheres is $\sqrt{\frac{3}{2}} \cdot a$, there exists a third order focus at $\varphi_M = \pi/2$ with a finite dispersion.

d) For particles which obey eq.3, the system acts as a mirror of zero focal power and angle of deflection 2π.

e) The whole system acts as two analysers in cascade connected in a symmetrical way. The first analysis is performed at $\varphi = \varphi_M$ and the second at I (see Fig.54)

f) The case discussed by Ritchie et al.[5] where the source S is located on the inner sphere, comes out as a limiting case.

It should be noted that electrostatic analysers with perfect focusing are an entirely new phenomenon in the field of electron optics[6].

References:

1. YARNOLD, G. D. and BOLTON, H. C., Sci. Instr. 26, 38 (1949)
2. HARROWER, G. A., Rev. Sci. Instr. 26, 850 (1955)

3. ZWORYKIN, V. K. et al., Electron Optics and the Electron Microscope, John Wiley and Sons, Ch.13, 1957

4. SAR-EL, H. Z., Israel AEC Report IA-883 (1965)

5. RITCHIE, R. H., CHEKA, J. S. and BIRKHOFF, R. D., Nucl. Instr. and Methods 6, 157 (1960), 8, 313 (1960)

6. See for example BORN, M. and WOLF, E., Principles of Optics, p.743, Pergamon Press, 1959, and Ref.3, Ch.16,17

Neutron Capture Gamma Ray Spectroscopy : G. Ben-David*, B. Arad* and Y. Tennenbaum*

The neutron scattering chamber at the outlet of Beam Tube No.1 has now been completed. It consists of 3 concentric cylinders having radii of 10 cm, 55 cm and 100 cm respectively. The innermost cylinder serves as the scattering cavity, containing the lead scattering crystal. The cavity walls are covered with borated plastic to absorb the thermal neutrons, except for inlet and outlet neutron beam holes (see Fig.63 ,p.313). The middle cylindrical section is filled with lead, and the outermost with borated paraffin, a 2" hole being left for the neutron exit beam. The 111 plane of the 3" x 3" x $\frac{1}{2}$" lead crystal is used, in the transmission mode. The maximum scattered thermal neutron flux is achieved at a scattering angle of 15' 30", which corresponds to a mean of .04 eV. The thermal neutron flux at the experimental position is at present 10^6 n/cm^2.sec at 2 MW reactor power. It is hoped to get a flux 3 or 4 times higher with a new reactor core grid arrangement at 5 MW power.

The use of the lead scattering crystal reduces the incident thermal flux by a factor of 100, compared with a factor of 10^5 for epithermal neutrons and gamma rays, thus achieving a signal-to-noise improvement of 10^3 for the epithermal neutron and gamma background components.

The external neutron beam will be used for the different experiments - spectroscopy of neutron capture gamma rays, and Mössbauer studies using neutron capture gamma rays. The spectroscopy will include

---

* Nuclear Physics Dept.

detailed studies of correlations between the capture gamma rays from enriched isotopes of Ti, using lithium drifted germanium counters and sodium iodide crystals as detectors.

E L E C T R O N I C S

Low Noise Charge Sensitive Preamplifier: J. Grünberg and L. Tepper

A low noise charge-sensitive preamplifier was designed and a number of units built. The amplifier is intended primarily for use with solid state detectors, but can also be used with ionization chambers and proportional counters.

The circuit is fully transistorized and includes a field effect transistor at the input stage. It is modelled on the usual scheme of a cascode and boot-strapping emitter follower[1]. The specifications are as follows:

Noise: $(10 + 0.2\ C_{in})$ keV, referred to silicon detectors. C_{in} is the external capacitance in pf at the input.

Sensitivity: 400 mV/pico Coulomb
100 mV/pico Coulomb
20 mV/pico Coulomb

Range: 0.1 MeV to 250 MeV (silicon)

Fall time: 100 μsec

The unit is housed in a small box (11 cm long) so that it can be used in relatively inaccessible spots.

Reference :

1. RADEKA, V., "Proc. NAS on Instrument Techniques in Nuclear Pulse Analysis", NSS, No. 40 (1963)

Fast Timing Circuits Using Storage Diodes : J. Grünberg and L. Tepper

A constant-charge pulse-shaper has been used as the basic element in two fast timing circuits using photomultipliers. The shaper is based on storage diodes (snap-off diodes) and delivers an approximately constant amount of charge at the output, almost independent of the input current pulse amplitude. These constant-charge pulses are delivered to a tunnel

diode, which in the sub-nanosecond range is a charge sensitive device.

A coincidence circuit and a time-to-amplitude converter were built and operated with a Co^{60} source, two plastic scintillators used with 56 AVP tubes, and a slow coincidence discriminator. With a range of 20 mA to 200 mA, the coincidence slope was 0.4 nsec for half-amplitude, while the time-to-amplitude converter showed a FWHM of 0.8 nsec on a multichannel analyzer.

Fast Counter : B. Remigolski

A Ring Counter based on a combination of tunnel diodes and fast transistors connected in the common base mode[1] was developed. The input requirements of the circuit are a sine wave of 0.5 V amplitude, or else positive pulses less than 5 nsec wide.

The circuit was tested in the frequency range of 100 - 250 Mc. For frequencies lower than 100 Mc a pre-shaper must be added.

Reference :

1. RADEKA, V., Nuclear Instr. and Methods, 22, 153 (1963)

Nucleonic Modules : B. Remigolski

The following modular units were designed as part of a more general modular system of plug-in units:

a) A fast amplifier with a rise time of 3.5 nsec and gain of 100. The amplifier uses two stages of current amplification, each stage having a gain of 10 and a rise time of 2 nsec. The stage itself is based on a current feedback loop of 3 fast transistors.

b) Variable coincidence unit.

The double triple coincidence unit includes:

(i) A fast amplifier (risetime 4 nsec) with a gain of 10.

(ii) A variable tunnel diode discriminator and shaper based on a combination of common base transistor and tunnel diodes.

(iii) A double triple slow coincidence unit with a resolution of 1 μsec. The circuit is capable of working in the mode of delayed coincidence.

Time-to-Amplitude Converter : R. Potascher

A fast time-to-amplitude converter was designed and several units built. The block diagram is given below.

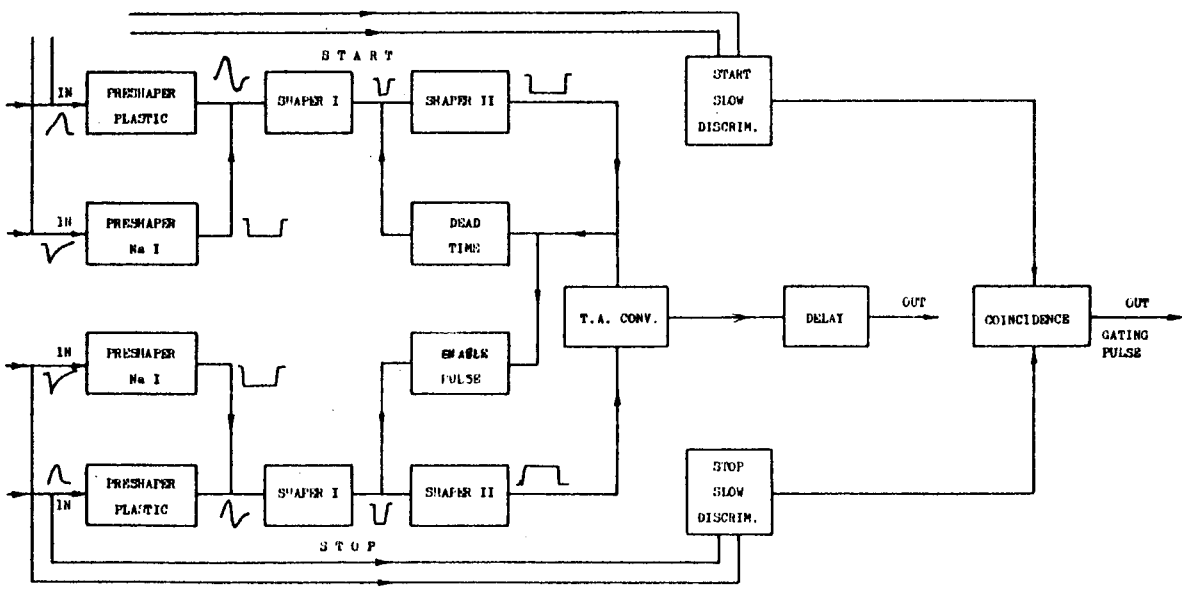

Fig. 55

Block diagram of time-to-amplitude converter

The converter is based on the start-stop principle and the usual method of charging a capacitor from a constant current source. Fast diodes are used as the current switching elements. The preshapers for pulses coming from plastic scintillators use zero crossing, while those for NaI scintillators use limiters. Both types of shaper are current sensitive. The main shapers are fast tunnel diode univibrators.

A slow coincidence circuit with a variable discrimination level is included for the gating pulses. An "enable" pulse is provided to trigger the stop shaper only when a start pulse has preceded the stop pulse. A dead time of 3 μsec is introduced after the start pulse.

The converter has two ranges, 30 nsec and 100 nsec. The time resolution measured as the FWHM on a multichannel analyzer is better than 10 psec using a mercury relay pulser as input source. Using two XP 1020 photomultipliers with plastic scintillators and a Co^{60} source in prompt coincidence, the resolution is 0.6 nsec for the low discrimination level and 0.35 nsec for the high discrimination level in the slow coincidence discriminators. Using a NaI scintillator and a 56 AVP photomultiplier in the start input the best time resolution for Co^{60} prompt coincidence was 0.85 nsec. With two NaI scintillators and 56 AVP photomultipliers the best resolution is 1.1 nsec. Linearity is better than 0.3% in the 100 nsec range and better than 0.5% in the 30 nsec range.

The unit was built as a "nucleonic module" (see previous item), and was developed as a continuation of previously described work[1]

Reference:

1. POTASCHER, R., Israel AEC Semi-Annual Report, Jan.-June 1964, IA-984, p.171

Spectrum Stabilizer : A. Senator, L. Tepper

Semiconductor detectors, as is known, show a deteriorated collection efficiency after being subjected to particle bombardment. This deterioration is greater the heavier the particles, and for fission fragments the impairment is particularly rapid.

A spectrum stabilizer[1,2], which is intended to present a steady spectrum at the input of a multichannel analyzer, was developed. It includes a preamplifier, the main amplifier and the detector itself. The stabilization is achieved by means of a variable gain amplifier to which the output of a differential ratemeter is fed back. The instrument was designed mainly for use with solid state detectors, but it is suitable for photomultipliers as well.

The block diagram of the stabilization system is given below. The amplifier gain is changed by means of the field effect transistor working below the pinch-off.

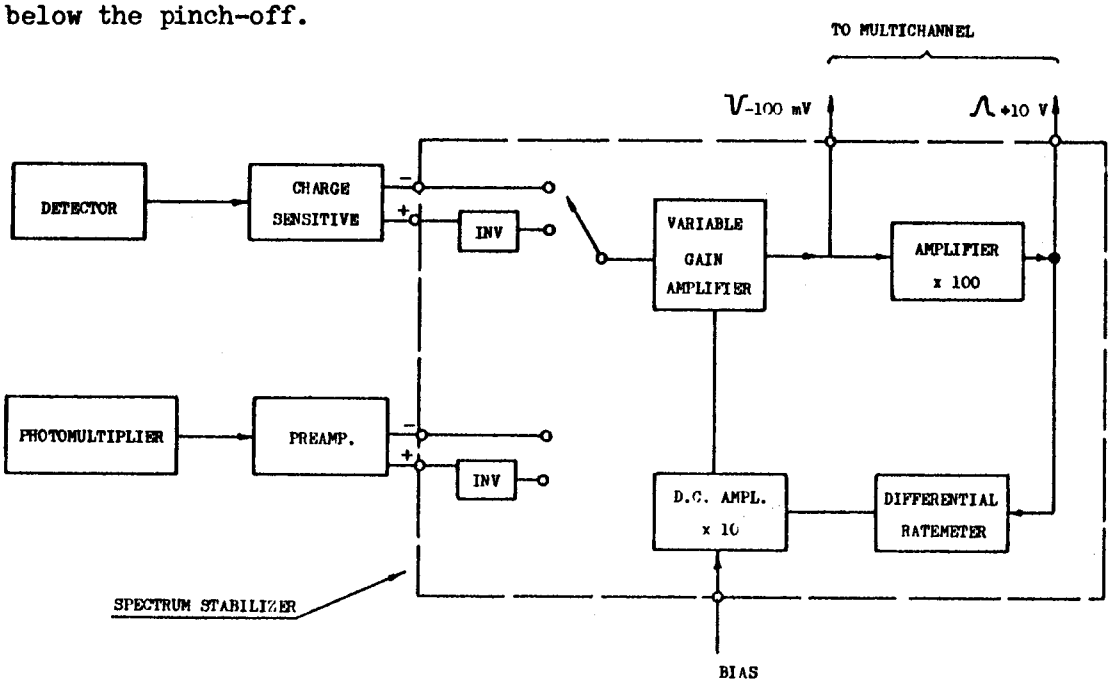

Fig. 56
Block diagram of stabilization system

The results measured on a 512 channel pulse height analyser are as follows:

Stabilization factor: for changes in input amplitude up to a factor of 2.5, the peak position remains in the same channel.

Long term stability: about 1 channel per day.

Temperature stability: 1 channel over a range of 30°-55°C.

Hunting effect (smearing): about 10% of the initial peak

Dynamic response: faster than 1 sec

A number of units were built and are in use.

A digital instrument which includes the changes of the multichannel analyzer in its stabilization loop, is now under development.

References:

1. DE WARD, H. Nucleonics 13, 36 (1955)
2. Cosmic Rad. Lab., RSI, 33, 1137 (1962)

Computation of the Fourier Transform in a Digital Differential Analyzer[1]:

A. Senator

The Fourier transform is of special importance in many problems of mathematical analysis. Several methods have been proposed for computing the Fourier transform with the help of digital and analogue computers. The present work describes how the problems can be solved on the digital differential analyzer (DDA)[2]. The proposed computation system consists of an interpolator of Lagrange, connected to an oscillator described by the weighting function $w(t)$:

$$w(t) = \sin \omega t$$

The speed and accuracy of computation is high and can be compared with the speed of a general purpose computer (8 minutes on the DDA compared with 1 minute on the G.P.C.).

References:

1. SENATOR, A., M.Sc. Thesis submitted to the Technion, Haifa, November 1955
2. SHANY, A. and KAMIL, Z., A Versatile Incremental Computer, 6th Annual Conference on Aviation and Astronautics, Feb. 24-25, 1964, Tel-Aviv and Haifa

Waveform Generator for a Mass Spectrometer : I. Ben Nun

A generator has been designed and built to supply slow sawtooth and triangular voltage waveforms.

The instrument includes:

(i) A stable voltage pedestal supply with an adjustable range of 0 to 100 V. This pedestal is needed in order to set a rough level from which to start a slow scanning sweep of 10 V.

(ii) A 0-100 V scanning sweep for searching for the proper pedestal level.

(iii) A very stable linear sweep, 10 V high, which "rides" on the selected pedestal.

An electrometer tube is used at the input stage of a Miller integrator. The reference voltages are temperature compensated.

The generator gives sweep times of 10, 100 and 1000 seconds, and the integral linearity and long-term stability are better than 0.2%.

Upper Audio-Frequency Heat Supply for a Mass Spectrometer : I. Ben Nun

Mass spectrometer measurements can be made more accurate by heating the ion source filament with frequencies in the range 10 to 30 kc/s, rather than with DC[1]. A supply was designed using a "resonant capacitor commutated SCR inverter"[2]. The basic circuit is an underdamped series resonant circuit in which the resistive component is the filament to be heated. When the SCR gates are triggered, alternating positive and negative half sine wave current pulses flow into the load. If both gates are triggered by the same source at a frequency twice the resonant frequency, the output is as shown in Fig. 57a. If the triggering frequency is decreased, the output is as shown in Fig. 57b. This variable current-pulse frequency provides smooth power control to the filament heating. The output power of the instrument is variable between 0 and 100 watt at an efficiency of 75%.

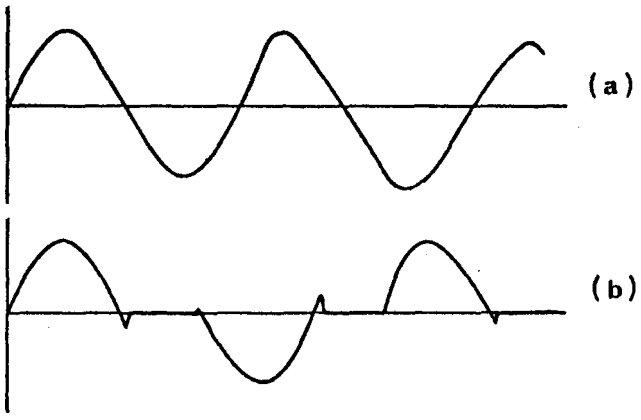

Fig. 57

Output of mass spectrometer heat supply.

References :

1. Advances in Mass Spectrometry,ed. Waldron J.D. p.473, Vol.I, Pergamon Press
2. SCR Manual, General Electric Comp., Auburn, N.Y., p.161

Linear Heating System for Crystals : M. Sidi

In certain solid state physics experiments it is necessary to heat a crystal linearly with time in order to search for energy lines. An instrument was designed to provide linear heating from -200°C to +400°C over a period of one hour. One of the main problems is the sensing element which must respond linearly to temperature changes, Another problem is the speed with which the transducer responds when energy is transferred to the heating element.

The body to be heated is included in a servo loop. A voltage ramp is provided to the input of the system. Because of the nonlinearity of the sensing element, some compensation is needed at the ramp voltage. The block

diagram of the whole system is given in Fig.58 and the block diagram of the ramp generator in Fig. 59 . The latter circuit is basically a dynamic integrator with a quasi-ideal current source feeding a Mylar capacitor of 10 μf. When the switch is opened the capacitor C charges through R (1000 Mohm). The output is

$$e_o(t) = \frac{EA}{RC}\left(t - \frac{1-A}{RC}\,t^2 + \frac{(1-A)^2}{(RC)^2}\,t^3 + \ldots\ldots\right) \qquad (1)$$

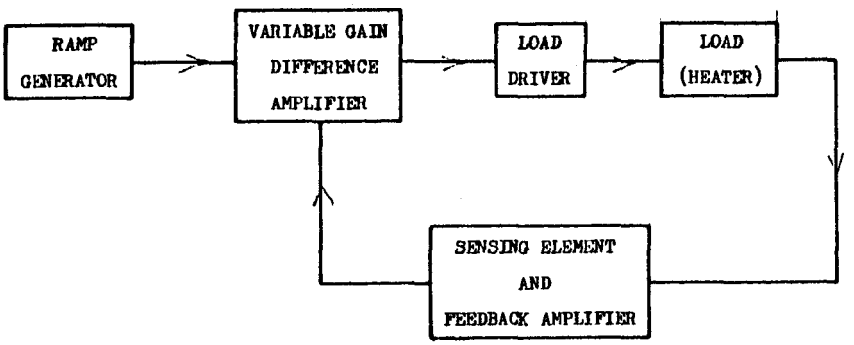

Fig. 58

Block diagram of linear heating system.

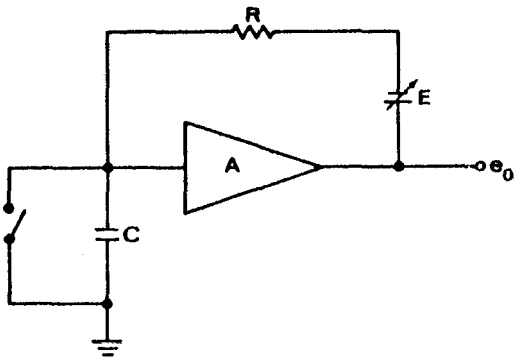

Fig. 59

Block diagram of ramp generator. E is a DC variable voltage supply.

The term $\frac{1 - A}{RC} t^2$ in expression (1) partly compensates the nonlinearity of the sensing element which displays similar square components. This circuit provides a linear ramp of 1 V with 0.7% nonlinearity over a period of one hour. The load driver uses SCR's which change the power supplied to the heating element by changing the phase of the firing. The load itself has the form shown in Fig. 60 . The cryostat is held at high vacuum. The heater wire can provide 300 W. The sensing element is a 10 ohm platinum wire. The feedback amplifier is a low drift D.C. amplifier with a gain of 100. The variable gain difference amplifier has a gain of from 25 to 200 with a common mode rejection of 10,000:1.

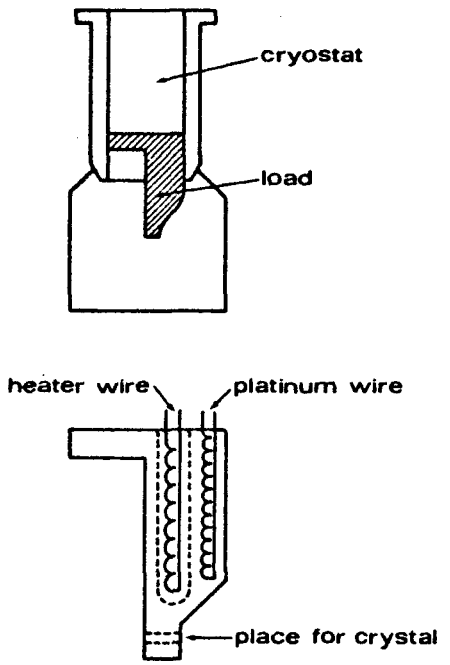

Fig. 60
Load and sensing element

The overall result was 1% integral linearity of temperature at the output, for heating from -200 to +400°C during one hour.

Parity Check for the 3 Dimensional Multichannel Analyzer : M. Sidi

A parity checking device was designed and built for the existing 3-dimensional pulse height multichannel analyzer[1]. The information for the analyzer is stored on punched paper tape, each event being recorded in four rows of 8 bits each. In order to make sure that the mechanical perforator is working properly a parity check is needed. The check is on those bits having binary values 2^2 to 2^7.

The circuit has three inputs, A, B and C (Fig.61), and one output, defined as follows:

0 Volt ≡ 0

-12 Volt ≡ 1

If there are one or three inputs (1) the output is (0). If there are two inputs (1) the output is (1).

The circuit described in the figure below is designed with a minimum number of active devices. Immunity to power supply variations is ± 7% of ± 12 V.

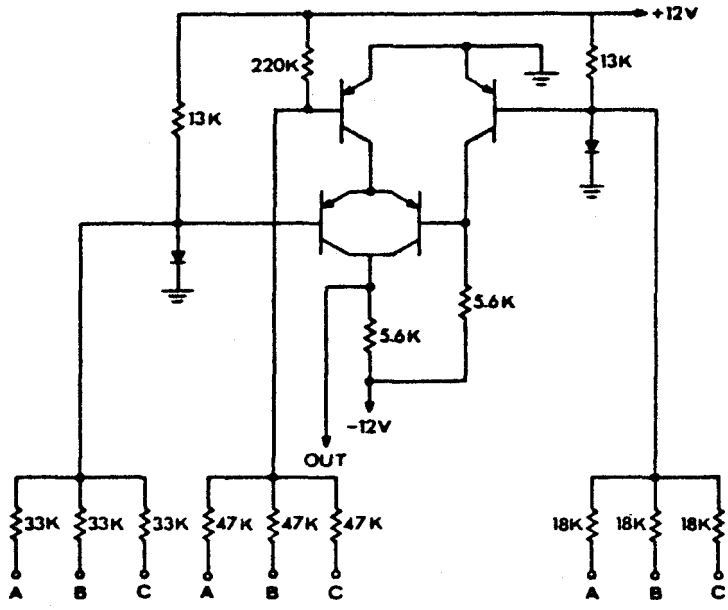

Fig.61

Parity check circuit

Reference:

1. SIDI, M. and FABIAN, Z., Israel AEC Report IA-900, p.161

Capacitance Bridge for Semiconductor Detectors : I. Zadicario and L. Tepper

A bridge was designed and built for the measurement of detector capacitance as a function of the applied bias voltage. It is particularly intended for use in the production of lithium drift type diodes. The bridge has three ranges : 0 - 10 pf, 0 - 100 pf and 0 - 1000 pf. The leakage currents tolerated in each range are 100 μA, 1 mA and 10 mA respectively. Maximum voltage rating is 600 V and accuracy better than 2%.

Portable Linear Ratemeter : I. Zadicario

A portable ratemeter has been designed, intended for monitoring and surveying purposes. There are four linear ranges: 0 - 30 cps, 0 - 300 cps, 0 - 3000 cps and 0 - 30000 cps. The time constants are internally adapted for the different ranges. The accuracy is better than 2% and the stability better than 10%. Sensitivity is 0.5 V negative. The instrument also contains a stabilized power supply (1200 V - 50 μA) for photomultipliers.

Fast Solid State Light Pulser : M. Sidi and L. Tepper

The characteristics and possible uses of a fast light emitting device were investigated.

The device is a Fairchild FSP-103 diode emitting a light pulse with a 1 nsec risetime, when pulsed into avalanche. The number of photons emitted is estimated at 100 when a 10 A pulse is delivered into the diode. This number increases with the current. The schematic circuit used for the excitation of the diode is shown in Fig. 62.

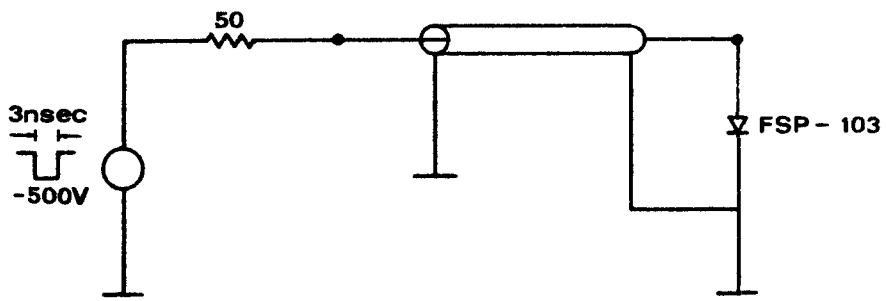

Fig. 62

Schematic circuit for light diode excitation

The light emission was measured with a 56 AVP photomultiplier operating at 2000 V. The spread in current amplitude at the anode of the phototube was about 20% of the minimum; the time spread was 0.35 nsec with the diode coupled directly to the tube, and 0.5 nsec with a scintillation crystal in between. The rise time of the pulse was about 4 nsec, the fall time 8 nsec.

It is thought that this type of diode may be very useful for the alignment of several photomultipliers with respect to signal propagation delay. Another possible use could be the focussing of fast phototubes.

Instrumentation for a Pulsed Nuclear Magnetic Resonance System :

J. Hershkovitz

In pulsed N.M.R. experiments, a sample is inserted in an intense DC magnetic field for the purpose of tipping the nuclear spin system by means of a massive RF pulse which lasts for a very short time. A short-lived free induction decay signal is thus produced and has to be recorded without noise or distortion.

A system was set up for this experiment. Some of the instruments required were bought and others were designed and built here. The system includes:

(i) A large magnet with a magnetic field of 26 kgauss, very well stabilized by means of a "Hall effect" element.

(ii) A transmitting system in the range of 2-30 Mc/s with a pulsed output of 5 kW, which leads to pulsed circularly polarized RF magnetic fields of the order of 50 gauss.

(iii) A receiving system with a recovery time of 5-10 μsec after the burst of RF field from the transmitter, and a sensitivity limited by thermal noise in the receiving end of the preamplifier. The detection is phase coherent.

The system works as follows. A constant amplitude sine wave generator is the RF source. Its output is split into two channels; one passes through a phase shifter (which controls the phase of the RF field, related to a reference signal), an RF gate (controlled by the pulse generator), and on to the transmitter, while the other goes via an attenuator to one of the two inputs of the receiver, being used there as a reference signal for phase detection. The free induction decay signal and the RF pulse overload are picked up by the RF preamplifier from the receiver coil. A special pulse from the pulse generator (quench pulse) helps to speed up the recovery of the receiver coil from the overload of the RF pulse. The action of the quench pulse is to lower the Q of the receiver coil until the ringing induced by the RF pulse has vanished, after which the Q rises to record the nuclear resonance signal.

In the first stage of the receiver, the free induction decay signal and the reference signal are combined to make possible phase coherent detection. Since the reference signal has a steady and large amplitude compared with the nuclear resonance signal, its rectified output is used for the automatic gain control of the receiver. After the detection of the signal, the video is amplified anf fed to a scope or to a lock-in-detector which improves the signal-to-noise ratio.

An Air Particle Monitoring System : I. Ben Nun and D. Boger

An environmental radiation monitoring station has to give a continuous indication of the activity of particles in the atmosphere. It must distinguish between normal activity and unusual activity resulting from special events like fresh fallout, etc. Due to the large variations in the normal activity, reliable measurements require averaging over long periods, leading to a delay of many hours before the results can be obtained. However this problem can be overcome by measuring the ratio of beta to alpha activity, which remains constant for normal activity.

A monitor C.R.C. 620 was modified and adapted to perform the ratio measurements. The output recorded is proportional to

$$\alpha + \beta - (k + 1)\,\alpha$$

where $\alpha \equiv$ integrated α radiation, $\beta \equiv$ integrated β radiation, $k \equiv \frac{\beta}{\alpha}$. For normal activity the output must be zero. The instrument was tested in several week-long runs and no significant departure from zero was detected, although there were tenfold increases in natural activity during every 24 hour period.

PHYSICS TECHNOLOGY

This laboratory is available for consultation in the fields of vacuum technology, low temperature technology, gas handling (especially inert or radioactive gases) and technology of special materials. Activities include participation in the construction of experimental apparatus, and research and development work on basic problems in these fields.

Sealing Mechanism of Vacuum Gasket Seals[1]: A. Roth and A. Inbar (Amilani).

The sealing mechanism of vacuum gasket seals was investigated and the following general expression for the conductance of the seal derived:

$$C = \frac{2\pi}{\ell n \frac{r_o}{r_i}} \frac{k}{8.12} A^2 . e^{-3\frac{P}{R}}$$

This equation gives the conductance, C, as a function of the nature and temperature of the gas (k), the geometry of the seal (r_o/r_i), the surface roughness (A), the tightening pressure (P) and the sealing factor (R).

The sealing factor (R) is a new quantity introduced to express the properties of the gasket material leading to the sealing effect. A special apparatus (sealometer) was developed [2] and built to measure R and nominal R values for various materials are being determined. With this data it will be possible to use the equation of the sealing process in the design of vacuum gasket seals and the prediction of their performance. It is intended to determine the dependence of R on the environmental conditions (high or low temperature, radiation, etc), so that the general equation can be used under these special conditions as well.

References:

1. ROTH, A. and AMILANI, A., Israel AEC Report, IA-1033 (1965)

2. ROTH, A., Israel Patent Appl. 24018/1965.

M E C H A N I C A L E N G I N E E R I N G

The following are typical of some of the projects carried out during 1965 by the Engineering Department.

Industrial Gamma Irradiation Facility - Experimental Stage

As the first step towards providing a facility for industrial irradiations with the 30,000 Curie Co^{60} source described previously[1], apparatus was designed and constructed for the irradiation of oranges. The apparatus consists of two contra-rotating tables on which cases of fruit are placed for exposure. The tables are located close to the aluminium window of the gamma cell and are driven by a roller chain from a gearbox connected to an explosion-proof motor. They can be rotated at 8 rpm or 1 rpm, or they can be set to remain stationary for a predetermined time, then turn through 180^{o}, stop again and then turn through a further 180^{o}.

A heavy shielding door made of steel was designed and installed inside the gamma cell, so that the area in which the fruit is irradiated can be closed off. This door also confines the ozone produced by the gamma radiation to a small area of the cell from which it can be evacuated without spreading to the whole cell. The door was designed so that it could be erected in the confined area of the cell by two men, without the need of a crane, and without having to introduce fixing bolts, etc. into the concrete walls. Foolproof safety interlocks were fitted so that in case of any fault or failure the Co source is automatically returned to its safe storage position.

Reference:

1. BARON (Balla), I., FOA, E., HARAM, S., LAPIDOT, M., Israel AEC Semi-Annual Report, July-Dec. 1964, IA-1021, p.146.

Combined Irradiation Facility in Beam Tube No.1

In order to exploit the beam tubes of the IRR-1 reactor more fully, facilities for two independent experiments have been installed in beam tube No.1.

Equipment has been constructed for producing a conically shaped neutron beam for the study of neutron capture gamma rays. A series of conical collimating plugs placed in the beam tube shapes the beam (Fig.63). The plug taper converges to a point 250 mm outside the beam tube cover. The monochromator crystal is placed at this position, sitting at the bottom of a hollow vertical plug inserted through the heavy external shielding. The crystal rests on a small tripod which is so arranged that its adjusting screws can be set from outside the cavity. To insert the crystal, the plug must be raised from the shielding. In its working position, the plug sits on a spherical, self-centering bearing, ensuring good reproducibility of its location. The angular position of the plug about its vertical axis can also be adjusted and measured by a 10 min graduated vernier scale.

The crystal cavity is lined with 1/4 inch thick neutron-absorbing boron plastic sheeting, and is shielded externally by lead bricks of approximately 50 cm thickness, surrounded by 45 cm thick borated paraffin blocks. The 10 ton shield is mounted on four wheels which run on rails in line with the beam tube axis. The shield assembly is driven by hand through a 1:100 reduction gearbox, giving quick and easy access to the beam tube. The neutron beam can be "switched-off" by filling the hole in one of the plugs with water. Gamma rays are stopped by moving into position an eccentric hole in a rotatable lead plug built into the beam tube cover. Both beam stoppers are operated by remote control.

A second independent experimental set-up, namely a loop for irradiating gases, has been placed in the same beam tube. A double-walled container 2 litres in volume is located at the core end of the

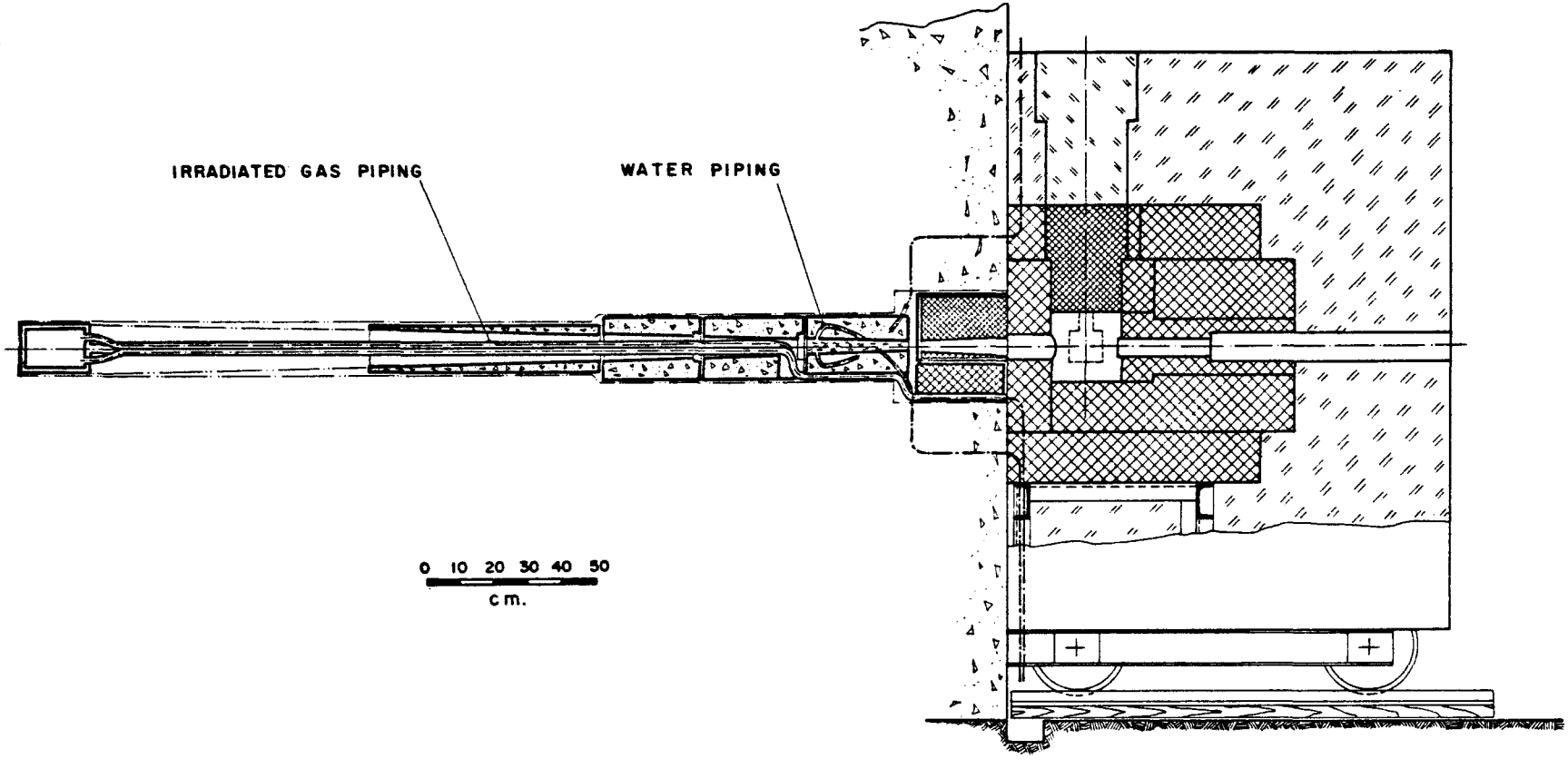

Fig. 63

Combined irradiation facility

beam tube, with its inner space connected by 1/4 inch tubes to a pumping and monitoring system outside the beam tube. The gas passes through two perforated partitions in the container to ensure turbulent flow. The space between the container walls is connected to a vacuum system for detecting leakage of irradiated gas, the outlet leading to the reactor hall exhaust system. By making all the parts that are located inside the beam tube of aluminium, neutron scattering is kept low, causing little disturbance to the other experiment.

Liquid Waste Disposal System

The liquid wastes from the operation of a nuclear research establishment fall into the low-level category and can generally be disposed of by discharge into the environmental soil. The favourable soil formations and geological and hydrological features at our location permit direct disposal of liquid waste into the sand-dunes provided that suitable precautions are taken to prevent a public health hazard. Our system is based on controlled delay and decay. All liquid waste from the laboratories is collected and monitored to ascertain the need for and type of treatment required prior to release to the environment.

Liquid waste is collected from the IRR-1 reactor building, the laboratories surrounding the reactor, the hot laboratories, the health physics laboratories, etc. No separate collection systems are provided to handle wastes known to be radioactive or of low or no activity. Small volumes of long-lived or more hazardous liquid wastes are collected in special containers and treated individually. Roof and surface drainage is not connected to the general collection system. All other drains, from sinks, plumbing fixtures etc., are connected by pipelines to a central liquid waste collection tank farm.

The tank farm is located at the lowest point on the periphery of the site of the Soreq Center. The ground at this point is inclined towards

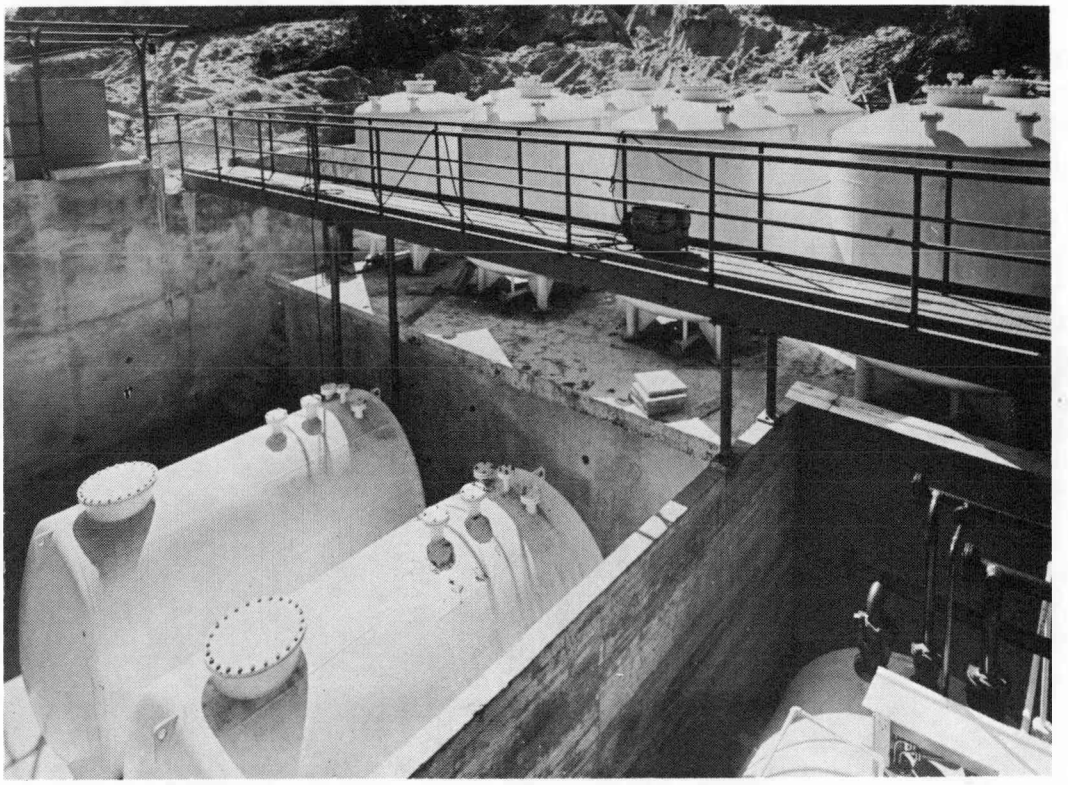

Tank farm for disposal of radioactive liquid waste

the surrounding sand dunes. The difference in level between the lowest laboratory floor and the tank farm is 10 meters, so that the liquid flows by gravity. There is also a 10 meter difference in level between the outlet (lowest) point of the tank farm and the point where the wastes are finally discharged to the sand dunes, so that again flow is by gravity.

The two main sources of liquid waste are the reactor (including the surrounding laboratories) and the hot laboratory. From each, a 3-inch diameter P.V.C. main pipeline (A, Fig.64 a) leads to a common distribution point (B) at the tank farm inlet. (Two additional pipelines, not shown in the figure, serve as emergency stand-bys.) From B the pipes lead to two manifolds, each serving four 10 m^3 tanks (Nos.11-14 and 21-24), with a common emergency tank (0). B can be set to direct the flow to both manifolds or to only one at a time. The manifolds are above the tanks and have a 1% slope. They are connected to the tanks by special junctions which automatically direct the flow into each tank in turn. Only when one tank is completely full does the next one begin to fill. Every tank has a level indicator. When a tank is full, the inlet valve between it and the junction is closed and the contents checked for activity. Each tank has a sampling station where samples are taken from three different heights. The samples are withdrawn by the suction effect of a water injector pump to ensure that there is no splashing. If the gross alpha plus beta-gamma activity of the samples is less than a certain amount the contents of the tank are discharged via a valve to manifold 3 where the flow is directed straight to the release point C. If the activity is too high, the contents of the tank are transferred via valves from manifold 3 to one of the hold-up tanks below (Nos.31-34). The hold-up tanks are also equipped with level indicators and sampling stations. After suitable decay the contents of these tanks are discharged via manifold 4. If the liquid waste is found to require special treatment it can be drawn by gravity from the common manifold of the collecting tanks, or by pumping from the hold-up tanks. The latter step is the only one for which a pump is needed.

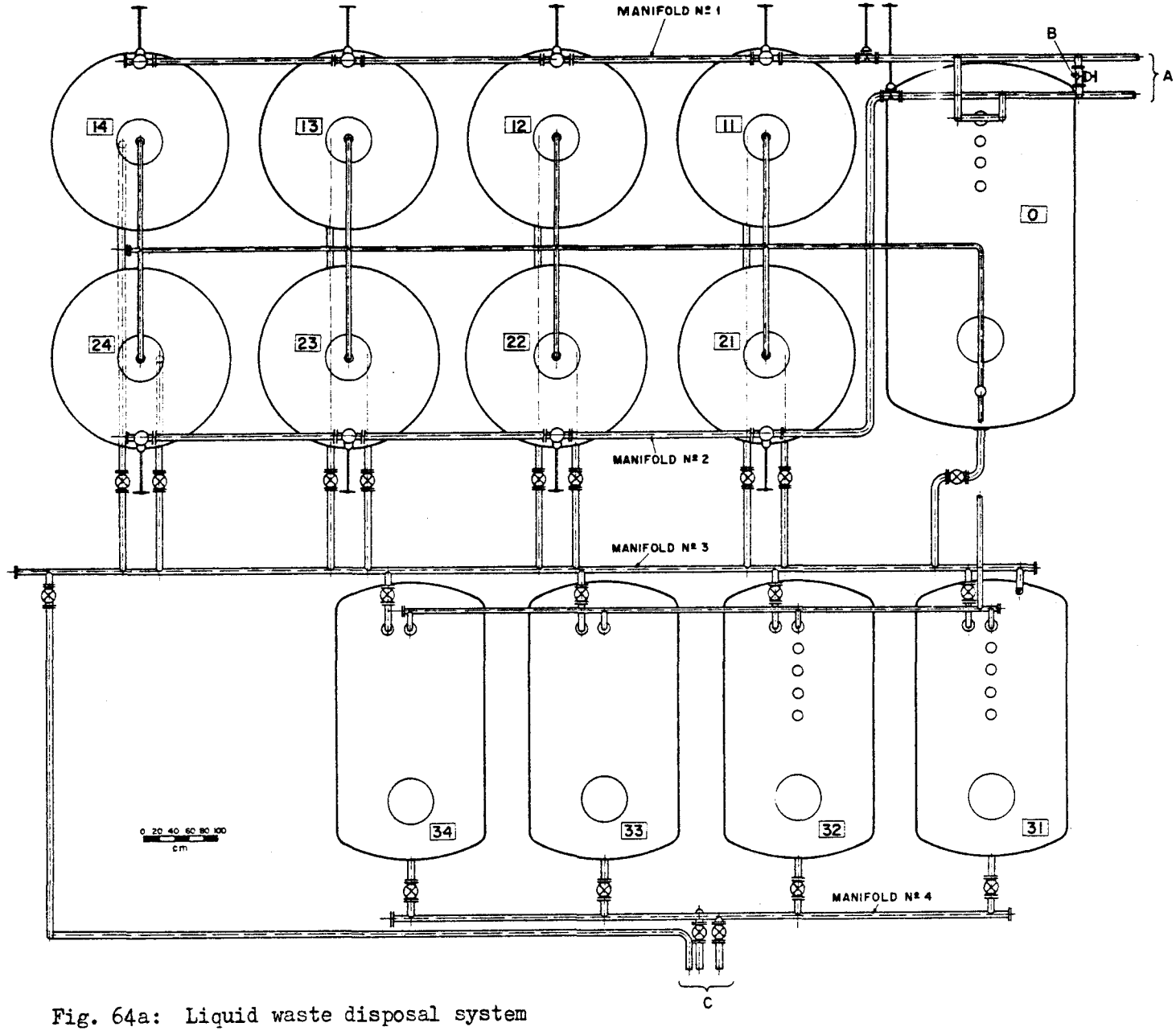

Fig. 64a: Liquid waste disposal system

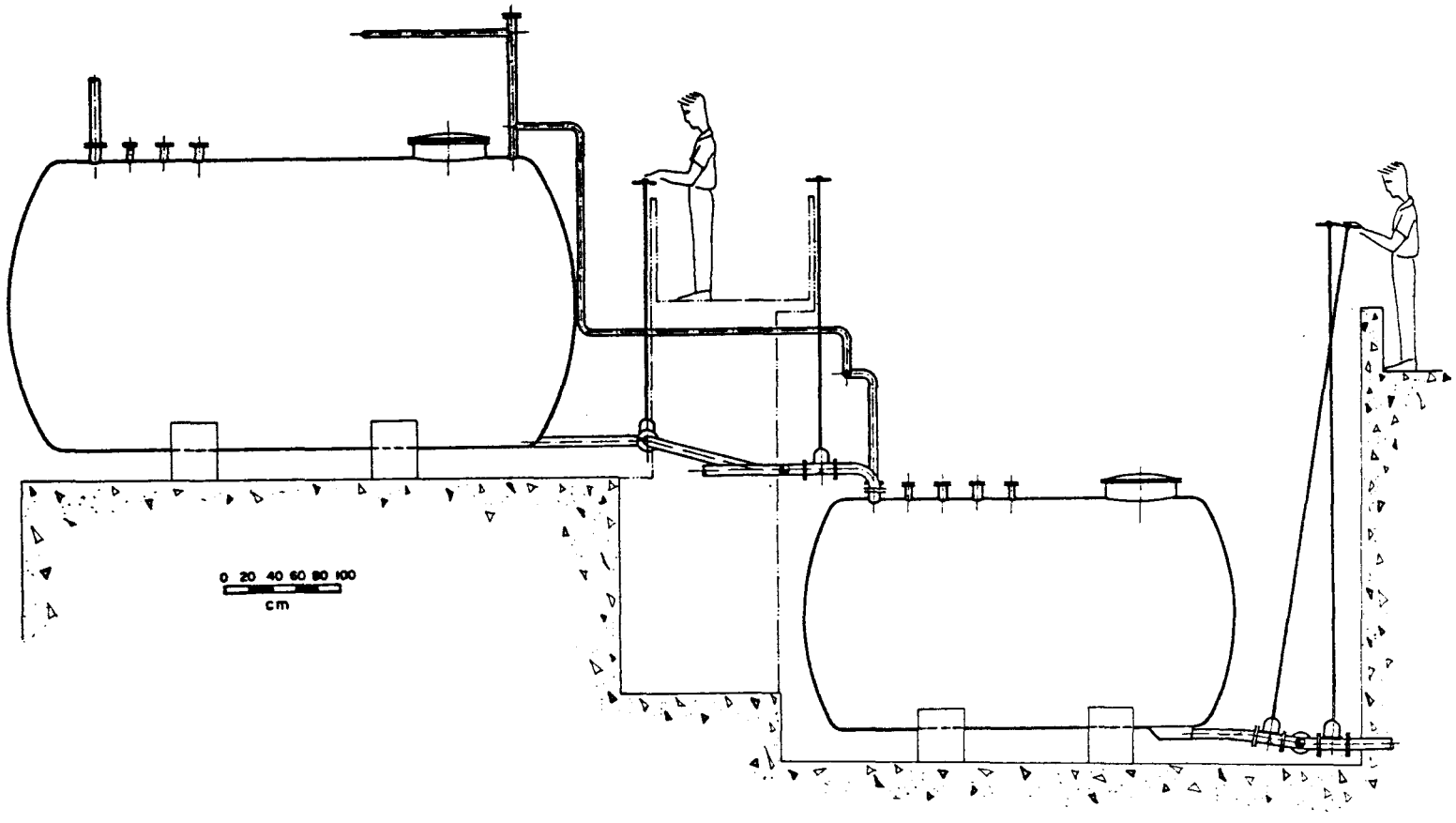

Fig. 64b

Liquid waste disposal system (side elevation)

Liquid level indicators, sampling stations, and valves are arranged along walkways, easy to reach and handle, and at the same time a safe distance away from the tanks (Fig.64b). The emergency collecting tank is equipped with a device which gives a signal in the health physics laboratory if liquid starts flowing into this tank.

NUCLEAR EDUCATION

In the period under review courses on various aspects of atomic energy were held for scientists and technicians from institutions throughout the country. During the summer vacation a 12-day science camp was held at the reactor site for 25 high school pupils about to enter their final year. The program included lectures and practical work in the laboratories.

Ten foreign scientists worked in our laboratories during the year on Israel AEC fellowships or fellowships granted by the Israel Ministry of Foreign Affairs under the supervision of the I.A.E.A. The scientists are listed on p. 320.

Six of our scientists participated in the following technical panels sponsored by the I.A.E.A.: Industrial Applications of Radioisotopes; Use of Nuclear Energy in Sea Water Desalination; Use of the Mössbauer Effect in the Chemistry and Physics of the Solid State; Isotope Techniques in Hydrology; Use of Isotopes in Agriculture.

Twenty-three of our scientists are part-time members of the faculties of institutions of higher education: Tel-Aviv University - 12; Bar-Ilan University - 6; Technion - Israel Institute of Technology - 3; Weizmann Institute of Science - 1; Hebrew University, Jerusalem - 1.

Twenty-four of our scientific staff are working towards a Ph.D. degree and nine towards an M.Sc.

The Second Conference on Nuclear Medicine was held in Tel-Aviv, 20-21 December, 1965, organized jointly by the Israel Radiological Society, the Soreq Nuclear Research Center and the Tel-Aviv University Medical School. About 100 physicians from Israel and 6 foreign countries participated, and 70 papers were presented. The I.A.E.A. and U.K.A.E.A. were officially represented.

Consultation and supervision were provided in the planning of a large Radium and Radioisotope Centre at the Rambam Government Hospital in Haifa.

LIST OF FELLOWS

Israel AEC

Dr. A. Abrahamson (USA)
Dr. M. Ash (USA)
Dr. C. Miller (USA)
Dr. W. Sherman (England)

Foreign Ministry

Dr. Artieda (Ecuador)
Mr. H. Brown (Ghana)
Dr. Y. Dafri (Thailand)
Dr. A. Katase (Japan)
Dr. Ku Aung Gy (Burma)
Mr. A. Simopoulos (Greece)
Dr. Y. Yoshida (Japan)

RESEARCH CONTRACTS

During 1965 the following contracts were in operation:

1. European Office of Aerospace Research of U.S.A.F.

   Optical and electrical properties of diamonds
   Microscopic theory of ferroelectricity
   Calculation of strength of optical spectra for transition metal ions in crystals

2. United States National Bureau of Standards

   Rare earth spectra
   Observation and analysis of neutral and singly-ionized spectra

3. Euratom (KBB - Euratom Association Karlsruhe Research Centre)

   The Doppler effect in fast reactors

4. Ford Foundation

   Study of ion-solvent interaction in mixed salt solutions in water

5. Israel Ministry of Development

   Aman reactions

6. Israel Citrus Marketing Board

   Mediterranean fruit fly irradiation

7. International Atomic Energy Agency

   Dynamic study of thyroxine deiodination

Twenty other research proposals were submitted to various international sponsors. Of these, five were approved by the end of 1965.

D O C U M E N T A T I O N

Storage and Retrieval of Information

During the period under review the following programs were completed and tested, within the framework of the Information Retrieval project:

1. The input program in COBOL and TAC language for the bibliographical material. This program translates the paper tape to computer language.
2. A program in COBOL which records errors in the above input. A recorded error causes rejection of the document concerned.
3. A program in COBOL for producing a sorted report of new documents introduced by program 1. Sorting keys incorporated into the program enable the sorting to be done according to the parameters indicated by the users (current number, authors, etc.)
4. The input program for the dictionary of keywords and for the subject index.
5. The central program of the system which provides answers for enquirers.

It has now been decided to discontinue development of this system since its specific requirements, as regards the organization of the information and the format of the input data, are not coordinated with parallel systems abroad. Such coordination is desirable to permit cooperation with other centers. Future work in this research will be directed towards a very close cooperation with Euratom in Brussels and with the IAEA in Vienna,in order to apply their results to our requirements.

Participation in Research Projects

Extensive calculations on ionic interaction in solution were carried out in cooperation with the Radiochemistry Department. A computer program was written for the solution of the simultaneous equations involved. The program solves the equations for all possible combinations of the parameters concerned, in turn. The program is still in the debugging stage.

Calculations of polynomials and angular momentum transformation matrix elements were carried out in connection with work being done in the Solid State Physics Department (see p.62; GAZITH, M., Israel AEC Report IA-1067 (1965)).

Library

Construction of the new library was completed. The functional layout was the subject of many meetings with the team responsible for the building. The transfer to the new premises was begun at the end of December.

The staff of the library prepared a complete author card file of the scientific publications of all the academic members of the Center for the years 1958-1965.

A thesaurus for the book collection in our library is in preparation, using the UDC classification, the subject headings of the NSA and the Engineers Council Thesaurus.

Publishing Activities

The department published 61 IA-reports, and 14 theses. It also prepared 44 papers for publication in journals and 30 papers for presentation at conferences.

Bibliographies and Translations

Fourteen bibliographies were compiled for the use of the Center's scientists, and 11 translations from various languages were prepared.

IA - REPORTS

IA-914 PASSY, N. and FEIGE, Y.
Radioactivity Measurements in Israel, September 1961 - June 1963

IA-928 HERMAN, H., BALLA, I. and REVEZ, G.
An Automatic Transporting and Dispensing System for Irradiated Materials

IA-930 SHENBERG, A.
Neutron Spectroscopy by Activation Analysis (Report in Hebrew)

IA-937 ROSEN, J.
Embedding of Various Relativistic Riemannian Spaces in Pseudo-Euclidean Spaces

IA-945 HARARI, H.
An Octet of Interactions

IA-960 ENGLMAN, R.
Phonon-Enhancement of Electron Self-Trapping

IA-961 ENGLMAN, R.
Zero-Phonon Lines in Diamond and Localized Modes

IA-964 HELD, S.
Some Remarks on the Assignments of the Furnace Absorption Spectra of Ce, Nd and Sm

IA-975 AVNI, A., FRIEDMAN, M., KESSLER, D. and SHATZ, M.
Monte Carlo Program for Interactions of High Energy Elementary Particles in Complex Nuclei

IA-978 AVNI, A.
Elastic and Inelastic Scattering of K^- by Complex Nuclei (Thesis in Hebrew)

IA-986 GIVON, M. and ZANGEN, M.
Recovery of Americium and Curium from an Irradiated Plutonium "Napkin-Ring" I. The Proposed Process

IA-987 SHILOH, M.
Complexes of the Trivalent Actinides with Inorganic Anions in Aqueous Solutions.(Thesis in Hebrew)

IA-989 FEIGE, Y. and GAIRON, P.
Relative Toxicity of Radionuclides

IA-990 HARARI, H.
The Use of Group Theoretical Methods for the Symmetries of Elementary Particles (Thesis in Hebrew)

IA-996 MOREH, R.
Study of the Energy Levels of O^{19}.(Thesis in Hebrew)

IA-998* BEN-DAVID (Davis) G.
Nuclear Physics Research at the IRR-1 Reactor

IA-1001 ROTHENSTEIN, W. and TABAK, D.
Philco-2000 Code for the Calculation of Resonance Escape Probability in Heterogeneous Reactors by the Monte Carlo Method

IA-1002 HORN, D.
Interaction between Leptons.(Thesis in Hebrew)

IA-1003 FEIGE, Y., SEVER (Strop) I. and ALTEROVITZ, S.
Calculation of Gamma Ray Energy Response for a Flat Silver Metaphosphate Glass Dosimeter

IA-1005 ZANGEN, M.
Solvent Extraction from Molten Salts IV. Kinetics of the Formation of Mercury (II) Bromide Species

---

* Internal Report

IA-1006 ABRAHAMSON, A.A.
Thomas-Fermi-Dirac Screening Functions for Neutral Atoms (Linearized Tables)

IA-1007 NEBENZAHL, I. and RAKAVY, G.
Calculation of the Energy Spectrum of Fission Neutrons

IA-1008 SZWARCBAUM (Shaviv) G.
The Doppler Effect in Fast Reactors

IA-1009 GAZITH, M.
Molal Osmotic Coefficients and Water Activities for Various Electrolytes

IA-1010 NEHARIN, A., CALDERON, M. and YACOBI, O.
Susceptibility of Callosobruchus Maculatus to High Rate Gamma Irradiation. A Preliminary Study

IA-1011 GOTSMAN, E.
The ωNN and ϕNN Coupling Constants

IA-1012 BRANDSTETTER, A.
Hyperfragment Production in Li^6 Loaded Emulsion. (Thesis in Hebrew)

IA-1013 ELIEZER, I.
Solubility and Structure of Mercuric Halides

IA-1014 ABRAHAMER, I., MARCUS, Y. and ELIEZER, I.
A Study of the Interaction between Lanthanide and Nitrate Ions

IA-1015 KAHAN, R.S., GOREN, R. and MONSELISE, S.P.
The Effect of Cobalt-60 Gamma Rays on Juice Constituents and the Peel Colour of Citrus Fruit (Preprint)

IA-1016 SCHOENFELD, I.
Spectrochemical Determination of Boron and Strontium in Reactor Waters

IA-1017* GILAT (Goldstein) H.
Study on the Possible Application of Radioisotopes in the Textile Industry

IA-1018 PADOVA, J.
Ion-Solvent Interaction. VI.A Thermodynamic Approach to Preferential Solvation in Mixed Solvents

IA-1019 BARNETT, B. and HAZONY, Y.
Theoretical Model for the Motion of Krypton in a Hydroquinone Clathrate

IA-1020 MARCUS, Y.
Anion Exchange of Metal Complexes XV. Anion Exchange and Amine Extraction of Lanthanides and Trivalent Actinides from Chloride Solutions

IA-1021 Research Laboratories, Semi-Annual Report for the Period July-December 1964

IA-1022 HAZONY, Y. and HILLMAN, P.
Mössbauer Studies on Hydroquinone-Kr-Clathrates

IA-1023 HARARI, H.
Electromagnetic Interactions and the Subgroups of SU(6)

IA-1024 AHARONY, A., RAKAVY, G. and TIKOCHINSKY, Y.
The Distorted Wave Approximation for Direct Nuclear Reactions. General Formulation and Program Description of DINUR (A Code Written for the Philco-2000 Computer)

IA-1025 NOTEA, A.
Evaluation of Fast Neutron Spectroscopy by Time of Flight Technique. (Thesis in Hebrew)

* Internal reports

IA-1028 ZANGEN, M.
Research on the Reaction between Alcohols and Phosphorus Pentoxide. (Thesis in Hebrew)

IA-1029 PENCINER, J., ELIEZER, I. and MARCUS, Y.
Anion Exchange of Metal Complexes. XVI. Chloride Complexes of Zinc, Cadmium and Mercury in Anhydrons Ethanol

IA-1030* LEVY, R.
Instrument for Measuring Level of Cryogenic Liquid

IA-1031 MARCUS, Y.
Solvent Extraction

IA-1032 IMRY, Y., PELAH, I. and WIENER, E.
Proton Dynamics in Hydrogen Bonded Ferroelectrics

IA-1033 ROTH, A. and AMILANI, A.
Sealing Factors, their Measurement and Use in the Design of Vacuum Gasket Seals

IA-1035 GAIRON, P.
Fast Neutron Dosimetry. Manual for Radiation Workers (Report in Hebrew)

IA-1036 CHEN, R. and HALPERIN, A.
On the Analysis of Thermally Stimulated Processes in Crystals

IA-1037 HELD, S.
Differentiation between ErI and ErII Spectra using only a DC as Excitation Source

---

* Internal reports

IA-1038 ZAMIR, D.
Nuclear Magnetic Resonance Study of Hydrogen Alloying in the Early Transition Metals

IA-1039 R.E. SZWARCBAUM (Shaviv) G. and YIFTAH, S.
Calculation of the Doppler Effect in Fast Reactors

IA-1040 GOTSMAN, E., FRISHMAN, Y.
Explicit Wave Functions for any Spin

IA-1041 ANBAR, M.
Reactions of the Hydrated Electron

IA-1043 List of Publications 1960-1964

IA-1044 MEYERSTEIN, D.
The Effect of Ionic Solutes on the Primary Products of Radiolysis of Water. (Thesis in Hebrew)

IA-1045 PEDATSUR, N.
The Radiolysis of Halides and the Properties of Halogen Atoms in Aqueous Solution. (Thesis in Hebrew)

IA-1047 BAER, M.
QMBLSQ, A Program for the Analysis of Multicomponent Exponential Decay Curves

IA-1048 ANBAR, M., PERLSTEIN, P.
Determination of the Gamma Flux in a Nuclear Reactor by the $N_2^{1414} - N_2^{1515}$ Isotopic Exchange Reaction

IA-1050 BEN-DAVID (Davis) G., ARAD, B., BALDERMAN, J. and SCHLESINGER, Y.
Further Study of Nuclear Resonant Scattering Using Neutron Capture Gamma Rays

IA-1051 CHEIFETZ, E.
Investigation of (n,α) Reaction with Thermal Neutrons. (Thesis in Hebrew)

IA-1052 HARARI, H.
On the Reduction of Direct Products of the Irreducible Representations of Su(n)

IA-1053 ASH, M.
Two Fast Reactors Studies
1. Study of Doppler Coefficient by Sinusoidal Fuel Heating
2. Multi-Level Model for Heavy Isotope Fission and Total Cross-Sections

IA-1054 IMRY, Y.
Proton Dynamics in Hydrogen Bonded Systems. (Thesis in Hebrew)

IA-1056 SUSS, Y.
Paramagnetic Resonance Spectrum of Co^{1+} in Single Crystals of Calcium Oxide

IA-1057 YIFTAH, S., GITTER, L. and ILAMED, Y.
Sodium Void and Doppler Coefficients for Fast Power Reactors

IA-1058 LOCKER, B.
Purification of a Sn^{121m} Source

IA-1059 ENGLMAN, R.
The Operator for Spin - Forbidden Transitions

IA-1060 RAFAELOFF, R. and ROY, A.
An Improved Preparation of Pure Uranium Tetrachloride

IA-1061 SCHOENFELD, I. and HELD, S.
Spectrochemical Methods for Determining Boron, Barium, Lithium and Rubidium in Mediterranean and Dead Sea Water

IA-1063 PELAH, I., IMRY, Y.
A New Interpretation of the Quasielastic Scattering of Slow Neutrons from Water

IA-1064 ABRAHAMER, I.
The Spectrophotometric Study of the Interaction between Nitrate and Lanthanide Ions. (Thesis in Hebrew)

IA-1065 ANBAR, M. and PERLSTEIN, P.
On the Mechanism of Radiolysis of Carbon Dioxide

IA-1071 Dual Purpose Nuclear Reactors for Desalination of Sea Water and Production of Electricity

IA-1072 RAFAELOFF, R. and ROY, A.
An Improved Preparation of Pure Uranium Tetrachloride

IA-1073 BAR, V.
The Influence of Electric Fields on the Luminescence and Conductivity of Zns Single Crystals. (Thesis in Hebrew)

PUBLISHED PAPERS

The following papers were published during 1965 .

1. AMIEL, S.
Non-Destructive Activation Analysis Based on Photoneutron Counting, Radiochemical Methods of Analysis, IAEA, 2, 101 (1965)

2. AMIEL, S.
Neutron Counting in Activation Analysis , Isotopes and Radiation Technol., 2, 339 (1965)

3. AMIEL, S.
Delayed Neutrons and Photoneutrons from Fission Products, Physics and Chemistry of Fission, IAEA, 2, 171 (1965)

4. AMIEL, S. and JULIANO, J.O.
Rapid and Non-Destructive Analysis of Sulfur and Calcium by Radioactivation and Photoneutron Counting, Anal. Chem., 37, 343 (1965)

5. AMIEL, S. and NIR, A.
Analysis of Oxygen-18 Based on the Reaction $O^{18}(\alpha,n)Ne^{21}$ Radiochemical Methods of Analysis, IAEA, 1, 293 (1965)

6. AMIEL, S. and PAISS, Y.
A Criterion for Selectivity in Recoil Labeling, Radiochim. Acta, 4 157 (1965)

7. ANBAR, M.
Reactions of the Hydrated Electron, in "Solvated Electrons", A.C.S. Advn. Chem. Ser., 50, 55 (1965)

8. ANBAR, M., GUTTMANN, S., RODAN, G.A. and STEIN, J.A.
The Determination of the Rate of Deiodination of Radioactive Thyroxine in Human Subjects ,J. Clin. Invest., 44, 1986 (1965)

9. ANBAR, M. and HART, E.J.
The Reactivity of Aromatic Compounds toward Hydrated Electrons, J. Am. Chem. Soc., 86, 5633 (1964)

10. ANBAR, M. and HART, E.J.
The Reaction of Haloaliphatic Compounds with Hydrated Electrons. J. Phys. Chem., 69, 271 (1965)

11. ANBAR, M. and HART, E.J.
The Reactivity of Metal Ions and Some Oxy-Anions toward Hydrated Electrons., J. Phys. Chem., 69, 973 (1965)

12. ANBAR, M. and HART, E.J.
The Effect of Solvent and of Solutes on the Absorption Spectrum of Solvated Electrons., J. Phys.Chem. 69, 1244 (1965)

13. ANBAR, M., INBAR, M. and TATA, J.R.
Dissociation of the Calorigenic Action of Thyroid Hormones from the Deiodination of l-Thyroxine in vivo., Acta Endocr. 48, 506 (1965)

14. ANBAR, M. and MEYERSTEIN, D.
Isotope Effects in the Radiolysis and Photolysis of H_2O - D_2O Mixtures , J. Phys. Chem., 69, 698 (1965)

15. ANBAR, M. and MEYERSTEIN, D.
Effects of Ligands on the Rate of Reduction of Cobalt (III) Complexes by Radiolytically Produced Hydrogen Atoms , Nature, 206, 818 (1965)

16. ANBAR, M. and MEYERSTEIN, D.
Effect of Linear Energy Transfer (LET) on the H/D Isotope Effect in the Formation of Hydrogen from Irradiated Water , Trans. Faraday Soc., 61, 263 (1965)

17. ANBAR, M. and NETA, P.
Tables of Bimolecular Rate Constants of Hydrated Electrons, Hydrogen Atoms and Hydrated Radicals with Inorganic and Organic Compounds , Intern. J. Appl. and Isotopes, 16, 227 (1965)

18. ANBAR, M. and NETA, P.
The Activation Energy of Reactions of Hydrated Electrons, Chem. Commun., 365 (1965)

19. ANBAR, M and THOMAS, J.K.
Pulse Radiolysis Studies of Aqueous Sodium Chloride Solutions, J. Phys. Chem., 68, 3829 (1964)

20. APPLEMAN, E.H. and ANBAR, M.
Intermediates in the Oxidation of Water by Perxenate , Inorg. Chem., 4, 1066 (1965)

21. BARNETT, B. and HAZONY, Y.
Theoretical Model for the Motion of Krypton in a Hydroquinone Clathrate, J. Chem. Phys., 43, 3462 (1965)

22. DOTHAN, Y. and HARARI, H.
Reduction Coefficients of the Product $8 \otimes 8 \otimes 8$ of SU(3) Supplemento al Nuovo Cimento 1, 3, 48 (1965)

23. ENGLMAN, R.
Zero Phonon Lines in Diamond and Localized Modes, J. Chem. Solids 26, 1039 (1965)

24. GOTSMAN, E.
Explicit Wave Functions for any Spin, Phys. Rev. 140 B1151, (1965)

25. GRUNBERG, T. and SOLD, U.
A Fast Solid State, Pulse Amplitude Divider and Multiplier, Nucl. Instr. Methods 34, 311 (1965)

26. LEHRER-ILAMED, Y.
On the Direct Calculations of the Representations of the Three-Dimensional Pure Rotation Group, Proc. Camb. Phil. Soc., 60, 61 (1964)

27. IMRY, Y., PELAH, I. and WIENER, E.
Proton Dynamics in Hydrogen-Bonded Ferroelectrics. J. Chem, Phys. 43, 2332 (1965)

28. LEVITZKI, A., PECHT, I. and ANBAR, M.
Oxidase-Like Activity of the Copper (II) Poly-L-Histidine Complex, Nature, 207, 1386 (1965)

29. LOW, W. and SUSS, J.T.
Paramagnetic Resonance Spectrum of CO^{1+} in Single Crystals of Calcium Oxide, Phys. Rev. Letters 15, 519 (1965)

30. MANTEL, M. and KUSHNIR, E.
Separation of the Radiolysis Products of O-Iodobenzoic Acid., J. Chromatog., 17, 624 (1965)

31. MARCUS, Y.
An Exchange Metal Complexes. XV. Anion Exchange and Amine Extraction of Lanthanides and Trivalent Actinides from Chloride Solutions, J. Inorg. Nucl. Chem. 28, 209 (1966)

32. MOAV, B.
The Determination of Manganese in Urine by Neutron Activation Analysis, Intern. Appl. Radiation Isotopes 16, 365 (1965)

33. MOAV, B., GITTER, S., WELWART, Y. and AMIEL, S.
Tracing and Trace Element Composition of Snake Venom by Activation Analysis, Radiochemical Methods of Analysis, IAEA, 1,205 (1965)

34. PADOVA, J.
Ion-Solvent Interaction in Mixed Solvents: III The Molar Refraction of Electrolytes, Can. J. Chem., 43, 458 (1965)

35. PEISACH, M.
The Preparation of Potassium Hexacyanocobalbate (III) Labelled with Cobalt-58 and -60 for Hydrological Studies, J.S. African Chem. Inst. 18, 1 (1965)

36. PELAH, I., KREBS, K. and IMRY, Y.
Inelastic Neutron Spectra and the Vibrational Modes of the Hydrogen Layer in Alkali and Alkaline Earth Hydroxides, J. Chem. Phys. 43, 1864 (1965)

36. PENCINER, J., ELIEZER, I. and MARCUS, Y.
An Exchange XVI. Chloride Complexes of Zn, Cd, Hg in Anhydrous EtOH, J. Phys. Chem., 69, 2955 (1965)

37. SCOTT, S.A. and NOTEA, A.
Monitoring Reactor Power by N^{17} Neutron Decay, Trans. Am. Nucl. Soc. 8, 70 (1965)

38. SHILOH, M. and MARCUS, Y.
A Spectrophotometric Study of Complex Formation of the Trivalent Actinides in Solution- I. Uranium, Israel J. Chem., 3, 123 (1965)

39. TADMOR, J.
Gas Chromatographic Separation of I^{131} Produced by Neutron Irradiation of Tellurium Compounds, Intern. J. Appl. Radiation Isotopes 16, 191 (1965)

40. TADMOR, J.
Gas Chromatographic Separation of P^{32} Produced by Neutron Irradiation, of Sulphur, J. Gas Chromat. 3, 121 (1965)

41. TADMOR, J.
Chromatography in the Preparation and Purification of Materials. Ann. N.Y.Acad. Sci., 137, 103 (1966)

42. WEISSLER, A., PECHT, I. and ANBAR, M.
Ultrasound Chemical Effects on Pure Organic Liquids. Science, 150, 1288 (1965)

43. ZANGEN, M.
Solvent Extraction from Molten Salts.IV Kinetics of the Formation of Mercury (II) Bromide Species, J. Phys. Chem. 69, 1835 (1965)

44. ZAMIR, D.
Nuclear Magnetic Resonance Study of Hydrogen Alloying in the Early Transition Metals, Group VB, Phys. Rev. 140, 271 (1965)

PAPERS PRESENTED AT CONFERENCES

1. THE OXFORD INTERNATIONAL CONFERENCE ON ELEMENTARY PARTICLES, OXFORD, SEPTEMBER, 1965

   ALEXANDER, G., HABER, B., SHAPIRA, A., YEKUTIEL, G. and GOTSMAN, E.
   Peripheral Production and Decay Parameters of N^* (1238) in
   $pp \rightarrow nN^*$ (1238) at 5.5 GeV/c

2. PROCEEDINGS OF THE INTERNATIONAL CONFERENCE ON ELECTRON DIFFRACTION AND THE NATURE OF DEFECTS IN CRYSTALS, MELBOURNE, AUSTRALIA, 16-21 AUGUST,1965

   LOW, W. and SUSS, J. T.
   E.S.R. Studies of Radiation Effects in Simple Oxides

3. GORDON CONFERENCE ON ION EXCHANGE, NEW LONDON, N.H., AUGUST, 1965

   MARCUS, Y.
   Cation Exchange in Molten Salts

4. GORDON CONFERENCE ON MOLTEN SALTS, MERIDEN, N.H., SEPTEMBER, 1965

   MARCUS, Y.
   Cation Exchange in Molten Salts

5. 16th JOINT PITTSBURG CONFERENCE ON ANALYTICAL CHEMISTRY AND APPLIED SPECTROSCOPY, FEBRUARY, 1965

   MARCUS, Y.
   Solvent Extraction

6. PROCEEDINGS OF THE IAEA SYMPOSIUM ON THE USE OF ISOTOPES AND RADIATION IN SOIL-PLANT NUTRITION STUDIES, ANKARA, TURKEY, JUNE, 1965

   NILUBOL, A. and KAFKAFI, U.
   Manganese Content of Soils and Plants as Determined by Activation Analysis

7. CITCE 16th MEETING, ELECTROLYTES, BUDAPEST, SEPTEMBER, 1965

PADOVA, J.
The Application of the Thermodynamic Treatment of a Fluid in the Electrostatic Field to Solutions of Electrolytes

8. PROCEEDINGS OF THE SYMPOSIUM ON INELASTIC SCATTERING OF NEUTRONS, BOMBAY, 15-19 DECEMBER, 1964, IAEA VIENNA, 1965

PELAH, I., WIENER, E. and IMRY, Y.
Indication of Proton Tunneling in KH_2PO_4 by Comparing Neutron Inelastic Scattering and Infrared Measurements

9. PAPER PRESENTED AT THE INTERNATIONAL CONFERENCE ON SAFETY, FUELS AND CORE DESIGN IN LARGE FAST POWER REACTORS, ARGONNE, OCTOBER 11th-13th,1965

FROELICH, R., ATT, K., SHAVIV, G. and YIFTAH, S.
Results of Doppler Coefficient Calculations for Fast Reactors and Comparison of Different Methods

10. 1st INTERNATIONAL CONFERENCE ON THERMAL ANALYSIS, ABERDEEN, 6-9th SEPTEMBER, 1965

RAFAELOFF, R., BOROWITZ, J. L. and ROY, A.
On the Liquidus of the UCl_4-$PbCl_2$ System

11. 3rd INTERNATIONAL VACUUM CONGRESS, STUTTGART, JUNE, 1965

ROTH, A. and AMILANI, A.
Sealing Factors, their Measurement and Use in the Design of Vacuum Gasket Seals

12. PAPER PRESENTED AT THE SYMPOSIUM ON PURIFICATION OF MATERIALS, NEW YORK ACADEMY OF SCIENCES, MAY 6-8th, 1965

TADMOR, J.
Chromatography in the Preparation and Purification of Materials

13. PROCEEDINGS OF THE 3rd INTERNATIONAL CONFERENCE ON THE PEACEFUL USES OF ATOMIC ENERGY, VOL. 13 p.225 (1965)

TADMOR, J. and GALRON, H.
Guide for the Hazards Evaluation of a Nuclear Chemical Installation

14. PRESENTED TO THE 8th EUROPEAN CONGRESS ON MOLECULAR SPECTROSCOPY, COPENHAGEN, DENMARK, AUGUST, 1965

WIENER, E., PELAH, I. and IMRY, Y.
ADP Phase Transition Studied by Infra Red Absorption

15. THIRD INTERNATIONAL CONFERENCE ON THE PEACEFUL USES OF ATOMIC ENERGY, GENEVA, 31 AUGUST - 9 SEPTEMBER, 1964

AMIEL, S.
Neutron Counting in Activation Analysis

ARAD, B., BEN-DAVID, G., NARDI, E. and PASTERNAK, M.
Neutron Flux Measurements in a Pool-Type Light-Water Moderated Research Reactor

ASCHNER, F. S., YIFTAH, S. and GLUECKSTERN, P.
Feasibility of Nuclear Reactors for Sea Water Distillation in Israel

BAR-OR, A., HIRSCH, G., GOLDSTEIN, I., and WYNBLATT, P.
Uranium Alloys

EPSTEIN, J. A., LEVIN, I. and RAVIV, S.
Electrochemical Reduction of Dilute Nitric Acid

FRIEDMAN, E.
Studies of Neutron Thermalization by a Modified Pulsed-Source Technique

HUMI, M., WAGSCHALL, J. J. and YEIVIN, Y.
Multi-Group Constants from Integral Data

KERTES, A.S. and HABOUSHA, Y.E.
Miscibility Gap in Extraction Systems Involving Alkylamines

MARCUS, Y., GIVON, M. and SHILOH, M.
The Chemistry of the Trivalent Actinides in Aqueous Solutions and their Recovery

MARGALITH, N. and YEIVIN, Y.
The Thermal Flux Distribution in the Moderator Region of a Rectangular Lattice of Cylindrical Fuel Elements

RAKAVY, G. and WAGSCHAL, J.J.
Generalization of the Fermi Age Theory and its Application to the Calculation of Resonance Escape Probability

ROTHENSTEIN, W., BEN-DAVID, G., HELHOLTZ, J., SEGAL, Y. and TABAK, D.
Reactor Physics Studies of Natural Uranium Light-Water Moderated Lattices

SZWARCBAUM, G., SIEGER, M. and YIFTAH, S.
Inelastic Scattering of High Energy Neutrons in Fast Reactors

TADMOR, J. and GALRON, H.
Guide for the Hazards Evaluation of a Chemi-Nuclear Installation

YIFTAH, S. and SIEGER, M.
Nuclear Cross Sections for Fast Reactors

AUTHOR INDEX

Abrahamer, I. 77, 78

Aladjem, A. 83

Alexander, G. 27, 28

Algave, A. 283

Amiel, S. 159, 164, 167, 168 169, 171, 197, 220

Amilani, A. (Inbar) 310

Anbar, M. 15, 96, 98, 99, 101, 109, 115, 117, 123, 125, 127, 128, 130, 131, 132, 134, 136, 138, 141, 142, 146, 153, 156, 177, 203, 207, 213

Ar, A. 213

Arad, B. 43, 293

Baer, M. 171, 175, 176

Balderman, J. 46

Bar, V. 67

Barkai-Golan, R. 276, 279

Barnett, B. 63

Bar-Nir, I.M. 31

Baruch, Z. 96

Ben-David, G. 43, 54, 293

Ben-Nun, I. 301, 309

Ben-Yehoshua, S. 273

Boazi, M. 21, 22, 23

Boger, D. 309

Boneh, Y. 53

Borowitz, J.L. 91

Braudo, C. 267

Brown, H. 183

Bukshpan, S. 49, 51

Caner, M. 61

Carmon, B. 96

Catz, A.L. 159, 161

Cheifetz, E. 53

Chen, R. 70

Cohen, I. 281

Cuperman, S. 73

Donagi, A. 247, 248, 251

Eden, Y. 199, 200, 201, 202

Eisenberg, A. 247

Eisenberg E. 270, 271, 272, 274, 278, 281, 282

Englman, R. 58, 59, 60, 61

Faraggi, M. 98, 142, 146

Feige, Y. 18, 235, 247

Finkel, M. 263

Finston, H.L. 22, 166, 198,200, 201

Fishel, D. 251

Foa, E. 256, 263

Fraenkel, Z. 55

Friedman, C. 101

Frishman, Y. 27

Froelich, R. 38

Galron, H. 218, 229
Gazith, M. 62
Gersten, A. 76
Gilat, J. 197, 198, 199, 201
Gilath, Ch. 258, 260, 263, 265, 266
Gindel, I. 214
Gitter, L. 35, 37, 213
Givon, M. 93
Glezer, A. 185
Gotsman, E. 27, 31
Gozez, Y. 54, 57
Grünberg, J. 295
Guttmann, S. 101, 203, 206

Halperin, A. 67, 70
Harari, H. 28, 29, 30, 31
Hazan, G. 57
Hazony, Y. 50, 56, 63
Hecht, E. 80
Held, S. 193, 195
Heller, A. 270
Hershkovitz, J. 307
Hoffmann, A.P. 9, 13, 14
Horn, D. 27, 30
Horowitz , A. 149

Ilamed, Y. 35, 37, 75, 76
Imry, Y. 65

Joskowicz, J. 74
Juliano, J.O. 167

Kafkafi, U. 198
Kahan, R.S. 270, 271, 272, 276, 278, 279, 281, 282
Kaldor, U. 102, 104, 106
Kanter, M. 214
Katase, A. 54, 57
Kedem, D. 48
Kertes, A.S. 80
Konigsbuch, M. 256
Kruger, S. 173

Lapidot, M. 283
Lask, S. 256, 263, 265
Latti, J. 200
Lemanska, M. 32
Levin, S. 63
Levinson, J. 67
Levitzki, A. 156, 177, 178
Lipkin, H.J. 28, 29, 31
Liquornik, M. 84
Locker, B. 56
Low, W. 66
Lubin, E. 211

Mantel, M. 180, 182, 183, 184
Marcus, Y. 77, 83, 84
Mazor, E. 267
Meilen, L. 55
Mero, F. 267
Meshkov, S. 28
Meyerstein, D. 96, 115, 117, 127, 128, 130, 131, 134

Milmann, Y. 224, 230, 233
Monselise, S.P. 278
Moreh, R. 46, 47, 54, 57

Nadel, D. 281
Nardi, E. 53, 55
Ne'eman, Y. 31
Neharin, A. 211
Neta, P. 127, 128, 130, 134 136, 138, 141
Nilubol, A. 198
Nir, A. 173
Notea, A. 4, 5, 6, 9, 12, 162 164, 168

Ott, K. 38

Padova, J. 78, 84, 182
Paiss, Y. 168, 169
Paran, M. 207
Pasternak, M. 49, 50, 51, 53
Pecht, I. 123, 177
Pelah, I. 63, 65
Peleg, B.A. 281, 282
Peleg, M. 84, 86
Peres, H. 174
Perlman, A. 270
Perlstein, P. 15, 153
Pfeffer, P. 260
Potascher, R. 297
Prulov, Y. 18, 235, 243, 244, 245, 247

Rafaeloff, R. 91, 94
Rajbenbach, A. 149, 150, 151
Remigolski, B. 296
Rodan, G.A. 203, 206, 207
Roth, A. 310
Rothem, T. 48, 56
Roy, A. 91
Ruppin, R. 58

Sar-El, H.Z. 289
Satchy, C. 278, 284
Schächter, O. 256
Schenberg, C. 196, 198, 200, 201, 202
Schiffer, D. 263
Schlesinger, Y. 43
Schoenfeld, I. 189, 191, 193, 195
Scott, S.A. 4, 5, 6, 9, 12
Segal, D. 13
Segev, M. 33, 34
Senator, A. 298, 300
Shalmon, E. 235, 247, 248, 251
Shamir, J. 93, 95
Shapira, A. 25, 26
Shavitt, I. 102, 104, 106
Shaviv, G. 38, 39, 40
Sherman, W.V. 113, 114, 152
Simopoulos, A. 50, 52
Sidi, M. 302, 305, 306
Sonnino, T. 22, 53, 173, 174

Soriano, J. 93, 95

Stein, G. 123

Stein, J.A. 203

Steinberg, M. 96

Stiller, M. 18, 235, 243, 244, 245

Stuhl, Z. 256, 258, 260, 263, 266

Suss, J.T. 66

Tadmor, J. 218, 224, 228, 230 233

Tal, A. 247

Tamir, Y. 200

Temkin-Gorodeiski, N. 272, 281

Tennenbaum, Y. 293

Tepper, L. 295, 298, 306

Thomas, J.K. 125

Wiener, E. (Avnear) 63

Wiernik, M. 180, 185

Yager, Z. 62

Yatom, C. 60

Yellin, E. 20, 166, 168

Yiftah, S. 32, 33, 34, 35, 37, 38, 39, 40

Zadicario, I. 306

Zamir, D. 58

Zangen, M. 79, 80, 89

Zaubermann, G. 271

Zehavi, D. 98, 142, 146

SUBJECT INDEX

Activation Analysis
Cm^{244} alpha source for the $O^{18}(\alpha,n)N^{21}$ reaction, 174
in forensic investigations, 200
of Au, Pt, Ag and Pd, in metal scraps, 200
of Br in agricultural samples by X-ray counting, 198
of Cu in snake venom, 213
of Fe in blood, 196
of Mn in soils and plants, 198
of Na, K, Cl, in body electrolytes, 201
of Na, K, Cl, in heart tissue, 201
of Na in analytical grade KCl, 202
of O in steel, by $O^{16}(n,p)N^{16}$ reaction, 199
of Si in oil samples, 202
of U, precision of analysis by delayed neutron counting, 199
of U in meteorites, by delayed neutron counting, 197

Aerosols
sizing of atmospheric aerosols, 248

Agriculture
see Irradiation of Agricultural Products

Aliphatic Compounds
dehalogenation of organic halogen compounds by aliphatic free radicals, 141
electron scavenging processes in irradiated alkane-perfluorocarbon solutions, 150
radiolysis of n-hexane-perfluorocyclobutane system, 151
radiolysis of n-pentane solutions of tetrachloroethylene, 149
reactivity towards Br and H atoms in aqueous solution, in radiolysis, 134
reactions with hydrated electrons, in radiolysis, 111
reactivity towards OH radicals in radiolysis, 128

Alkali Halides
radiolysis of, 134

Alkali Metals
influence on spectroscopic det. of B and Sr, 191
spectrochemical det. in reactor water, 189

Alpha Particles
alpha particle associated fission, 54

Alpha Sources
Cm^{244}, as α source for analytical uses of the $O^{18}(\alpha,n)Ne^{21}$ reaction, 174

Aluminium
Al^{28} in activation analysis, 202

Americium
solvent extraction of Am III and Am VI from HNO_3, 79

Ammonia
computation of properties of, 104

Ammonium Dihydrogen Phosphate
phase transition of, 63

Analytical Chemistry
det. of Cs in sea water, 182
det. of thorium in urine, 183
det. of dissolved gases in natural waters, 180
det. of iodine in urine, 184
microcoulometric det. of chloride ions, 185
spectrophotometric det. of Cr III, 189

Aromatic Compounds
reaction of H atoms and OH radicals with benzoate ions in radiolysis, [mechanism, 132
reactions with hydrated electrons in radiolysis, 112
reactivity towards H atoms in radiolysis, 130
reactivity towards OH radicals in radiolysis, 127

Arsenic
preparation of $AsOF_3$, 95

Barium
spectrochemical det. of, 195

Biochemistry
ceruloplasmin, oxidase activity towards D-isoascorbate and [L-ascorbate, 178
poly-L-histidine copper complex as an oxidase, 177
radiosensitization of rabbit-liver enolase by copper ions, 156

Biology and Medicine
Cu as tracer in snake venom studies, 213
det. of Na, K, Cl, in body electrolytes, 201
det. of Na, K, Cl, in heart tissue, 201
dynamic study of thyroxine deiodination in humans, 203
effect of cortisol on Ca metabolism in the rat, 207
Fe^{58} as a blood tracer in ferrokinetic studies, det. by activation [analysis, 196

Biology and Medicine (contd)
reverse transpiration in plants, 214
thyroxine metabolism in tumor-bearing rats, 206
trace element composition of snake venoms, 213
transfer of Ce^{144} via placenta and during lactation to offspring [in mice, 211

Blood
Fe^{58} as a blood tracer in ferrokinetic studies, 196

Boron
spectrochemical det. of, 191, 195

Bromine and Bromide Ions
det. in agricultural samples by activation analysis, 198
formation in radiolysed bromide solutions, 134
radiolytic debromination of 2-bromopropionate ions, 136
radiolytic formation of tetravalent Br, reactions with halides and [halogens, 138
radiolytic isotopic exchange between bromopropionate and bromide, [mechanism, 138
reactivity of aliphatic compounds towards Br atoms in radiolysed [aqueous solutions, 134

Caesium
Cs^{137} in fallout, 235
Cs^{137} in food, 244
Cs^{137} in milk, 243
det. in sea water, 182

Calcium
metabolism in rat, effect of cortisol, 207

Californium
neutron emission in ternary fission of Cf^{252}, 55

Carbon
C^{12}, nuclear levels of, 161
C^{14} as a tracer, 258

Carbon Dioxide
in radiolysis - see Radiolysis

Cation Exchange
in molten salts, 84

Cerium
transfer of Ce^{144} via placenta and lactation to offspring in mice, 211

Chlorine and Chloride Ions
Cl^{36} in study of thermal decomposition of perchlorates, 96
Cl^{38} as a tracer for the study of reactions in sprays, 257
det. in body electrolytes by activation analysis, 201
det. in heart tissue by activation analysis, 201
interaction with OH radicals in radiolysis, 125
micro-coulometric det. of chloride ions, 187

Chromium
Cr^{51} as tracer, 260
radiolysis of dichromate ions in nitric acid solution, 148

Clathrates
model for motion of Kr in hydroquinone clathrate, 63

Cobalt
Co^{60} gamma source - see Gamma Irradiation Facility; see also Irradiation [of Agricultural Products
paramagnetic resonance spectrum of Co^{1+}, 66

Complexes
lanthanide - nitrate complexes, 77
metal ion, radiolytic reaction with hydrated electrons, mechanism, 109
poly-L-histidine copper complex as an oxidase, 177
reduction of Co(III) complexes by radiolytically produced H atoms, [mechanism, 131

Computer Programs
for analysis of gamma spectra, 175
for analysis of multicomponent exponential decay curves, 176
for environmental hazards evaluation in nuclear accidents, 224
for evaluation of Doppler integral in analysis of resonant gamma [scattering data, 44
for reactor physics problems, 32
LCAO-SCF computation of properties of $CH_2 = CH_2$, 106
LCAO-SCF computation of properties of H_2O_2, 102
LCAO-SCF computation of properties of NH_3, 104
Monte Carlo calculations, 39, 40

Copper
in snake venom, 213
poly-L-histidine copper complex as an oxidase, 177
radiosensitization of rabbit liver enolase by copper ions, 156

Cross Sections
for fast reactors - see Reactor Physics

Crystals and Crystal Structure
see also Diamonds
lattice dynamics, covalency effects in trigonal distortion in metal [ion crystals, 61
lattice dynamics, infrared spectra of small ionic crystals, 58
lattice dynamics, Jahn-Teller effect for 3-fold degeneracies, 61
lattice dynamics, model for motion of Kr in a clathrate, 63

Crystals and Crystal Structure (contd)
mean square displacement of iodine in ICN crystal, 53
Mössbauer effect of Co^{57} impurities in LiOH crystals, 52
$NH_4H_2PO_4$ phase transition studies by IR absorption, 63
paramagnetic resonance spectrum of Co^{1+} in CaO, 66
radiation damage in simple oxides, 66
symmetry of PO_4 group in $NH_4H_2PO_4$ and KH_2PO_4, 63
tetrahedral symmetry, intensity calculations of absorption bands, 62
thermal properties, specific heats of clathrates, 63
thermal properties, vibronic theory of ferroelectrics, 60

Curium
Cm^{244} and Cm^{242} as alpha sources, 174

Decay Curves
computer program for analysis of multicomponent decay curves, 176

Decay Schemes
see also Nuclear Levels
of Sn^{121m} and Te^{121m}, 56

Delayed Neutrons
from N^{17}, for reactor power monitoring, 12
from N^{17}, measured by He^3 spectrometer, 164
half-life of delayed neutron precursors Se^{86} and Se^{87}, 168
in analysis of U in meteorites, 197
precision of analysis of U by, 199

Deuterium
in radiolytic studies - see Radiolysis
isotopic exchange - see Isotope Effects

Diamonds
electroluminescence and dark-current in semiconducting diamonds, 67
thermoluminescence in semiconducting diamonds, 70

Dielectric Constants
calculation by vibronic theory of ferroelectrics, 60

Documentation
list of IA reports issued, 323
list of papers presented at conferences, 335
list of published papers, 331
participation in research projects, 322
storage and retrieval of information, 321

Doppler Effect
broadening of gamma spectra, 161
in reactors - see Reactor Physics

Dosimetry
for Co^{60} source, 284

Electrodeposition
of Ta and Sn from molten salts, 83

Electrolytes
eletrolyte solution theory, 78
ion-solvent interaction, 78

Electron Spin Resonance
see Paramagnetic Resonance

Electrons, hydrated
$e^-_{aq} + e^-_{aq} \rightarrow H_2$, H/D isotope effect in radiolysis in aqueous solutions, [117, 120
$e^-_{aq} + e^-_{aq}$ reaction, mechanism of in radiolysis, 116
H/D isotope effect in hydrogen generated photolytically from the [$e^-_{aq} + e^-_{aq}$ reaction, 115
in radiolysis of nitrate solutions, 145
in radiolytic debromination of 2-bromopropionate, 136
in radiolytic isotope exchange between bromopropionate and bromide [ions, 139
mechanisms of reactions in radiolysis, 109
reactions with aliphatic compounds in radiolysis, 111
reactions with aromatic compounds in radiolysis, 112
reactions with metal ions and metal ion complexes in radiolysis, 109
reduction of transition metal complexes in radiolysis, 131

Electrons, solvated
electron scavenging processes in irradiated alkane-perfluorocarbon [solutions, 150
electron scavenging processes in irradiated cyclohexane solutions, 114
reactivity in irradiated 2-propanol, towards various solutes, 113

Electronics
see also Instrumentation
air particle monitoring system, 309
capacitance bridge for semiconductor detectors, 306
digital differential analyzer for computation of the Fourier [transform, 300
fast counter, 296
fast solid state light pulser, 306
fast timing circuits using storage diodes, 295
instrumentation for a pulsed nuclear magnetic resonance system, 307
linear heating system for crystals, 302
low noise charge-sensitive preamplifier, 295
nucleonic modular units, 296
parity check for 3-dimensional multichannel analyzer, 305

Electronics (contd)
portable linear ratemeter, 306
spectrum stabilizer, 298
time-to-amplitude converter, 297
upper audiofrequency heat supply for a mass spectrometer, 301
waveform generator for a mass spectrometer, 301

Elementary Particles
bootstrap calculation for the mass of the intermediate vector boson, 27
calculation of helicity amplitudes of wave functions for any spin, 25
Regge recurrences, algebraic structure and relation to symmetry [schemes, 31
SU(3), predictions for 3-particle states, 31
SU(6), electromagnetic interactions in, 30
SU(6), meson and baryon masses in, 29
SU(6), tests of relativistic SU(6) in proton-antiproton annihilation, 28
SU(12), Γ_0 selection rules in proton - anti-proton annihilation, 28
U(12), classification of spin states, 30
U(12), experimental tests of broken U(12), 30

Ethylene
computation of properties of, 106

Fallout Monitoring
after 2nd Chinese nuclear test, 247
contamination around IRR-1 reactor, 247
of air, 235
of food, 244
of milk, 243
of rain, 235
of soil, 245

Ferroelectrics
calculation of dielectric constants, 60
Mössbauer effect in ferroelectric iodine compounds, 51
phase transition of $NH_4H_2PO_4$, infrared spectra, role of protons, 63
vibronic theory of, 60

Fission
alpha particle associated fission in U^{235}, 54
evaporation calculations, 55
fission products - see Nuclear Safety
neutron emission in triple fission, 55
photoneutron emission from U^{235} fission products in heavy water, 167
recoil labelling of CH_3I by fission iodine, 168, 169
saddle point calculations, 53

Gallium
solvent extraction of Ga III from bromide solutions, 80
spectrochemical det. in U-Ga alloys, 193

Gamma Irradiation Facility
see also Irradiation of Agricultural Products
calibration of Co^{60} irradiation facility, 284
det. of ozone in Co^{60} irradiation facility, 283
improvements for industrial use, 311

Gamma Radiation
scattering of - see Scattering

Gamma Spectra
computer program for analysis of, 175

Gas Chromatography
det. of dissolved gases in natural waters, 180

Gold
Au^{198} as a tracer, 260
det. by activation analysis, 200

Halogens and Halides
see also specific halogens
radiolysis of alkali halides in CO_2-saturated aqueous solutions, 134
radiolytic dehalogenation of organic halogen compounds on reaction [with aliphatic free radicals, 141
radiolytic formation of tetravalent Br, reactions with halides and [halogens, 138

Hazards Evaluation
see Nuclear Safety

Health Physics
see also Fallout Monitoring, Nuclear Safety
survey of dental X-ray machines, 251

Helium
He^3 neutron spectrometer, 164

Hot Atoms
energy distribution in gaseous media, calculation by elastic [scattering from spherical potential, 171
recoil labelling by, criteria for selectivity in, 168
recoil labelling of CH_3I by, effect of noble gases on, 169

Hydrogen
abstraction by OH radicals from bromopropionate, radiolytic, 138
abstraction from aliphatic compounds by OH radicals, radiolytic, 128
abstraction from benzoate by H atoms and OH radicals, radiolytic, 133

Hydrogen (contd)
alloying with V and Nb, 58
atomic, in radiolysis of aqueous solutions, 117
atomic, in radiolysis of chloride ions, 126
atomic, in radiolysis of H_2O_2 in nitric acid solutions, 144
atomic, in radiolysis of nitrate solutions, 143
atomic, in radiolytic debromination of 2-bromopropionate, 136
atomic, in radiolytic isotope exchange between bromopropionate and bromide ions, 143
$e^-_{aq} + H \rightarrow H_2$ reaction in radiolysis, H/D isotope effect, 120
$H + H \rightarrow H_2$ reaction in radiolysis, H/D isotope effect, 121
isotopic exchange - see Isotope Effects
"molecular", production in radiolysis of aqueous solutions, mechanism, 115, 117
reaction of H atoms with benzoate ions in radiolysis, mechanism, 132
reactivity of aliphatic compounds towards H atoms in radiolysed aqueous solutions, 134
reactivity towards aromatic compounds in radiolysis, electrophilic substitution, 130
reduction of Co(III) complexes by H atoms in radiolysis, 131

Hydrogen Peroxide
computation of properties of, 102
preparation of O^{18}-labelled H_2O_2, 96
radiolysis of H_2O_2 in nitric acid solution, mechanism, 143
radiolytic formation of $H_2O_2{}^{18,18}$ and $H_2O_2{}^{16,18}$ in H_2O^{18} solutions containing $H_2O_2{}^{16,16}$, mechanism, 123
reaction with NO_2, 98

Hydroxyl Radicals
in radiation damage to enolase, in presence of Cu ions, 157
in radiolysis of aqueous solutions, 117
in radiolysis of H_2O_2 solutions, 124
in radiolysis of nitrate solutions, 143
in radiolytic debromination of 2-bromopropionate, 136
in radiolytic isotope exchange between bromopropionate and bromide ions, 139
interaction with chloride ions in radiolysis, 125
reaction with benzoate ions in radiolysis, mechanism, 133
reaction with H_2O_2 in radiolysed nitric acid solution, 145
reactivity of aromatic compounds towards, in radiolysis, 127
reactivity towards aliphatic compounds, in radiolysis, electrophilic substitution, 128
role in hydrolysis of dichromate ions, 149
scavengers of, CD_3OH, 115, 118
scavengers of, H_2O_2, 123, 127

Industrial Applications of Radioisotopes
see also Irradiation of Agricultural Products, Radioisotope Tracing, [Gamma Irradiation Facility
checking of mixing conditions in a paper mill, using Na^{24}, 263
corrosion studies, using Cl^{38}, 265
det. of polyelectrolyte residuals after purification of water, using [C^{14}, 258
det. of weight distribution of carbon black in rubber using Na^{24}, 266
spray reactions, laboratory apparatus for study of reactions which can [be carried out in an "Aman" spray reactor, using Cl^{38}, 256

Information, Storage and Retrieval, 321

Infrared Spectra
of small ionic crystals, model for calculating, 58
in phase transition studies of $NH_4H_2PO_4$, role of protons, 63

Instrumentation
see also Electronics, and Mechanical Engineering
electrostatic analysers, cylindrical and spherical, 289
neutron scattering chamber, 293

Iodine and Iodide Ions
deiodination of iodoaromatic compounds, 101
det. in urine, 184
formation in radiolysed iodide solutions, 135
I^{131} in milk and sheep thyroids, 247
mean square displacement of iodine in ICN crystal, calculated from [Mössbauer fraction, 53
Mössbauer effect in ferroelectric iodine compounds, 51
Mössbauer effect in I_2CL_6, 51
Mössbauer effect in molecular iodine crystals, 50

Iron
Fe^{28}, as stable tracer in blood, det. by activation analysis, 196

Irradiation Facility
Co^{60} - see Gamma Irradiation Facility
neutron beam facility, 312

Irradiation of Agricultural Products
see also Industrial Applications of Radioisotopes, and Gamma [Irradiation Facility
of avocado pears, to extend ripening period, 271
of fungi attacking citrus, 279
of Mediterranean Fruit Fly, to sterilize, 281
of Mediterranean Fruit Fly, susceptibility of different developmental [stages, 282
of Shamouti oranges inoculated with fungi, 276
of stored potatoes, to prevent sprouting, 272

Irradiation of Agricultural Products (contd)
of strawberries, to extend storage life, 273
of sugar beets, to delay sucrose decomposition, 270
of Valencia oranges, 278
list of projects, 282

Isotopes
see individual elements; see also Radioisotope and Stable Isotope Tracing, Labelled Compounds, Industrial Applications of Radioisotopes, Nuclear Safety

Isotope Effects
H/D isotope effect in $e^-_{aq} + H \rightarrow H_2$ in radiolysis, 120
H/D isotope effects in formation of hydrogen from 2 radicals in radiolysed aqueous solutions, 117
H/D isotope effect in hydrogen generated photolytically from the reaction $e^-_{aq} + e^-_{aq}$. 115
H/D isotope effect in reduction of water by metals and ions, 99

Isotopic Exchange
between bromopropionate and bromide, radiolytic, mechanism, 138
between $N_2^{14,14}$ and $N_2^{15,15}$, radiolytic, mechanism, 153

Jahn-Teller Effect
for 3-fold degeneracies, 61

Krypton
model for motion of Kr in a hydroquinone clathrate, 63

Labelled Compounds
see also Radioisotope and Stable Isotope Tracing, and Industrial Applications of Radioisotopes
preparation of Hg^{197}-labelled neohydrin, 22
preparation of O^{18}-labelled H_2O_2, 96

Labelling
recoil labelling of CH_3I, effect of noble gases on, 169
recoil labelling, criteria for selectivity in, 168

Lanthanides
see also individual elements
interaction of lanthanide ions with nitrate ions, 77
nitrates of, in molten alkali nitrates, 84
preparation of PrF_4, 93
preparation of PrO_2, 94

Lead
phase diagram of UCl_4-$PbCl_2$ system, 91

Lithium
Li^7, nuclear levels of, 161
spectrochemical det. of, 189, 195

Luminescence
electroluminescence and dark-current in semiconducting diamonds, 67
thermoluminescence in semiconducting diamonds, 70

Manganese
det. in soils and plants by activation analysis, 198

Mathematics
fourth order three point difference scheme for solving linear second [order differential equations, 76
Hamilton-Cayley theorem for matrices with non-commutative elements, 76
structure of TA-algebras, 75

Mercury
Hg^{197} and Hg^{203} in preparation of labelled neohydrin, 22

Mechanical Engineering
combined neutron irradiation facility in reactor beam tube No.1, 312
improvements in the Co^{60} irradiation facility for industrial [purposes, 311
liquid wastes disposal system, 314

Medicine
see Biology and Medicine

Metals
see also individual metals, and Alkali Metals
hydrogen alloying in transition metals, NMR studies, 58
metal ions and their complexes, reaction with hydrated electrons in [radiolysis, 109
U - Ga alloys, spectrochemical det. of Ga in, 193

Meteorites
assay of U in, 197

Methyl Iodide
recoil labelling of, 169

Molecules and Molecular Structure
computed properties of CH_2CH_2, 106
computed properties of H_2O_2, 102
computed properties of NH_3, 104
nuclear coupling, Jahn-Teller effect for 3-fold degeneracies, 61

Molten Salts
cation exchange between sodium zeolite and $CsNO_3$ or $Ca(NO_3)_2$ in [molten $NaNO_3$, 84
electrodeposition of Ta and Sn from, 83
extraction of Zn halides from, 89
Nd nitrates in molten alkali nitrates, 84
solubility of water in, 86

Monte Carlo Calculations
for fast reactors, 39, 40

Mössbauer Effect
absolute recoilless fraction of ZnTe, 49
in ferroelectric iodine compounds, 51
in molecular iodine crystals, 50
of Co^{57} impurities in LiOH crystals, 52
mean square displacement of iodine in ICN crystal, calculated from the [Mössbauer fraction , 53
model for motion of Kr in a hydroquinone clathrate, 63
studies of ferrite structures, 48

Neodymium
nitrates of, in molten alkali metals, 84

Neon
a triplet at 2.8 MeV in Ne^{21}, 159
Ne^{21} nuclear levels, lifetime of by Doppler broadening, 162

Neutrons
see also Elementary Particles, and Delayed Neutrons
fast neutron spectroscopy by time-of-flight technique, 162
He^3 neutron spectrometer, 164
neutron emission in triple fission, 55
neutron irradiation facility, 312
neutron scattering chamber, 293
photoneutron emission from U^{235} thermal fission products in heavy [water, 169
quasielastic scattering in water, 65

Nickel
in ZnO, calculation of spectrum, 62

Niobium
NMR studies of niobium hydride, 58

Nitrates
radiolysis of nitrate and nitric acid solutions, mechanism, 142

Nitric Acid
radiolysis of nitric acid solutions - see Radiolysis

Nitrogen
molecular nitrogen, radiolytic production in cyclohexane solutions [of N_2O, 114
N^{17} delayed neutrons measured by He^3 spectrometer, 164
radiolytic isotope exchange in N_2, 153

Nitrogen Dioxide
reaction with H_2O_2, 98

Nitrous Oxide
as electron scavenger in radiolysis - see Radiolysis

Nuclear Levels
see also Decay schemes
C^{12} 4436 keV level, lifetime by Doppler broadening, 161
Li^7 477 keV level, lifetime by Doppler broadening, 161
Na^{23}, mean life of 1st and 2nd excited states, 46
O^{16}, O^{17} and O^{18} levels, 47, 48
resonance scattering of gamma rays from highly excited nuclear [levels, 43
Te 7.53 MeV level, coincidence measurement of, 45
Tl 7.64 level, width, 44
triplet at 2.8 MeV in Ne^{21}, 159

Nuclear Magnetic Resonance
study of hydrogen alloying in transition metals, 58

Nuclear Reactions
(d,p) reactions in study of O isotope levels, 47
energy distribution of hot atoms in a gaseous medium, 171
(n,α) reactions with thermal neutrons, 57
(n,γ) cross sections of the products of (n,2n) reactions, 166
$O^{18}(\alpha,n)Ne^{21}$, Cm^{244} as α source in analytical uses of, 174
(t,p) reactions in study of O isotope levels, 47
tritium from $N^{14}(n,t)C^{12}$ reaction with 14 MeV neutrons, 173

Nuclear Safety
see also Fallout Monitoring, and Health Physics
computer program for environmental hazards evaluation, 224
radiation doses from a hypothetical accident, under various atmospheric [conditions, 218
relative hazards of fission products, 228
sizing of atmospheric aerosols, 248
Sutton's equation, 233
turbulent atmospheric diffusion, 230

Nuclei and Nuclear Models
evaporation calculations, 55
saddle point calculations for fission, 53

Oxygen
det. in steel by activation analysis, 199
energy levels of O isotopes, 47
O^{17} and O^{18}, a source of neutrons in reactor coolant water, 4
preparation of O^{18}-labelled H_2O_2, 96

Ozone
det. in gamma irradiation cell, 283

Palladium
det. by activation analysis, 200

Paramagnetic Resonance Spectra
of Co^{1+} in single crystals of CaO, 66
studies of radiation effects in simple oxides, 66

Perturbation Theory
for reactor calculations, 32

Phase Diagrams
of UCl_4-$PbCl_2$ system, 91

Phase Transitions
of $NH_4H_2PO_4$, infrared spectra, role of protons, 63

Plant Biology
Mn in plants, det. by activation analysis, 198
reverse transpiration in plants, 214

Plasma Physics
build-up of beam-generated plasma, 73
plasma formation by laser beams, review, 74
radiation by growing plasma oscillations, 73

Platinum
det. by activation analysis, 200

Potassium
det. in body electrolytes by activation analysis , 201
det. in heart tissue by activation analysis, 201

Praseodymium
preparation of PrF_4, 95
preparation of PrO_2, 94

Propanol
as solvent in radiolysis - see Radiolysis

Protons
see also Elementary Particles
proton tunneling in $NH_4H_2PO_4$, 63

Publications
see Documentation

Quantum Mechanics, General
Jacobi polynomials and angular momentum transformation matrix elements, 62
operator for spin-forbidden transitions in ions, 59

Radiation
see also Health Physics, Irradiation of Agricultural Products, Irradiation Facilities, Nuclear Safety, Radiolysis
damage in crystals, 66
radiosensitization of rabbit liver enolase by Cu ions, 156

Radicals
see also Hydroxyl Radicals, Hydrogen Atoms
dehalogenation of organic halogen compounds on reaction with aliphatic free radicals, 141

Radioactivity
see also Decay Schemes, Industrial Applications of Radioisotopes, Nuclear Safety, Radioisotopes, Radioisotope and Stable Isotope Tracing
of submerged springs, use for tracing flow, 267

Radiochemical Separation
of Fe from blood plasma, 196
of tritium, 173

Radioisotope and Stable Isotope Tracing
see also Labelled Compounds, and Industrial Applications of Radioisotopes
flow of submerged radioactive springs, 267
in studies of thermal decomposition of perchlorates, using Cl^{36}, 96
of blood, by stable Fe^{58}, 196
of Cu in snake venom, 213
of reverse transpiration in plants, using tritium, 214
of sand movement on the sea bed, using Au^{198} or Cr^{51}, 260
of silt movement in a wadi, using Cr^{51}, 263

Radioisotope Training Center, 25

Radioisotopes
half-life of short-lived Se isotopes, 168
production, 24

Radiolysis
carbon dioxide as electron scavenger in radiolysis of alkali halides, 134
carbon dioxide as electron scavenger in radiolytic debromination of 2-bromopropionate, 136
2-D-2 propanol as reference in competition kinetics, 134

Radiolysis (contd)
debromination of 2-bromopropionate ions in CO_2-saturated aqueous [solution, 136
deuterated methanol, as OH radical scavenger, 115,118
$e^-_{aq} + e^-_{aq}$ reaction, mechanism of, 116
electron scavenging processes in irradiated alkane-perfluorocarbon [solutions, 150
electron scavenging processes in irradiated cyclohexane solutions, 114
formation of $H_2O_2^{18,18}$ and $H_2O_2^{16,18}$ in H_2O^{18} solutions containing [$H_2O_2^{16,16}$, mechanism, 123
formation of tetravalent Br, reactions with halides and halogens, 138
H/D isotope effect in $e^-_{aq} + H \rightarrow H_2$ reaction, 120
H/D isotope effect in formation of hydrogen from 2 radicals in aqueous [solutions, 117
H/D isotope effect in hydrogen generated photolytically in the reaction [$e^-_{aq} + e^-_{aq}$, 115, 120
H_2O_2 as OH radical scavenger, 127
interaction of chloride ions with OH radicals, by pulse radiolysis, 125
isotopic exchange between bromopropionate and bromide ions, 138
nitrous oxide as electron scavenger in cyclohexane solutions, 114
nitrous oxide, as electron scavenger in 2-propanol solutions, 113, 114
nitrous oxide as electron scavenger in isotopic exchange between [bromopropionate and bromide, 140
nitrous oxide as electron scavenger in radiolysis of alkane- [perfluorocarbon solutions, 150
nitrous oxide as electron scavenger in radiolysis of benzophenone in [2-propanol, 153
of alkali halides in CO_2-saturated aqueous solutions, 134
of dichromate ions in nitric acid solutions, 146
of n-hexane - perfluorocyclobutane system, 151
of N_2-saturated aqueous solutions of alkali halides, 136
of N_2O-saturated aqueous solutions of alkali halides, 134
of nitrate and nitric acid aqueous solutions, 142
of tetrachloroethylene in n-pentane, 149
of water, 117, 122
radiolytic isotope exchange in N_2
radiosensitization of enolase by copper ions, 156
reaction of H atoms and OH radicals with benzoate ions, mechanism, 132
reactions of hydrated electrons produced in, 109
reactivity of aliphatic compounds towards Br and H atoms in aqueous [solutions, 134
reactivity of aliphatic compounds towards OH radicals, 128
reactivity of aromatic compounds towards H atoms, 130
reactivity of aromatic compounds towards OH radicals, 127
reactivity of solvated electrons towards solutes in irradiated [2-propanol, 113

Radiolysis (contd)
reduction of benzophenone in 2-propanol, 152
reduction of Co(III) complexes by H atoms, 131

Reaction Mechanisms
hydrogen abstraction - see Hydrogen
in radiolysis - see Radiolysis
of hydrated electrons - see Electrons

Reactor IRR-1
analysis of reactor water, 18
automatic control, 13
burn-up in MTR type fuel element, experimental evaluation, 14
contamination in vicinity of, 247
experiments installed in the reactor, 2
operation and utilization, 1
power monitoring, local and integral methods, N^{17} delayed neutron [monitor, 12
spectroscopic det. of alkali metals in reactor water, 189

Reactor Physics
collision density for fast reactor conditions, 34
Doppler coefficients for fast reactors, calculated by different [methods, 38
effect of changes in cross-section increments on the total Doppler [effect in fast reactors, 37
effect of Pu isotopic composition on the Doppler coefficient in fast [reactors, 39
fundamental fast reactor calculations, 33
Monte Carlo investigation of the heterogeneity of fast reactor [cores, 39
Monte Carlo investigation of the interaction between resonances of [fertile and fissile isotopes in fast reactor cores, 40
one-dimensional multigroup perturbation codes, 32
sodium void and Doppler effects in large fast power reactors, 35

Reactor Safety
see Nuclear Safety

Resonances
see Elementary Particles, Reactor Physics

Resonant Scattering
see Scattering

Rubidium
spectrochemical det. of, 189

Scattering
computer calculations for resonant scattering, 44
elastic scattering of hot atoms in gaseous media, calculation of energy [distribution, 171
inelastic components in scattering of gamma rays from Te, 45
resonance fluorescence of gamma rays using gaseous and liquid sources, 56
resonant scattering of gamma rays from highly excited nuclear levels, 43
width of Tl 7.64 MeV level by resonant gamma scattering, 44

Scavengers
in radiolysis - see Radiolysis
electron scavengers - see Electrons

Selenium
half-life of short-lived Se^{86} and Se^{87}, 168

Silicon
det. by activation analysis, 202

Silver
det. by activation analysis, 200

Snake Venom
trace element composition of, 213

Sodium
det. by activation analysis, 201
Na^{23}, mean life of 1st and 2nd excited states, 46
Na^{24}, as a tracer, 263

Soil
det. of Mn in, by activation analysis, 198
det. of Sr, 245

Solvent Extraction
of Am III and Am VI from HNO_3, synergism in, 79
of Ga III from bromide solutions, synergism in, 80
of Zn halides from molten salts, 89

Spectra
see also Infrared Spectra, and Spectroscopy
angular momentum transformation matrix elements, calculation, 62
gamma spectra, computer program for analysis of, 175
intensity calculations of absorption bands using static and vibrational [electric fields, 62
of ions, operator for spin-forbidden transitions, 59
splitting of optical bands, covalency effects in trigonal distortion, 61

Spectroscopy
det. of alkali metals in reactor water, 189
det. of B, Ba, Li, Ru in Mediterranean and Dead Sea water, 195
det. of Ga in U-Ga alloys, 193
influence of alkali metals on intensity of B and Sr lines, 191

Spin
calculation of helicity amplitudes of wave functions for any spin, 27
classification of spin states in U(12), 30
spin-forbidden transitions, matrix operator for, 59

Strontium
spectrochemical det. of, 191
Sr^{90} in fallout, 235
Sr^{90} in food, 244
Sr^{90} in milk, 243
Sr^{90} in soil, 245

Tantalum
electrodeposition from molten salts, 83

Tellurium
7.53 MeV level, inelastic components in scattering of gamma rays, 45

Thallium
det. of 7.64 MeV level by nuclear resonant gamma ray scattering, 44

Thermal Decomposition
of perchlorates, catalytic effect of chlorides in, 96

Thorium
det. in urine, 183

Thyroxine
deiodination in humans, 203
metabolism in rats, 206

Tin
electrodeposition from molten salts, 83

Tracers
see Radioisotope and Stable Isotope Tracing, and Labelled Compounds

Tritium
production of in the reaction $N^{14}(n,t)C^{12}$ with 14 MeV neutrons, 173
as a tracer in plant studies, 214

Uranium
assay in meteorites, by delayed neutron counting, 197
phase diagram of UCl_4 - $PbCl_2$ system, 91
precision of det. by delayed neutron counting, 199
spectrochemical det. of Ga in U-Ga alloys, 193
U^{235}, alpha particle associated fission in, 54

Vacuum Technology
sealing mechanism of vacuum gasket seals, 310

Vanadium
NMR studies of vanadium hydride, 58

Water
excited water molecules, in radiolysis of water, 117
excited water molecules, reaction with HNO_3 in radiolysis, 145
model for structure of liquid water, based on quasielastic neutron [scattering data, 65
radiolysis of, 115, 117, 122 ; (see also Radiolysis)
reactor coolant, measurement of flow rate, 6
reactor coolant, N^{16} activity in, 5
reactor coolant, neutron activities in, 4
reactor coolant, spectroscopic analysis, 189
reduction by metals and ions, isotope effect in, 99
sea water, spectrophotometric det. of Cs, 182
sea water, spectroscopic analysis, 195

Zinc
extraction of Zn halides from molten salts, 89